NASA/TM–2018-219810

Preliminary Error Characterization and Parametric Error Model for the Automatic Dependent Surveillance – Contract Extended Projected Profile Message

Nelson M. Guerreiro and Matthew C. Underwood
Langley Research Center, Hampton, Virginia

March 2018

NASA STI Program . . . in Profile

Since its founding, NASA has been dedicated to the advancement of aeronautics and space science. The NASA scientific and technical information (STI) program plays a key part in helping NASA maintain this important role.

The NASA STI program operates under the auspices of the Agency Chief Information Officer. It collects, organizes, provides for archiving, and disseminates NASA's STI. The NASA STI program provides access to the NTRS Registered and its public interface, the NASA Technical Reports Server, thus providing one of the largest collections of aeronautical and space science STI in the world. Results are published in both non-NASA channels and by NASA in the NASA STI Report Series, which includes the following report types:

- TECHNICAL PUBLICATION. Reports of completed research or a major significant phase of research that present the results of NASA Programs and include extensive data or theoretical analysis. Includes compilations of significant scientific and technical data and information deemed to be of continuing reference value. NASA counter-part of peer-reviewed formal professional papers but has less stringent limitations on manuscript length and extent of graphic presentations.

- TECHNICAL MEMORANDUM. Scientific and technical findings that are preliminary or of specialized interest, e.g., quick release reports, working papers, and bibliographies that contain minimal annotation. Does not contain extensive analysis.

- CONTRACTOR REPORT. Scientific and technical findings by NASA-sponsored contractors and grantees.

- CONFERENCE PUBLICATION. Collected papers from scientific and technical conferences, symposia, seminars, or other meetings sponsored or co-sponsored by NASA.

- SPECIAL PUBLICATION. Scientific, technical, or historical information from NASA programs, projects, and missions, often concerned with subjects having substantial public interest.

- TECHNICAL TRANSLATION. English-language translations of foreign scientific and technical material pertinent to NASA's mission.

Specialized services also include organizing and publishing research results, distributing specialized research announcements and feeds, providing information desk and personal search support, and enabling data exchange services.

For more information about the NASA STI program, see the following:

- Access the NASA STI program home page at http://www.sti.nasa.gov

- E-mail your question to help@sti.nasa.gov

- Phone the NASA STI Information Desk at 757-864-9658

- Write to:
  NASA STI Information Desk
  Mail Stop 148
  NASA Langley Research Center
  Hampton, VA 23681-2199

NASA/TM–2018-219810

Preliminary Error Characterization and Parametric Error Model for the Automatic Dependent Surveillance – Contract Extended Projected Profile Message

Nelson M. Guerreiro and Matthew C. Underwood
Langley Research Center, Hampton, Virginia

National Aeronautics and
Space Administration

Langley Research Center
Hampton, Virginia 23681-2199

March 2018

Acknowledgments

The authors wish to thank Mike Palmer, Doug Mielke, Mike Day, Tom Britton, and Jim Sturdy, and other members of the Airspace and Traffic Operations Simulation development team for providing software support; Bryan Barmore for technical oversight of the effort; as well as all others who contributed to this effort.

This work was supported by the NASA SMART-NAS for Safe Trajectory Based Operations Project, TBO sub-project. The support and guidance from project management and technical lead personnel are greatly appreciated.

Available from:

NASA STI Program / Mail Stop 148
NASA Langley Research Center
Hampton, VA 23681-2199
Fax: 757-864-6500

Table of Contents

List of Figures

List of Tables

Acronyms

4DT	=	Four-Dimensional Trajectory
AIDL	=	Aircraft Intent Description Language
ADS-C	=	Automatic Dependent Surveillance – Contract
ANSP	=	Air Navigation Service Provider
ASTOR	=	Aircraft Simulation for Traffic Operations Research
ATN-B2	=	Aeronautical Telecommunication Network – Baseline 2
ATOS	=	Air Traffic Operations Simulation
ATSU	=	Air Traffic Service Unit
CAS	=	Calibrated Air Speed
CI	=	Cost Index
DST	=	Decision Support Tool
EPP	=	Extended Projected Profile
ETA	=	Estimated Time of Arrival
FAA	=	Federal Aviation Administration
FANS	=	Future Air Navigation System
FL	=	Flight Level
FMS	=	Flight Management System
FOM	=	Figure of Merit
GPS	=	Global Positioning System
ILS	=	Instrument Landing System
IPI	=	Intermediate Projected Intent
KDEN	=	Denver International Airport
KIAD	=	Washington Dulles International Airport
KLAS	=	Las Vegas McCarran International Airport
KLAX	=	Los Angeles International Airport
KORD	=	Chicago O'Hare International Airport
KSFO	=	San Francisco International Airport
LNAV	=	Lateral Navigation
MOT	=	Middle-of-Turn
NAS	=	National Airspace System
NASA	=	National Aeronautics and Space Administration
NextGen	=	Next Generation Air Transportation System
NM	=	Nautical Mile
RAP	=	Rapid Refresh
RF	=	Radius-to-Fix
RL	=	Route Length
RNAV	=	Area Navigation
RNP	=	Required Navigation Performance
RPFMS	=	Research Prototype Flight Management System

RT	=	Route Type
RTA	=	Required Time of Arrival
STAR	=	Standard Terminal Arrival Route
TBO	=	Trajectory-Based Operations
TCP	=	Trajectory Change Point
VNAV	=	Vertical Navigation
VOR	=	Very High Frequency Omnidirectional Range
VOR-DME	=	Very High Frequency Omnidirectional Range with Distance Measuring Equipment
VORTAC	=	Very High Frequency Omnidirectional Range with Tactical Air Navigation System
WC	=	Wind Condition

1 Introduction

Trajectory-based Operations (TBO) are a key component of the Next Generation Air Transportation System (NextGen) [1, 2]. TBO are based on the premise that, in the near future, aircraft operating in the National Airspace System (NAS) will be managed more strategically based on a four-dimensional trajectory (4DT). A 4DT defines the lateral, vertical, and temporal path of an aircraft and can be computed by automation, computed by the aircraft, or synchronized between these two agents. TBO extends this premise by providing separation, sequencing, spacing, and merging services to flights based on these 4DTs, thus providing efficiency, capacity, and safety benefits [2].

A critical component of TBO is the ability for a consistent and accurate 4DT representation to be shared and synchronized between airborne and ground systems as well as amongst various ground automation systems. Sharing of the 4DT is important to ensure that all stakeholders of a given flight have a common baseline from which to build situation awareness of the present and future states of any aircraft at any time during the flight. Additionally, through management and sharing of the 4DT, preferences regarding how the trajectory of a given flight should be modified can be developed and shared with other stakeholders of the flight. Furthermore, for the Air Navigation Service Provider (ANSP), sharing the 4DT amongst various ground-based automation platforms assists in system-wide benefit realization by considering the widespread system-level impacts that result from specific decisions.

In today's NAS, no comprehensive trajectory information is broadcast from the flight deck to ground-based automation systems. Several ground-based automation platforms have independent, domain-specific trajectory generators that build trajectory representations based on constraints in the NAS. These systems typically do not share their trajectory representations, and if they do, the information that is passed to other systems is usually inadequate (constraints with insufficient detail) and is only passed in one direction with no opportunity for negotiation. This leads to un-coordinated decision making without the input of all stakeholders.

The Aeronautical Telecommunication Network—Baseline 2 (ATN-B2) standard [3] defines the Extended Projected Profile (EPP) trajectory that can be sent via Automatic Dependent Surveillance-Contract (ADS-C) from an aircraft to ground automation. The EPP trajectory message contains a representation of the reference trajectory from an aircraft's Flight Management System (FMS). The EPP is included in the ATN-B2 standard as one method for facilitating trajectory synchronization between airborne and ground systems. The ATN-B2 standard has been mandated by EUROCONTROL [4], but not by the Federal Aviation Administration (FAA).

Several studies [5, 6, 7, 8, 9] have demonstrated potential uses for, and illustrated shortcomings of, the data contained within the EPP trajectory. However, none of these studies has attempted to characterize the EPP error that results from an aircraft's own trajectory prediction error. The objective of this analysis and paper is to produce an initial characterization of the accuracy of the EPP message under a limited set of conditions. This is intended to be an initial characterization that produces an order of magnitude understanding about the potential limitations in the use of the shared EPP trajectory information. In addition, a parametric error model is identified that could serve to support fast-time predictive analyses on a larger number of use cases.

This report is organized as follows. Section 2 describes the content of the EPP message and explains anticipated uses and limitations of the EPP as found in literature. Section 3 describes the design of the EPP error characterization analysis, the simulation approach used, and the calculation methodology of the error metrics. Section 4 discusses the qualitative EPP error characterization, with the associated experiment figures presented in Appendix A-Appendix F. Section 5 describes the development of the parametric error model, with associated model calibration and validation figures shown in Appendix G, while section 6 presents the conclusions for this analysis.

2 Background

This section of the document provides an overview of how ADS-C contracts and reports are initiated and operationally executed, discusses the contents of the EPP message, and highlights potential uses of the EPP message. It also discusses the identified shortcomings of the EPP message found in the literature.

2.1 ADS-C Operational Overview

ADS-C is an application that provides automatic reports from an aircraft's FMS to an ANSP. ADS-C reports can be requested by the ANSP in one of three types of contracts – an on-demand one-time report, a periodic contract, and an event-driven contract. The aircraft system is capable of providing ADS-C reports to support contract requests. The ADS-C report's content, and the conditions under which the report is sent, vary depending on the type of contract request and the conditions specified in the request [3]. Figure 1 illustrates how an ADS-C contract is originated and executed.

A contract is initiated through a request sent from the ANSP (Air Traffic Service Unit, or ATSU, in the figure) to the aircraft's FMS. The aircraft's FMS sends a message that either accepts the request, partially accepts the request, or rejects the request, at which point the controller is notified. Once the ADS-C contract is no longer required, a cancellation message is sent from the ANSP to the aircraft's FMS [3].

Only one contract of a given type can be set up per aircraft with any given ANSP. When the ANSP sends a request to an aircraft system for a periodic or event contract, and either of these two contracts is already in place with that aircraft, the new contract will override the previous contract for that type. An ADS-C contract may be established between an aircraft and an ANSP prior to the entry into the ANSP's airspace, and an ADS-C contract may remain in effect after an aircraft has exited an ANSP's airspace [3].

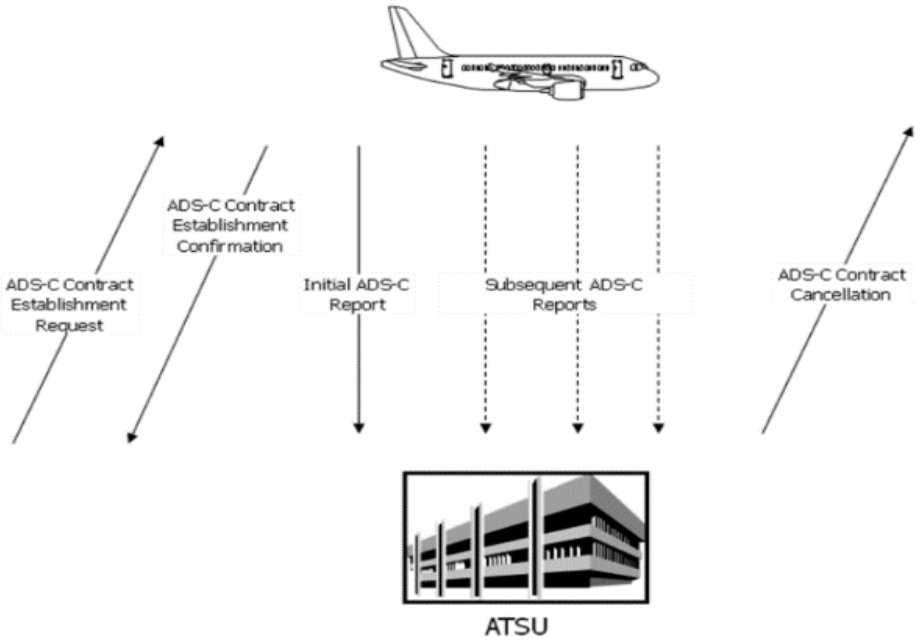

Figure 1. ADS-C operational diagram [3].

2.2 EPP Message Elements

The EPP message provides a set of trajectory points that are a representation of the aircraft's four-dimensional FMS reference trajectory. It extends and improves upon the Intermediate Projected Intent (IPI) trajectory downlink message, which was available in Future Air Navigation Systems (FANS) 1/A. The EPP message contains information based on the route and performance data that has been entered into the aircraft's Flight Management System (FMS), including up to 128 trajectory change points (TCPs) and constraints (e.g., altitude, time, etc.) at each waypoint [3, 7]. Figure 2 defines the data contained in the EPP message. Note that the minimum required set of data for an EPP trajectory point is the latitude and longitude position.

```
ExtendedProjectedProfile ::= SEQUENCE
        {
        computation-time        [0]     DateTimeGroup,
        way-point-sequence      [1]     SEQUENCE SIZE (1..128) OF SEQUENCE
                {
                latitude                [0]     Latitude,
                longitude               [1]     Longitude,
                level                   [2]     EPPLevel                OPTIONAL,
                name                    [3]     WaypointName            OPTIONAL,
                estimated-time          [4]     ETA                     OPTIONAL,
                estimated-speed         [5]     SpeedIASMach            OPTIONAL,
                vertical-type           [6]     VerticalType            OPTIONAL,
                lateral-type            [7]     LateralType             OPTIONAL,
                level-constraint        [8]     LevelConstraint         OPTIONAL,
                speed-contraint         [9]     SpeedConstraint         OPTIONAL,
                time-constraint         [10]    RTA                     OPTIONAL,
                ...
                },
        current-gross-mass      [2]     GrossMass               OPTIONAL,
        trajectory-intent-status [3]    TrajectoryIntentStatus  OPTIONAL,
        ...
        }
```

Figure 2. ADS-C EPP message contents [3].

2.3 Anticipated Uses of the Extended Projected Profile Message

Data contained within the EPP message are anticipated to facilitate trajectory synchronization between aircraft and ANSP automation, as well as to provide data required for automated conformance monitoring. As stated by Bronsvoort, et al in [10], "The goal of air-ground trajectory synchronization is to produce trajectories in disparate systems whose discrepancies are operationally insignificant, increasing the likelihood of flying the planned conflict-free and preferred trajectories." Trajectory synchronization is anticipated to occur through several means, including augmentation of ground-based trajectory generation systems with FMS-calculated and inferred intent data from the EPP message, and calibration of the ground-based trajectory generators utilizing data contained within the EPP message. Once the trajectories are synchronized, they can be used for conformance monitoring.

2.3.1 Augmentation of Ground-Based Trajectory Generators

Decision Support Tools (DSTs) serve many functions in air traffic management, including separation assurance, forecasting of sector loading [6], supporting time-based metering into terminal areas, and updating flight route information in ground systems [9], among others. A common requirement among all of these DSTs is the ability to accurately, and timely, predict an aircraft's future state. Ground-based trajectory predictors and generators are used by several DSTs in order to model the aircraft's anticipated future path. Paglione, et al, provide an example of a generic trajectory prediction and generation process, noting that some trajectory predictors may require more, different, or less information that the example. In general, the trajectory predictor requires the flight plan, flight number, the aircraft type, the filed cruise speed, and the desired cruise altitude. Additionally, the trajectory predictor will have an estimate of the initial condition from surveillance data. With the route from the flight plan converted from named waypoints and procedures (e.g., jet routes, Standard Terminal Arrival Routes (STARs)) into a series of latitude/longitude points, the initial condition is joined to the converted route. Once the lateral path is ascertained, procedural altitude and speed constraints are added at different points along the route (e.g., speed and/or altitude constraints at waypoints on the STAR). Finally, the trajectory prediction process involves the calculation of the trajectory using physics-based modeling. During this step, the lateral and vertical paths, and speed profile, are merged to reproduce the predicted behaviors identified in the previous steps (i.e., following the converted route, meeting specified constraints) while following appropriate aircraft

dynamics and reflecting environmental effect, such as wind. The output of this process is an aircraft's predicted flight path with respect to time [11].

Ground-based trajectory generators must overcome several impediments in order to provide an accurate representation of an aircraft's intent. Regarding lateral uncertainty, as mentioned in the previous paragraph, the flight plan is used to determine the lateral path of the aircraft. Yet, as the aircraft executes its trajectory, unforeseen conditions such as weather or the actions of traffic aircraft may affect the flight and require changes to the lateral path. Common examples of these are vectors and direct-to maneuvers, which are communicated verbally between the ANSP and flight crew, and often are not captured by ANSP automation systems. Mondoloni and Bayraktutar state that the intent error caused by vectoring is among the highest-impact factors that affect prediction accuracy, due to the significant effects on cross-track and along-track error [12]. In a study published by MITRE, the author states that only approximately 30 percent of the lateral maneuvers were entered into the ANSP automation within an en route facility [13]. Furthermore, regarding longitudinal uncertainty, ground-based trajectory generators often have inadequate knowledge of an aircraft's speed schedule and weight, which results in inaccuracies in the climb and descent portions of the flight [6, 14].

In order to address trajectory uncertainty, work conducted by Paglione, et al [11], and Bronsvoort, et al [15], demonstrated that ground-based trajectory generation systems can benefit significantly from using data from the aircraft's FMS-generated trajectory (e.g., via the EPP message). Bronsvoort, et al [10], describe two approaches for using such information. The first approach is to directly employ the EPP message as the trajectory to be used by ANSP DSTs; however, arguments have shown that this is not the most practical use for the EPP message (see Section 2.4.2). The second approach is to augment the data used for ground-based trajectory generation with data contained in the EPP message. Because the FMS is the most accurate source of aircraft intent and other parameters required for trajectory generation, it follows that trajectory predictors in ground systems can improve accuracy when using EPP-derived intent and parameters [10].

Haugg, et al [8], state that the most beneficial data taken directly from the EPP message for a ground-based trajectory generator is the speed profile, especially the climb Calibrated Airspeed (CAS) or Mach number. Additionally, the use of the climb and descent profile data, along with the time prediction data from the EPP, would further improve ground-based trajectory generation. A ground-based trajectory generator may also benefit to a certain extent from a better air-ground trajectory synchronization if, for example, the aircraft's preferred Top of Descent or Top of Climb points are known in advance and are dynamically updated.

Šošovička, et al [5], re-iterate the findings of Haugg, et al, and posit that the highest benefit for the ground-based trajectory predictors occurs when the aircraft-derived data from the EPP message is used in conjunction with knowledge of how the aircraft is handled in any given sector (e.g., hand-off altitudes, entry/exit points). The authors add that, since ground-based trajectory generators do not have accurate knowledge of the weight of the aircraft, weight information available in the EPP can increase the accuracy of ground-based trajectory predictions.

In addition to the aforementioned direct use of data elements in the EPP message in ground-based trajectory generation systems (e.g., speed data, climb/descent profile data, weight), an additional use is to derive aircraft intent information from the EPP message and use it when building a trajectory in a ground-based trajectory generator. Bronsvoort, et al [7], propose a method that uses the EPP message to reconstruct the commands, guidance modes, and control strategies available to the FMS to plan the trajectory to be followed. These are modeled using the Aircraft Intent Description Language (AIDL) [16, 17], which is a formal language designed to express aircraft intent in a rigorous and standardized manner. In a recent example, the aircraft intent was used as input to a trajectory predictor used by Airservices Australia. The study determined that the proposed method can be used to achieve air-ground trajectory synchronization, based on an example flight, but there were some notable shortcomings to this approach (discussed in Section 2.4).

2.3.2 Calibration of Ground-based Trajectory Generators

In addition to its usefulness in deriving aircraft intent, the EPP can be used to calibrate aircraft performance characteristics unknown to the ground-based trajectory generator. This allows for synchronization of the current trajectory with the trajectory prediction process [10]. This calibration can be sufficiently accurate if the provisional solutions do not deviate too far from the intent associated with the original EPP. Bronsvoort, et al [9], demonstrated that the EPP message could be successfully used to determine an aircraft performance model calibration function that accounts for any variables not specifically recorded in the EPP.

With trajectory predictor calibration, a ground-based trajectory predictor can perform high accuracy "what-if" computations that anticipate the FMS behavior upon changes in aircraft intent. These "what-if" trajectories are essential for successful trajectory negotiation. In addition, re-computing the trajectory on the ground by a calibrated trajectory predictor provides superior trajectory information between the EPP TCPs rather than using basic interpolation [10].

2.3.3 Conformance Monitoring

A recognized feature of TBO is that, by using 4DTs to manage the flight, it should be possible to generate more efficient solutions to strategic traffic flow management and separation management problems. Correspondingly, the use of 4DTs in these scenarios results in a higher likelihood of using the more complex clearances in congested airspace. Complex clearances – typically composed of lateral, vertical, and temporal dimensions of the aircraft's trajectory – may be too detailed for human conformance monitoring. Therefore, a need exists for automated conformance monitoring – both on the flight deck and for the ANSP.

The EPP can play a crucial role in this conformance monitoring. An envisioned ANSP conformance monitoring DST uses surveillance reports and alerts the controller when the aircraft is outside the conformance margins allowed by the clearance. Some clearances may involve the use of procedures that have well-defined tolerances (e.g., clearances involving Required Navigation Performance (RNP) and Required Time of Arrival (RTA)). It is impractical to ask a human controller to monitor conformance for errors at the level of precision required for 4DTs. The EPP is required for the conformance monitoring function because it defines the aircraft's intent in complying with a clearance, and can be easily used within a DST.

2.4 Identified Shortcomings of the Extended Projected Profile Message

Although the EPP message is regarded in the literature as the practical solution for achieving trajectory synchronization, there are some shortcomings within the message standard. These deficiencies may lead to inaccurate trajectory synchronization, which, as Bronsvoort, et al state, can lead to unnecessary tactical intervention [10], thus likely causing a loss of efficiency. In the following sections, the identified inadequacies of the EPP message – both in terms of useful data missing from the message standard and of possible misuse of the data contained within the EPP message – are discussed.

2.4.1 Missing Data from the EPP Message

While the EPP message contains sufficient data to perform the functions outlined in the previous section, there are some data elements missing from the ADS-C standard that would increase the accuracy of trajectory synchronization between the aircraft's FMS and ground-based trajectory generators. This section discusses these elements and the implications of not having them as part of the standard.

The EPP message contains turn geometry information for fly-by turns and supports Radius-to-Fix (RF) legs. However, it does not contain turn geometry information for fly-over waypoints. Mondoloni and Bayraktutar include turn modeling in their list of high-impact factors that affect prediction accuracy [12]. Bronsvoort, et al [7], discuss the impacts of the lack of turn radii for a fly-over waypoint in the EPP message standard. Typically, a fly-over waypoint contains two turns with different radii – the first (R_1 in Figure 3) when overflying the waypoint, WP_1, to turn in the direction of the next waypoint, WP_2, and a second (R_2 in Figure 3) to intercept the track between WP_1 and WP_2. P_A represents the point where the first turn ends and the next begins, P_B represents the point where the second turn ends and the aircraft is on track to WP_2, and the red line indicated by Δd_0 is the track that the aircraft intends to follow.

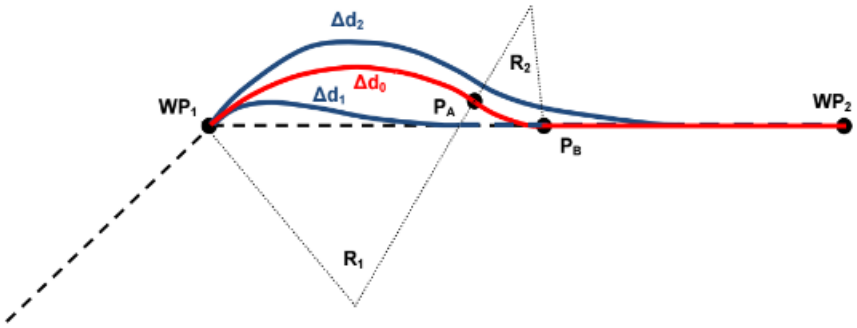

Figure 3. Lateral profile of a fly-over maneuver [7].

Because the turn radii information is not in the EPP message for fly-over waypoints, assumptions need to be made when generating the lateral trajectory, and resulting lateral trajectories produced by disparate ground-based trajectory generation systems. The lack of this information may result in significantly different lateral paths (e.g., Δd_1 or Δd_2 in Figure 3). These assumptions introduce both lateral and longitudinal trajectory errors due to ambiguities in the distance flown between WP_1 and WP_2. Bronsvoort, et al [7], concluded that the knowledge of the turn radii for fly-over waypoints is therefore crucial for unambiguous definition of the lateral path.

Additionally, while the EPP message includes data regarding the aircraft's current gross mass (i.e. the mass of the aircraft at the time when the reference trajectory used for the EPP message was generated), it does not provide information about predicted fuel burn. Mondoloni and Bayraktutar also include lack of aircraft weight in their list of high-impact factors that affect prediction accuracy [12]. Between subsequent EPP messages, the gross mass of the aircraft decreases due to fuel burn. If the periodicity of the EPP reports is large (i.e., a large time interval between subsequent EPP reports), significant differences may exist between the ground-based trajectory generation system's prediction of the gross mass and the actual gross mass of the aircraft. These errors affect the vertical trajectory, especially during the climb phase of flight, but less-so during the descent phase of flight [6, 9, 10].

The EPP message does not include information about the temperature and wind forecast that the FMS used for trajectory calculations, nor does it include the actual temperature and winds that the aircraft is experiencing at the time the trajectory calculation is performed [9, 10]. Mondoloni and Bayraktutar include lack of wind forecast and wind gradient modeling in their list of high-impact factors that affect prediction accuracy [12]. Complicating matters further, Bronsvoort, et al, describe the differences between weather information accessible by ground-based trajectory generators and the FMS, as well as differences between airline forecasting methods, data sources, and FMSs manufactured by different companies:

> *The ground system has access to a complete weather grid that is updated every hour, whereas the FMS is limited in the number of wind points that it accepts and it may not be updated as frequently, at least for most current FMS implementations. Additionally, airlines are inconsistent with different practices and procedures for handling the wind data that is provided to the aircraft. The sources of weather data used by the airline may also be different than ATC. To complicate matters, different FMS manufacturers have different approaches to process wind data and to blend forecast with sensed wind* [10].

Inconsistencies also exist in the FMS's calculations of the Estimated Time of Arrival (ETA) at waypoints along the trajectory due to errors in the predicted groundspeeds that result from differences between actual and forecast winds [6]. It was proposed to include wind information in the EPP message; however, the proposal was rejected to reduce complexity and to limit bandwidth requirements [9]. These discrepancies and lack of information cause errors between the trajectory calculated by an FMS and a trajectory calculated by a ground-based trajectory generator with respect to the longitudinal and time components of the trajectories.

The EPP message does not provide a direct representation of user preference [10]. Most FMSs perform cost trade-offs in the form of selecting a Cost Index (CI) to attribute a fuel-cost to time. The cost index is

typically specific to an airline and considered "sensitive" information; therefore, operators are reluctant to make the information available to the ground via data-link. While this information would not necessarily be useful for trajectory generation, it would be beneficial for ANSP DSTs used in separation assurance for ranking conflict resolution advisories, and in traffic flow management for delay allocation [10].

Finally, Bronsvoort, et al [10], state that in order to conduct accurate trajectory synchronization as described in the concepts in Section 2.3, a key element is missing in the EPP – an error estimate or Figure of Merit (FOM) associated with the EPP that informs ground automation the expected accuracy of the prediction. This information could be used by the ground system to determine the level of reliability of the EPP and thus decide whether to map the EPP directly onto a native trajectory, or to re-compute a new trajectory.

2.4.2 Misuse of Data Contained within the EPP Message

The EPP message provides ground-based trajectory generators with a standardized, un-matched representation of the FMS reference trajectory. The current concepts of use in Section 2.3 are predicated on the philosophy that the airborne trajectory computation process is superior and, hence, the effectiveness and feasibility of any constraints imposed by the ANSP are checked with the FMS in the loop. The most trivial approach to the trajectory synchronization problem is for the ground to use the EPP trajectory directly in ANSP DSTs.

Klooster, et al [18], provide several arguments against the direct use of the EPP trajectory. The most impactful reason is that a direct overwrite of the ground-computed trajectory with the airborne trajectory representation can lead to instabilities and inconsistencies due to differences in the trajectory computations by each trajectory generator.

The EPP only provides a representation of the active reference trajectory within the FMS based on the current active flight plan, implying that the EPP is only valid for the current clearance held by the aircraft when it is in a coupled path guidance mode (i.e., coupled Lateral Navigation (LNAV) and Vertical Navigation (VNAV)) [10]. Haugg, et al, reiterate this point, stating that it is important to consider the guidance mode, which is indicated in the EPP trajectory status portion of the message, because predictions may not be relevant when not in a coupled path guidance mode [8].

3 Analysis Design

The literature discusses different ways that information from an EPP trajectory can be used in ground-based trajectory prediction. However, there is no known effort that has attempted to characterize a Figure of Merit (FOM) or an error estimate for the EPP message under a given set of conditions. The objective of this analysis was to produce an initial characterization of the accuracy of the EPP message under a limited set of conditions. This was intended to be an initial characterization to produce an order of magnitude understanding, identify further limitations in the use of the shared EPP trajectory information, and to provide a preliminary method for calculating error estimates for the EPP message points.

As stated in the previous section, the EPP message provides a set of trajectory points that are a representation of the aircraft's four-dimensional FMS reference trajectory. Under the assumption of "good FMS trajectory prediction," and without any atmospheric uncertainty (no wind), the as-flown trajectory should follow the FMS reference trajectory closely. In fact, the error between these two could be characterized as the guidance and control error and can be easily quantified within a simulated environment. Then, the remaining difference between the as-flown trajectory and the EPP data can be denoted as the error associated with the EPP representation of the reference trajectory. The EPP error can be characterized against the as-flown trajectory (which includes the guidance and control error), or directly against the FMS's reference trajectory. In this analysis, we primarily focus on the EPP error against the as-flown trajectory but also compare the differences between the FMS reference trajectory and the EPP trajectory.

The EPP message is a sampling of the FMS reference trajectory. As such, we can characterize error with respect to the reported points easily. However, characterizing error at positions between the reported points requires making assumptions about how to estimate the aircraft's position at any time between those reported points. The EPP trajectory reports on lateral trajectory change points (e.g., flight pan waypoints), vertical trajectory points (i.e., the top-of-descent and the Mach/CAS crossover altitude), and speed change points. In this analysis, we consider only the errors at the EPP reported points and do not consider the speed change points.

The approach used in this analysis was to simulate a set of scenarios using a medium-fidelity simulation and compare the EPP and FMS trajectories to the as-flown trajectories. A set of independent variables were selected to try to generate trajectory differences that could try to answer the following set of research questions:

- What are the differences between an FMS reference trajectory and the EPP trajectory for a set of common trajectory points?
- How do the EPP trajectories compare to the realized trajectories as a function of look-ahead time?
- What parameters contribute to EPP trajectory error?
- Can parametric error models be identified for the EPP message?

3.1 Simulation Environment

NASA's Airspace and Traffic Operations Simulation (ATOS) platform was used as the simulation environment for this study. The ATOS platform contains a network of real-time simulators that can be used for batch studies and real-time human-in-the-loop experiments [19]. Each Aircraft Simulation for Traffic Operations Research (ASTOR) aircraft within the ATOS platform utilizes a high fidelity six degree-of-freedom dynamics model, an emulated flight management system, and an emulated auto-throttle system. The ASTOR is also equipped with a pilot model that can simulate the actions of a human pilot in executing a flight plan through climb, cruise, and descent phases.

The Research Prototype Flight Management System (RPFMS) of the ASTOR was modified to include the ADS-C and EPP messaging capability of ATN-B2. The RPFMS is a high-fidelity FMS simulation with added research capabilities, such as a multiple RTA capability. The RPFMS was modified to include the ability to receive an ADS-C contract request for periodic EPP trajectory information, the ability to respond to and execute the ADS-C contract request, and the ability to encode the FMS reference trajectory into an EPP trajectory, based on the ATN-B2 specification.

Table 1 shows an example of the EPP trajectory data from one of the experiment scenarios used in this study. The basic information for each reported point includes: the point sequence number; the latitude and

longitude position; the altitude in 10's of feet; the waypoint name where applicable; the estimated time; the estimated speed; the vertical and lateral types, to include the fly-by radius in tenths of a nautical mile (NM) where applicable; and the speed, altitude, or time constraints applicable to that point. The gray entries in Table 1 (e.g., sequence 7, 8) indicate the speed change points that were not considered in this analysis.

Table 1. Example EPP message contents.

Sequence	Lat./Long.	Altitude [/10]	Name	Time[1]	Speed	Vertical Type[2]	Fly-By Radius [*10]	Lateral Type[3]	Level Constraint	Speed-Constraint	Time-Constraint
1	N40040458W107554962	3500	EKR	181	M801		515	64			
2	N40209575W106299611	3500		741	M801	2					
3	N40216178W106264949	3371		763	K280	256					
4	N40230153W106191248	3181	CSPAD	811	K280			64	27000A		
5	N40266847W105595400	2674	FRNCH	945	K280		103	64	21000A		
6	N40237803W105410735	2196	SKARF	1079	K280			64	17000A		
7	N40222137W105312534	1934		1154	K280	32					
8	N40214045W105262175	1900		1195	K250	64					
9	N40214045W105262175	1900	TOMSN	1195	K250			64	19000B17000A	K250B	
10	N40197262W105139473	1647		1304	K250	32					
11	N40173840W104570970	1300		1477	K210	64					
12	N40173840W104570970	1300	BEOND	1477	K210			64	13000	K210B	
13	N40168210W104531685	1228	SWAYN	1522	K210			64	12000A		
14	N40158058W104461062	1100	KAILE	1603	K210		66	64	11000	K210B	
15	N40145178W104425038	1050	BJETN	1648	K210		28	64	10500A		
16	N40124355W104409922	1000	JEEPR	1683	K210		32	64	10000		
17	N40096990W104410242	1000	JOBOB	1723	K210			64	10000		
18	N40073004W104410521	937		1758	K210	32					
19	N40058310W104410692	899		1781	K202	64					
20	N40058310W104410692	899	KUURT	1781	K202			64	9000A		
21	N40058310W104410692	899		1781	K202	32					
22	N40019682W104411140	800		1844	K181	64					
23	N40019682W104411140	800	KIKME	1844	K181			64	8000A		
24	N40019682W104411140	800		1844	K181	32					
25	N39588175W104411505	700		1901	K164	64					
26	N39588175W104411505	700	LEETS	1901	K164			64	7000A		
27	N39588175W104411505	700		1901	K164	32					
28	N39569639W104411720	641		1939	K138	64					
29	N39538222W104412083	541	R-16L	2014	K138			64			

[1] Relative to EPP message computation time.

[2] Vertical types: 2 – ToD, 256 – xOVER, 32 – speed change begin, 64 – speed change end. Speed change points not considered in this analysis.

[3] Lateral types: 64 – flight plan waypoint.

The ATOS platform was used to simulate a set of ASTORs executing a set of flight plans while providing EPP trajectory reports at a pre-defined interval. As will be discussed in more detail later in this section, three flight plans were chosen to represent short, medium, and long flights across the NAS. Each flight was initiated at the start of the cruise phase of flight and flew the flight plan, through the descent phase, and terminated just prior to reaching the destination. Each flight was providing EPP trajectory information at a 60-second interval. The frequent EPP trajectory report interval provided a large amount of EPP trajectory samples while also matching the FMS trajectory update interval. The choice to begin each scenario at the start of the cruise phase of flight was selected because the aircraft is not using a VNAV path guidance and is therefore not attempting to adhere to the vertical path in the EPP trajectory during the climb phase of flight. This is one limitation for the use of the EPP trajectory.

The ASTOR state trajectory data, FMS reference trajectory data, and EPP trajectory data were collected for each scenario. For each flight, the as-flown trajectory was gathered at a 1-Hertz frequency, a complete FMS trajectory prediction was gathered every 60 seconds during the cruise phase of flight, and a complete EPP trajectory was gathered every 60 seconds throughout the flight. These trajectories were used in post-processing to extract the EPP error information.

3.2 Independent Variables

In order to address the research questions, the research team chose a set of five independent variables. The independent variables selected were route length, route type, wind magnitude error, wind direction error, and RTA condition. The independent variables are discussed in the following sections and were selected based on surveys of the literature and subject matter expertise, and directly affect the trajectory in different, quantifiable ways.

3.2.1 Route Length and Route Type Conditions

The two independent variables that relate to the route of flight are the route length and the route type. The route length was chosen to help identify whether longer flight plans have the same or different EPP error characteristics when compared to shorter flight plans. The route type is used to distinguish between a full route and a sparse route, where a sparse route will have significantly fewer flight plan waypoints than a full route, and may have different EPP error characteristics.

Three route lengths and two route type conditions were chosen as independent variables in order to characterize the accuracy of the EPP message. This section describes assumptions made when looking for and generating the scenario flight plans, a description of the independent variables, the route generation process, and the details of each route used in this study. The STAR charts and approach plates used in developing these routes can be found in Figure 124 through Figure 131 located in Appendix I.

3.2.1.1 Route Design Considerations

Two considerations were made for this study concerning route design. The first consideration is that all routes are fully connected from their respective initialization points to their respective runways (i.e., there are no route discontinuities in the FMS). This is done in order to calculate a trajectory from the aircraft's current position to the runway threshold so that the trajectory representation provided by the EPP message is complete. The second consideration is that the researchers desired for all of the flights to travel in the same general direction so that one scenario could contain three aircraft flying different routes based on length while utilizing a common wind field with some desired nominal headwind component. The direction chosen for the flights was from West to East.

3.2.1.2 Description of Independent Variables

The route length was chosen to be one of three conditions – long, medium, or short. These are represented as conditions RL1, RL2, and RL3, respectively, as seen in Table 2. The long route length (RL1) is represented by a flight plan from Los Angeles International Airport (KLAX) to Washington Dulles International Airport (KIAD). The medium route length (RL2) is represented by a flight plan from Las Vegas McCarran International Airport (KLAS) to Chicago O'Hare International Airport (KORD). The short route length (RL3) is represented by a flight plan from San Francisco International Airport (KSFO) to Denver International Airport (KDEN). The details of the route design for these flights, including details

about each route's waypoints, can be found in Appendix H. A schematic of these three flight plans for the full route conditions can be seen in Figure 4.

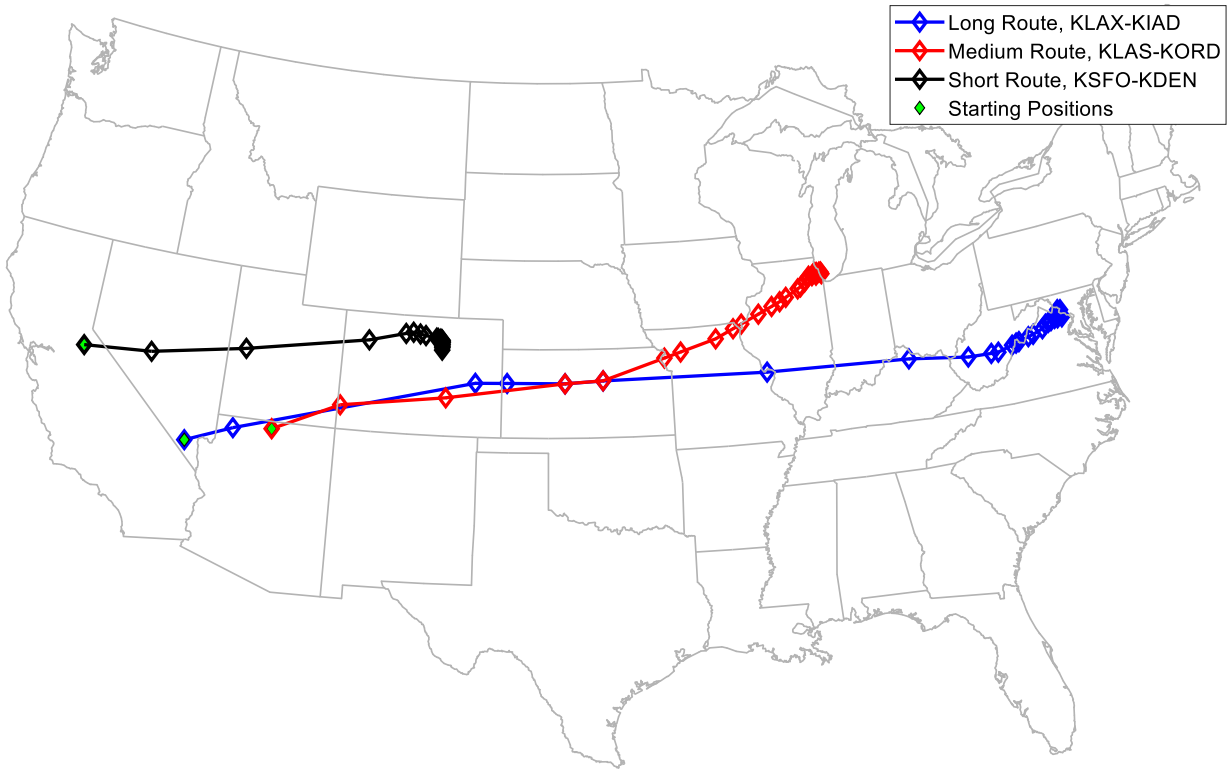

Figure 4. Long, medium, and short routes and their lateral waypoint locations.

The route type was chosen to be either a full route (i.e., a route similar to what an aircraft would fly on a normal day) or a sparse route (i.e., a route with a minimal set of waypoints in the cruise phase of flight). The full route was designated the condition name RT1 while the sparse route was designated the condition name RT2. The details of the differences between the full route waypoints and the sparse route waypoints can also be found in Appendix H.

Table 2. Flight route length and type independent variables.

Route Length		Route Type	
Condition Name	**Value**	**Condition Name**	**Value**
RL1	Long (approx. 2,400 NM)	RT1	Full
RL2	Medium (approx. 1,600 NM)	RT2	Sparse
RL3	Short (approx. 1,000 NM)		

3.2.2 Wind Conditions

Wind forecast error is widely known to be a significant contributor to trajectory prediction error. In this study, nine wind conditions were chosen to demonstrate the impact of both wind forecast magnitude error and wind forecast direction error. These wind forecast errors affect the FMS trajectory predictions, which, in turn, affect the EPP trajectories. In this section, the assumptions made regarding wind conditions are presented, the methodology for selecting winds is discussed, and a description of the wind conditions used in this study is provided.

3.2.2.1 Assumptions Made Regarding Wind Conditions

In this study, variations in wind direction within each scenario (i.e., headwind, crosswind, tailwind) as a function of latitude, and longitude were not considered. A single direction wind field was used at all altitudes. This was done primarily for data analyses purposes – the objective was to maintain a constant wind direction in order to quantify the impacts of wind direction on the EPP trajectory. The majority of scenarios tested feature wind conditions with a headwind component, with a subset of scenarios featuring a crosswind or tailwind condition.

It should be noted that the impact of a headwind component was assumed equivalent to the impact of a tailwind condition, with the exception of the direction of the error. For example, it is postulated that the impact of a stronger that forecast headwind will cause the time error at a waypoint to be positive (i.e., the aircraft will arrive at the waypoint later than its estimated time of arrival). Conversely, the impact of a similar magnitude, stronger than forecast tailwind would likely produce a similar magnitude negative time error at that waypoint. In order to minimize the number of scenarios in this study, we focused our scenarios around a headwind condition.

Finally, the temporal effects of wind were disregarded. While, in the physical world, the magnitude and direction of the wind varies as a function of time, this would make this initial data analysis more complicated. Thus, the wind field direction and magnitude is held constant throughout each scenario.

3.2.2.2 Methodology for Selecting Wind Magnitude and Direction

The wind magnitudes used in this analysis we selected using the analysis presented in Appendix J. For wind magnitude, the desire was to have one condition with no wind magnitude forecast error, one condition with wind forecast magnitude greater than true wind magnitude, and one condition with wind forecast magnitude smaller than true wind magnitude. Thus, the magnitude conditions of 25th percentile, 50th percentile, and 75th percentile wind magnitude from Appendix J were chosen, with the 50th percentile magnitude selected as the true wind magnitude condition.

The selection of wind direction error was guided by the desire to have a transition between a nearly pure headwind condition and a nearly pure tailwind condition. Using the 50th-percentile wind magnitude condition, the wind directions of 080, 110, 140, 170, 215, and 260 degrees were selected as the wind forecast direction conditions. Those are equivalent to 0, 30, 60, 90, 135, and 180 degrees of wind forecast direction error, respectively, given that the true wind direction is from 080 degrees in all scenarios.

3.2.2.3 Description of Wind Conditions

The nine wind conditions in this study consisted of: one condition with no winds, one condition with perfect knowledge of the winds, two wind forecast magnitude error conditions, and five wind forecast direction error conditions. The nine wind conditions are presented in Table 3.

The first wind condition (WC0) was that of no winds at all. This condition was chosen to allow the research team to identify errors between the aircraft's reference trajectory and the EPP trajectory due to the different trajectory representations.

The second wind condition chosen for this study is a perfect knowledge wind condition (WC1). In this condition, the wind magnitude and wind direction are the same between the true wind and the forecast wind. Even in this perfect wind condition, there can be trajectory prediction errors in the FMS because the FMS only samples the wind forecast at the waypoints of the flight plan, and only at a few altitude levels. Furthermore, the FMS uses wind blending between the sensed winds and the forecast winds to create wind predictions. Thus, this wind condition allowed for potential rounding, translation, and wind-blending impacts on the EPP errors to be assessed.

The third (WC2) and fourth (WC3) wind conditions simulated featured wind forecast magnitude errors, prompting quantifiable errors into the FMS reference trajectory. In each of these conditions, the direction of the truth wind (i.e., the wind that the aircraft dynamics model physically experienced) and the direction of the forecast wind (i.e., the wind data used by the FMS for wind prediction computations) remained the same across all conditions (i.e., wind from 080 degrees). However, the magnitudes changed between the 25th percentile, 50th percentile, and 75th percentile, where the 50th percentile represented the true wind magnitude condition. The wind forecast magnitude conditions are shown in Figure 5.

The fifth through ninth wind conditions (WC4-WC8) simulated featured wind direction forecast errors, also inducing quantifiable errors into the FMS reference trajectory. In each of these conditions, the magnitude of the truth wind and the magnitude of the forecast wind remained the same across all conditions (i.e., at the 50th percentile magnitude). However, the direction of the wind in the forecast varied from 080 degrees (the truth wind direction) to 260 degrees (180-degree wind forecast direction error). The wind forecast direction conditions are shown in Figure 6.

Table 3. Scenario wind conditions.

Condition Number	Qualifier	Truth Wind Magnitude Percentile	Truth Wind Direction	Forecast Wind Magnitude Percentile	Forecast Wind Direction
WC0	No Wind	N/A	N/A	N/A	N/A
WC1	Perfect Knowledge (Truth = Forecast)	50th	From 080°	50th	From 080°
WC2	Positive Magnitude Error (Truth > Forecast)	50th	From 080°	25th	From 080°
WC3	Negative Magnitude Error (Truth < Forecast)	50th	From 080°	75th	From 080°
WC4	30° Direction Error	50th	From 080°	50th	From 110°
WC5	60° Direction Error	50th	From 080°	50th	From 140°
WC6	90° Direction Error	50th	From 080°	50th	From 170°
WC7	135° Direction Error	50th	From 080°	50th	From 215°
WC8	180° Direction Error	50th	From 080°	50th	From 260°

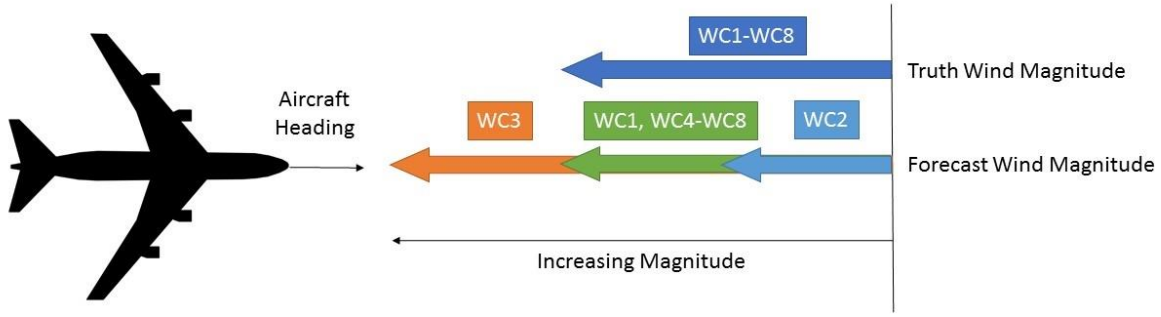

Figure 5. Wind forecast magnitude description.

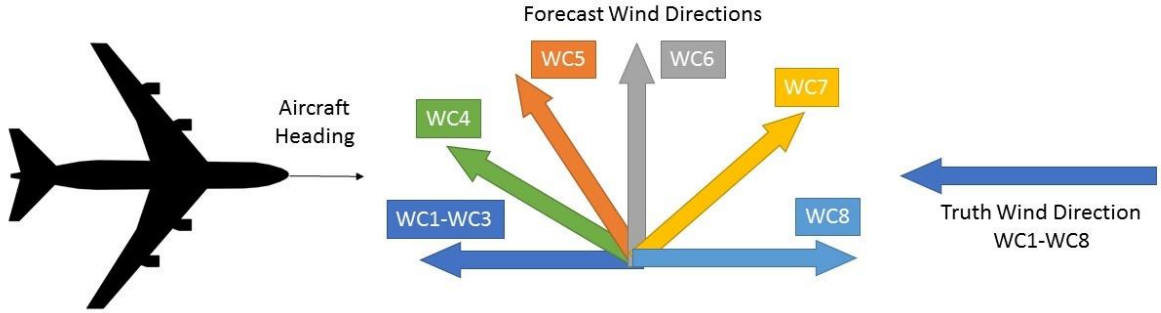

Figure 6. Wind forecast direction description.

3.2.3 RTA Conditions

The use of an RTA waypoint on a route is expected to have an impact on the EPP error characteristics. In order to understand this impact, four RTA conditions were tested. The first condition (No RTA) involved no RTA on the route. The second condition (RTA1) involved an RTA waypoint near the end of the cruise segment for each flight. In this condition, an RTA was assigned to the waypoints WOJOW, KEOKK, and EKR of the long, medium, and short routes, respectively. The third condition (RTA2) involved an RTA in the descent portion of the flight, just after the top-of-descent point. In this condition, an RTA was assigned to the waypoints HESEE, BDF, and TOMSN of the long, medium, and short routes, respectively. The fourth condition (RTA3) involved an RTA to a waypoint at the entry to the terminal area (defined as a point just prior to reaching 10,000 feet). In this condition, an RTA was assigned to the waypoints KILMR, BENKY, and KAILE of the long, medium, and short routes, respectively.

In each RTA condition, an RTA tolerance of +/- 30 seconds was used. It is important to note that the RPFMS used in this analysis has dynamic RTA tolerances that can result in internal tolerances of up to 120 seconds when far from the RTA waypoint and 30-second tolerance as the flight approaches the RTA point.

Table 4. Scenario RTA conditions.

Condition	Description
None	No RTA constraint
RTA1	An RTA constraint en route at a waypoint just prior to top of descent
RTA2	An RTA constraint in descent at a waypoint just after the top of descent
RTA3	An RTA constraint in descent at a waypoint close to the terminal area

3.3 Test Scenarios

A select combination of the conditions of each independent variable above resulted in the experiment matrix, shown in Table 5. The experiment matrix consists of 13 scenario runs, each consisting of one long, one medium, and one short route length flight simulated simultaneously. That equates to 39 flight datasets of as-flown trajectories, FMS trajectories, and EPP trajectories.

Table 5. Test matrices.

Scenario Number	Route Length	Route Type	Wind Condition	RTA Condition
1	RL1, RL2, RL3	RT1	WC0	No RTA
2	RL1, RL2, RL3	RT1	WC1	No RTA
3	RL1, RL2, RL3	RT1	WC2	No RTA
4	RL1, RL2, RL3	RT2	WC2	No RTA
5	RL1, RL2, RL3	RT1	WC3	No RTA
6	RL1, RL2, RL3	RT1	WC4	No RTA
7	RL1, RL2, RL3	RT1	WC5	No RTA
8	RL1, RL2, RL3	RT1	WC6	No RTA
9	RL1, RL2, RL3	RT1	WC7	No RTA
10	RL1, RL2, RL3	RT1	WC8	No RTA
11	RL1, RL2, RL3	RT1	WC2	RTA1
12	RL1, RL2, RL3	RT1	WC2	RTA2
13	RL1, RL2, RL3	RT1	WC2	RTA3

The test matrix was devised to achieve the following data comparisons:

- Compare the EPP trajectories to the FMS trajectories (scenario 1)
- Investigate the impact of wind forecast sampling by the FMS (scenario 2 vs. scenario 1)
- Compare the EPP errors of the full routes with those of the sparse routes (scenario 3 and 4)
- Investigate the impact of wind forecast magnitude error on EPP errors (scenarios 2, 3, 5)
- Investigate the impact of wind forecast direction error on EPP errors (scenarios 2 and 6-10)
- Investigate the impact of RTA constraints on EPP errors (scenarios 2 and 11-13)

The above list corresponds to the analysis presented in sections 4.1-4.6.

Each scenario in Table 5 resulted in three flown trajectories and multiple EPP and FMS trajectories because the FMS and EPP trajectories were recorded approximately once-per-minute for each flight. As an example of the output data of each scenario, scenario 1 resulted in 219, 135, and 84 FMS trajectories for the long, medium, and short routes, respectively. Scenario 1 also had 236, 158, and 102 EPP trajectories for those same three route lengths. The number of EPP trajectories for each flight, in general, exceeded the number of FMS trajectories because the FMS trajectory in the RPFMS were not updated after top-of-descent but the EPP trajectory continued to be generated using the last FMS reference trajectory.

3.4 Dependent Variables

The dependent variables for the EPP error analysis were the cross-track error, vertical error, and time error. The three dependent variables were computed based on the state data point closest to the trajectory reported point.

Figure 7 illustrates the method used to determine the closest state data point for a given trajectory point. The determination was done with respect to the closest lateral position in the latitude-longitude plane. Point P_3 represents the latitude, longitude, altitude, and time of a reported EPP trajectory point. Point P_3 may also have an associated non-zero fly-by radius, R, and may or may not be associated with a two-dimensional waypoint position, WPT_i, such as a flight plan waypoint. Given the position, P_3, and the radius, R, the position of the geometric middle-of-turn (MOT), P_2, was computed using Great-Circle distances and the track angle change, θ, associated with the difference between the track-in and track-out of the point P_3. The distance, d, between the points P_3 and P_2 is given by:

$$d = R\left(\frac{1}{cos\left(\frac{\theta}{2}\right)} - 1\right) \quad \textbf{(1)}$$

Once the point P_2 had been computed, the closest state data point, P_1, was identified. Finally, the point $P_1{}'$ was estimated by intersecting the perpendicular line at the middle-of-turn with the line between the two closest state data points as shown in Figure 7. Note that the point P_2 inherits the same altitude and time as that reported in the EPP point P_3.

The closest interpolated state data point, $P_1{}'$, is a 4-dimensional point in latitude, longitude, altitude, and time from the state data. The cross-track error for the i^{th} trajectory point can thus be defined as,

$$E_{xtrk,i} = GCD\left(P_{2,i}, P_{1,i}{}'\right) \quad \textbf{(2)}$$

where GCD is a positive-definitive Great-Circle distance function. The vertical error is defined as,

$$E_{vert,i} = Altitude_{P_{1,i}'} - Altitude_{P_{2,i}} \quad \textbf{(3)}$$

and the time error can be defined as,

$$E_{time,i} = Time_{P_{1,i}'} - Time_{P_{2,i}} \quad \textbf{(4)}$$

The cross-track error is computed in units of feet as is the altitude error. The time error is computed in terms of seconds.

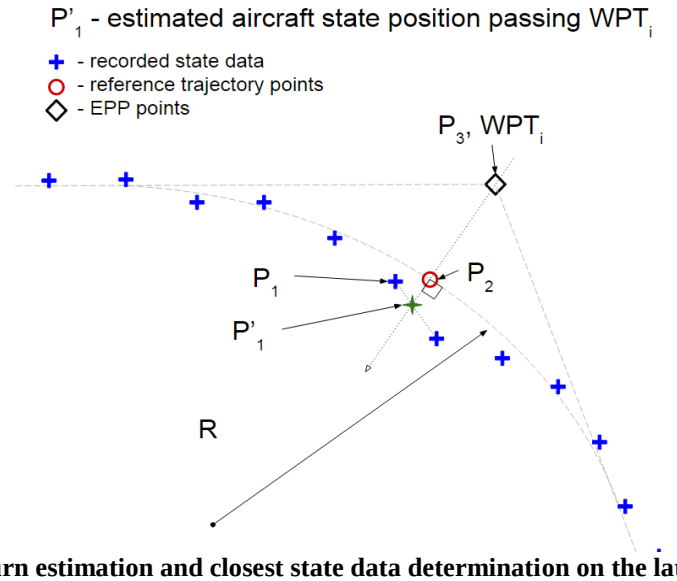

Figure 7. Middle-of-turn estimation and closest state data determination on the latitude-longitude plane.

The point P_2 must be estimated for the EPP trajectory. As was described above, to estimate this point, the track-in and track-out for point P_3 is required. This track in and out must be estimated given the other points provided in the EPP trajectory because the EPP trajectory does not directly provide track information. One area where this is problematic is for the first point in the EPP trajectory, which, in general, is a point somewhere ahead of the aircraft's current position. Thus, the track into this first EPP point must be assumed to be from the current aircraft position, which may not necessarily be an accurate assumption. Note that, in the case of the FMS trajectory, the point P_2 is estimated and available and does not need to be re-computed for this error analysis.

3.5 Data Processing

The data processing of each scenario involved computing the EPP error metrics of cross-track, vertical, and time error for each point in each EPP and each FMS trajectory. Each EPP and FMS trajectory contained a set of trajectory points ahead of the aircraft and all the way to the destination airport. As the flight sequenced a waypoint, these trajectories became smaller in terms of number of trajectory points. The error metrics were only computed for the lateral type points, plus the top-of-descent (label name "ToD" in the data) and crossover altitude (label name "xOVER" in the data) vertical type points. The error metrics were only computed to a point on the trajectory close to the scenario termination altitude of 6000 feet. These waypoints were MAAAY, MONKZ, and LEETS for the long, medium, and short routes, respectively.

As an example, Scenario 1 of Table 5 consisted of 7457 analysis points from the FMS trajectories and 7740 analysis points from the EPP trajectories. That consisted of 3590 data points for the long route, 2467 data points for the medium route, and 1400 data points for the short route from the FMS trajectories. Similarly, this consisted of 3647 data points for the long route, 2554 data points for the medium route, and 1539 data points for the short route from the EPP trajectories. Each of the experiment scenarios consisted of approximately the same number of analysis data points for the EPP cross-track, vertical, and time errors.

In much of the figures and discussion of Section 4, the EPP error metrics are presented as a function of the time horizon. The time horizon refers to the difference between the estimated time-of-arrival at a waypoint and the time the trajectory was generated. Some may also refer to this as the "time-to-go" to that waypoint at trajectory generation time.

4 EPP Error Preliminary Analysis

In this section, a preliminary characterization of EPP trajectory errors is presented. The characterization is a qualitative discussion of the EPP trajectory errors observed in the simulated scenarios. In section 4.1, a baseline scenario with no wind is used to compare the EPP and FMS trajectory errors. Section 4.2 compares the no-wind condition scenario with the perfect wind forecast condition scenario to assess the impacts of FMS wind sampling. Section 4.3 looks at the impact of long flight segments by comparing the full and sparse route scenarios. In section 4.4, the impacts of wind forecast magnitude error on EPP trajectory errors are discussed. Section 4.5 discusses the EPP error impacts resulting from wind forecast direction error. Finally, section 4.6 investigates the effects of RTA waypoints on the EPP errors. For ease of reading, the figures associated with this section's analysis and discussion are presented in Appendix A-Appendix F.

4.1 No Wind Baseline Scenario – EPP and FMS Comparison

The baseline scenario with zero wind magnitude [RL1-RL3, RT1, WC0, No RTA] allows for the comparison of the EPP error data against the FMS error data. The FMS error here represents the combination of the trajectory prediction error and the guidance error in following the desired flight plan. The EPP error is a combination of this FMS error, the error associated with transforming the FMS reference trajectory into the EPP format, the error associated with computing the geometric middle-of-turn, and the error that results from the EPP message itself being "stale." Staleness here refers to an EPP message that may not be a representation of the most recent FMS reference trajectory (assuming that the EPP message update interval is larger than the FMS trajectory's update interval).

4.1.1 Cross-Track Error

The FMS cross-track error is a function of the error in the prediction of the MOT point for a fly-by waypoint combined with the fact that the middle-of-turn point is, itself, not a point that the guidance algorithm is targeting. The FMS computes a MOT point along a constant radius turn using the estimated groundspeed at a fly-by waypoint and assuming a constant bank angle for that turn. In some cases, such as with very small track angle changes (~1-2 degrees or smaller), the FMS will not compute a turn radius or MOT point, thereby adding to the cross-track error at those points. The EPP, because it is generated from the FMS reference trajectory, necessarily inherits this guidance and prediction error. In addition to these errors, the EPP, in general, will have higher cross-track errors because the EPP message does not contain the FMS's estimated MOT point. Instead, the EPP trajectory contains the waypoint's position and a predicted fly-by radius that must be used to estimate this point. The EPP message also limits the resolution of this reported fly-by radius to the nearest $1/10^{th}$ of a NM, thereby creating additional possibility for errors.

Figure 8 shows the EPP cross-track error for the no wind baseline run as a function of the time horizon. Figure 9 shows the FMS cross-track error for the same run. The figures show the EPP or FMS cross-track errors for each point of each EPP or FMS reference trajectory, respectively, for each route length of the baseline run. The largest value of time horizon for any given point's error profile is representative of how far in time that point is in the flight plan relative to the scenario starting position. The time horizon represents the difference between the predicted waypoint crossing time in the EPP or FMS trajectory and the computation time of the EPP or FMS trajectory. Both figures indicate a steady cross-track error for each waypoint throughout the scenario run, which is expected when there is no wind error affecting the trajectory predictions of the FMS. However, the scale of the cross-track error does show a larger cross-track error for some of the EPP points as compared to the same points in the FMS cross-track error. This is due partially to the resolution of the EPP reported turn radius, which is reported to the nearest 0.1 NM. However, this fly-by radius resolution contributes minimally to the cross-track error difference for small track angle change turns as can be seen in Figure 133. The worst-case error difference due to the radius resolution will be more evident for larger track angle changes and can be even worse if a floor or ceiling rounding approach is used for composing EPP radius values.

Figure 10-Figure 12 show the comparison of the cross-track median error and median error difference for each of the trajectory points in the EPP and FMS trajectories for the long, medium, and short routes,

respectively, in the no wind baseline scenario. For the long route (RL1), the median error difference is largest at the points NOOTN, HYS, FLM and HVQ in the en route phase of flight, and at the point BBONE in the descent phase of flight. For the medium route (RL2), the median error difference is largest at the point PUB in the en route phase of flight, and at the points BDF and PETAH in the descent phase of flight. For the short route (RL3), the median error difference is largest at the points INSLO and EKR in the en route phase of flight, and at the points BJETN, JEEPR in the descent phase of flight. The majority of these points are associated with either very large fly-by radii (as seen in Figure 13), or very small track angle changes (as seen in Figure 14), or both. Large radius and small track angle change turns will have the highest sensitivity to the method used to estimate the MOT point that is subsequently used to compute the cross-track error. Figure 15 and Figure 16 show the FMS cross-track error as a function of the fly-by radius and the track angle change, respectively. The cross-track error for most of the FMS trajectory points in the no wind baseline scenario is less than 20ft with the exception of the points NOOTN, FLM, PUB, and PETAH.

4.1.2 Vertical Error

The vertical error is the difference between the actual crossing altitude at a point and the predicted altitude in each EPP or FMS trajectory. Figure 17 shows the vertical error for the EPP trajectory points versus time horizon for the no wind baseline scenario [RL1-RL3, RT1, WC0, No RTA] while Figure 18 shows the vertical error for the same FMS trajectory points. While the two datasets show similar characteristics, there are two distinguishing features when comparing these two figures. First, the EPP error data has trajectory errors all the way down to zero time horizon for all points whereas the FMS error data terminates just prior to zero time horizon for some of the trajectory points. This is because, in the prototype FMS used in this analysis, the FMS reference trajectory is not re-computed in the descent phase of flight (the last reference trajectory is computed prior to top-of-descent) while that same FMS reference trajectory is used to generate EPP trajectory reports in the descent phase. Second, there is some level of "noise" in the EPP error data, which is attributed to truncation or rounding of the reported altitude to increments of 10 feet.

The vertical error profiles of both the EPP and FMS show relatively constant error profiles with the exception of a few points. The points BURTT, ToD, and xOVER in the long route show some variation in their vertical error with time horizon. This variation is due to re-computations and updates to the descent profile as the flight progresses, where the inflection points in the error data represent the sequencing of a flight plan waypoint. Note also that BURTT happens sequentially after the ToD and before the xOVER points in the flight, and that the ToD and xOVER points have dynamically generated positions based on the descent profile computations, which explains why the predicted altitude at BURTT is changing.

Figure 19 shows the median vertical error for the EPP and FMS trajectory points of the long route as well as the magnitude of the difference between the EPP median vertical error and the FMS median vertical error. The largest median vertical errors occur at the points ToD, BURTT, xOVER, KILMR, OTTTO, and MAAAY. With the exception of the ToD point, all points have a median vertical error of less than 50 feet magnitude. The ToD point has a median vertical error of ~160 feet, which is a direct result of the way this point is defined in both the EPP trajectory and the FMS trajectory. The ToD point is defined by the intersection of the cruise altitude with the descent path. The implication of this definition is that the aircraft has already begun intercepting the descent path as it sequences the predicted latitude and longitude position of the ToD point, leading to a below-path (negative) vertical error. The difference between the EPP and FMS vertical error median at all points is less than 10 feet, which is the resolution of the EPP trajectory point altitudes.

Figure 20 shows the median vertical error for the EPP and FMS trajectory points of the medium route as well as the magnitude of the difference between the EPP median vertical error and the FMS median vertical error. The largest median vertical errors occur at the points ToD, DRAMS, xOVER, and BENKY. The ToD median vertical error indicates just over 200 feet below path while DRAMS shows approximately 60 feet above path for both the EPP and FMS data. Both xOVER and BENKY are within 50 feet median

vertical error and the vertical median error difference is within the 10-foot resolution between the EPP and FMS for all points.

Figure 21 shows the median vertical error for the EPP and FMS trajectory points of the short route as well as the magnitude of the difference between the EPP median vertical error and the FMS median vertical error. The largest median vertical errors occur at the points ToD, xOVER, TOMSN, JEEPR, and JOBOB. The ToD median vertical error also indicates just over 200 feet below path while xOVER, TOMSN, JEEPR, and JOBOB show less than 100 feet median vertical error. All other points are within 50 feet median vertical error and the vertical median error difference is within the 10-foot resolution between the EPP and FMS for all points.

4.1.3 Time Error

The time or temporal error is the difference between the actual crossing time at a point and the predicted time in each EPP or FMS trajectory. Figure 22 shows the temporal error for the EPP trajectory points versus time horizon for the no wind baseline scenario [RL1-RL3, RT1, WC0, No RTA] while Figure 23 shows the temporal error for the same FMS trajectory points. There are two characteristic differences between the EPP and FMS temporal errors. First, the EPP temporal errors exhibit a "stair-stepping" pattern when compared to the FMS temporal errors. This is the result of the resolution of the time component in the EPP trajectory points (1-second resolution). The RPFMS reported trajectory points were provided as floating point numbers with a ten-millisecond resolution. This is confirmed in Figure 24 where the distribution of the time error difference between the EPP trajectory times and their source FMS trajectory times is within this 1-second resolution. Second, as discussed previously, FMS trajectories are not re-computed beyond the top-of-descent point so the error data appears to end prior to zero time horizon for some points. In fact, the FMS computed error would be constant if computed and shown for time horizons after the top-of-descent (similar to the trends in the EPP error data). This lack of ETA updates beyond the top-of-descent point, however, is an artifact of the RPFMS simulation and may not be consistent with how operational FMSs handle trajectory updates.

The FMS error data shows discontinuities, or "jumps," in the temporal error data at different points in the time horizon. These discontinuities represent a new FMS trajectory prediction (typically associated with the sequencing of a waypoint) where the RPFMS re-computes the FMS trajectory instead of simply updating ETA information. The linear decrease in the temporal error as the time horizon decreases represents the FMS trajectory prediction error that is reduced as the aircraft gets closer to sequencing a trajectory point. In general, this particular FMS and aircraft simulation combination has trajectory predictions that are biased towards earlier than actual waypoint crossing predicted times; other FMS/aircraft combinations may exhibit the opposite behavior. Trajectory points with temporal error that does not converge to zero error represent points in the descent phase of flight where the FMS trajectory is not being updated.

4.1.4 EPP and FMS Comparison Findings

In comparing the EPP and FMS trajectories in the no wind baseline scenario, we have shown the level of error that can be expected in composing an EPP trajectory from an FMS trajectory. These cross-track, vertical, and time error differences are attributed to the limited resolution of the EPP trajectory point information as well as the assumptions made in re-constructing certain points not reported with the EPP trajectory, such as the MOT point. Specifically, the encoding of the turn radius information with $1/10^{th}$ nautical mile resolution for an EPP fly-by trajectory point only adds a small amount of error for small track angle change turns but the estimation of the MOT point can be problematic, especially if the turn radius is very large. The vertical and temporal errors in the EPP data follow the FMS error data closely and the errors are primarily due to the 10-foot and 1-second resolutions for these two parameters, respectively. When compared to the standard separation criterion of 5 nautical miles and 1000 feet, the cross-track and vertical errors are both within approximately 0.1%, which could be considered negligible for most purposes. The temporal error is within one second.

The scenario used here also defines the trajectory prediction error of the RPFMS in the absence of wind. These errors are small for most FMS trajectory points: less than 50 feet cross-track error, less than 10 feet

vertical error, and a conservative time error within 30 seconds inside two hours of time horizon. The outlier points for error occur at the top-of-descent and altitude crossover points (where the lateral position is dynamically computed) as well as other trajectory points close to these vertical points.

4.2 Baseline Scenario – No Wind versus Perfect Wind

The comparison of the baseline run with no wind [RL1-RL3, RT1, WC0, No RTA] against the baseline run where the wind forecast is perfect [RL1-RL3, RT1, WC1, No RTA] (referred to here as the "perfect wind" baseline scenario) is intended to highlight any differences in the EPP and FMS trajectories in the presence of a non-zero wind field. This comparison is important because the FMS only samples the forecast wind at discrete points of the flight plan (namely, at the flight plan waypoints and at a few discrete altitudes for the descent phase). In addition, the FMS uses wind blending (where the aircraft-sensed wind information is blended with the upstream forecast wind) to compute wind predictions for waypoints within some distance from the aircraft's current position. As such, the FMS trajectories will have some non-zero prediction error that results from this sampling and blending of the wind information and will affect the EPP trajectory data. The comparison is also important because it allows us to see the impact on the EPP trajectories of the nominal headwind that is used in the perfect wind scenario, which is the baseline scenario used for all of the comparisons that follow.

4.2.1 Cross-track Error

Figure 25 shows the EPP cross-track error for the perfect wind baseline scenario [RL1-RL3, RT1, WC1, No RTA] as a function of the time horizon. Figure 26 shows the FMS cross-track error for the same run. The figures show the EPP or FMS cross-track errors for each point of each EPP or FMS reference trajectory, respectively. Qualitatively, the cross-track errors show the same type of pattern between the EPP and FMS errors as in the no wind baseline scenario. Namely, the EPP errors are larger than the FMS errors as expected. The EPP median cross-track errors and the cross-track error differences between the perfect wind scenario and the no wind scenario are shown in Figure 27, Figure 28, and Figure 29 for the long, medium, and short route points, respectively.

The EPP errors are smaller in the perfect wind scenario (Figure 25) versus the no wind scenario (Figure 8) for most trajectory points. For example, the waypoint PUB has approximately 150 feet cross-track error in the perfect wind scenario as compared to approximately 225 feet in the no wind scenario. The smaller cross-track errors appear to be a result of the smaller turn radii predicted in the perfect wind scenario. In this scenario, the wind is nearly pure headwind, which results in smaller groundspeed for the same airspeed and requires a smaller turn radius for a given turn, as shown in Figure 30. Figure 31 shows that there exist some turn radii that produce better cross-track performance (e.g., the executed turn is the closest to the predicted turn) with respect to the FMS predictions. Turns with larger and smaller radii are likely to have higher cross-track errors. For the perfect wind baseline run in the presence of a headwind, this minimum cross-track error occurs for points with predicted fly-by-radius around 40 nautical miles, as can be seen in Figure 31 for the FMS trajectory points.

4.2.2 Vertical Error

Figure 32 shows the vertical error for the EPP trajectory points versus time horizon for the perfect wind baseline scenario [RL1-RL3, RT1, WC1, No RTA]. Qualitatively these vertical errors are close to the vertical errors in the scenario with no wind. Figure 33, Figure 34, and Figure 35 show the comparison of the median vertical error and the median error difference between the no wind baseline scenario and the perfect wind baseline scenario and the long, medium, and short routes, respectively. Most of the errors are close to zero, or within 15 feet, with the exception of BURTT, BBONE, and KILMR on the long route. These three points have median error differences under 100 feet, although their median error magnitudes are nearly identical and of opposite sign, indicating an above-path or a below-path sequencing of the waypoint, or vice versa. Nonetheless, the vertical error profiles show just over 200 feet as the worst-case median error in both baseline scenarios, which occurs at the ToD point.

4.2.3 Time Error

Figure 36 shows the temporal error for the EPP trajectory points versus time horizon for the perfect wind baseline scenario [RL1-RL3, RT1, WC1, No RTA]. Qualitatively these temporal errors are not much different from the temporal errors for the no wind baseline scenario [RL1-RL3, RT1, WC0, No RTA] (Figure 22). The means and standard deviations of the time errors were binned by time horizon; these are shown in Figure 37 in order to compare the two scenarios. The temporal error data shows smaller standard deviations for the scenario with perfect wind as compared to the scenario with no wind, but the differences in the temporal error curves are not statistically significant. The slightly better performance in the scenario with wind could be attributed to the wind blending between the sensed and forecast wind used by the FMS in trajectory prediction, but the actual reason is not clear from this data.

4.2.4 Summary

As expected, there do not appear to be any major differences between the baseline scenario with no wind and the baseline scenario with perfect wind, with respect to the cross-track, vertical, and temporal errors in the EPP trajectory data. The observed differences in errors are related to the presence of a headwind in one scenario but not the other, which affects the predicted groundspeed at the trajectory points.

4.3 Impact of Sparse Versus Full Routes

In this section, the differences between the full routes scenario [RL1-RL3, RT1, WC2, No RTA] and the sparse route scenario [RL1-RL3, RT2, WC2, No RTA] are compared. Note that the scenarios were both run in the presence of a true wind with magnitude larger than the forecast magnitude (WC2) in order to assess the impact of the forecast winds on a flight plan with long legs (e.g., the sparse flight routes). Any significant differences in EPP errors profile will manifest themselves in the cruise phase of the flight because the descent portion of both scenarios is identical in terms of the flight plan waypoints.

4.3.1 Cross-Track Error

The EPP cross-track errors for the full routes scenario [RL1-RL3, RT1, WC2, No RTA] can be seen in Figure 38. Figure 39 shows the EPP cross-track errors for the sparse routes scenario [RL1-RL3, RT2, WC2, No RTA]. Qualitatively, there are some differences between the two figures. First, the sparse route does not contain some of the waypoints of the full route, e.g., FLM, which in intentional. Second, the error magnitudes of some of the points are significantly different, as is the case with NOOTN. To compare the differences in the errors, we plot the median errors for each point.

Figure 40, Figure 41, and Figure 42 show the median cross-track error (top) and the median cross-track error difference (bottom) for the waypoints common to both the full and the sparse routes scenarios, and for the long, medium, and short routes, respectively. The median cross-track error appears to be the largest at the waypoint NOOTN for the long route (Figure 40). A closer look at the data revealed that the difference is linked to different turn radii at the point NOOTN resulting from different track angle change to go direct to HVQ in the sparse routes scenario (~7 degrees) versus the track angle change to go directly to PUB in the full routes scenario (~3 degrees). A similar phenomenon with large median error differences occurs at the point HVQ, the effective end of the sparse en route portion of the flight plan. All other points on the long route have a median error difference less than 15 feet cross-track error. Similar median cross-track error differences are observed at the end point of the medium sparse route, IRK, in Figure 41, although the start of the sparse route at DVC does not have as large of a median cross-track error difference as in the long route. All other points on the medium route are within 10 feet for median cross-track error difference. For the short route in Figure 42, there is no significant difference in the median cross-track error and all points have median cross-track errors within 10 feet. Qualitatively, with the exception of the start and end waypoints of the sparse routes, the cross-track error profiles of the full and sparse routes are similar.

4.3.2 Vertical Error

The EPP vertical error for the points of the full routes scenario [RL1-RL3, RT1,WC2, No RTA] can be seen in Figure 43. Figure 44 shows the vertical error for the points of the sparse routes scenario [RL1-RL3, RT2, WC2, No RTA]. Qualitatively, there is very little difference between these two vertical error profiles.

We do note, however, the discontinuity that appears in the vertical error of some of the route points, both on the full routes and the sparse routes. This discontinuity is due to the piece-wise linear FMS wind blending function, which triggered a significant update to the vertical profile as the wind predictions changed when the flight sequenced one of the route's en route waypoints. The points with the large discontinuity in vertical error are those on the descent profile without any hard "AT" altitude constraints, where an update to the predicted winds can have a significant impact on the predicted crossing altitudes. These types of error discontinuities are governed by the algorithms that each FMS uses to convert a wind forecast into a set of wind predictions along the route.

Figure 45, Figure 46, and Figure 47 show the median vertical errors (top) and the median vertical error difference (bottom) for the waypoints common to both the full and the sparse routes scenarios, and for the long, medium, and short routes, respectively. In all instances, the vertical error profiles are the same and the median vertical error difference is within 10 feet, which is the EPP reported altitude resolution. This is to be expected because the primary difference between the full and the sparse routes is in the en route phase of flight where the aircraft is level at the cruise altitude and no significant difference would be expected in the EPP reported altitudes.

4.3.3 Time Error

The EPP time error for the points of the full routes scenario [RL1-RL3, RT1,WC2, No RTA] can be seen in Figure 48. Figure 49 shows the time error for the points of the sparse routes scenario [RL1-RL3, RT2, WC2, No RTA]. Qualitatively, there are differences between the two temporal error profiles, particularly with respect to the magnitude and slope of the time error after approximately 5000 seconds of time horizon. The EPP time error for the sparse routes scenario shows smaller temporal error and a relatively constant slope in this region of time horizon. These differences can also be seen in Figure 50, which shows the binned mean and standard deviation of the time error as a function of each route length and route type, and the time horizon for all route points.

The time error differences between the full routes and the sparse routes are the combined result of two different aspects of trajectory prediction used by the FMS. First, the FMS only implements wind information at discrete waypoints. As such, the sparse routes have less en route waypoints and, thus, less wind information. For example, in the sparse long route, the FMS has wind information for the waypoints NOOTN and HVQ, which are approximately 1500 nautical miles apart, whereas, in the full long route, the FMS has wind information at six additional waypoints between NOOTN and HVQ. This explains the smoother time error profiles of the sparse routes in Figure 49 as compared to the error profiles of the full routes in Figure 48. The second aspect of FMS trajectory prediction that contributes to the time error differences is the wind blending. As described before, the wind blending blends the true winds with the forecast winds out to approximately 700 nautical miles ahead of the aircraft, where, at that horizon, the predicted winds are equal to the forecast winds. In the case of the sparse routes, there are less opportunities for the wind blending to include wind forecast errors in the wind predictions during the long route legs. This explains why the time error profiles converge at or below approximately 5000 seconds time horizon as this horizon is where the impact of wind blending begins to include wind forecast data that may exist for the scenarios we have tested here.

The FMS wind blending is intended to improve trajectory predictions in the presence of wind forecast error. In this particular set of runs, the wind blending made the time error in the trajectory predictions worse, as evidenced by the sparse routes scenario. In that scenario, the very long route legs led to the true wind information being used for a longer period where there were no downstream waypoints within the wind-blending horizon. Because the true wind field used in the scenario was uniform and static for any given altitude, the time error is smaller for the sparse routes in time horizons outside the wind-blending horizon. This may not have been true, however, if the true wind field were not uniform.

4.3.4 Summary

The differences between the EPP errors of a sparse route and a full route can be attributed primarily to the wind predictions that an FMS generates given its wind blending scheme. The higher the number of waypoints in a flight plan, the higher the number of wind data points. When those waypoints fall within

the wind blending horizon of the FMS, the wind predictions are a blend between the aircraft's current sensed wind and the forecast wind at that point. The predicted wind has an impact on the predicted groundspeed, which in turn has an impact on the predicted turn radius. The predicted wind also has an impact on the descent profile and the location of the top-of-descent point. Cross-track errors are impacted by the differences in turn radii between the full and sparse route scenarios. The vertical errors between the full routes and sparse routes scenario are nearly identical because the sparseness portion of the routes only affected the en route phase of flight where the altitude is constant for the scenarios tested. Wind blending can lead to discontinuities between subsequent trajectory predictions in the FMS, which can lead to discontinuities in the vertical errors. EPP time errors are also impacted by the wind predictions generated by an FMS's wind blending scheme. Wind blending may have a negative impact on the EPP time errors in some circumstances.

4.4 Wind Magnitude Error Effects

Wind magnitude error effects were investigated using a set of three scenarios. These scenarios represent the conditions where: the true wind magnitude was equal to the forecast wind magnitude [RL1-RL3, RT1, WC1, No RTA], the true wind magnitude was larger than the forecast wind magnitude [RL1-RL3, RT1, WC2, No RTA], and the true wind magnitude was smaller than the forecast wind magnitude [RL1-RL3, RT1, WC3, No RTA]. In all scenarios, the true and predicted wind direction was from 080 degrees, or nearly pure headwind.

4.4.1 Cross-Track Error

Figure 51 shows the cross-track errors for all route lengths and all route points of the three wind magnitude conditions tested: truth equal to forecast (WC1), truth greater than forecast (WC2), and truth less than forecast (WC3) [RL1-RL3, RT1, No RTA]. The cross-track errors from these three wind conditions indicate nearly symmetrical error profiles with respect to the perfect wind conditions. For example, at long time horizons, the EPP reported waypoint FLM has approximately 90 feet cross-track error in the perfect wind condition (WC1), approximately 101 feet cross-track error in the under-forecast wind magnitude case (WC2), and approximately 78 feet cross-track error in the over-forecast wind magnitude case (WC3). At zero time horizon, these cross-track errors all converge to 96.3 feet cross-track error. This symmetry is seen with many of the EPP reported points and is to be expected because the wind forecast error tested was also symmetric.

The cross-track error symmetry described above is not necessarily present for all points with a fly-by radius, as seen in Figure 52 for the points FLM and WOJOW of the long route. In this case, WOJOW has an asymmetric error profile when compared to the perfect wind condition. This asymmetry is related to the cross-track error being reported as a magnitude only; that is, we do not differentiate between left or right of course with positive and negative values in this metric. In fact, the points exhibiting this asymmetry indicate points where the fly-by radius was over-predicted in one case and under-predicted in the other, when compared to the average fly-by radius that would produce zero cross-track error.

One other major difference between the points FLM and WOJOW is the magnitude of the fly-by radius; FLM has a reported fly-by radius of 92 NM compared to the WOJOW reported fly-by radius of 17.1 NM, in the perfect wind condition case. FLM also had a reported fly-by radius as large as 96.3 NM in the WC2 condition and as low as 87.5 NM in the WC3 condition whereas, WOJOW only had a reported fly-by radius as large as 17.1 NM and as low as 16.3 NM in those same two conditions. Given that WOJOW has a track angle change of approximately 18 degrees, we also see "stair-stepping" in the WOJOW cross-track error profile in increments of approximately 7 feet, which is a function of the EPP radius resolution consistent with the chart in Figure 133.

The convergence of the cross-track errors at zero time horizon is a result of the wind blending where, as the aircraft gets closer to a specific waypoint, the wind blending is helping to reduce the amount of wind prediction error and the predicted turn radius is changing. Trajectory points whose errors do not converge are those in the descent phase of flight, where the trajectory re-computations are suppressed in this FMS simulation.

Figure 53, Figure 54, and Figure 55 show the boxplots of the cross-track error data for each waypoint of the long, medium, and short routes, respectively, for the three wind conditions tested. The figures indicate that the cross-track error differences between the magnitude error scenarios are more distinct to the en route waypoints. For example, for the long route points in Figure 53, the points SELLS, HYS, FLM, HVQ, and WOJOW have the most variation in the cross-track error for these three wind conditions. Along with NOOTN, these are also the en route points of the long route that have a track angle change significant enough to report a fly-by radius value; other en route points of the long route do not contain a fly-by radius value in the EPP message. Similar characteristics are observed in Figure 54 and Figure 55 for the points DVC, PUB, SLN, and IRK of the medium route, and the points INSLO and EKR of the short route. Once again, these en route points are also the ones that have the largest reported fly-by radius so a higher level of cross-track error can be expected due to the MOT point estimation.

4.4.2 Vertical Error

Figure 56 shows the EPP vertical errors for all route lengths and all route points of the three wind magnitude conditions tested: truth equal to forecast (WC1), truth greater than forecast (WC2), and truth less than forecast (WC3) [RL1-RL3, RT1, No RTA]. As expected, the differences in vertical error between these runs can be seen at the points that are in the descent profile and prior to the first hard altitude constraint. This can be seen more clearly in the boxplots of Figure 57, Figure 58, and Figure 59. The first waypoints with a hard "AT" altitude constraint on the descent profiles of the long, medium, and short routes are KILMR, BENKY, and BEOND, respectively. As such, we note that the points between the ToD point and these points exhibit some vertical error variation due to wind blending as well as the trajectory update that occurs with the discontinuity of each point's error profile at approximately 1800 seconds time horizon. This discontinuity is an artifact of this simulation and is the consequence of the simultaneous sequencing of the waypoint, FLM, on the long route, and the update to the wind predictions due to wind blending, which caused a discontinuity in the wind magnitude prediction of approximately four knots between subsequent trajectory updates. What this discontinuity does show is that, there can be a high sensitivity in the vertical error to the wind magnitude prediction. As expected, the variation decreases as the points approach the hard "AT" altitude constraint points.

4.4.3 Time Error

Figure 60 shows the EPP time errors for all route lengths and all route points of the three wind magnitude conditions tested: truth equal to forecast (WC1), truth greater than forecast (WC2), and truth less than forecast (WC3) [RL1-RL3, RT1, No RTA]. As expected, the time errors are nearly symmetrical, with respect to the perfect wind condition, and decrease as the aircraft approaches each point. The time errors reach a non-zero constant value for waypoints in the descent phase of flight due to the lack of FMS trajectory updates in this region, as seen in Figure 61. This non-zero error is 15 seconds or less for the condition with truth wind magnitude greater than forecast (headwind stronger than forecast leads to late actual waypoint crossing times) and greater than -25 seconds for the condition with truth wind magnitude smaller than forecast (headwind weaker than forecast leads to early actual waypoint crossing times).

4.4.4 Summary

Symmetric wind magnitude error affected the cross-track, vertical, and time errors in a nearly symmetric way with respect to the baseline perfect wind condition tested here. The predicted cross-track error is related to the predicted fly-by radius, which changes as the predicted wind at a point changes, especially in the wind-blending region of the trajectory. As discussed before, large turn radius values coupled with small track angle changes can have a significant impact on the cross-track error. The vertical errors are more prevalent at waypoints in the descent profile without any hard "AT" altitude constraints where the predicted crossing altitude is free to change as the predicted winds also change. The time error is directly related to the over- or under-prediction of the headwind magnitude and approaches zero as the time horizon to a waypoint decreases.

4.5 Wind Direction Error Effects

The impacts of wind direction error on EPP errors is described in this section. Five scenarios for wind direction forecast error were investigated and compared against the scenario with perfect wind forecast. The wind direction error scenarios [RL1-RL3, RT1, No RTA] were: no direction error (WC1), 30 degrees direction error (WC4), 60 degrees direction error (WC5), 90 degrees direction error (WC6), 135 degrees direction error (WC7), and 180 degrees direction error (WC8). These scenarios, as listed, span the realm of conditions from perfect knowledge of a nearly pure headwind (WC1) to a 180-degree wind direction error indicating a nearly pure forecast tailwind (WC8).

4.5.1 Cross-Track Error

The cross-track errors for the six wind-direction error conditions can be seen in Figure 62. For the majority of the points, the cross-track errors are larger at large time horizons as the wind direction error increases. As the time horizon decreases, the cross-track errors converge to the cross-track error in the perfect wind condition. This convergence is the result of the FMS wind blending, which corrects for the wind forecast error as the flight approaches a waypoint. The cross-track error trends seen in Figure 62 are caused by the prediction error in the groundspeeds at each waypoint, which, in turn, affect the predicted turn radius for those points. As an example, WOJOW has a predicted turn radius of 17.1 NM and a cross-track error of less than 10 feet in the perfect wind condition case. In the condition with 180 degrees of wind direction error, WC8, WOJOW has a reported turn radius of 22.4 NM and cross-track error of 397 feet at long time horizons that converge to the radius and cross-track error of the perfect wind condition. The difference in radius for this 17.7-degree turn at the long time horizon between these two conditions can contribute approximately 388 feet of additional cross-track error, per equation (11) and Figure 133. The cross-track errors are also smaller for lower altitude points with speed constraints, where the groundspeed predictions have smaller magnitude errors.

4.5.2 Vertical Error

The vertical errors for the six wind-direction forecast error conditions can be seen in Figure 63. The trends in the vertical profile error are similar to those seen in the cross-track error, where the larger wind direction errors lead to the largest vertical errors. We do note that, for some points, such as BURTT and PHOOW, the vertical errors for the 135-degree direction error condition are slightly larger than the vertical errors for the 180-degree direction error condition. This is because that portion of the long route is better aligned with the 135-degree error wind direction thereby resulting in slightly higher forecast tailwind than in the 180-degree direction error condition.

The vertical errors are largest for the descent points just prior to the first “AT” altitude-constrained waypoint. The different wind-direction error forecasts result in different forecast tailwind magnitude, which affect the groundspeed predictions and vertical path predictions at those un-constrained waypoints. The vertical errors in the constrained portion of the vertical path are small and nearly identical in all wind direction error conditions.

In the wind conditions tested, the vertical error is positive in the long time horizon because the wind forecast simulates increasing tailwind as the wind direction error increases. The increasing tailwind has the effect of moving the predicted top-of-descent point earlier in the flight, thereby resulting in a predicted path that is below the actual path flown in the presence of the true winds.

4.5.3 Time Error

The time errors for the six wind-direction forecast error conditions can be seen in Figure 64. As the wind-direction forecast error increases from zero to 180 degrees, the error at long time horizons also increases. Similar to the vertical error trends, this is due to the increasing forecast tailwind that produces decreasingly earlier predicted crossing times at each waypoint as compared to the actual waypoint crossing times. As such, the time errors are generally positive, indicating later waypoint crossing times when compared with the predictions.

Figure 64 shows a nearly linear increase in time error as the time horizon increases. This is especially true for regions outside any wind blending horizon (time horizon greater than ~5000 seconds). The time

errors approach zero as the time horizon approaches zero for en route waypoints. Descent waypoints reach a non-zero time error that is the time error at the last trajectory prediction just prior to the top-of-descent point.

The "lobes" observed on the 180-degree wind direction forecast error are an artifact of the FMS's wind blending. They occur when the current track of the aircraft causes a wind direction interpolation that is to the right of course in on one leg and to the left of course on the next leg. This causes a discontinuity in the predicted wind magnitude that results in the discontinuity observed in the time errors and is a simulation artifact.

4.5.4 Summary

Wind direction forecast error has a direct impact on the FMS predicted trajectories and EPP trajectories that is related to over- or under- predicted headwind or tailwind components at each waypoint. These over- or under-predicted along-track winds result in groundspeed prediction errors that affect the cross-track errors, vertical errors, and time errors in the EPP message. The groundspeed predictions affect the predicted fly-by radius, the vertical path predicted altitudes for unconstrained waypoints, and the predicted waypoint crossing times, all of which manifest themselves in the EPP trajectory.

4.6 Impact of Time Constrained Routes

In this section, we investigate the impact of RTA waypoints on the EPP errors. Three different conditions were tested with each of the route lengths and compared with the equivalent non-RTA scenario: an RTA just prior to the top-of-descent point (RTA1), and RTA just after the top-of-descent point (RTA2), and an RTA close to the terminal area (RTA3, just prior to reaching 10,000 feet). The baseline scenario for comparison is the scenario with a wind magnitude greater than the forecast magnitude [RL1-RL3, RT1, WC2, No RTA].

The RTA capability of the RPFMS, and the assumptions of that capability, have an impact on the EPP errors. In the absence of an RTA, the FMS updates the reference trajectory at frequency of once per minute. This update to the reference trajectory assumes the aircraft is following the FMS programmed speed profile. However, when an RTA exists on the active route, the reference trajectory is updated much less frequently, and each update reflects a change to the FMS speed profile necessary to correct any RTA error. The reference trajectory is only updated when a provisional trajectory prediction indicates that the estimated time at the RTA point is outside the allowable tolerance. This less frequent update to the reference trajectory in the presence of an RTA serves as a dead-band to prevent reactionary speed changes from occurring too frequently as the result of wind prediction and guidance errors, and to reduce the number of changes in the descent vertical path. In the ATOS simulation used here, the EPP message is composed from this infrequently updated reference trajectory, which leads to significant differences in the EPP error characteristics for a scenario with an RTA waypoint as compared to a scenario without an RTA waypoint.

4.6.1 Cross-Track Error

Figure 65 shows the cross-track errors as a function of time horizon for the long route points and the baseline wind condition with no RTA [RL1, RT1, WC2, No RTA] as well as the condition with an RTA just prior to the top-of-descent point [RL1, RT1, WC2, RTA1]. For the later scenario, the RTA waypoint is WOJOW. We can see that the condition with RTA has cross-track error profiles with long regions of constant cross-track error that are not seen in the baseline condition with no RTA. As explained above, this is related to the FMS's limited update rate for the reference trajectory, which leads to several EPP messages being generated from the same reference trajectory. In Figure 66, we can see this reduced reference trajectory update from the cross-track errors for the FMS's reference trajectory with and without RTA. For example, we note that the waypoint FLM only has two updates in the reference trajectory in the RTA condition scenario: one at 7870 and one at 3301 seconds time horizon.

We note that the magnitude of the cross-track error for the waypoint WOJOW at long time horizons is larger in the scenario with an RTA when compared to the no RTA scenario. In both scenarios, the cross-track error converges to less than 8 feet as the time horizon approaches zero. This larger error at long time horizons is related to a larger prediction error in the fly-by radius. The turn radius prediction at WOJOW

in the RTA condition scenario increases from 17.3 to 19.5 NM as the time horizon increases. Comparatively, in the non-RTA condition, the fly-by radius decreases from 17.9 to 17.1 NM as the time horizon increases. In the non-RTA condition, the fly-by radius variation comes purely from groundspeed prediction error due to the wind forecast error in the presence of constant indicated cruise speed. In the RTA condition, however, the speed profile is allowed to vary to achieve the RTA and, combined with the wind forecast error, can lead to larger groundspeed variations that consequently produce larger fly-by radius variations. For example, in the non-RTA condition, the cruise speed is a constant Mach 0.801, whereas, in the RTA condition, the initial Mach is 0.787 to meet the RTA but increases to Mach 0.843 just prior to crossing WOJOW to correct for the stronger than forecast headwind.

FLM also appears to have larger cross-track errors when there is an RTA at WOJOW as compared to the cross-track errors with no RTA. From Figure 67, we see that the points NOOTN, SELLS, HYS, FLM, HVQ, WOJOW, and BBONE have the largest cross-track error differences between the no RTA condition and the RTA condition scenarios. With the exception of BBONE, these are the en route points with reported fly-by radii that would be susceptible to groundspeed prediction error due to RTA speed adjustments and wind forecast error.

In Figure 68 we see the cross-track errors as a function of time horizon for the long route points and the baseline wind condition with no RTA [RL1, RT1, WC2, No RTA] as well as the condition with an RTA just after to the top-of-descent point [RL1, RT1, WC2, RTA2]. In this RTA condition, the RTA waypoint is HESEE. Figure 69 shows a comparison of the cross-track errors at each of the route points for these same two conditions. The same set of points, NOOTN, SELLS, HYS, FLM, HVQ, WOJOW, and BBONE, show the largest variation in cross-track error due to changes in the reported fly-by radius. There is also a large cross-track error at the xOVER point in the RTA condition at long time horizons because, in those trajectory predictions, the xOVER point falls on the arc of the turn at WOJOW and has cross-track error magnitudes close to those reported for WOJOW. We also note that the cross-track error at the RTA waypoint, HESEE, is small and constant for both conditions because HESEE has a track angle change of less than one degree and no reported fly-by radius.

Figure 70 shows the cross-track errors as a function of time horizon for the long route points and the baseline wind condition with no RTA [RL1, RT1, WC2, No RTA] as well as the condition with an RTA in the terminal area [RL1, RT1, WC2, RTA3]. In this RTA condition, the RTA waypoint is KILMR. Figure 71 shows a comparison of the cross-track errors at each of the route points for these same two conditions. These figures show the same trend seen in the RTA1 and RTA2 conditions, where the en route points with reported turn radius have the largest cross-track error variations. WOJOW shows up again as the point with the largest cross-track error variation because it has the largest track angle change in the points for the long route. Note that KILMR's cross-track error remains below 10 feet with only minor variation resulting from EPP trajectories where KILMR is the first trajectory point and the cross-track error computation can be somewhat noisy.

Figure 72 - Figure 83 show the cross-track errors as a function of time horizon and for each point of the medium and short routes with the baseline wind condition with no RTA [RL2-RL3, RT1, WC2, No RTA] as well as the three RTA conditions [RL2-RL3, RT1, WC2, RTA1-RTA3]. These figures show that, in the case of the medium route (RL2), the cross-track errors have the largest variation for the en route waypoints with a fly-by radius in the case of the cruise RTA (RTA1). That variation is smaller in the condition with the RTA after top-of-descent (RTA2) and almost non-existent in the condition with the RTA close to the terminal area (RTA3). In the case of the short route (RL3), cross-track errors are comparable with and without RTA with the exception of the point FRNCH, which shows very large cross-track error in the RTA conditions. This large error is due to the change in speed profile computed to achieve the RTAs, which translates to changes in the predicted turn radius at a descent point that does not have a speed constraint. For example, in the RTA1 condition of Figure 78, the initial turn radius prediction at FRNCH is 11 NM whereas the final prediction just before reaching FRNCH is 14.1 NM. The difference in these two radii for this 25-degree turn can produce approximately 470 feet of cross-track error.

4.6.2 Vertical Error

Figure 84-Figure 89 show a comparison of the vertical errors between the baseline wind condition with no RTA [RL1-RL3, RT1, WC2, No RTA] and the condition with an RTA in the cruise phase of flight [RL1-RL3, RT1, WC2, RTA1], for all three route lengths. Figure 90-Figure 95 show a comparison of the vertical errors between the baseline wind condition with no RTA [RL1-RL3, RT1, WC2, No RTA] and the condition with an RTA just after the top-of-descent [RL1-RL3, RT1, WC2, RTA2], for all three route lengths. Figure 96-Figure 101 show a comparison of the vertical errors between the baseline wind condition with no RTA [RL1-RL3, RT1, WC2, No RTA] and the condition with an RTA close to the terminal area [RL1-RL3, RT1, WC2, RTA3], for all three route lengths. There does not appear to be any clear distinction between the vertical errors when the RTA is in cruise versus when the RTA is in the descent portion of the flight. The primary difference between the no RTA condition and the RTA conditions is that the RTA conditions have higher levels of variation in vertical error for the waypoints in descent just prior to the first hard "AT" altitude constraint. This is a result of the RTA capability's adjustment of the cost index, and subsequent change of the FMS speed profile, to meet the required waypoint crossing time as the wind and trajectory predictions change. Note also that, in the RTA conditions, the vertical error for these unconstrained waypoints is, larger than in the condition without RTA, especially at longer time horizons.

4.6.3 Time Error

Figure 102-Figure 104 show a comparison of the time errors between the baseline wind condition with no RTA [RL1-RL3, RT1, WC2, No RTA] and the condition with an RTA in the cruise phase of flight [RL1-RL3, RT1, WC2, RTA1], for all three route lengths. Figure 105-Figure 107 show a comparison of the time errors between the baseline wind condition with no RTA [RL1-RL3, RT1, WC2, No RTA] and the condition with an RTA just after the top-of-descent [RL1-RL3, RT1, WC2, RTA2], for all three route lengths. Figure 108-Figure 110 show a comparison of the time errors between the baseline wind condition with no RTA [RL1-RL3, RT1, WC2, No RTA] and the condition with an RTA close to the terminal area [RL1-RL3, RT1, WC2, RTA3], for all three route lengths. Note that, in each of these figures, the time error for the RTA waypoint is emphasized. In most of the runs, the time error for the RTA waypoint remains within the RTA tolerance of 30 seconds used in these scenarios. The time error for the remaining non-RTA waypoints, however, can be larger than in the condition when there is no RTA on the route. Even in regions of short time horizon, there are instances of waypoint crossing time error predictions that are larger than the non-RTA condition time errors for the same waypoint. Thus, perhaps intuitively, having an RTA on a route ensures small magnitude time errors for the RTA waypoint at the expense of larger time errors for the non-RTA waypoints.

4.6.4 Summary

The presence of an RTA on a route contributes to the EPP errors in several ways under the conditions tested. The EPP cross-track, vertical, or time errors can be larger than in a condition without RTA because the RTA capability makes several changes to the FMS speed profile in order to try to achieve an RTA within the required tolerance. When these speed adjustments occur in the presence of wind forecast error, it is common for the FMS speed profile to initially change in one direction (e.g., higher speed) but then to correct in the opposite direction (e.g., slower speed). This happens as the time horizon to the waypoint is reduced and the wind forecast error is eliminated by the FMS's wind blending. Changes in the speed profile also lead to changes in the fly-by radius computed and reported for waypoints. Similarly, changes in speed profile lead to changes in the vertical path of the flight, especially for waypoints without an altitude constraint.

The EPP errors in this section were based on EPP trajectories generated from an FMS reference trajectory that remained constant for long periods, and was only updated when the RTA waypoint was found to be out of tolerance. Perhaps if the provisional route computations that this simulated FMS computes between reference trajectory updates were used to generate the EPP message, the results in this section may have been somewhat different. That analysis is left for a future study.

5 Parametric Error Model

The qualitative analysis of section 4 provides a good initial look at the level of cross-track, vertical, and time errors that one might expect to see in an EPP trajectory under a given set of conditions. This qualitative analysis is useful but does not allow for the real-time estimation of the EPP trajectory errors; for this, an error model is needed. For an error model to be useful, that error model should have the ability to estimate the expected level of error for any EPP trajectory point at the time the EPP trajectory is composed or received.

In this section, error models were designed for the cross-track, vertical, and time errors of an EPP message. These models were identified using a subset of the data collected for this analysis. As was highlighted in the previous section, the EPP errors have characteristics that are linked to the trajectory predictions of the specific FMS that generated that EPP message. As such, the models developed here are highly dependent on the FMS simulation within the ATOS environment and may not be suitable as generic models of EPP errors. Additional data would need to be collected using a variety of FMS representing the prediction and EPP encoding capabilities of the current, or future, air traffic system for more generic EPP error models. Nonetheless, because the ATOS and RPFMS models used in this analysis are medium- to high-fidelity models, we can expect that these error models are good first estimates of the magnitude of the errors expected in the real environment, although this could only be verified with field data.

5.1 Model Design

The cross-track, vertical, or time errors can be modeled using a linear relationship. The relationship between the error observations, y_i, the error model estimates, $\widehat{y_i}$, and their residuals, ε_i, is shown in equation (5).

$$y_i = \widehat{y_i} + \varepsilon_i \tag{5}$$

The i^{th} error model estimate, $\widehat{y_i}$, is given by equation (6), where $\widehat{\beta_0}$-$\widehat{\beta_n}$ are the model parameters and $x_{1,i}$-$x_{n,i}$ are the independent variable measurements of the i^{th} observation.

$$\widehat{y_i} = \widehat{\beta_0} + \widehat{\beta_1} x_{1,i} + \cdots + \widehat{\beta_n} x_{n,i} \tag{6}$$

The model identification requires the selection of an appropriate set of independent variables and model parameters that reduce the residuals between the observations and the estimates. The qualitative error analysis of section 4 was used to guide the selection of an appropriate set of candidate independent variables. The model parameters were estimated using MATLAB's stepwise regression function, where independent variables are added and removed from the regression model based on their statistical significance to the model fit. The error models identified below were selected by sequentially adding the most significant independent variables until the change in R-squared for the model fit reduced to less than 0.01, or one percent.

5.2 Independent Variables

The independent variables selected for the error model identification are shown in Table 6. The time horizon, t_h, was an obvious selection for a regressor because of the trends observed in the time error figures of section 4. In some regions of time horizon, the time error trend is nearly linear. The square of the time horizon was also used as an explanatory variable in the model identification. The time horizon variable can be obtained from the EPP trajectory directly.

The cross-track errors in the previous section revealed a significant dependency on the reported fly-by radius, R, but the relationship did not appear to be purely linear. Based on the trends of Figure 13, a bias term for points with a non-zero fly-by radius, $I_{R>0}$, was also included in model identification, as was the square of the radius. Conversely, a bias term, $I_{R=0}$, was included for those points with no reported fly-by radius (very small or no track angle change) in order to try and capture the small cross-track errors for these points. These variables can be derived from the EPP trajectory data.

Regressors related to the track angle change were also included in the model identification. The track angle change, θ, as well as the sine and coversine of that angle (based on Figure 14) were used as regressors.

The track angle change can be derived from the EPP trajectory data points, using the aircraft's current state as needed to estimate the track angle change for the first EPP trajectory point.

Table 6. Independent variables used in error model identification.

Var.	Name	Units	Description	Source
t_h	time horizon	sec.	The EPP point time minus the EPP computation time (the time-to-go to the EPP point at EPP generation time). $t_h > 0$	EPP trajectory
R	radius	N.M.	The EPP point reported fly-by radius. $R \geq 0$	EPP trajectory
$I_{R>0}$	radius bias	-	A bias term for the points with non-zero reported fly-by radius. $I_{R>0} := [R > 0] = 1, otherwise\ 0$	Derived from EPP trajectory data
$I_{R=0}$	no-radius bias	-	A bias term for the points with no reported fly-by radius. $I_{R=0} := [R > 0] = 0, otherwise\ 1$	Derived from EPP trajectory data
θ	track angle change	deg.	The absolute value of the track angle change for the reported point.	Derived from EPP trajectory data
S_θ	sine of track angle change	-	The sine of the track angle change. $S_\theta = \sin\theta$	Derived from EPP trajectory data
V_θ	coversine of track angle change	-	The coversine of the track angle change. $V_\theta = 1 - \sin\theta$	Derived from EPP trajectory data
E_{HW}	headwind error	knots	The difference between the true and the predicted wind magnitude. $E_{HW} = Headwind_{true} - Headwind_{predicted}$	Estimated from wind forecast data (not part of EPP trajectory)
I_{DES}	descent point bias	-	A bias term for the points after the top-of-descent point. $I_{DES} := [i > i_{TOD}] = 1, otherwise\ 0$ for the i^{th} point in the EPP trajectory.	Derived from EPP trajectory data
I_{CRU}	cruise point bias	-	A bias term for the points up-to and including the top-of-descent point. $I_{CRU} := [i \leq i_{TOD}] = 1, otherwise\ 0$ for the i^{th} point in the EPP trajectory.	Derived from EPP trajectory data
I_{TX}	ToD or xOVER bias	-	A bias term for the *ToD* and *xOVER* points. $I_{TX} := [i = i_{TOD}] = 1, [i = i_{xOVER}] = 1\ otherwise\ 0$ for the i^{th} point in the EPP trajectory.	EPP trajectory
I_{TOD}	ToD bias	-	A bias term for the *ToD* point. $I_{TOD} := [i = i_{TOD}] = 1, otherwise\ 0$ for the i^{th} point in the EPP trajectory.	EPP trajectory
I_{XVR}	xOVER bias	-	A bias term for the *xOVER* point. $I_{XVR} := [i = i_{xOVER}] = 1, otherwise\ 0$ for the i^{th} point in the EPP trajectory.	EPP trajectory
I_{BTX}	between ToD and xOVER bias	-	A bias term for the points between the *ToD* and *xOVER* points. $I_{BTX} := [i > i_{TOD}\ \&\ i < i_{xOVER}] = 1, otherwise\ 0$ for the i^{th} point in the EPP trajectory.	EPP trajectory
I_{SH}	short horizon bias	-	A bias term for the points within a short time horizon. $I_{SH} := [t_h < 1000] = 1, otherwise\ 0$	Derived from EPP trajectory data
I_{MH}	medium horizon bias	-	A bias term for the points within a medium time horizon. $I_{MH} := [t_h \geq 1000\ \&\ t_h < 4000] = 1, otherwise\ 0$	Derived from EPP trajectory data
I_{LH}	large horizon bias	-	A bias term for the points within a long time horizon. $I_{LH} := [t_h i > 4000] = 1, otherwise\ 0$	Derived from EPP trajectory data
I_{AT}	AT altitude bias	-	A bias term for the points in the EPP trajectory with an "AT" altitude constraint. $I_{AT} \in \{0,1\}$	Derived from EPP trajectory data
I_{PREALT}	pre AT-altitude bias	-	A bias term for the points in the EPP trajectory prior to the first "AT" altitude constrained point. $I_{PREALT} \in \{0,1\}$	Derived from EPP trajectory data
I_{PRESPD}	pre speed constraint bias	-	A bias term for the points in the EPP trajectory prior to the first speed constrained point. $I_{PRESPD} \in \{0,1\}$	Derived from EPP trajectory data

The EPP cross-track, vertical, and time errors of the previous section showed significant dependencies on the wind forecast error. Although the qualitative analysis was done with respect to wind magnitude forecast error and wind direction forecast error, separately, the EPP error dependencies are more likely related to the along-track wind forecast error. Both the wind magnitude error and direction error can be converted to a headwind error at the EPP points. This headwind error regressor, E_{HW}, is defined as the difference between the true headwind and the predicted headwind at a point. For the measured data, the track into a waypoint is used as the direction for the true and predicted headwind computation. The headwind error regressor can be computed from the analysis data, however, in model implementation, this parameter would have to be estimated using external data not available in the EPP trajectory.

The remaining independent variables are a set of biases intended to capture the error dependencies on specific types of EPP points, such as points that are part of the descent phase of flight, or points that are part of the cruise phase of flight. The descent point bias, I_{DES}, isolates the points after the top-of-descent, whereas, the cruise point bias, I_{CRU}, isolates the points up-to and including the top-of descent point. The bias term, I_{TX}, captures dependencies common to both the ToD and the xOVER points while bias terms, I_{TOD} and I_{XVR}, capture individual dependencies of these two points. Also related is the I_{BTX} bias, which captured dependencies from points that lie between these same two points. The bias terms, I_{SH}, I_{MH} , and I_{LH}, help separate the time horizon into three regions that could help capture wind blending dependencies. The final three bias terms, I_{AT}, I_{PREALT}, and I_{PRESPD}, capture the dependencies of points with and without altitude and/or speed constraints, focused mainly on the points just prior to one of these constraints. All of these bias terms can be derived from the EPP trajectory data.

In addition to the explanatory variables already mentioned, a few combinations of these variables were also used in the model identification. Specifically, the model identification also included: $I_{SH} * t_h$, $I_{MH} * t_h$, $I_{LH} * t_h$, $I_{DES} * t_h$, $I_{CRU} * t_h$, $I_{SH} * E_{HW}$, $I_{MH} * E_{HW}$, $I_{LH} * E_{HW}$, $I_{DES} * E_{HW}$, $I_{CRU} * E_{HW}$, $I_{TX} * E_{HW}$, $I_{DES} * (1 - I_{AT})$, $I_{DES} * I_{PREALT}$, $I_{DES} * I_{PRESPD}$, $E_{HW} * t_h$, and $I_{LH} * E_{HW} * t_h$. In total, 39 explanatory regressors were used in model identification. The same set of 39 regressors were used in the cross-track, vertical, and temporal error model identifications.

The EPP error models were identified using a subset of scenario runs. The baseline runs with no wind [RL1-RL3, RT1, WC0, No RTA] and with perfect wind [RL1-RL3, RT1, WC1, No RTA] were both included in the identification data set to capture dependencies in the absence of wind error. Two wind forecast error conditions ([RL1-RL3, RT1, WC2, no RTA] and [RL1-RL3, RT1, WC5, No RTA]) were included in the identification data set to capture the dependencies on the wind forecast error. The sparse route type and the RTA conditions were not used in the model identification.

The EPP error models were validated against a single wind forecast error condition that was not used in the model identification. The error models were validated against the 135-degree wind forecast direction error condition [RL1-RL3, RT1, WC7, No RTA] to evaluate the model predictive capabilities.

5.3 Cross-Track Error Model

The identified EPP cross-track error model includes five explanatory variables and a bias term. The cross-track error model takes the form seen in equation (7). Table 7 lists the model parameters estimates and their standard errors. This EPP cross-track error model has an R-squared value of 0.8500.

The cross-track error model aligns well with the qualitative analysis of section 4. The cross-track errors are predominantly a function of the turn radius, the track angle change, and the headwind error.

The cross-track error model fit can be seen in Figure 111 and Figure 112. Figure 111 shows the cross-track errors of the identified model against those of the model identification data set. Figure 112 shows the same data versus the time horizon parameter. Overall, the model shows a good fit to the identification data.

The validation of the cross-track error model can be seen in Figure 117 and Figure 118. These validation figures indicate a reasonable model, although, there are some indications that there may be other explanatory variables that have yet to be identified.

$$\hat{E}_{xtrk,i} = \hat{\beta}_{0,xtrk} + \hat{\beta}_{1,xtrk} * I_{R>0,i} + \hat{\beta}_{2,xtrk} * R_i + \hat{\beta}_{3,xtrk} * R_i^2 + \hat{\beta}_{4,xtrk} * \theta_i + \hat{\beta}_{5,xtrk} * E_{HW,i} \qquad \textbf{(7)}$$

Table 7. EPP cross-track error model parameter estimates.

Parameter	Estimate	Standard Error
$\hat{\beta}_{0,xtrk}$	5.8159	-
$\hat{\beta}_{1,xtrk}$	-17.4052	0.4513
$\hat{\beta}_{2,xtrk}$	0.0319	0.0147
$\hat{\beta}_{3,xtrk}$	0.0126	0.0001
$\hat{\beta}_{4,xtrk}$	1.2437	0.0134
$\hat{\beta}_{5,xtrk}$	0.5203	0.0104

5.4 Vertical Error Model

The identified EPP vertical error model includes eight explanatory variables and a bias term. The vertical error model takes the form seen in equation (8). Table 8 lists the model parameter estimates and their standard errors. This EPP vertical error model has an R-squared value of 0.5541.

$$\hat{E}_{vert,i} = \widehat{\beta}_{0,vert} + \widehat{\beta}_{1,vert} * E_{HW,i} + \widehat{\beta}_{2,vert} * I_{DES} + \widehat{\beta}_{3,vert} * I_{TX} + \widehat{\beta}_{4,vert} * I_{TOD} + \widehat{\beta}_{5,vert} * I_{BTX} + \widehat{\beta}_{6,vert} * I_{CRU} * E_{HW} + \widehat{\beta}_{7,vert} * I_{TX} * E_{HW} + \widehat{\beta}_{8,vert} * E_{HW} * t_h \quad \textbf{(8)}$$

Table 8. EPP vertical error model parameter estimates.

Parameter	Estimate	Standard Error
$\hat{\beta}_{0,vert}$	3.2635	-
$\hat{\beta}_{1,vert}$	9.9304	0.2526
$\hat{\beta}_{2,vert}$	-17.0391	1.5873
$\hat{\beta}_{3,vert}$	93.9648	3.0644
$\hat{\beta}_{4,vert}$	-296.2090	3.8219
$\hat{\beta}_{5,vert}$	172.8946	3.1350
$\hat{\beta}_{6,vert}$	-19.3875	0.2517
$\hat{\beta}_{7,vert}$	13.9122	0.3106
$\hat{\beta}_{8,vert}$	0.0013	0.000031

The vertical error model has two dependencies on the headwind error variable. The first is a direct relationship to the headwind error. The second is a combinatory regressor with the headwind error multiplied by the time horizon parameter, which accounts for the wind blending effects of the FMS. The remaining terms in the vertical error model capture the vertical error differences of different types of points in the EPP message related to the different phases of flight.

The vertical error model fit can be seen in Figure 113 and Figure 114. Figure 113 shows the vertical errors of the identified model against those of the model identification data set. Figure 114 shows the same data versus the time horizon parameter. The model does seem to indicate that some explanatory regressors may still be missing that could help improve the model fit.

The validation of the vertical error model can be seen in Figure 119 and Figure 120. These validation figures indicate a relatively weak model, where some model estimates could still be more than 1000 feet in error when compared to the actual error value. This is especially true for medium and long time horizons.

5.5 Time Error Model

The identified EPP temporal error model includes six explanatory variables and a bias term. The temporal error model takes the form seen in equation (9). Table 9 lists the model parameter estimates and their standard errors. This EPP time error model has an R-squared value of 0.8074.

$$\hat{E}_{time,i} = \hat{\beta}_{0,time} + \hat{\beta}_{1,time} * t_h + \hat{\beta}_{2,time} * t_h^2 + \hat{\beta}_{3,time} * E_{HW} + \hat{\beta}_{4,time} * I_{PREALT} + \hat{\beta}_{5,time} * I_{MH} * E_{HW} + \hat{\beta}_{6,time} * E_{HW} * t_h \quad \textbf{(9)}$$

Table 9. EPP temporal error model parameter estimates.

Parameter	Estimate	Standard Error
$\hat{\beta}_{0,time}$	16.1021	-
$\hat{\beta}_{1,time}$	0.0014	0.00017
$\hat{\beta}_{2,time}$	0.00000031	0.000000013
$\hat{\beta}_{3,time}$	-2.5949	0.0992
$\hat{\beta}_{4,time}$	-20.4580	0.3758
$\hat{\beta}_{5,time}$	0.7012	0.0840
$\hat{\beta}_{6,time}$	0.0017	0.000013

The cross-track error model indicates that the time horizon and headwind error variables contribute a significant portion to the time error. The time horizon and the square of the time horizon are both parameters in the model. The headwind error appears in three other terms of the model, including a combinatory term that includes the time horizon. This combinatory terms accounts for the integrated nature of the time error, where longer time horizons with a headwind error contribute to larger time errors. The pre- AT-altitude bias term, I_{PREALT}, indicates the errors are likely to be larger prior to entering the constrained portion of a route.

The temporal error model fit can be seen in Figure 115 and Figure 116. Figure 115 shows the time errors of the identified model against those of the model identification data set. Figure 116 shows the same data versus the time horizon parameter. Overall, the model shows a reasonable fit to the identification data, with some points showing over-estimation of time errors and others showing under-estimation of the time errors.

The validation of the temporal error model can be seen in Figure 121 and Figure 122. These validation figures also indicate a reasonable model, with a slight under-estimation of time errors for the validation scenario.

6 Conclusion

In this work, a set of scenarios were run in a high-fidelity aircraft and FMS simulation to perform an initial characterization of EPP trajectory errors. Linear regression was also used to identify a set of EPP error models. Because this analysis was performed in a simulation environment, the results are highly dependent on the assumptions and algorithms within that environment and may not be directly applicable to the errors that may be present in the real system and with an operational FMS. In fact, there are many different types of FMS capabilities in the system today, each of which has different trajectory prediction capabilities and accuracies. A field investigation would be required to understand EPP errors under real conditions, thus qualifying this analysis as preliminary. Nonetheless, this analysis does point to some important characteristics of EPP trajectory errors.

The EPP errors were characterized under the following set of conditions: no wind, perfect wind, full versus sparse routes, with wind forecast magnitude error, with wind forecast direction error, and under RTA operations. The following is a set of observations that were gathered from the conditions simulated:

- In the presence of no wind, when comparing EPP and FMS trajectory errors:
  - EPP cross-track errors can be as much as 100-200 feet larger than FMS errors, especially for large radius turns of en route waypoints, primarily due to MOT estimation
  - EPP vertical errors differ from FMS errors only by the EPP altitude resolution of 10 feet
  - EPP time errors differ from FMS errors only by the EPP time resolution of 1 second
- In the absence of wind forecast error, EPP trajectory error magnitudes are:
  - Less than 50 feet cross-track error for most points; on the order of 200 feet for large turn radius turns
  - Less than 10 feet vertical error for most points; on the order of 200 feet for the top-of-descent point
  - Within 30 seconds time error inside two hours of time horizon
- In the presence of wind forecast error, EPP trajectory errors are:
  - Related to the along-track wind forecast error
    - Groundspeed affects the predicted turn radius
    - Groundspeed affects the location of the ToD point and, thus, the descent vertical path
    - Groundspeed affects the ETA at points
  - Reduced within the wind-blending region of the FMS
- In the presence of RTA operations, EPP errors can be larger than without RTA, especially at long time horizons, due to the changing cost index and changing speed profile
- Depending on the conditions, FMS wind blending can have a positive or a negative impact on the EPP trajectory errors
- EPP trajectory errors inherit the FMS's trajectory prediction errors but, in general, are larger than the FMS trajectory errors
- EPP vertical errors are more pronounced for points in the descent profile prior to an altitude constrained point

Based on the findings of this analysis, some recommendations are made regarding the ATOS simulation capability and its FMS and EPP trajectory generation functionality:

- The FMS should generate trajectory updates after TOD, even if the vertical path does not change, in order to provide updated ETA information for EPP trajectories
- The FMS should generate the EPP message based on the provisional route computation when an RTA operation is active

References

[1] NextGen Joint Planning and Development Office, "Concept of Operations for the Next Generation Air Transportation System, Version 3.2," JPDO, Washington, D.C., 2011.

[2] NextGen Joint Planning and Development Office, "JPDO Trajectory-Based Operations (TBO) Study Team Report," JPDO, Washington, D.C., 2011.

[3] RTCA, Inc., "DO-350A; Safety and Performance Requirements Standard for Baseline 2 ATS Data Communications," RTCA, Inc., Washington, 2016.

[4] Directorate-General for Energy and Transport, *Data Link Services (DLS) Mandate,* Brussel: European Commission, 2005.

[5] R. Šošovička, P. Veselý and J. Svoboda, "Estimation of Aircraft Performance Parameters from ADS-C EPP Data," in *2015 Integrated Communication, Navigation and Surveillance Conference (ICNS)*, Herndon, 2015.

[6] J. Bronsvoort, G. McDonald, M. Paglione, C. M. Young, A. Fabian, J. Boucquey and C. Garcia Avello, "Demonstration of Improved Trajectory Prediction Using Future Air Navigation Systems," *Air Traffic Control Quarterly,* vol. 21, no. 4, pp. 355-381, 2013.

[7] J. Bronsvoort, G. McDonald, J. Hochwarth and E. Gallo, "Air to Ground Trajectory Synchronisation through Extended Predicted Profile (EPP), A Pilot Study," in *14th AIAA Aviation Technology, Integration, and Operations Conference*, Atlanta, 2014.

[8] E. Haugg, M. Poppe, S. Herr, T. Pütz, J. Svoboda and R. Šošovicka, "The Usability of ADS-C EPP Data for Air Traffic Control Applications," in *2015 IEEE/AIAA 34th Digital Avionics Systems Conference* , Prague, 2015.

[9] J. Bronsvoort, G. McDonald, M. Paglione, C. M. Young, J. Boucquey, J. K. Hochwarth and E. Gallo, "Real-Time Trajectory Predictor Calibration through Extended Projected Profile Down-Link," in *Eleventh USA/Europe Air Traffic Management Research and Development Seminar (ATM2015)*, Lisbon, 2015.

[10] J. Bronsvoort, G. McDonald, S. Torres, J. Hochwarth, J. Boucquey, M. Paglione, C. Young and M. Vilaplana, "Use of the Extended Projected Profile (EPP) in Trajectory Management," in *16th AIAA Aviation Technology, Integration, and Operations Conference*, Washington, D.C., 2016.

[11] M. Paglione, I. Bayraktutar, G. McDonald and J. Bronsvoort, "Lateral Intent Error's Impact on Aircraft Prediction," *Air Traffic Control Quarterly,* vol. 18, no. 1, pp. 29-62, 2010.

[12] S. Mondoloni and I. Bayraktutar, "Impact Of Factors, Conditions, and Metrics On Trajectory Prediction Accuracy," in *Sixth USA/Europe Air Traffic Management Research and Development Seminar (ATM2005)*, Baltimore, 2005.

[13] K. S. Linsday, "Results of a URET Operational Utility Experiment," MITRE Center for Advanced Aviation System Development, McLean, 2000.

[14] R. A. Vivona, K. T. Cate and S. M. Green, "Comparison of Aircraft Trajectory Predictor Capabilities and Impacts on Automation Interoperability," in *11th AIAA Aviation Technology, Integration, and Operations (ATIO) Conference*, Virginia Beach, 2011.

[15] J. Bronsvoort, G. McDonald, M. Paglione, C. Garcia-Avello, I. Bayraktutar and C. M. Young, "Impact of Missing Longitudinal Aircraft Intent on Descent Trajectory Prediction," in *30th Digital Avionics Systems Conference*, Seattle, 2011.

[16] C. Querejeta, M. A. Vilaplana, E. Gallo, J. Lopez-Leones and F. A. Navarro, "Predicting Aircraft Trajectory". European Patent EP2040137B1, 16 May 2012.

[17] J. López-Leonés, M. A. Vilaplana, E. Gallo, F. A. Navarro and C. Querejeta, "The Aircraft Intent Description Language: A key enabler for Air-Ground synchronization in Trajectory-Based Operations," in *26th Digital Avionics Systems Conference*, Dallas, 2007.

[18] J. Klooster, S. Torres, D. Earman, M. Castillo-Effen, R. Subbu, L. Kammer, D. Chan and T. Tomlinson, "Trajectory Synchronization and Negotiation in Trajectory Based Operations," in *29th Digital Avionics Systems Conference*, Salt Lake City, 2010.

[19] M. E. Peters, M. G. Ballin and J. S. Sakosky, "A Multi-Operator Simulation for Investigation of Distributed Air Traffic Management Concepts," in *AIAA Modeling and Simulation Technologies conference and Exhibit, August 5-8*, Monterey, California, 2002.

[20] S. Benjamin, C. Alexander, S. Weygandt, D. Dowell, M. Hu, T. Alcott, T. Smirnova, J. Olson, J. Brown, E. James and J. Kenyon, *Improvements in HRRRv2/RAPv3 for Aug 2016 Implementation at NCEP for More Accurate Warm-Season and Cold-Season NWP*, Salt Lake City: NOAA, 2016.

[21] M. T. Palmer and M. G. Ballin, "A High-Performance Simulated On-Board Avionics Architecture to Support Traffic Operations Research," in *AIAA Modeling and Simulation Technologies Conference*, Austin, 2003.

Appendix A: Figures - No Wind Baseline Scenario

1. *Cross-Track Error*

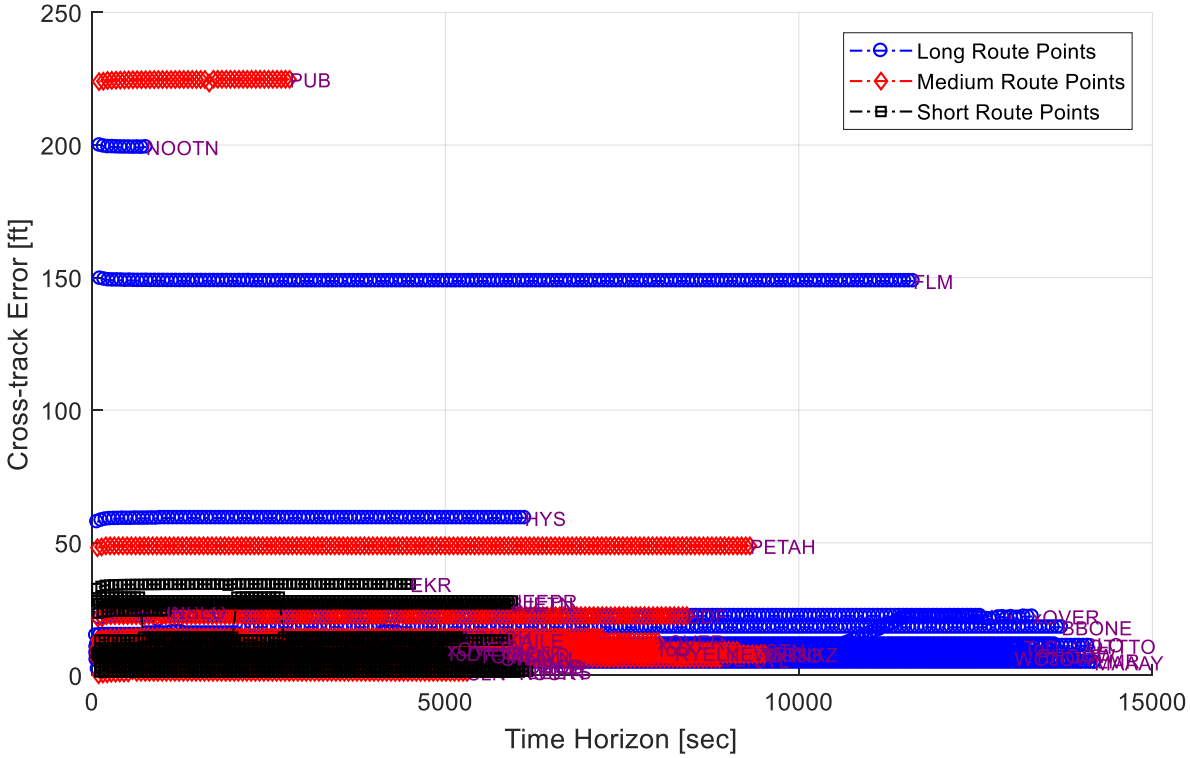

Figure 8. Cross-track error for EPP points as a function of the time horizon [RL1-RL3, RT1, WC0, No RTA].

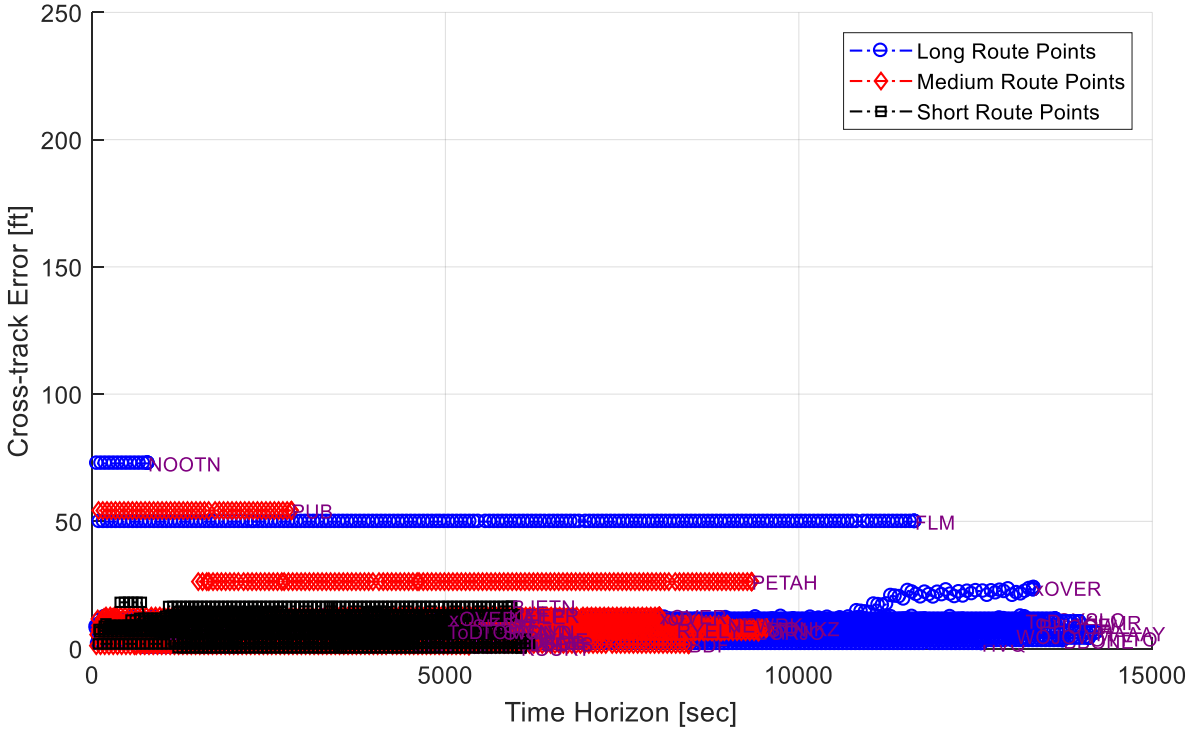

Figure 9. Cross-track error for FMS points as a function of the time horizon [RL1-RL3, RT1, WC0, No RTA].

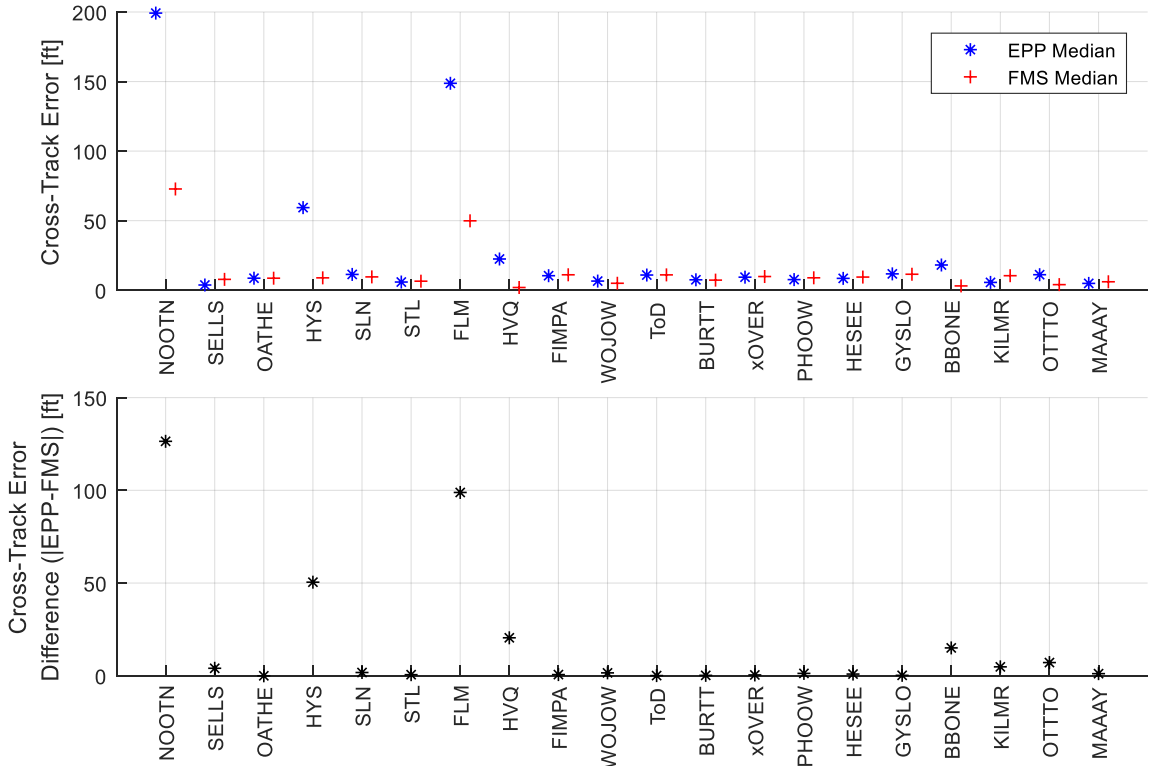

Figure 10. EPP and FMS median cross-track error (top) and error difference (bottom) for the trajectory points of the long route [RL1, RT1, WC0, No RTA].

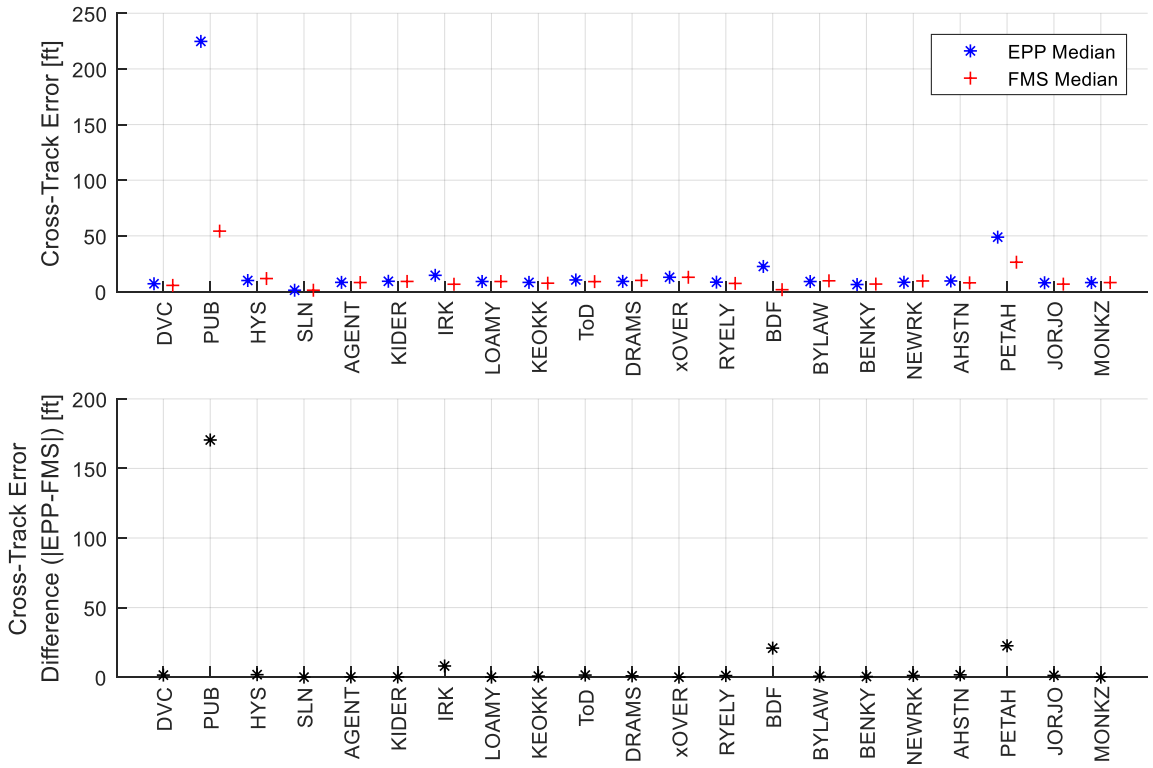

Figure 11. EPP and FMS median cross-track error (top) and error difference (bottom) for the trajectory points of the medium route [RL2, RT1, WC0, No RTA].

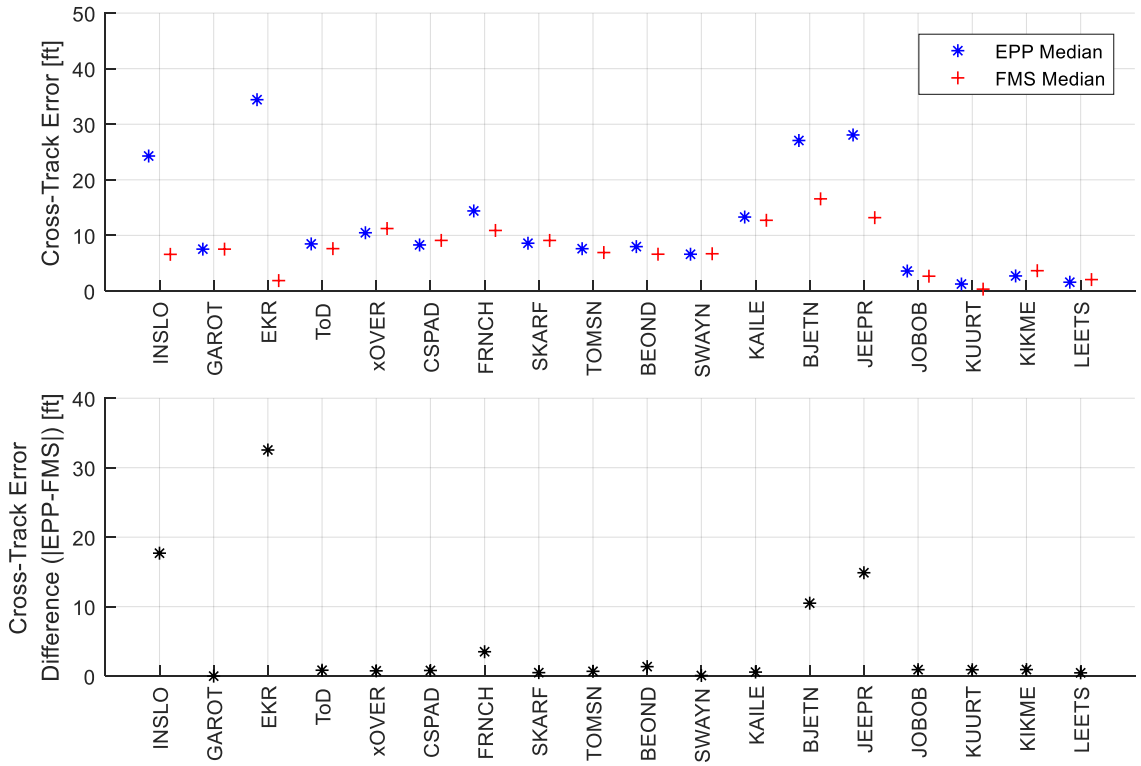

Figure 12. EPP and FMS median cross-track error (top) and error difference (bottom) for the trajectory points of the short route [RL3, RT1, WC0, No RTA].

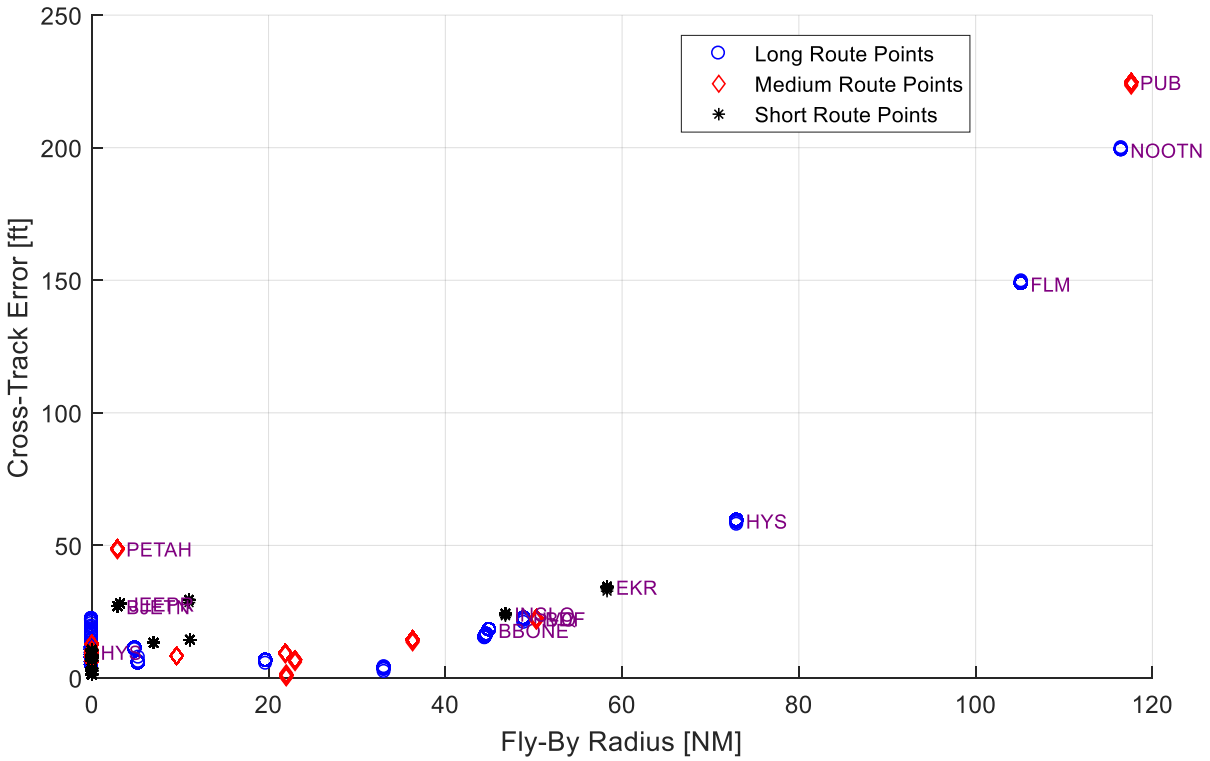

Figure 13. Cross-track error versus fly-by radius for EPP trajectory points [RL1-RL3, RT1, WC0, No RTA].

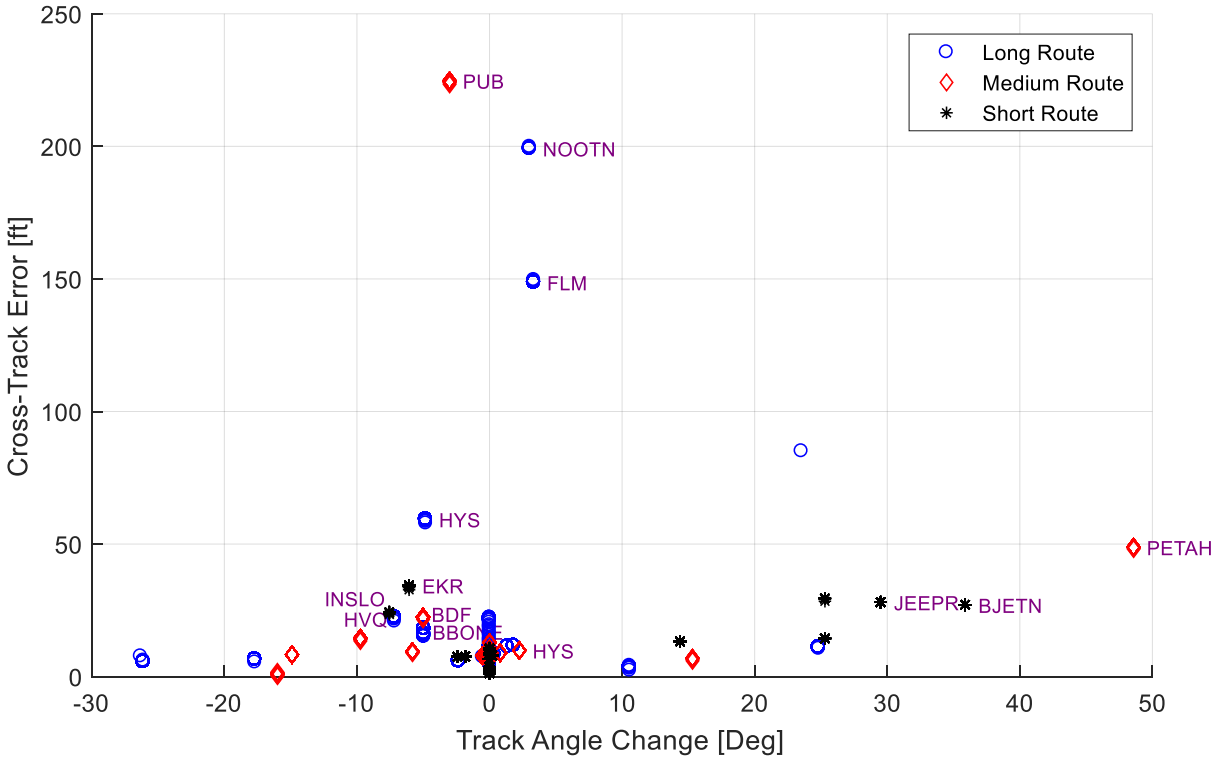

Figure 14. Cross-track error versus track angle change for EPP trajectory points [RL1-RL3, RT1, WC0, No RTA].

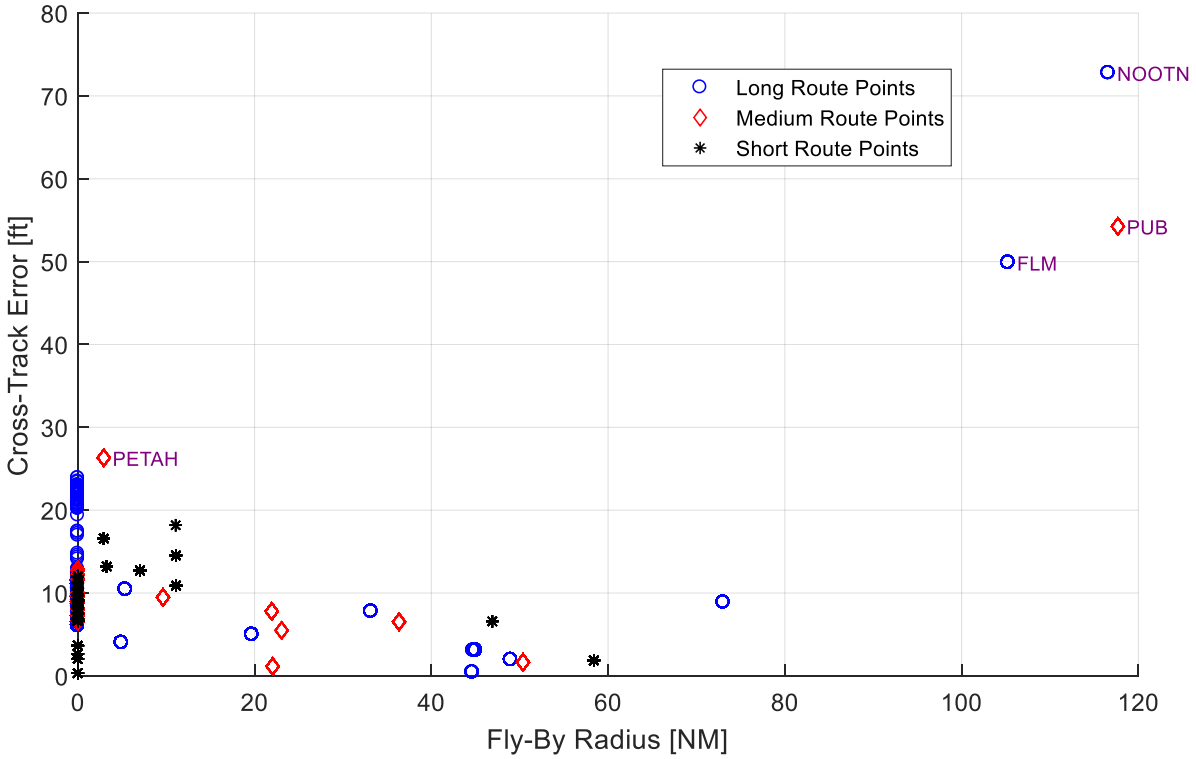

Figure 15. Cross-track error versus fly-by radius for FMS trajectory points [RL1-RL3, RT1, WC0, No RTA].

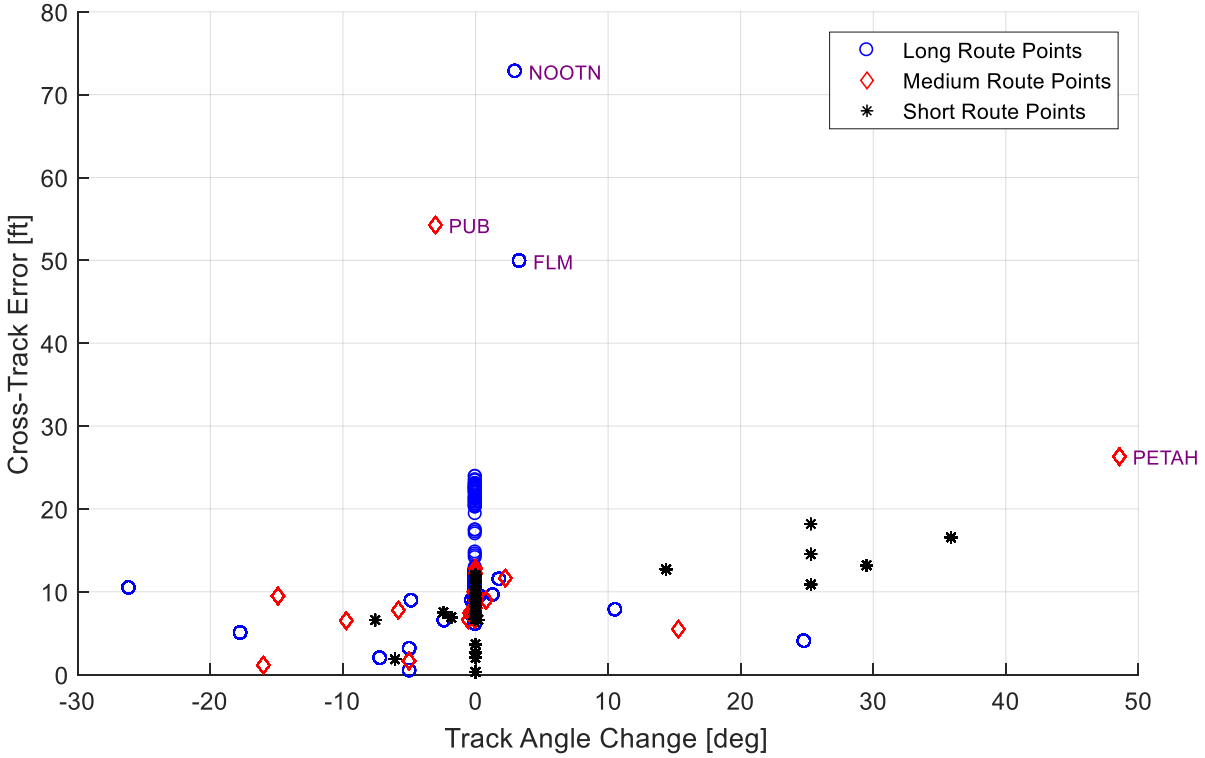

Figure 16. Cross-track error versus track angle change for FMS trajectory points [RL1-RL3, RT1, WC0, No RTA].

2. Vertical Error

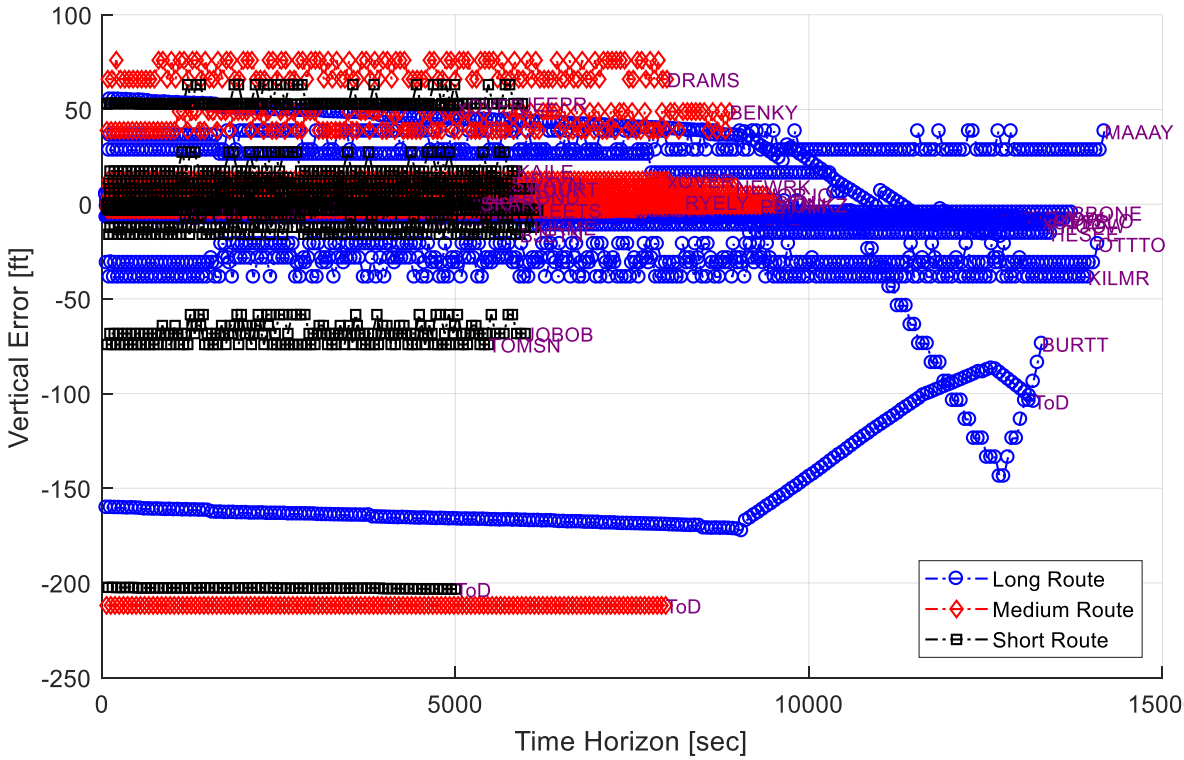

Figure 17. Vertical error for EPP trajectory points as a function of the time horizon [RL1-RL3, RT1, WC0, No RTA].

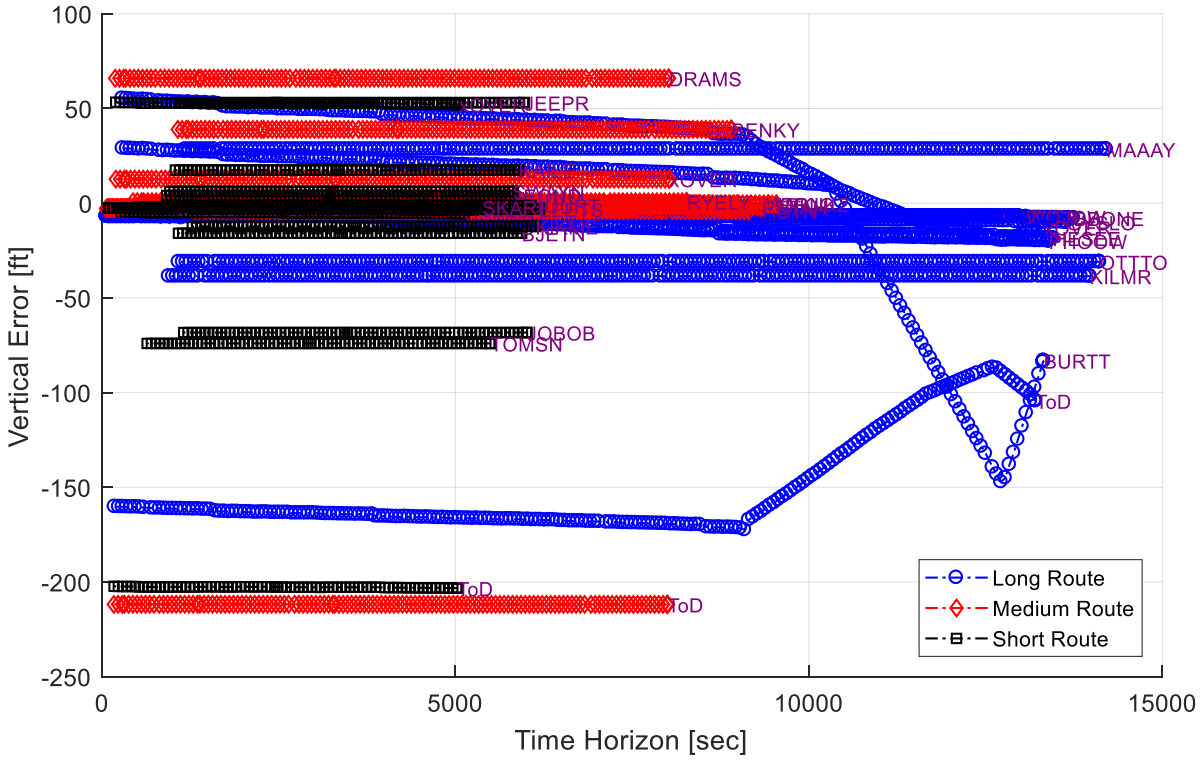

Figure 18. Vertical error for FMS trajectory points as a function of the time horizon [RL1-RL3, RT1, WC0, No RTA].

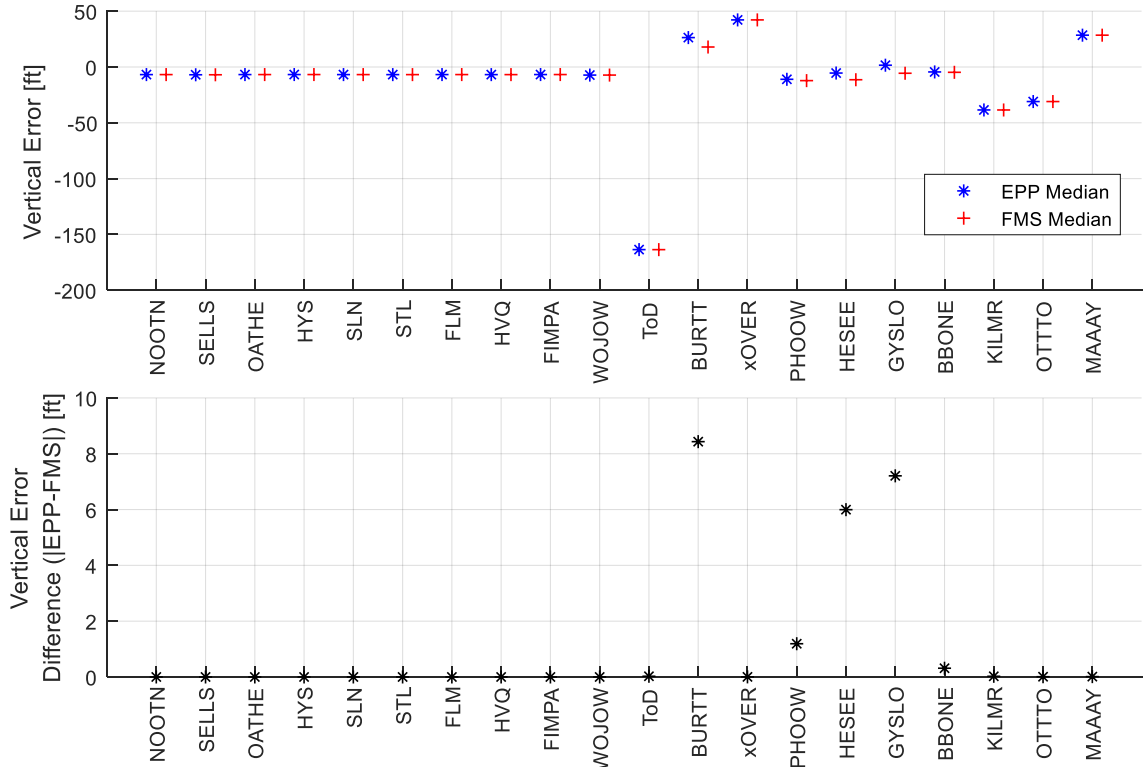

Figure 19. EPP and FMS median vertical error (top) and error difference (bottom) for the trajectory points of the long route [RL1, RT1, WC0, No RTA].

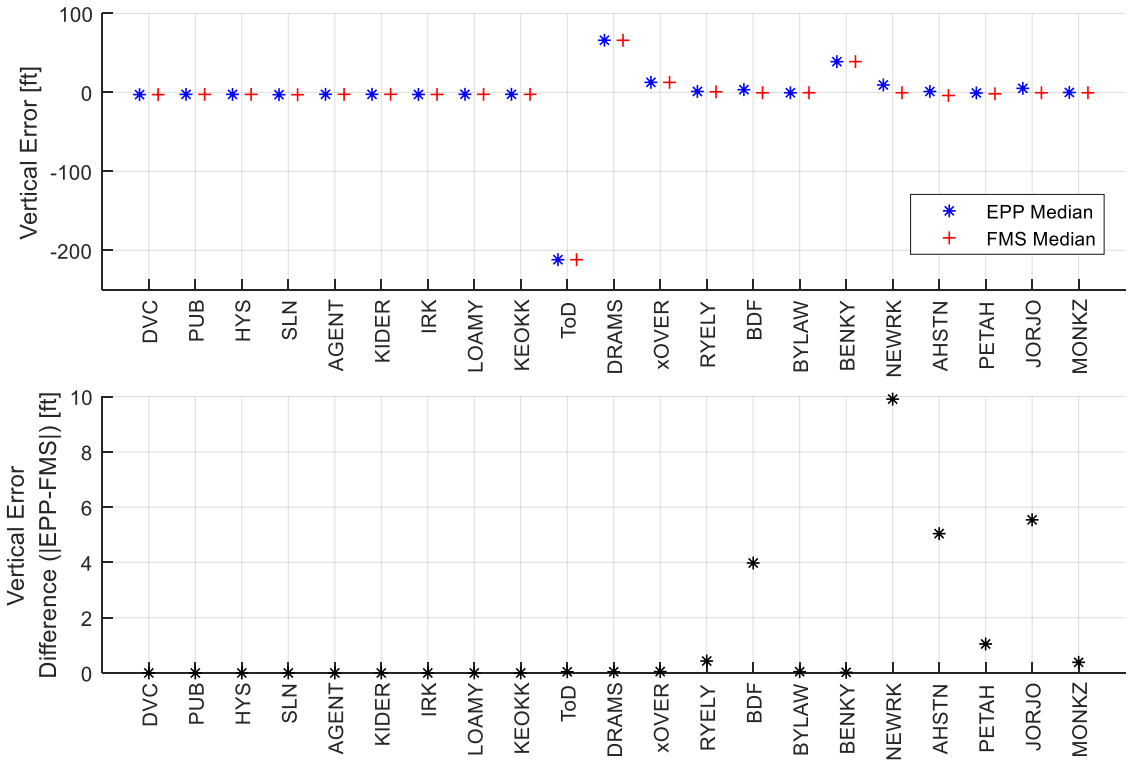

Figure 20. EPP and FMS median vertical error (top) and error difference (bottom) for the trajectory points of the medium route [RL2, RT1, WC0, No RTA].

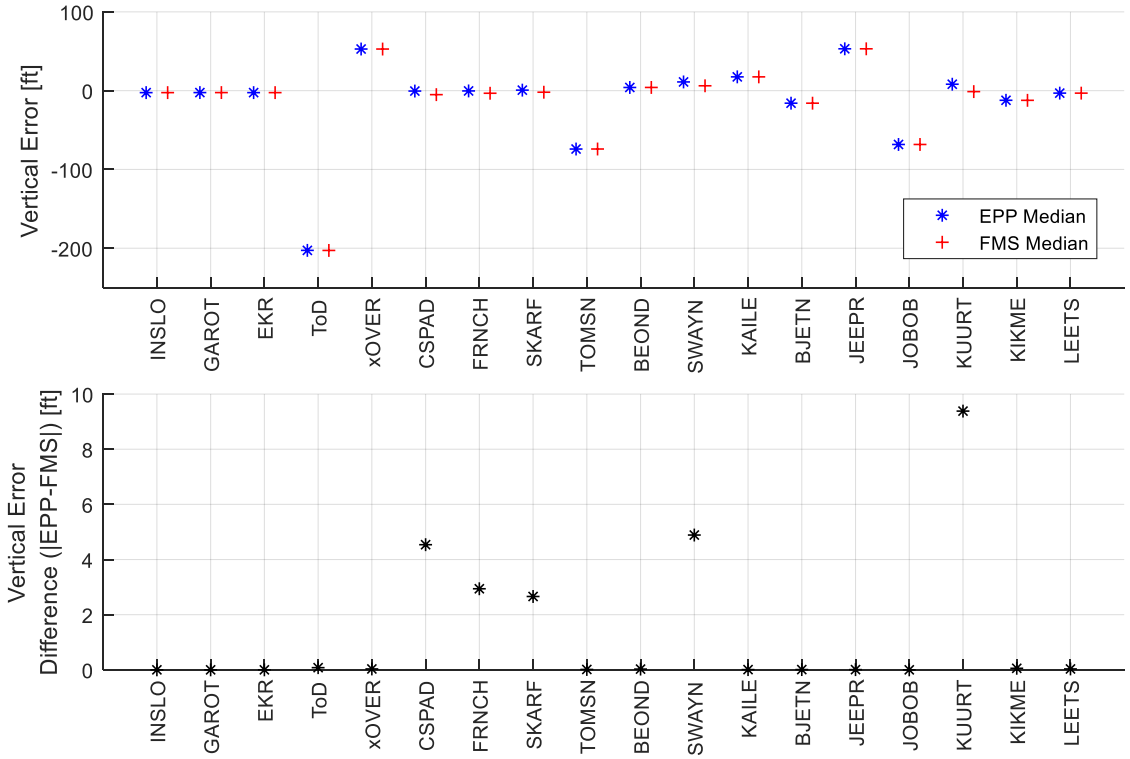

Figure 21. EPP and FMS median vertical error (top) and error difference (bottom) for the trajectory points of the short route [RL3, RT1, WC0, No RTA].

3. *Time Error*

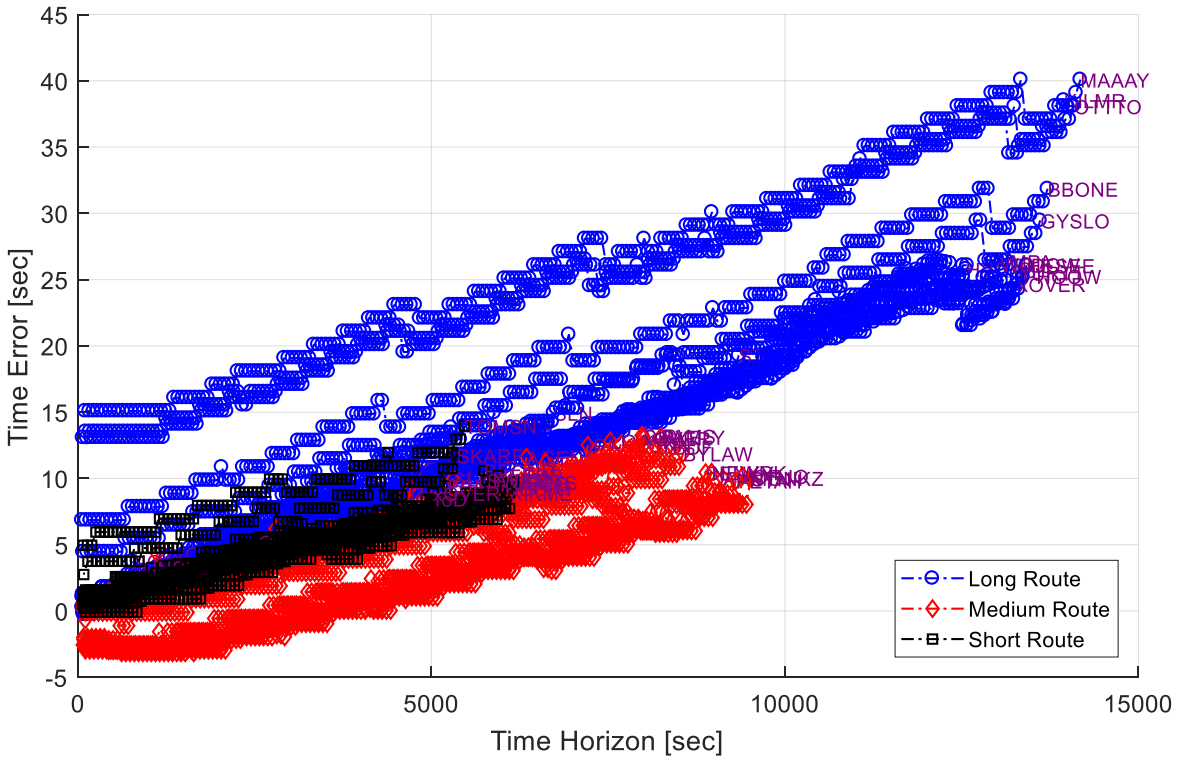

Figure 22. Time error for EPP trajectory points as a function of the time horizon [RL1-RL3, RT1, WC0, No RTA].

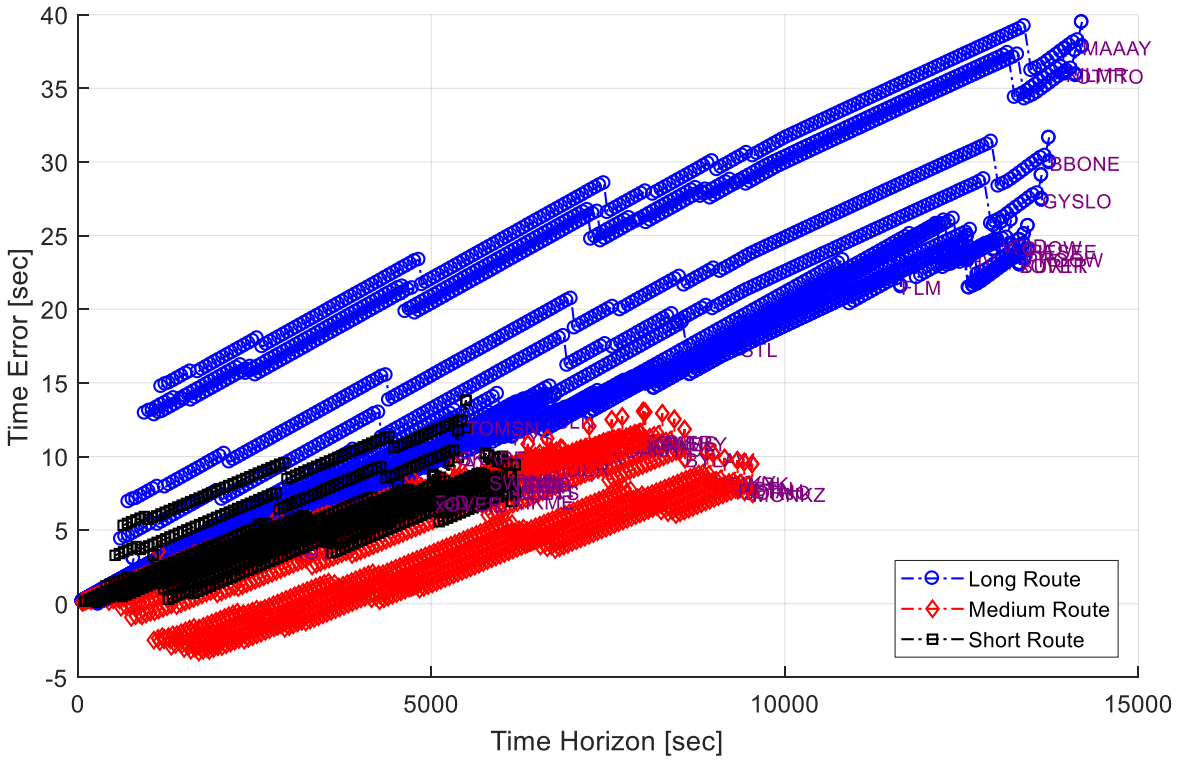

Figure 23. Time error for FMS trajectory points as a function of the time horizon [RL1-RL3, RT1, WC0, No RTA].

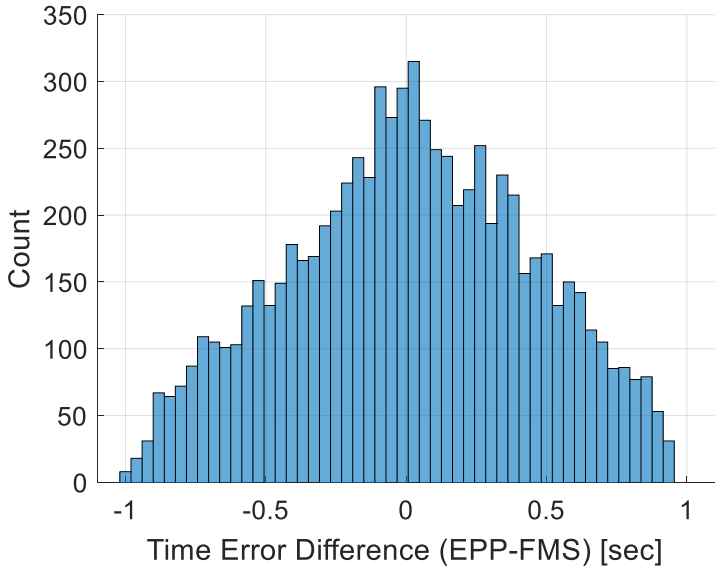

Figure 24. Distribution of the time error difference between EPP and FMS trajectory points [RL1-RL3, RT1, WC0, No RTA].

Appendix B: Figures – No Wind Versus Perfect Wind

1. *Cross-Track Error*

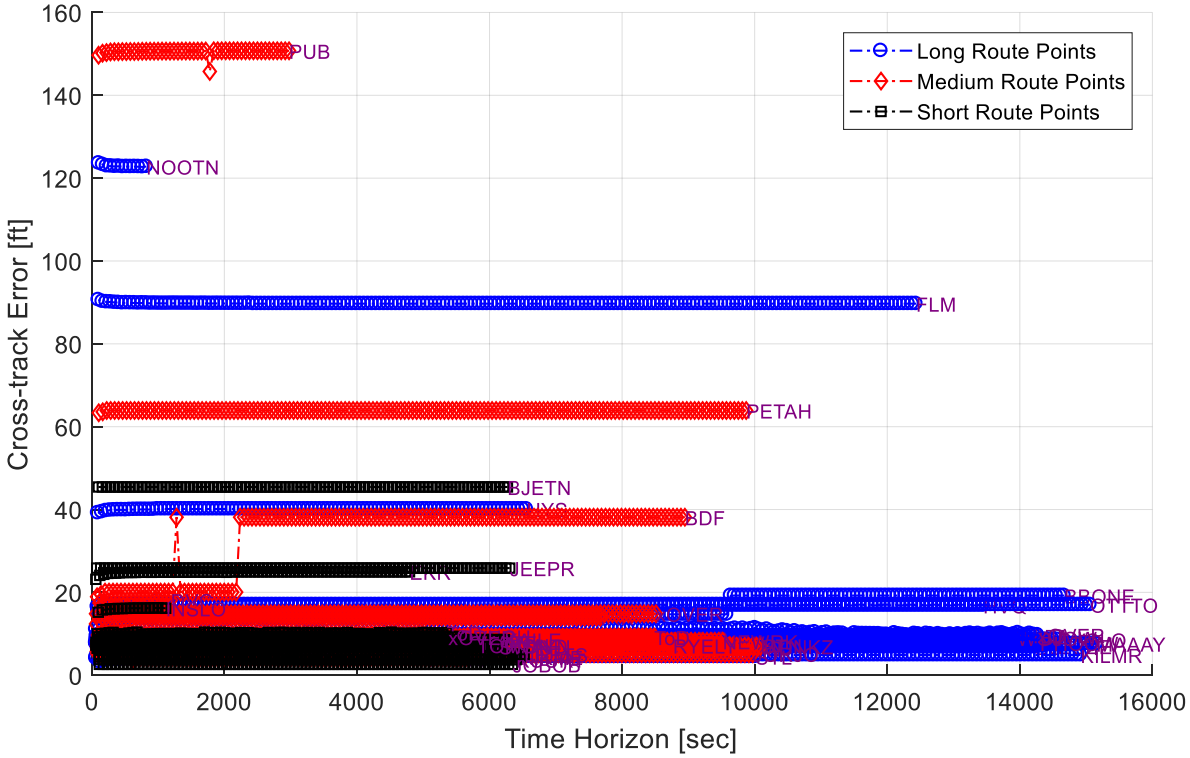

Figure 25. Cross-track error for EPP points as a function of the time horizon [RL1-RL3, RT1, WC1, No RTA].

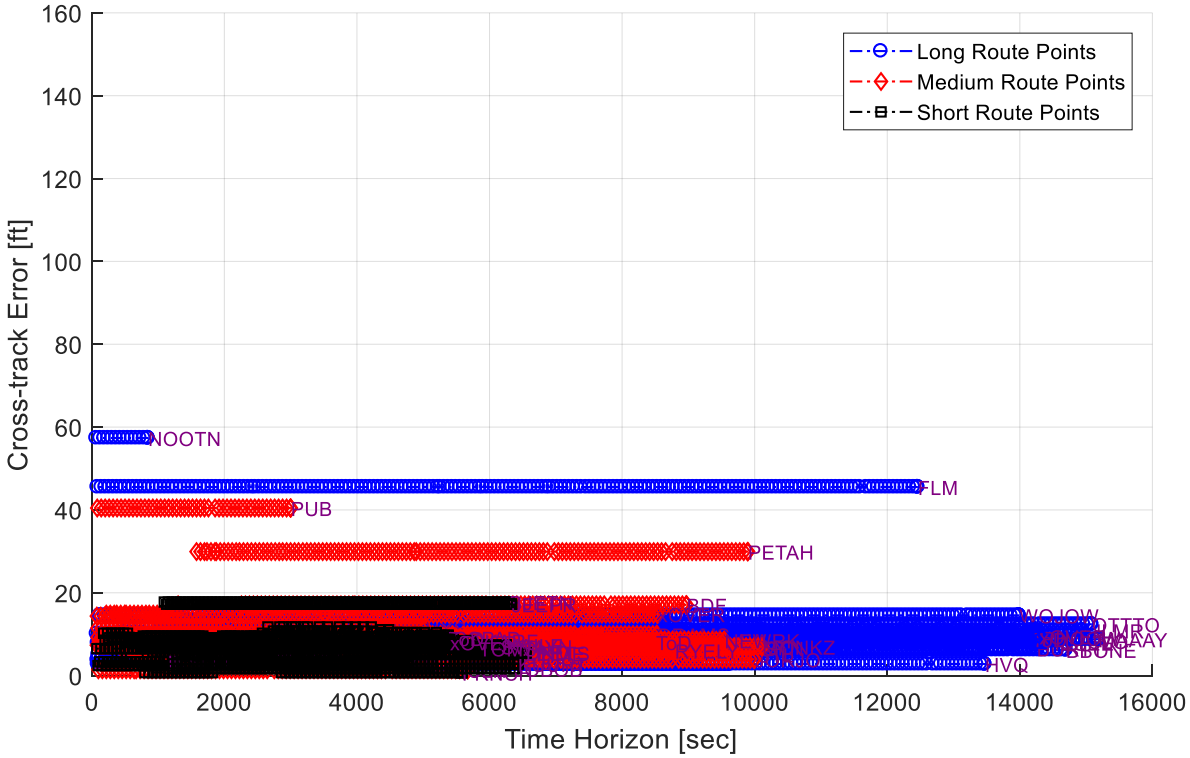

Figure 26. Cross-track error for FMS points as a function of the time horizon [RL1-RL3, RT1, WC1, No RTA].

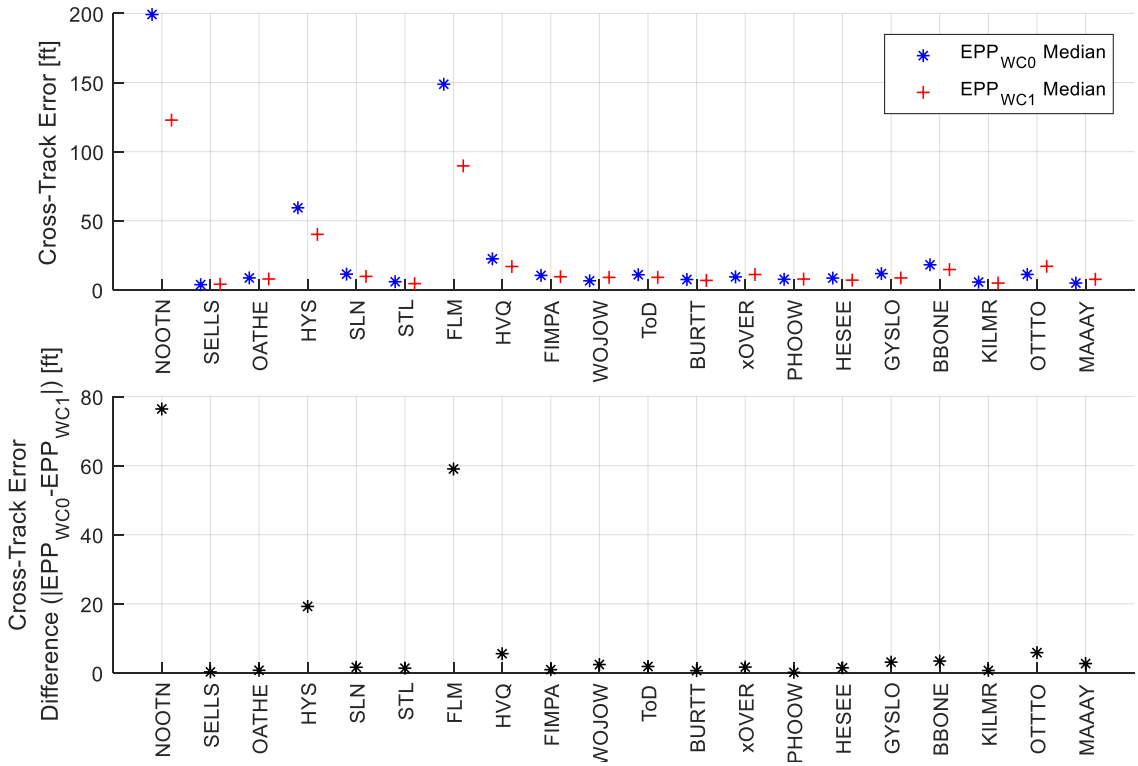

Figure 27. No wind (EPP_{WC0}) and perfect wind (EPP_{WC1}) median cross-track error (top) and error difference (bottom) for the trajectory points of the long route [RL1, RT1, No RTA].

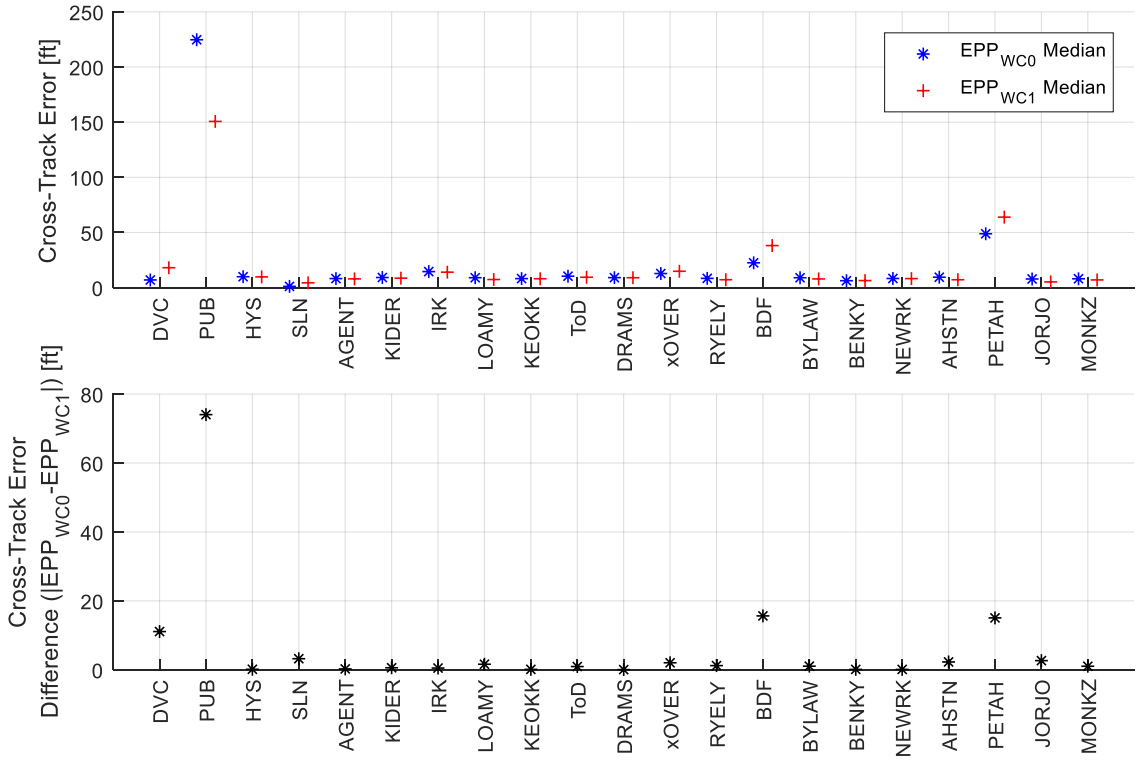

Figure 28. No wind (EPP_{WC0}) and perfect wind (EPP_{WC1}) median cross-track error (top) and error difference (bottom) for the trajectory points of the medium route [RL2, RT1, No RTA].

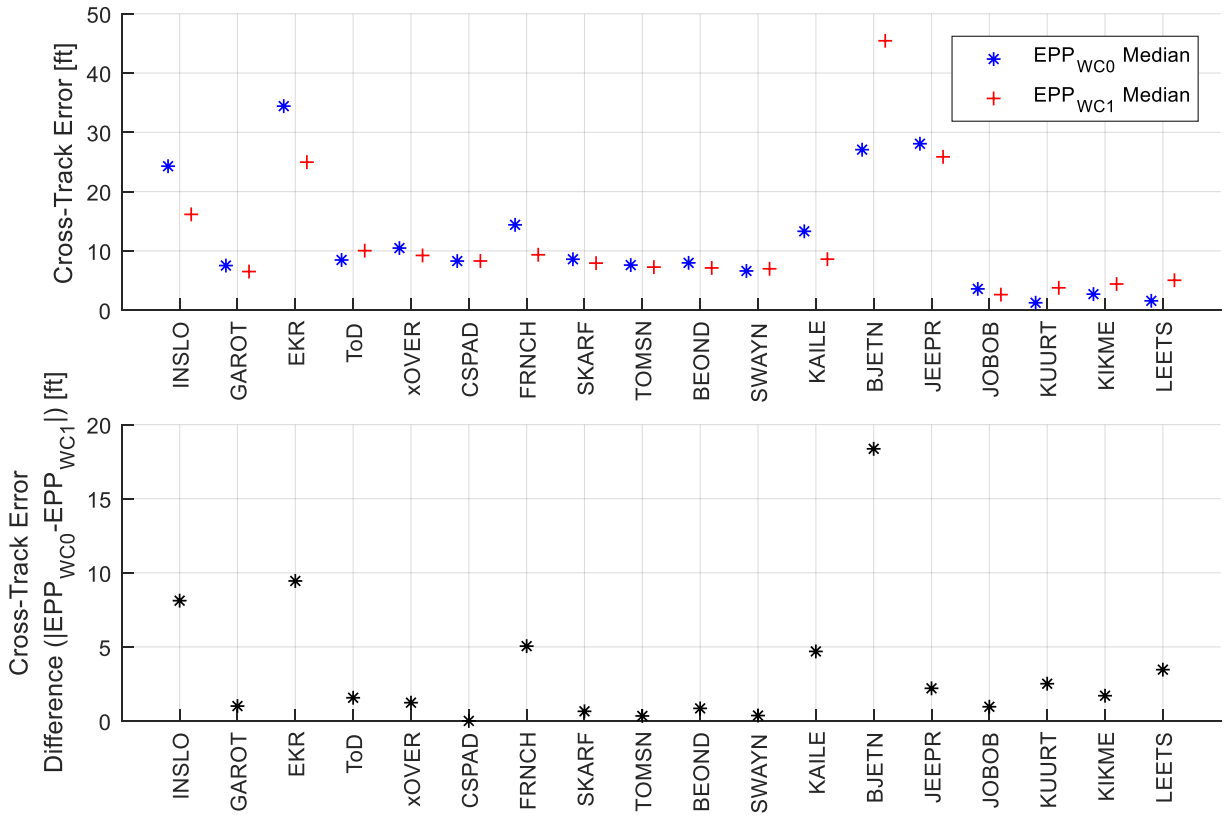

Figure 29. No wind (EPP_{WC0}) and perfect wind (EPP_{WC1}) median cross-track error (top) and error difference (bottom) for the trajectory points of the short route [RL3, RT1, No RTA].

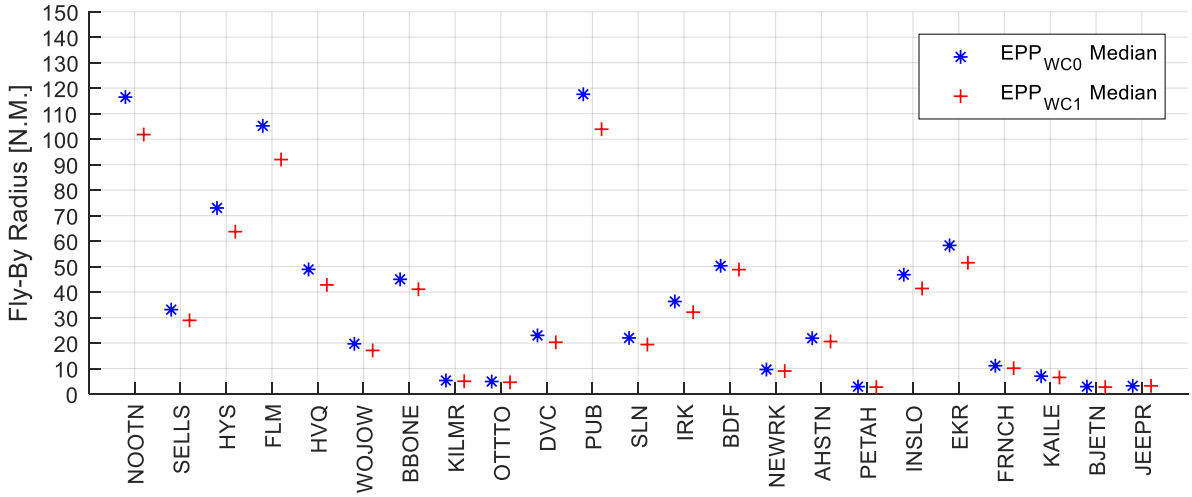

Figure 30. EPP median fly-by radius for no wind scenario (EPP_{WC0}) and perfect wind scenario (EPP_{WC1}) for all trajectory points with non-zero reported radius [RL1-RL3, RT1, No RTA].

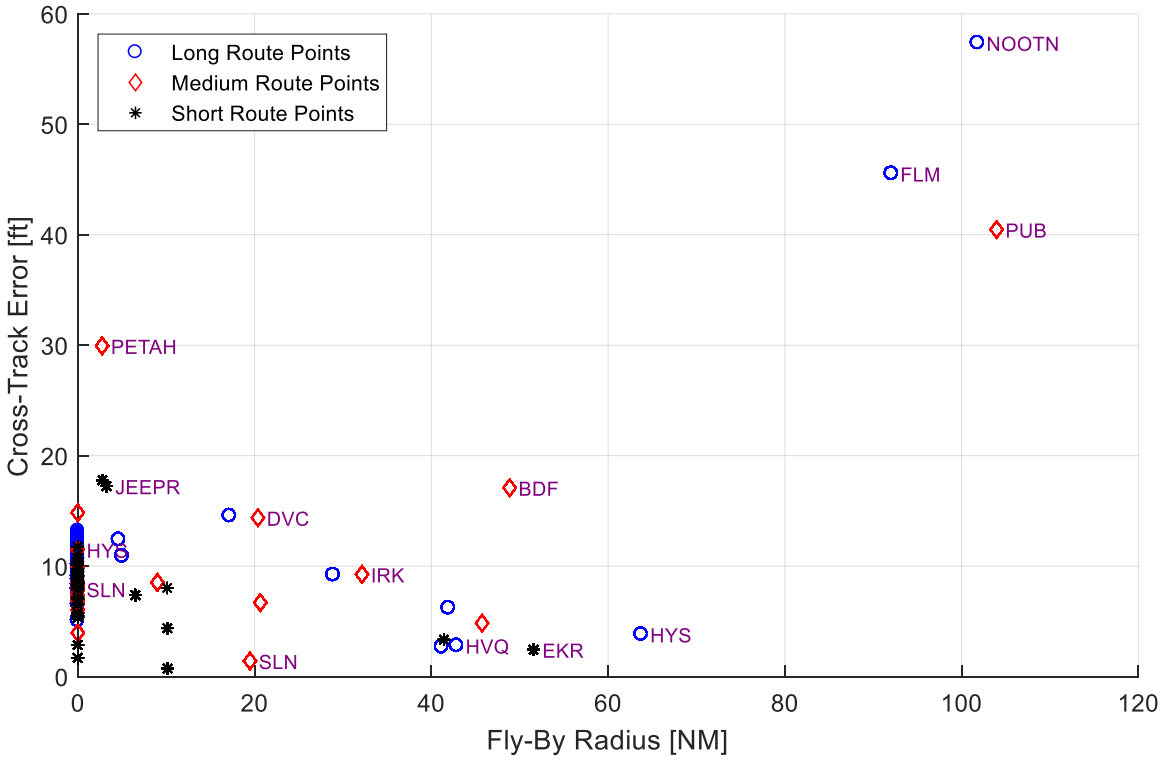

Figure 31. Cross-track error versus fly-by radius for FMS trajectory points [RL1-RL3, RT1, WC1, No RTA].

2. *Vertical Error*

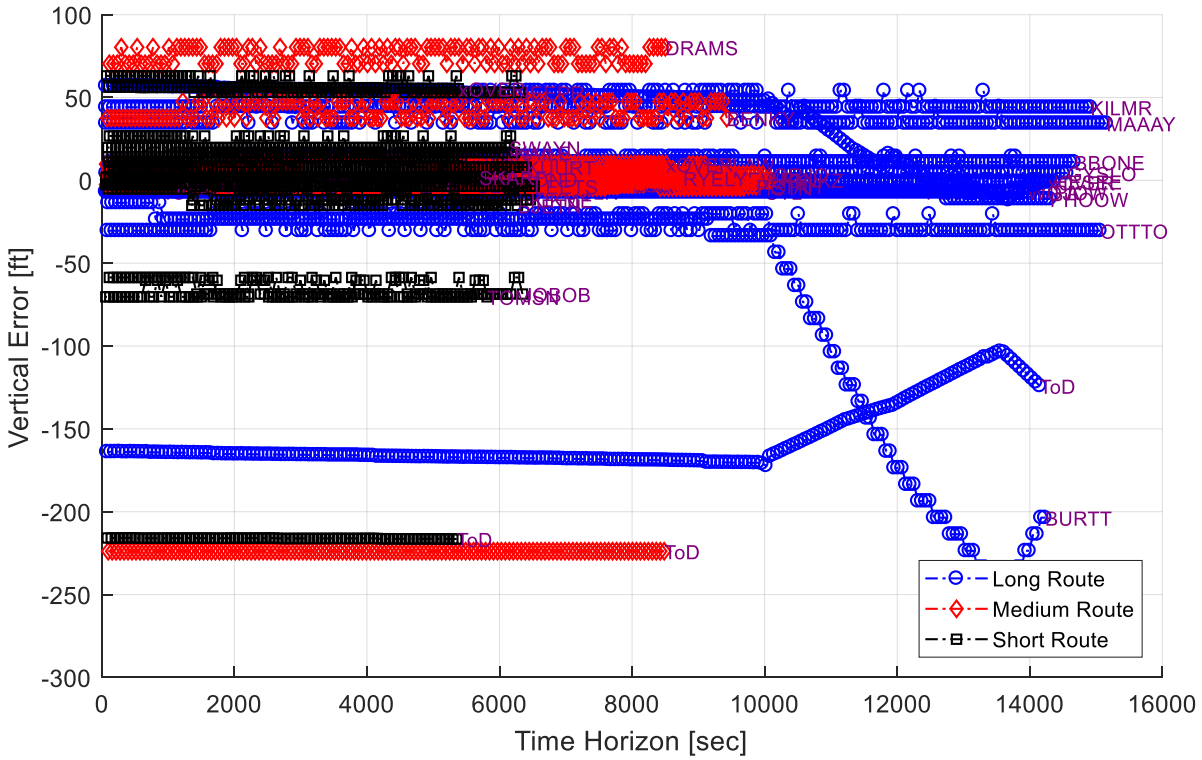

Figure 32. Vertical error for EPP trajectory points as a function of the time horizon [RL1-RL3, RT1, WC1, No RTA].

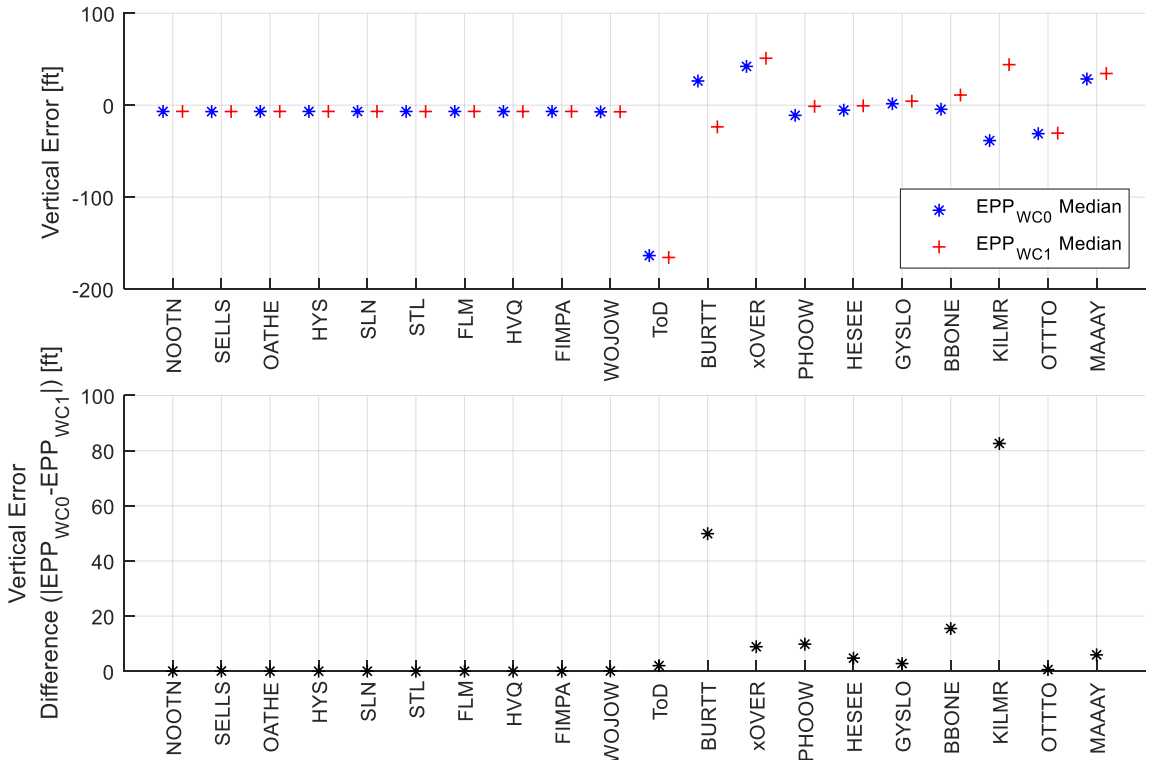

Figure 33. No wind (EPP_{WC0}) and perfect wind (EPP_{WC1}) median vertical error (top) and error difference (bottom) for the trajectory points of the long route [RL1, RT1, No RTA].

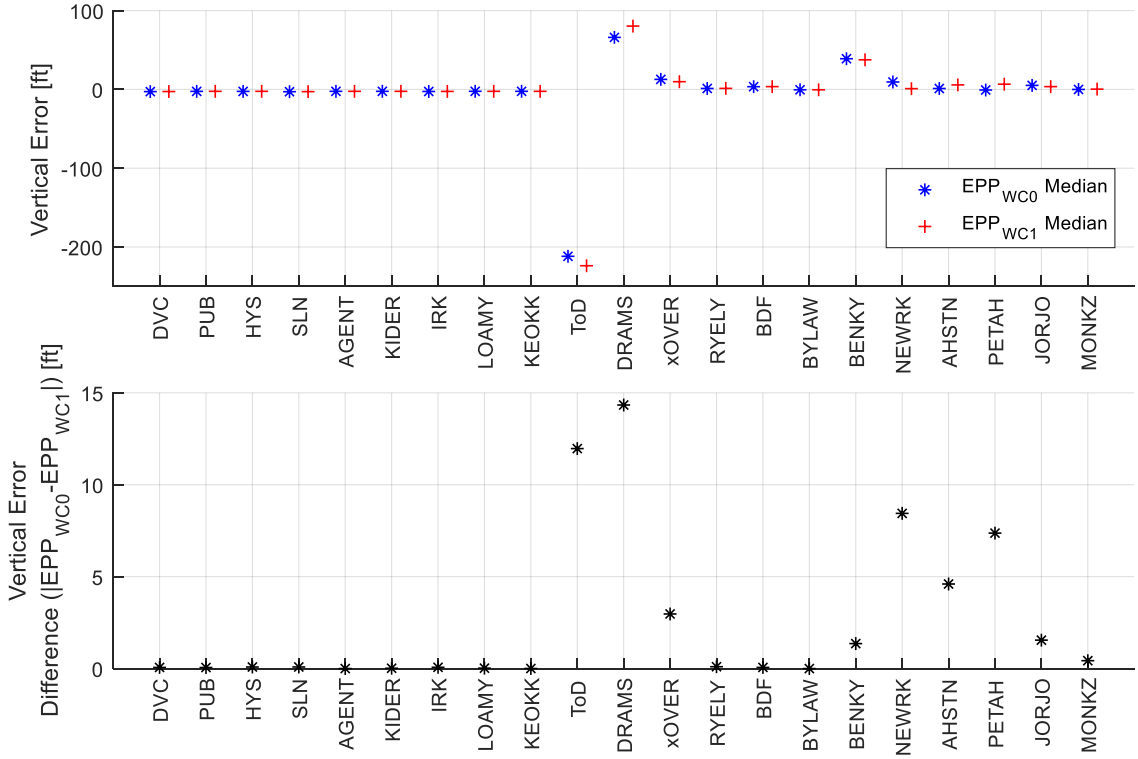

Figure 34. No wind (EPP_{WC0}) and perfect wind (EPP_{WC1}) median vertical error (top) and error difference (bottom) for the trajectory points of the medium route [RL2, RT1, No RTA].

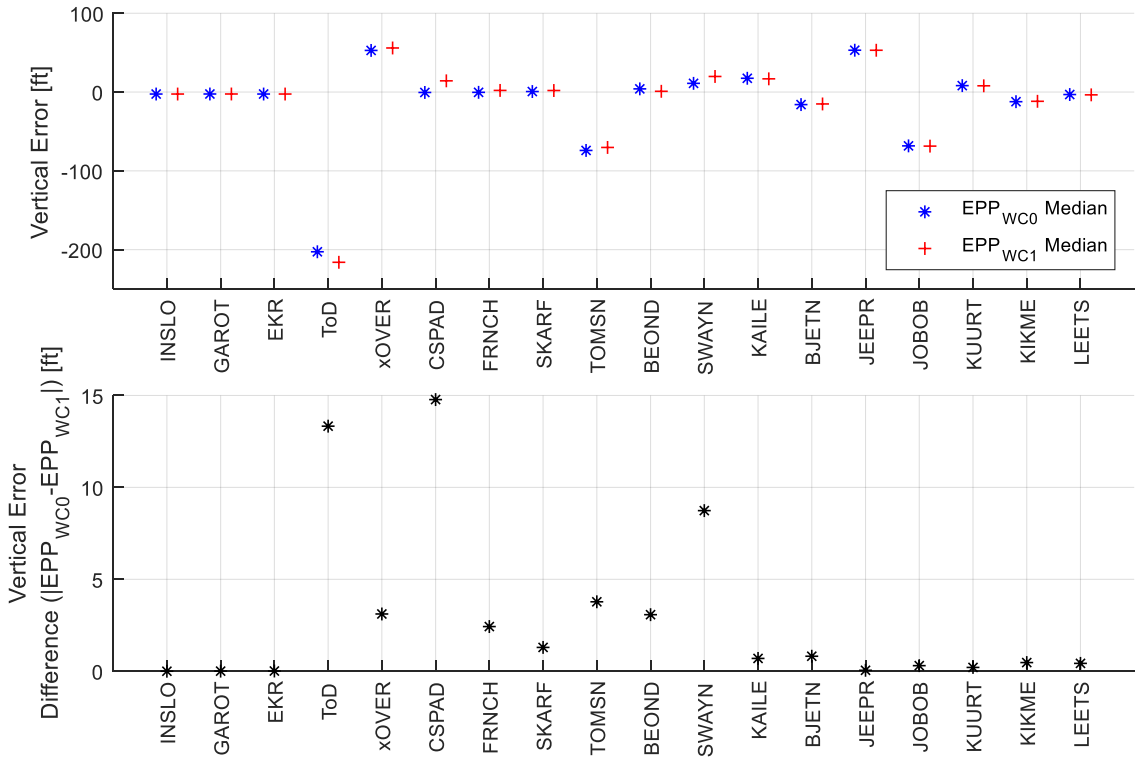

Figure 35. No wind (EPP_{WC0}) and perfect wind (EPP_{WC1}) median vertical error (top) and error difference (bottom) for the trajectory points of the short route [RL3, RT1, No RTA].

3. Time Error

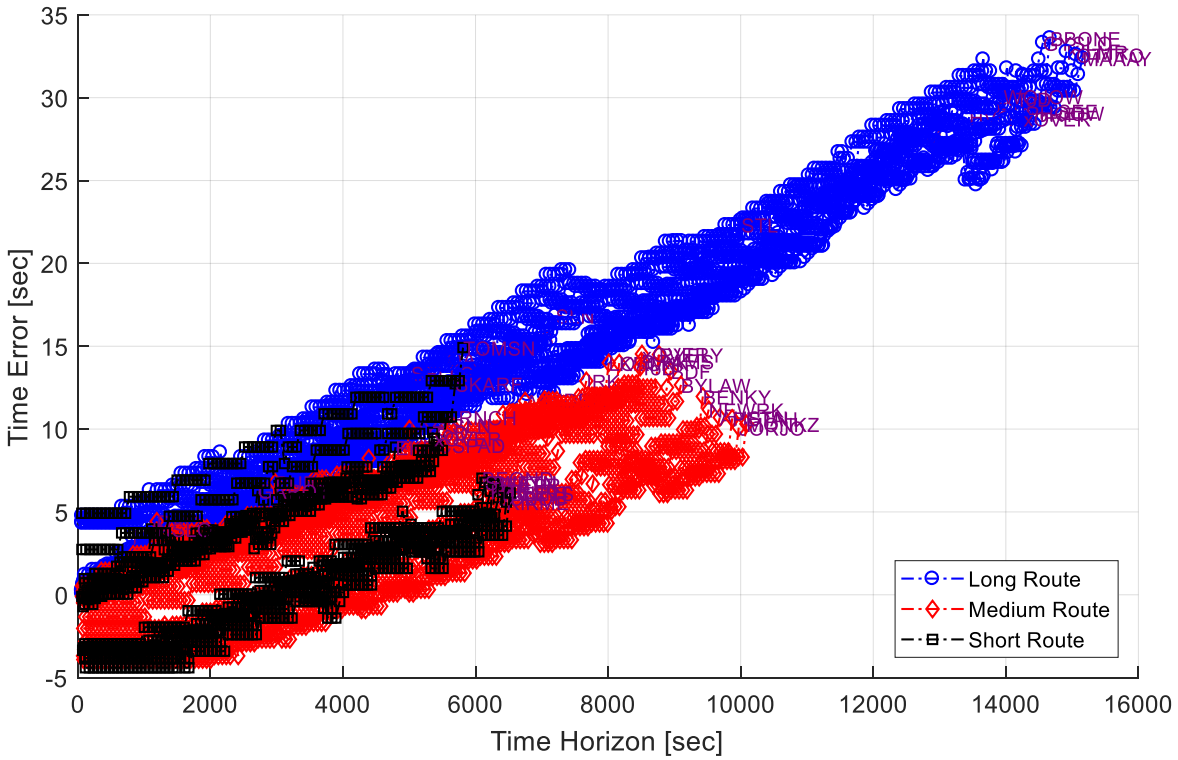

Figure 36. Time error for EPP trajectory points as a function of the time horizon [RL1-RL3, RT1, WC1, No RTA].

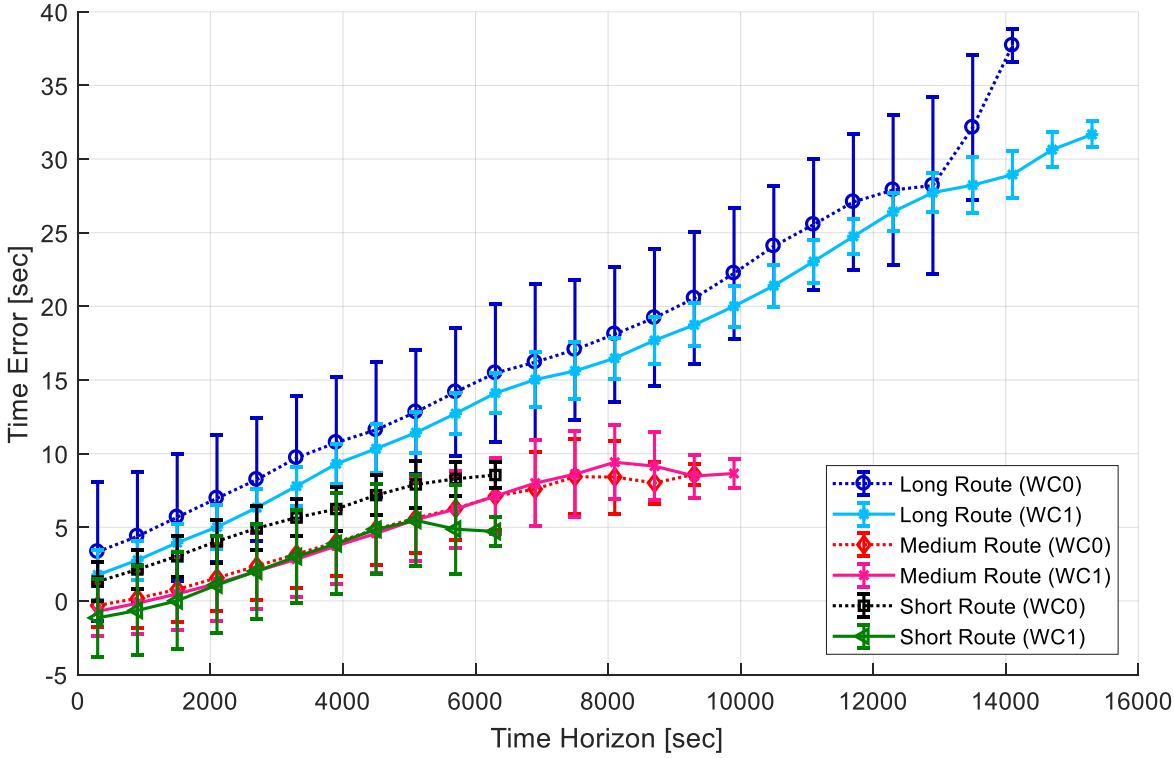

Figure 37. Binned temporal error mean and standard deviation for all trajectory points in the no wind [RL1-RL3, RT1, WC0, No RTA] and the perfect wind [RL1-RL3, RT1, WC1, No RTA] scenarios.

Appendix C: Figures – Sparse Versus Full Routes

1. *Cross-Track Error*

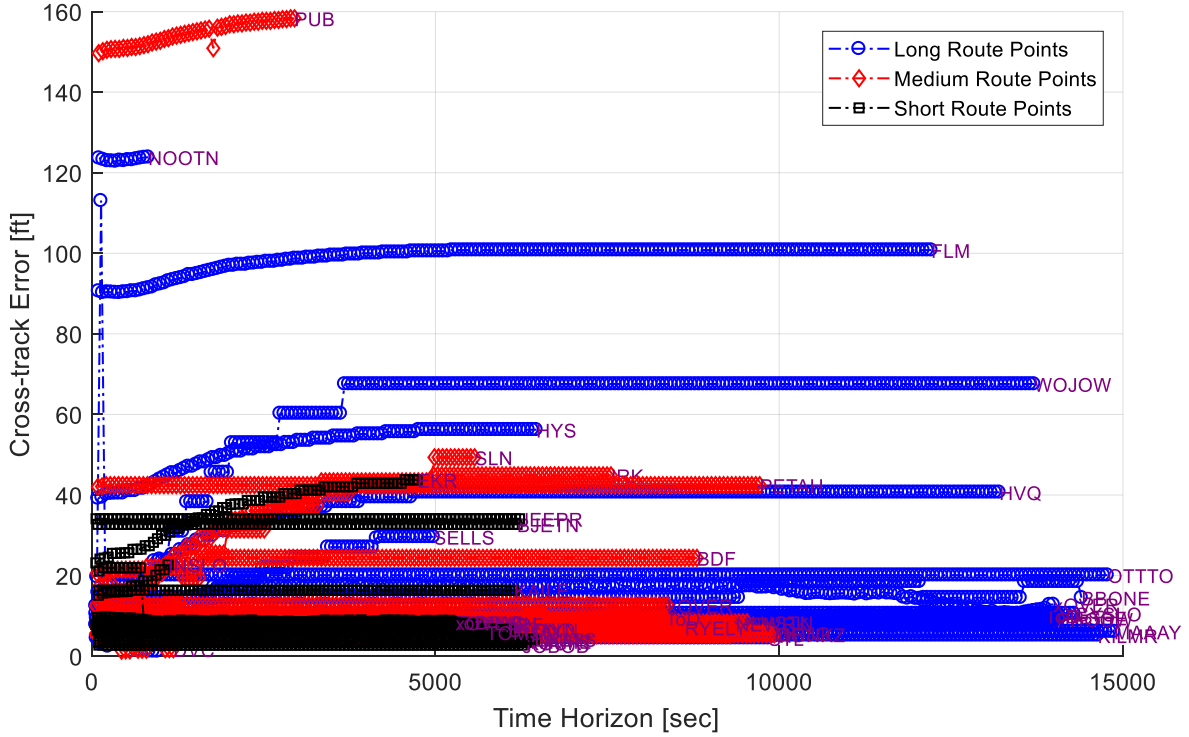

Figure 38. Cross-track error for EPP points as a function of the time horizon for the full routes scenario [RL1-RL3, RT1, WC2, No RTA].

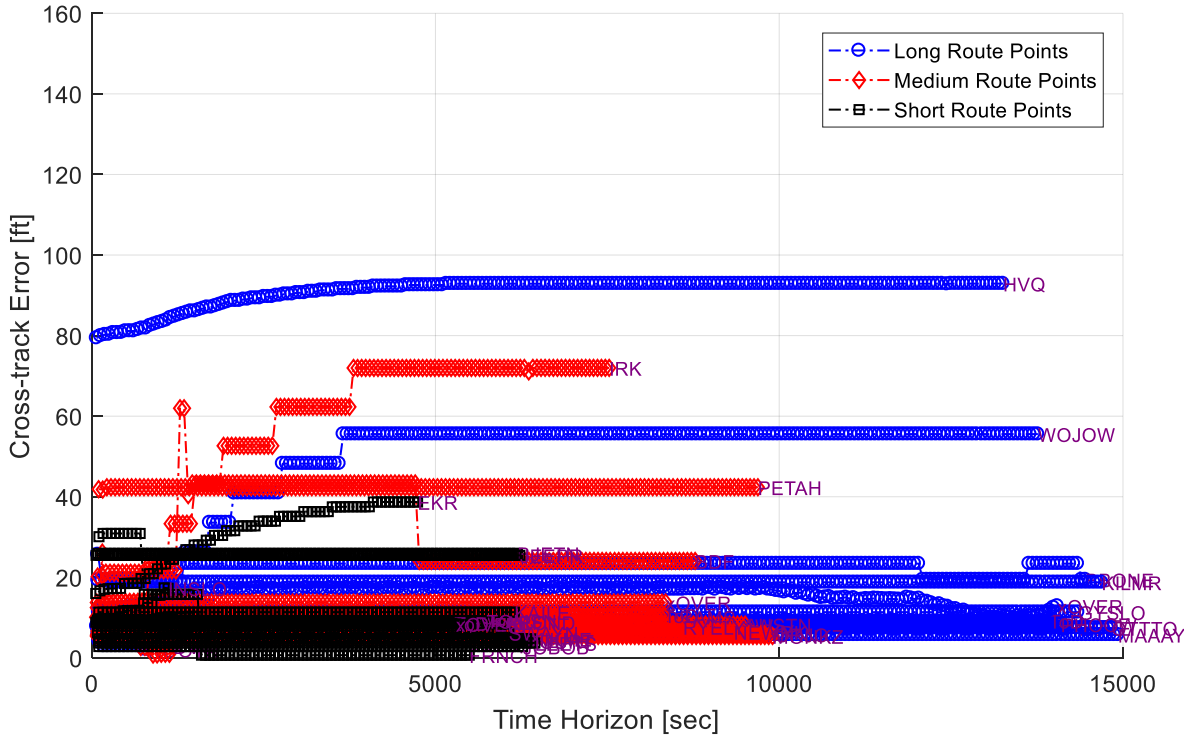

Figure 39. Cross-track error for EPP points as a function of the time horizon for the sparse routes scenario [RL1-RL3, RT2, WC2, No RTA].

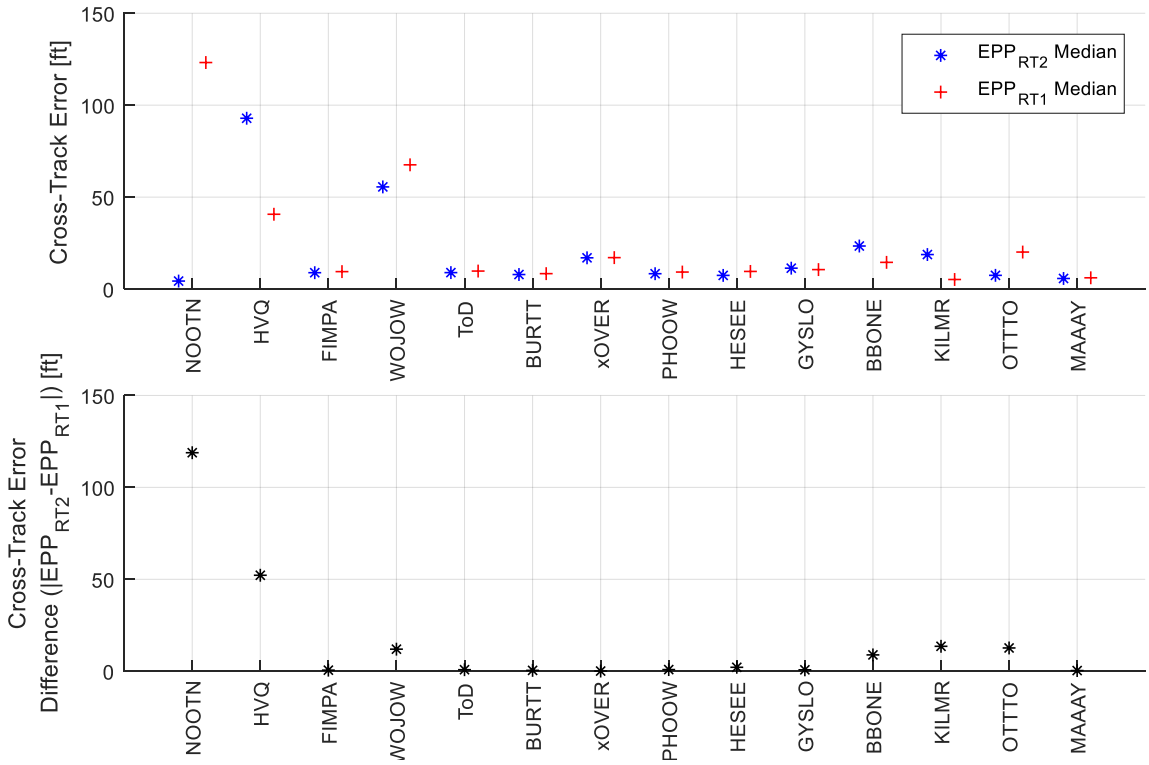

Figure 40. Sparse route (EPP_{RT2}) and full route (EPP_{RT1}) median cross-track error (top) and error difference (bottom) for the trajectory points of the long route [RL1, WC2, No RTA].

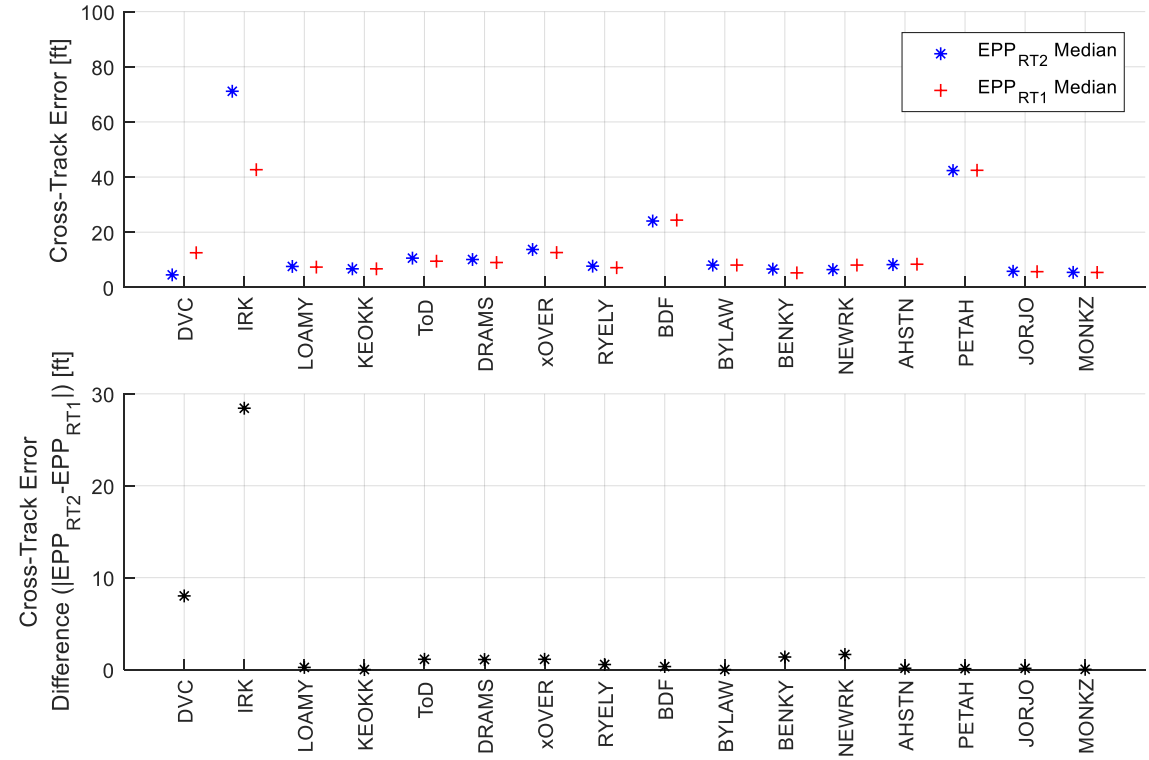

Figure 41. Sparse route (EPP_{RT2}) and full route (EPP_{RT1}) median cross-track error (top) and error difference (bottom) for the trajectory points of the medium route [RL2, WC2, No RTA].

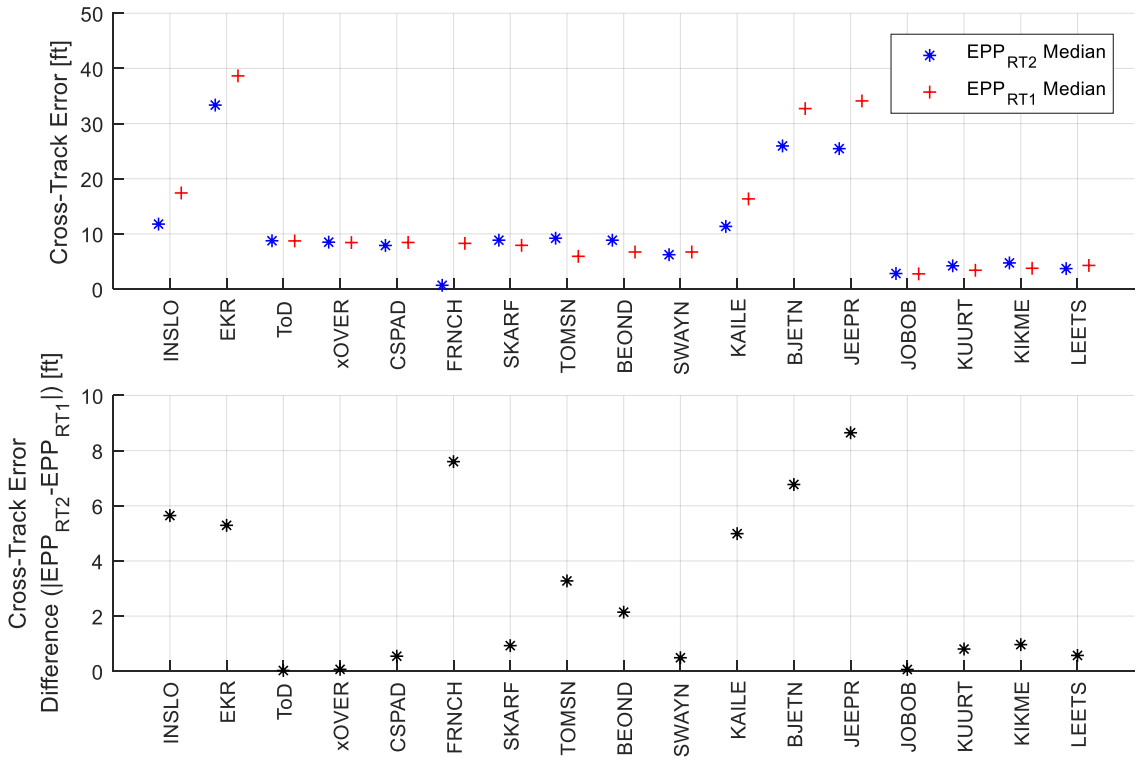

Figure 42. Sparse route (EPP_{RT2}) and full route (EPP_{RT1}) median cross-track error (top) and error difference (bottom) for the trajectory points of the short route [RL3, WC2, No RTA].

2. Vertical Error

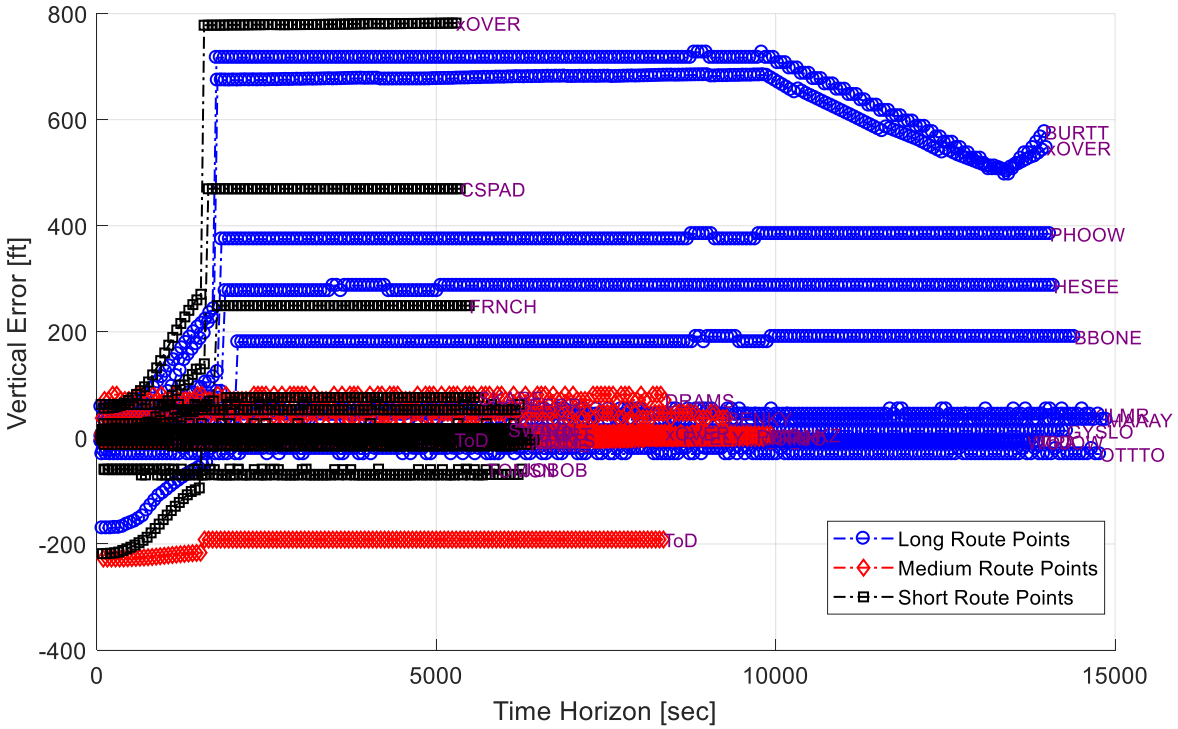

Figure 43. Vertical error for EPP trajectory points as a function of the time horizon for the full routes scenario [RL1-RL3, RT1, WC2, No RTA].

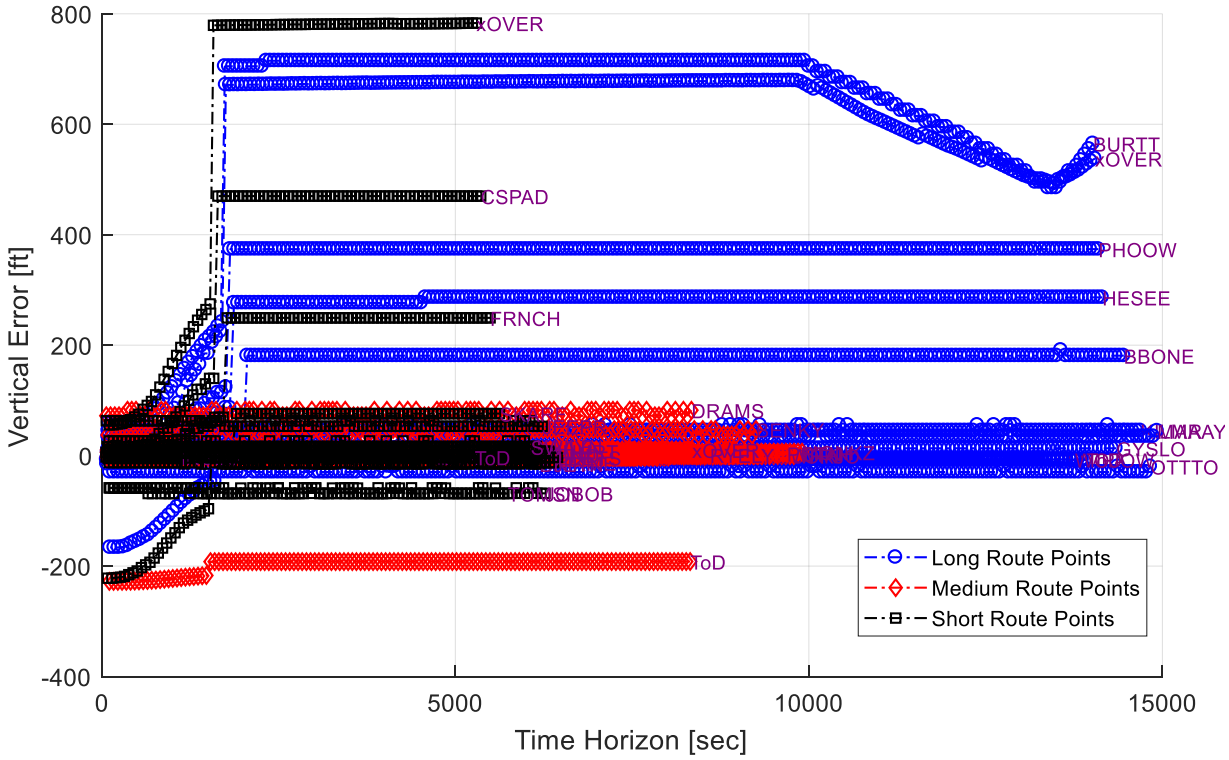

Figure 44. Vertical error for EPP trajectory points as a function of the time horizon for the sparse routes scenario [RL1-RL3, RT2, WC2, No RTA].

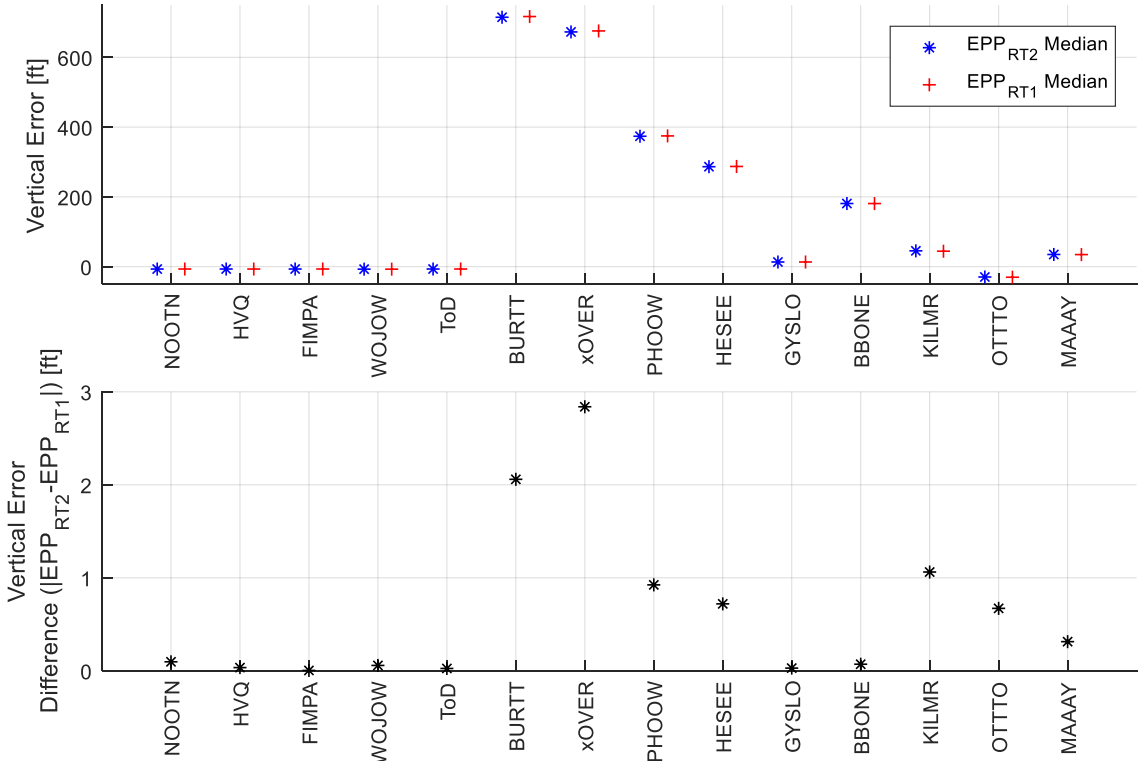

Figure 45. Sparse routes (EPP_{RT2}) and full routes (EPP_{RT1}) median vertical error (top) and error difference (bottom) for the trajectory points of the long route [RL1, WC2, No RTA].

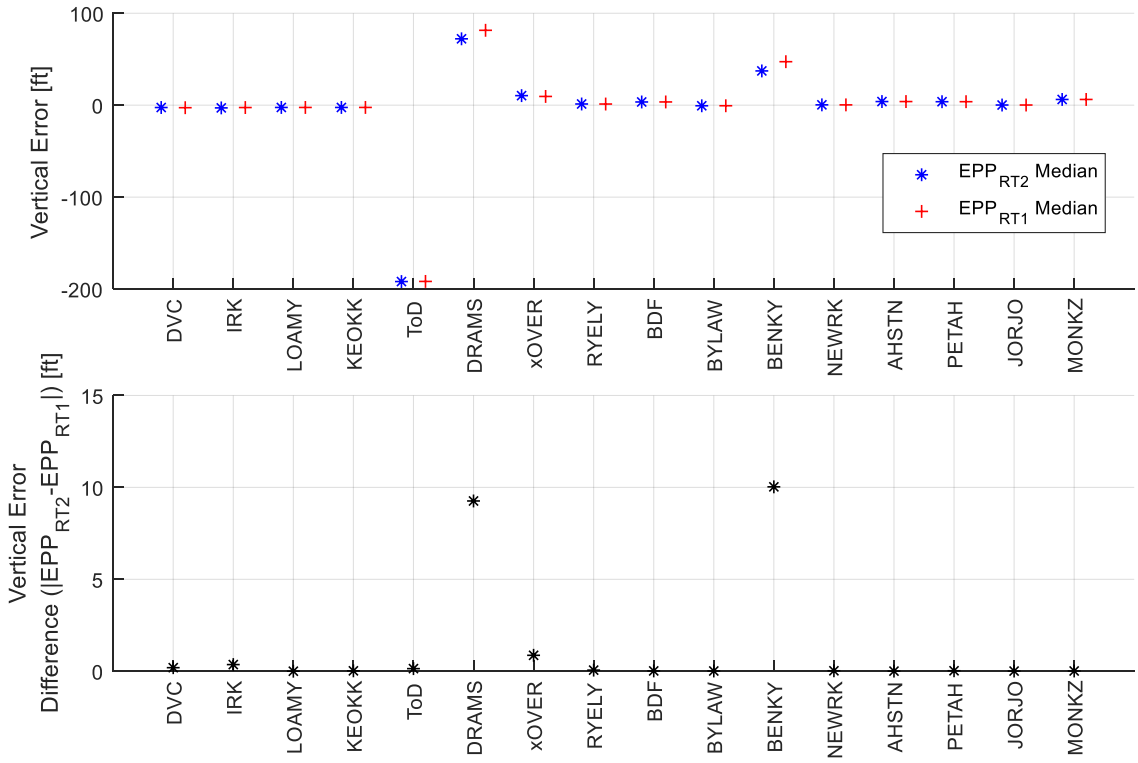

Figure 46. Sparse routes (EPP_{RT2}) and full routes (EPP_{RT1}) median vertical error (top) and error difference (bottom) for the trajectory points of the medium route [RL2, WC2, No RTA].

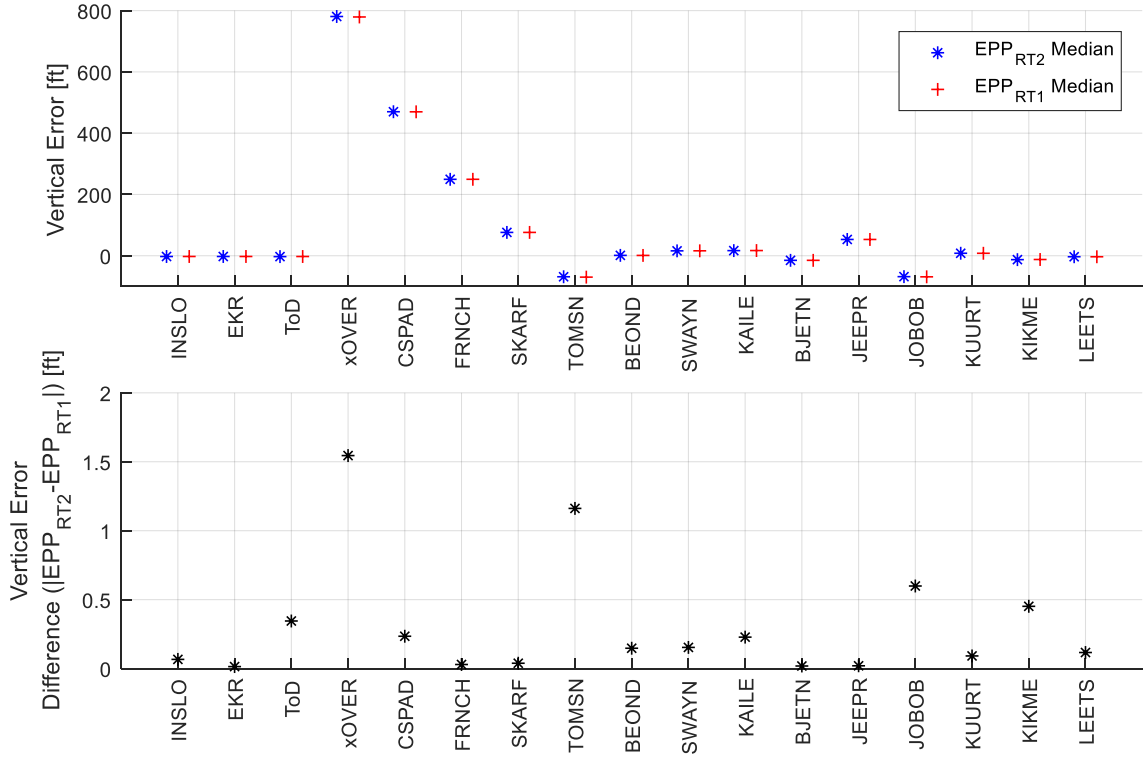

Figure 47. Sparse routes (EPP_{RT2}) and full routes (EPP_{RT1}) median vertical error (top) and error difference (bottom) for the trajectory points of the short route [RL3, WC2, No RTA].

3. *Time Error*

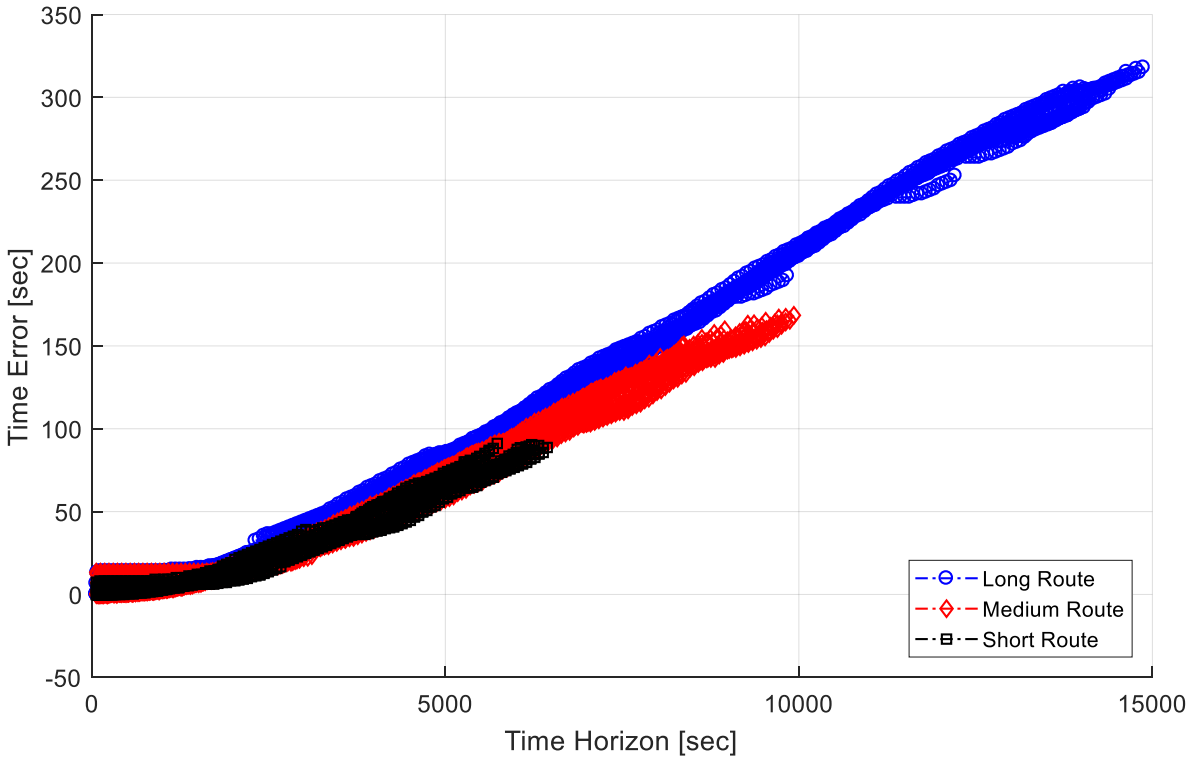

Figure 48. Time error for EPP trajectory points as a function of the time horizon for the full routes scenario [RL1-RL3, RT1, WC2, No RTA].

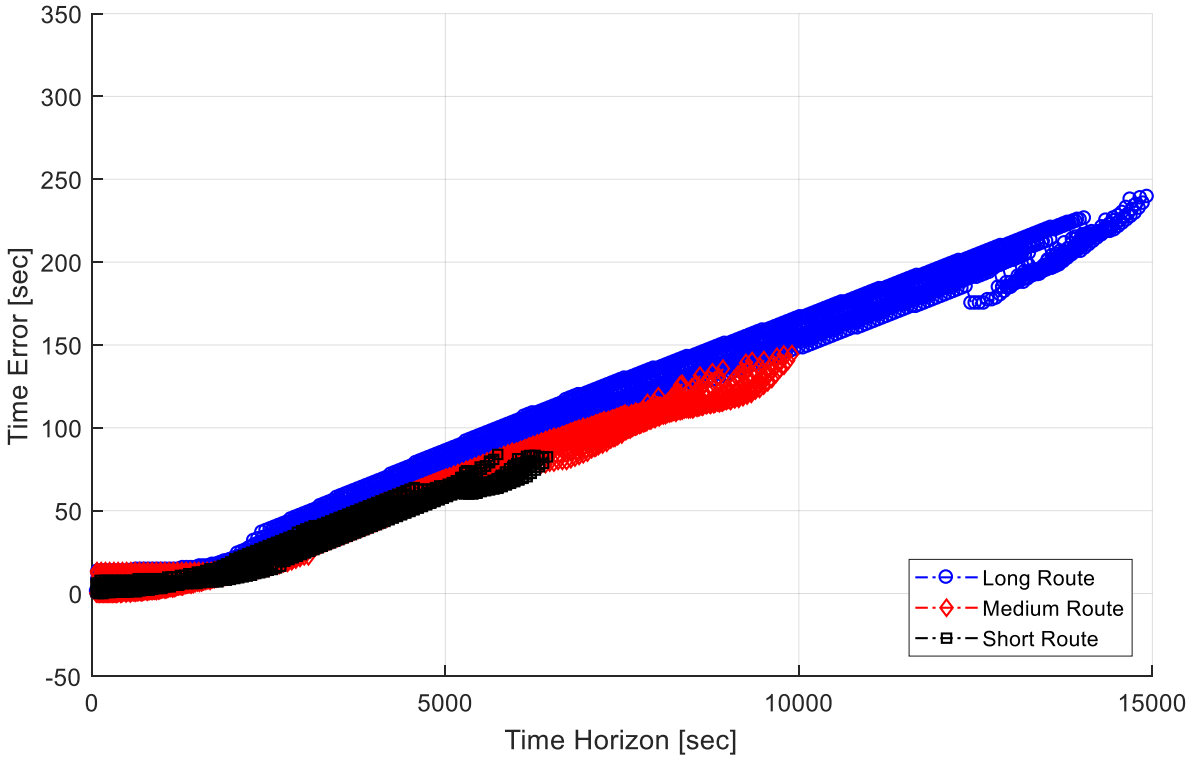

Figure 49. Time error for EPP trajectory points as a function of the time horizon for the sparse routes scenario [RL1-RL3, RT2, WC2, No RTA].

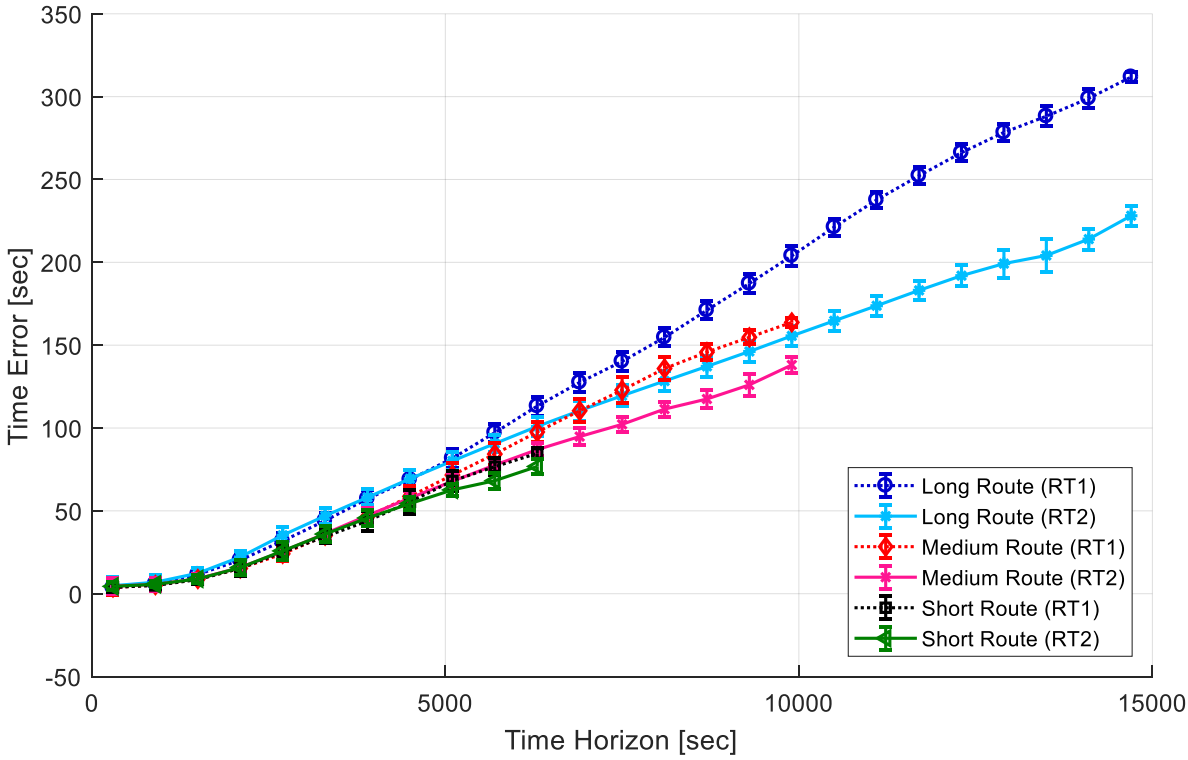

Figure 50. Binned temporal error mean and standard deviation for all trajectory points in the full routes scenario [RL1-RL3, RT1, WC2, No RTA] and the sparse routes scenario [RL1-RL3, RT2, WC2, No RTA].

Appendix D: Figures – Wind Magnitude Error

1. *Cross-Track Error*

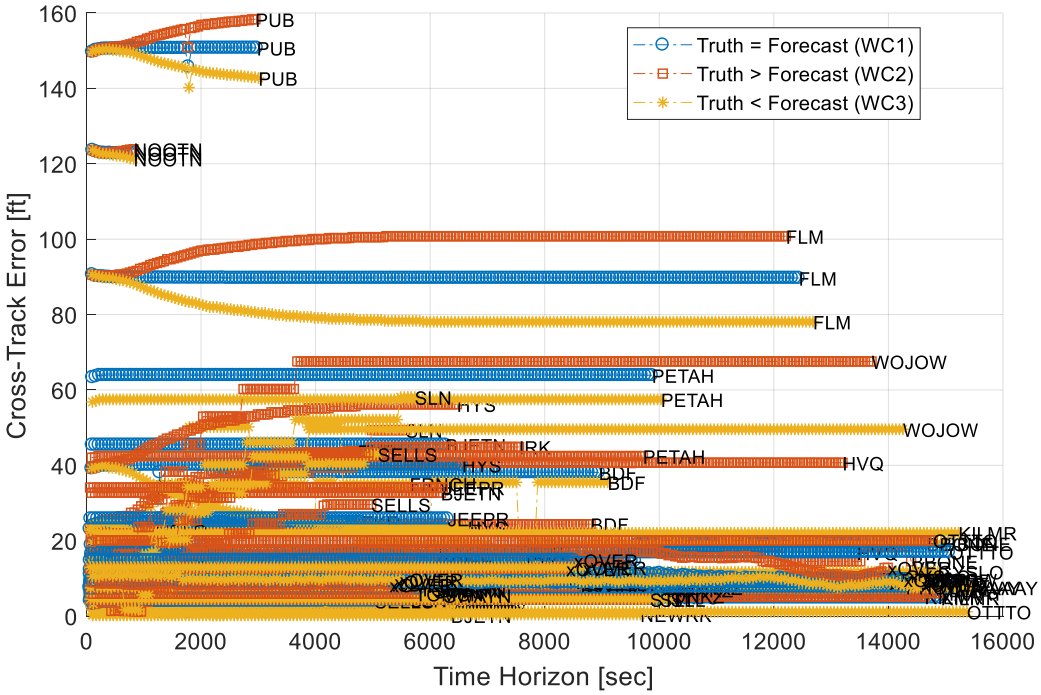

Figure 51. EPP cross-track error for the perfect wind condition (WC1), the true wind magnitude greater than forecast (WC2), and the true wind magnitude less than forecast (WC3) [RL1-RL3, RT1, No RTA].

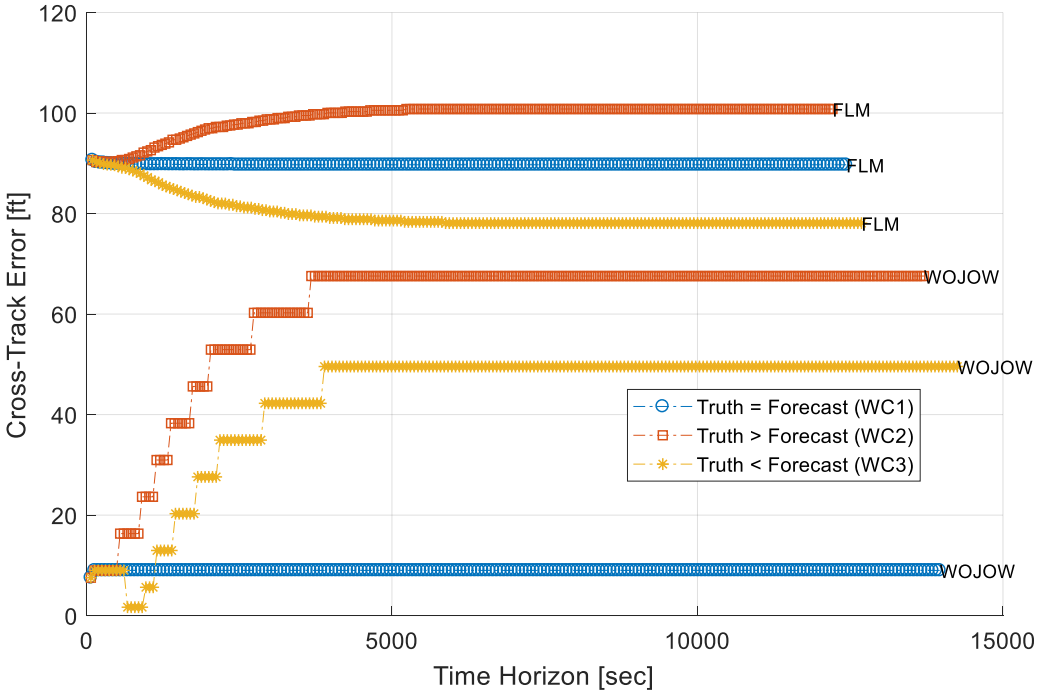

Figure 52. Cross-track error for a subset of EPP points (FLM and WOJOW) for the perfect wind condition (WC1), the true wind magnitude greater than forecast (WC2), and the true wind magnitude less than forecast (WC3) [RL1-RL3, RT1, No RTA].

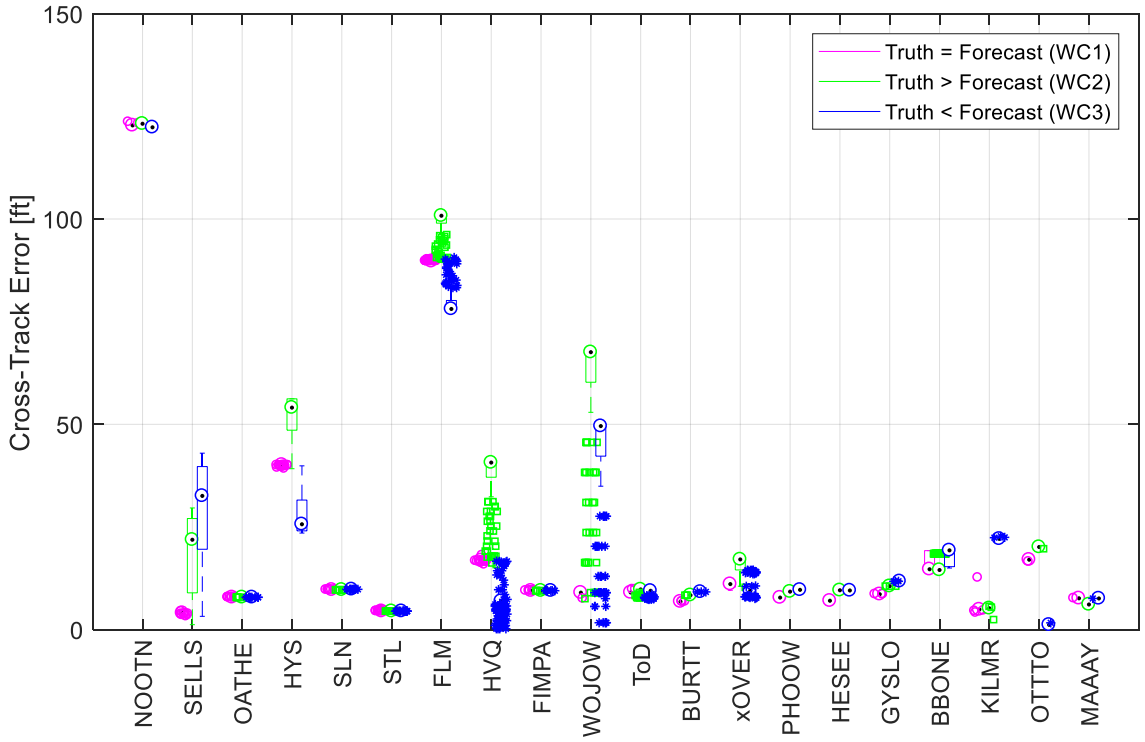

Figure 53. Boxplot of the cross-track error for each EPP point of the long route for the perfect wind condition (WC1), the true wind magnitude greater than forecast condition (WC2), and the true wind magnitude less than forecast condition (WC3) [RL1-RL3, RT1, No RTA].

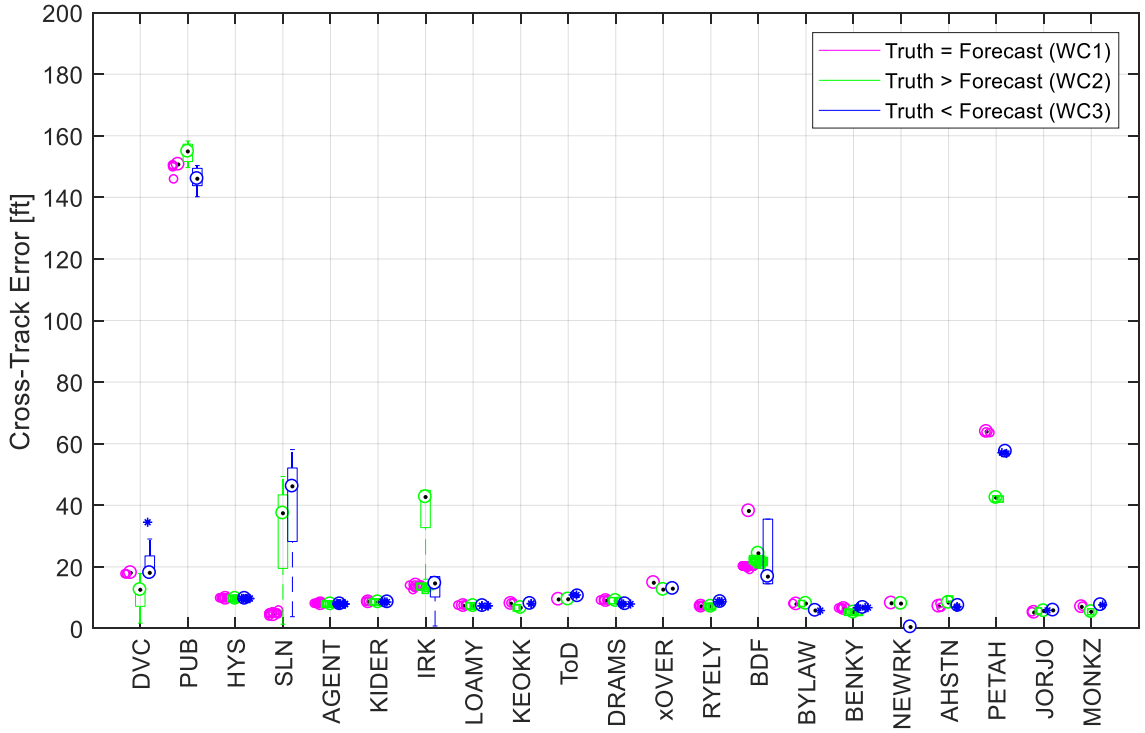

Figure 54. Boxplot of the cross-track error for each EPP point of the medium route for the perfect wind condition (WC1), the true wind magnitude greater than forecast condition (WC2), and the true wind magnitude less than forecast condition (WC3) [RL1-RL3, RT1, No RTA].

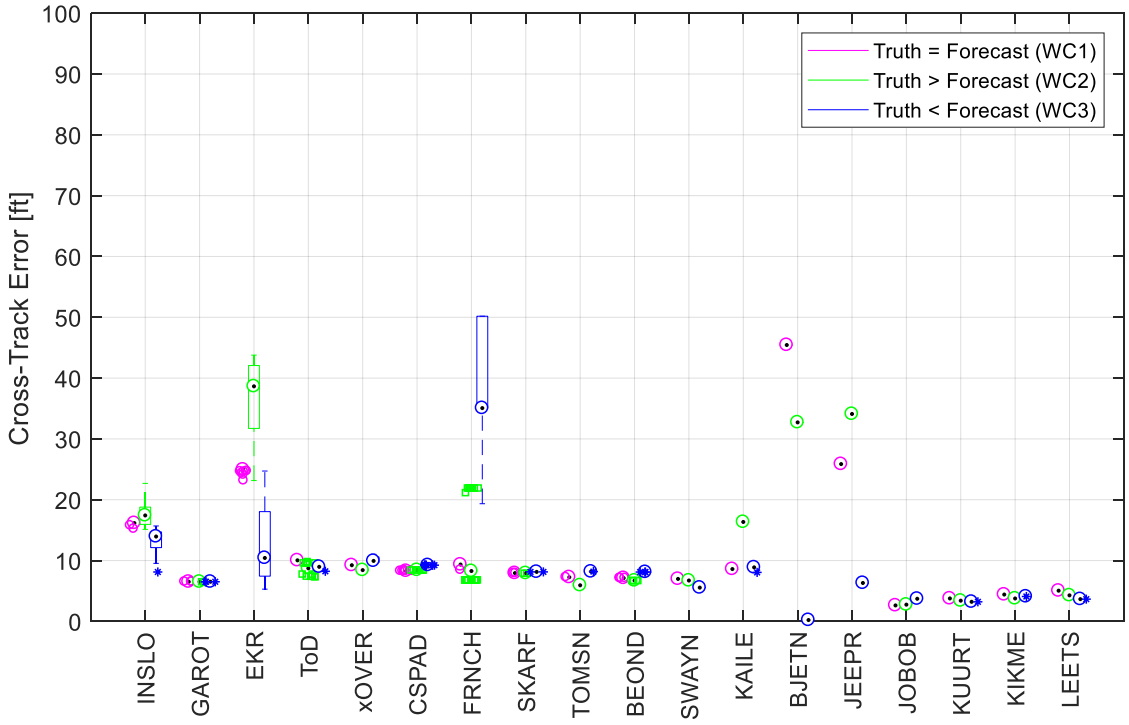

Figure 55. Boxplot of the cross-track error for each EPP point of the short route for the perfect wind condition (WC1), the true wind magnitude greater than forecast condition (WC2), and the true wind magnitude less than forecast condition (WC3) [RL1-RL3, RT1, No RTA].

2. Vertical Error

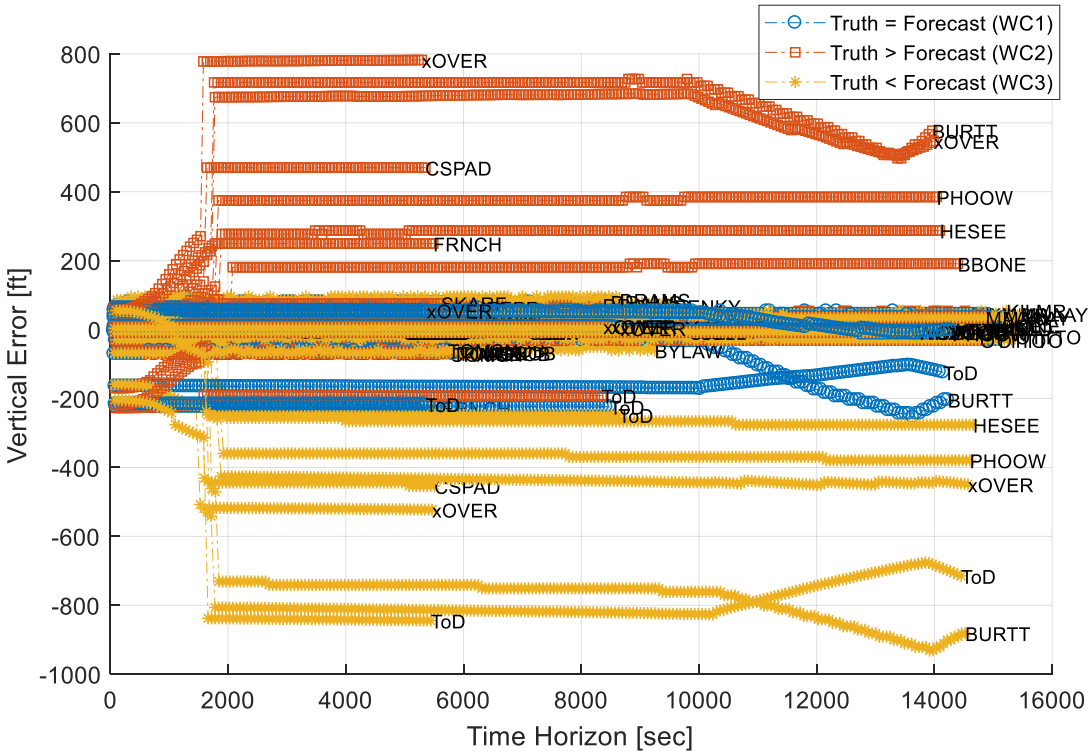

Figure 56. Vertical error for EPP points for the perfect wind condition (WC1), the true wind magnitude greater than forecast (WC2), and the true wind magnitude less than forecast (WC3) [RL1-RL3, RT1, No RTA].

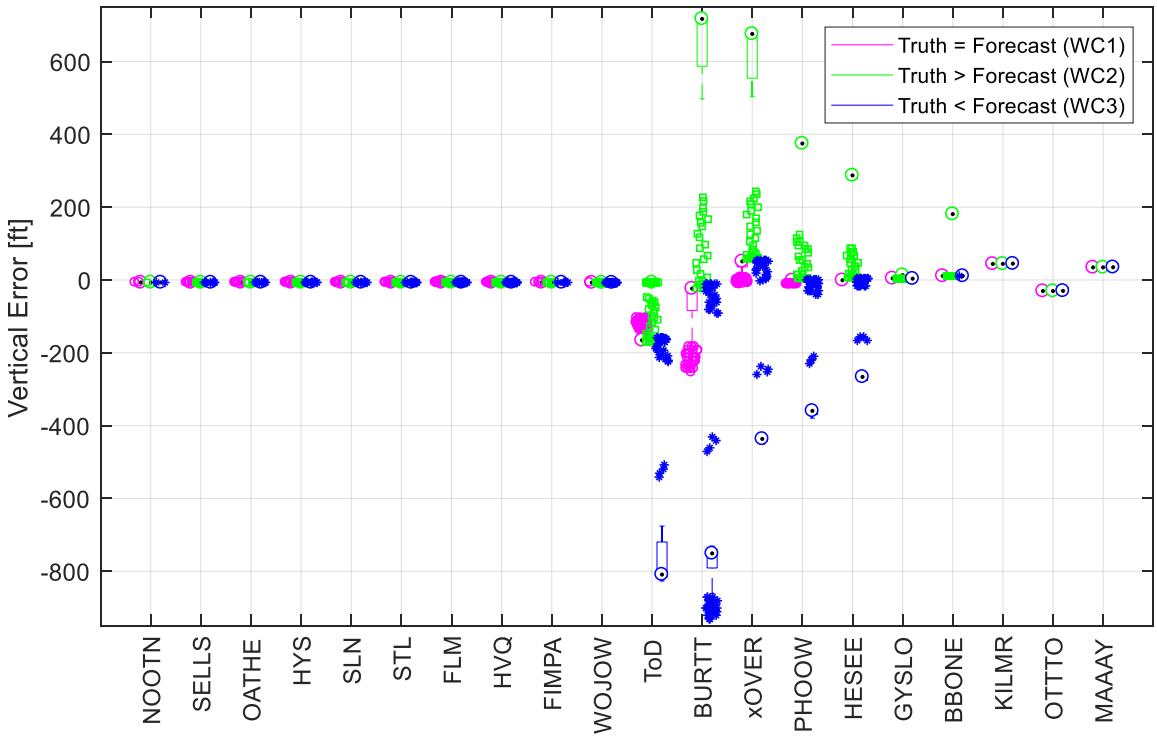

Figure 57. Boxplot of the vertical error for each EPP point of the long route for the perfect wind condition (WC1), the true wind magnitude greater than forecast condition (WC2), and the true wind magnitude less than forecast condition (WC3) [RL1-RL3, RT1, No RTA].

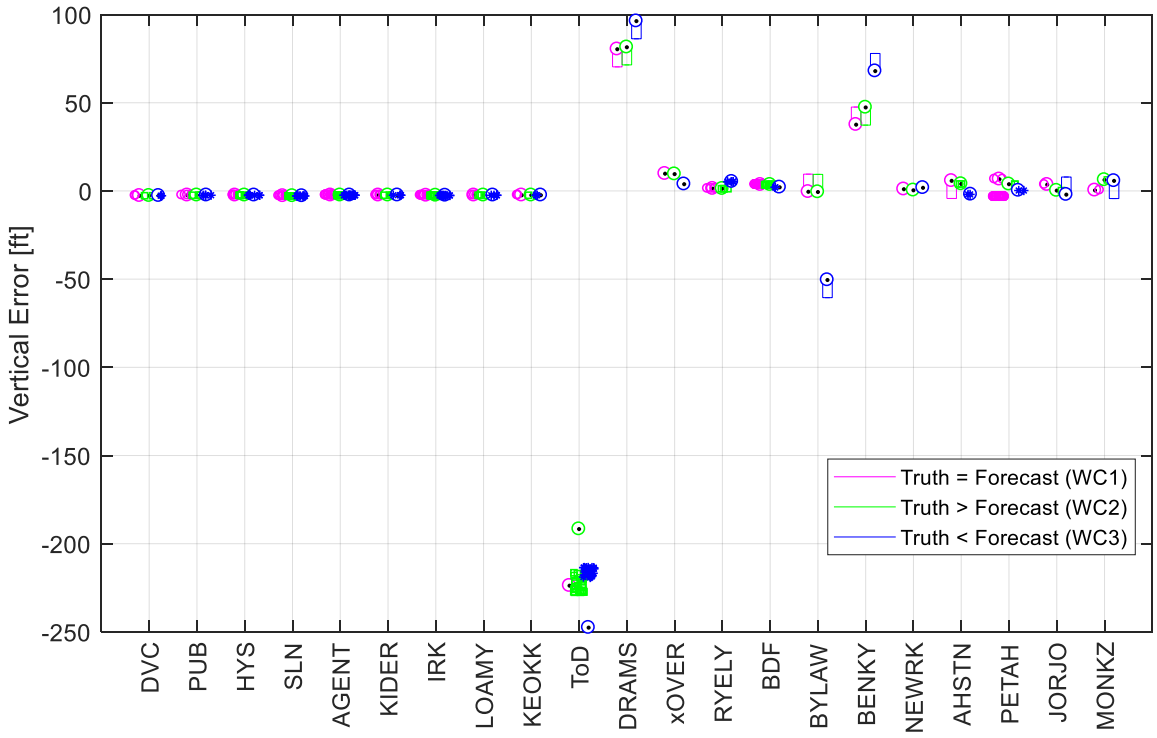

Figure 58. Boxplot of the vertical error for each EPP point of the medium route for the perfect wind condition (WC1), the true wind magnitude greater than forecast condition (WC2), and the true wind magnitude less than forecast condition (WC3) [RL1-RL3, RT1, No RTA].

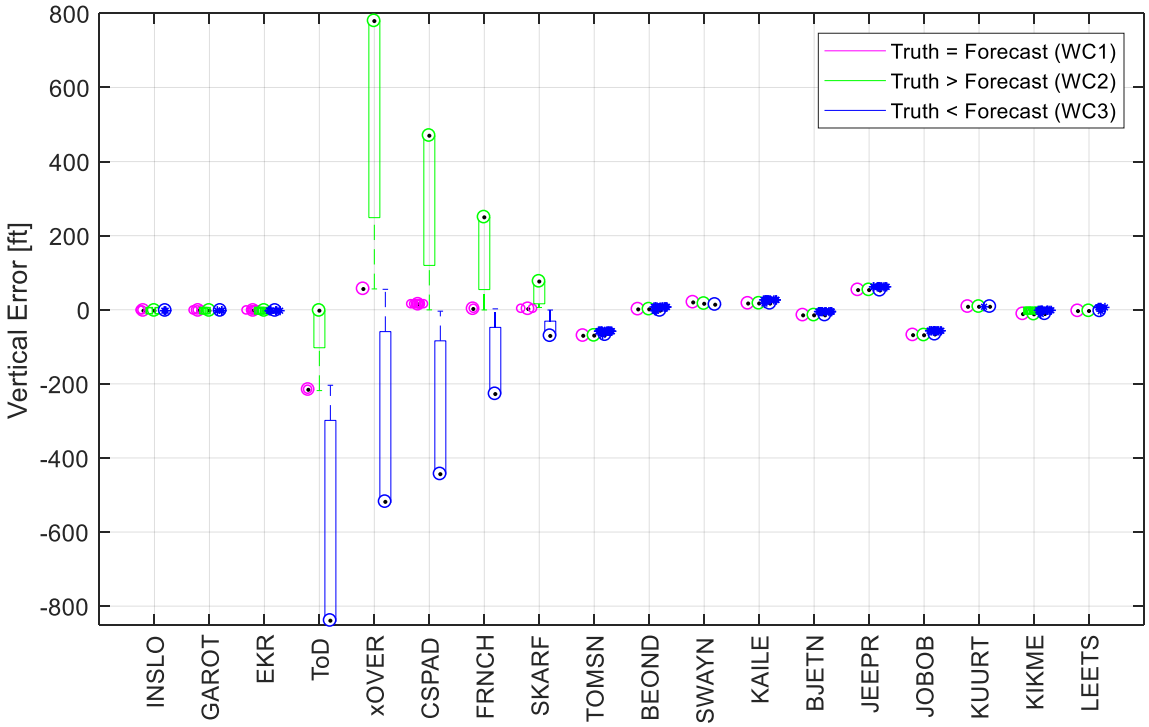

Figure 59. Boxplot of the vertical error for each EPP point of the short route for the perfect wind condition (WC1), the true wind magnitude greater than forecast condition (WC2), and the true wind magnitude less than forecast condition (WC3) [RL1-RL3, RT1, No RTA].

3. Time Error

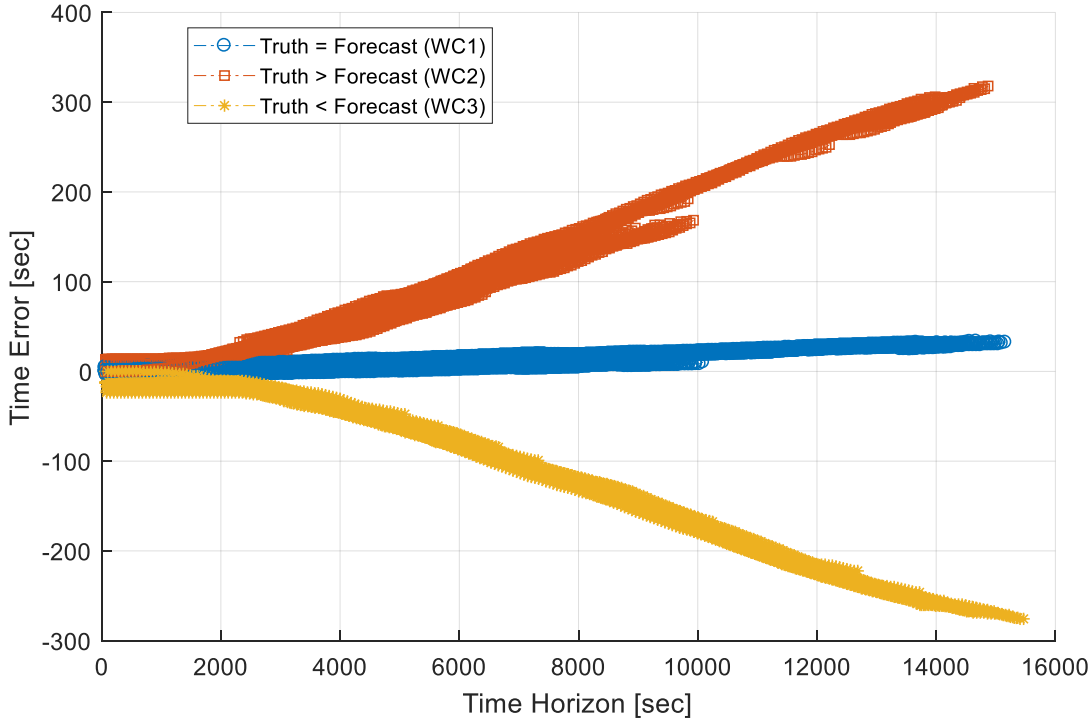

Figure 60. Time error for EPP points for the perfect wind condition (WC1), the true wind magnitude greater than forecast (WC2), and the true wind magnitude less than forecast (WC3) [RL1-RL3, RT1, No RTA].

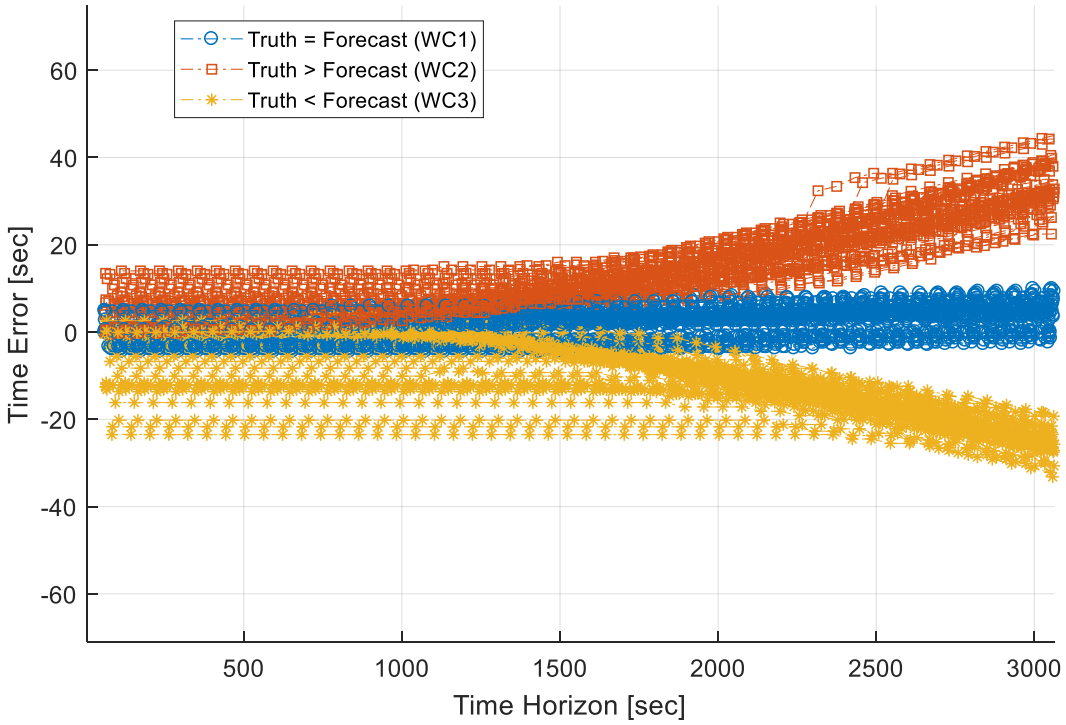

Figure 61. Short time horizon EPP time errors for the perfect wind condition (WC1), the true wind magnitude greater than forecast (WC2), and the true wind magnitude less than forecast (WC3) [RL1-RL3, RT1, No RTA].

Appendix E: Figures – Wind Direction Error

1. *Cross-Track Error*

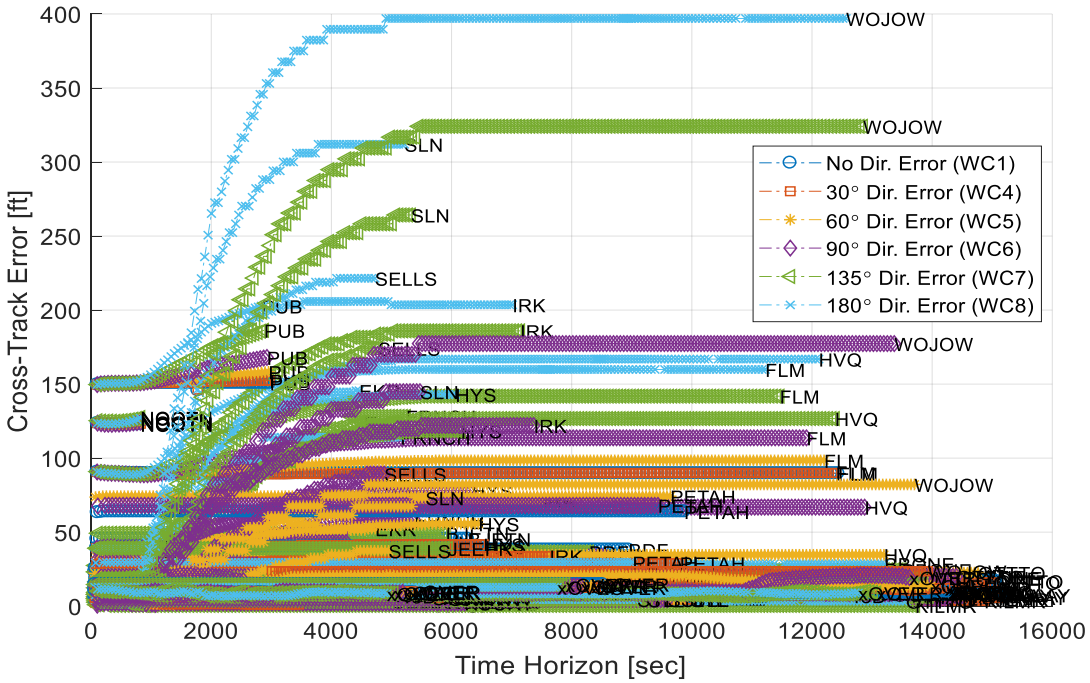

Figure 62. Cross-track error for EPP points of all route lengths with the perfect wind condition (WC1) and several wind direction error conditions (WC4-WC8) [RL1-RL3, RT1, No RTA].

2. *Vertical Error*

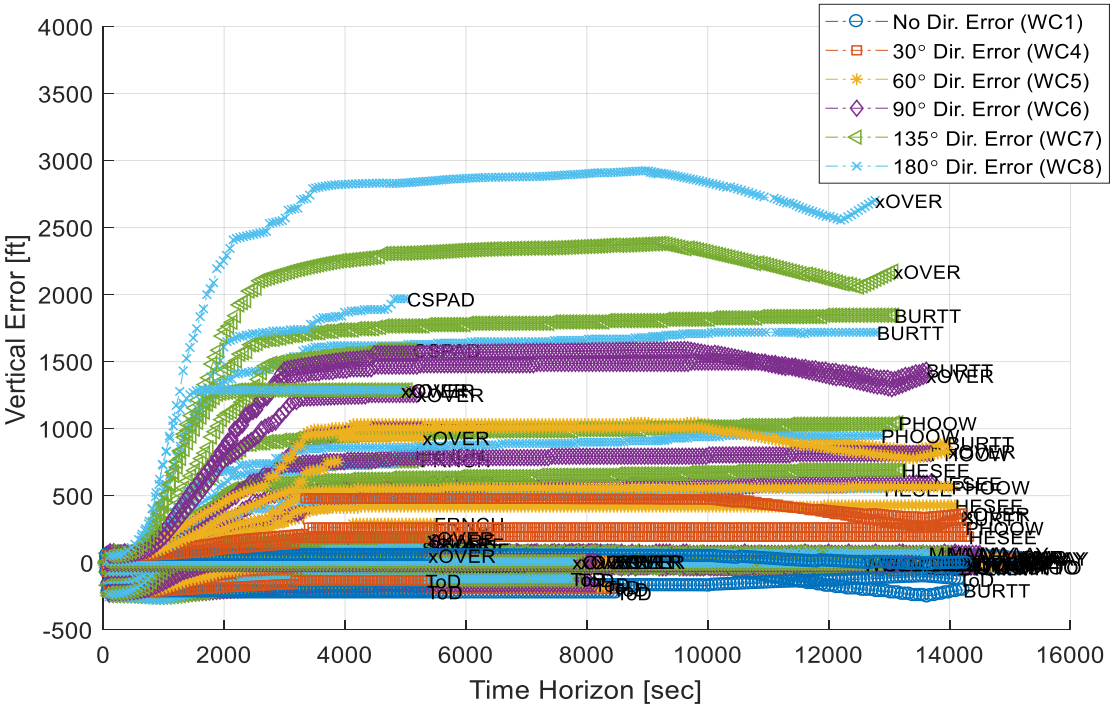

Figure 63. Vertical error for EPP points for all routes with the perfect wind condition (WC1) and several wind direction error conditions (WC4-WC8) [RL1-RL3, RT1, No RTA].

3. Time Error

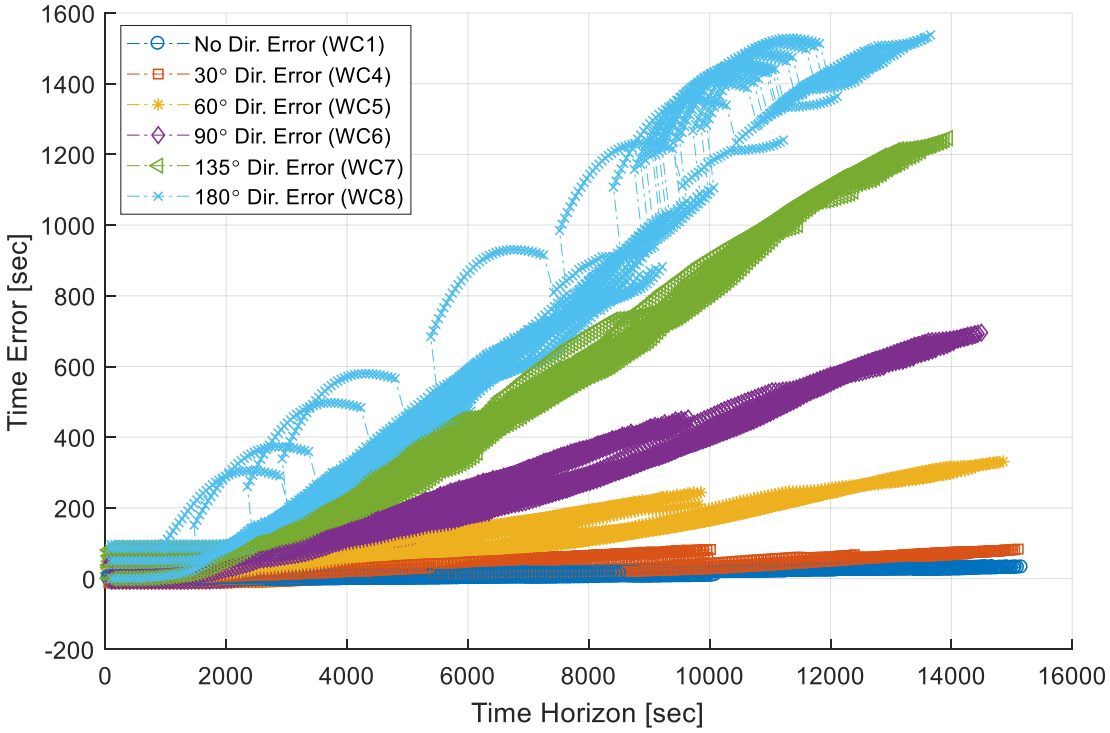

Figure 64. Time error for EPP points for all route lengths with the perfect wind condition (WC1) and several wind direction error conditions (WC4-WC8) [RL1-RL3, RT1, No RTA].

Appendix F: Figures – Time Constrained Routes

1. *Cross-Track Error*

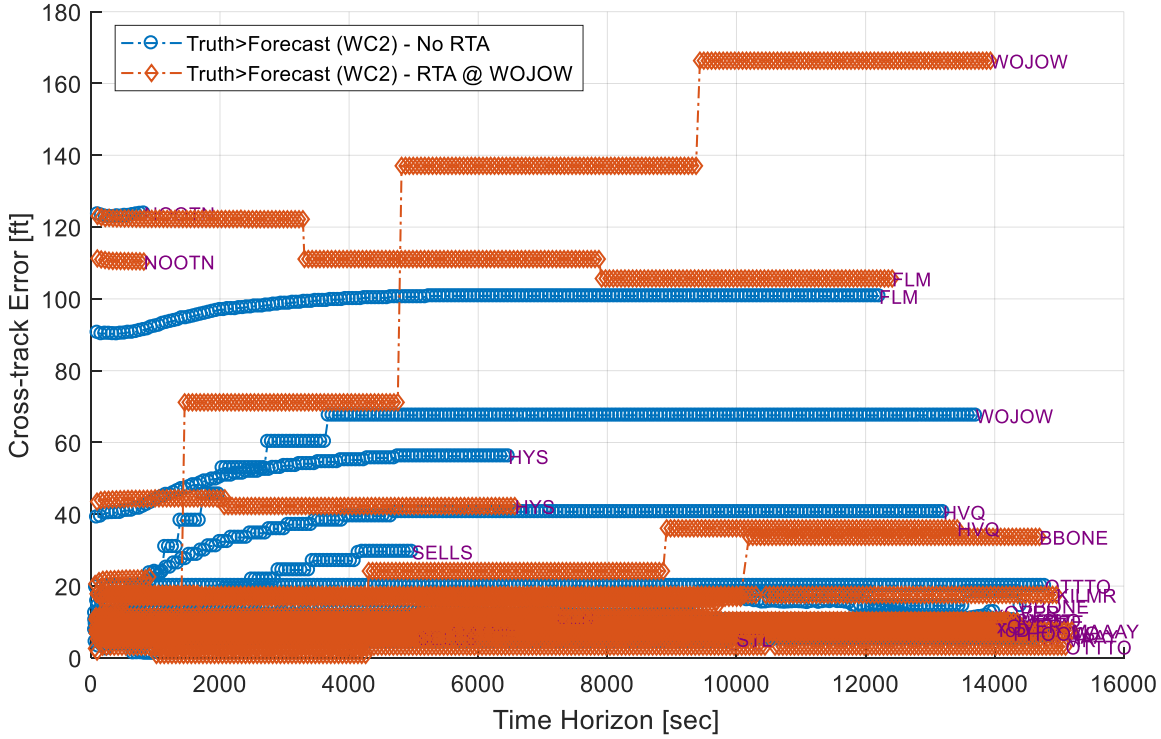

Figure 65. EPP cross-track error for the points of the long route, with true wind magnitude greater than forecast condition, without RTA (No RTA) and with an RTA (RTA1) in the cruise portion of flight [RL1, RT1, WC2].

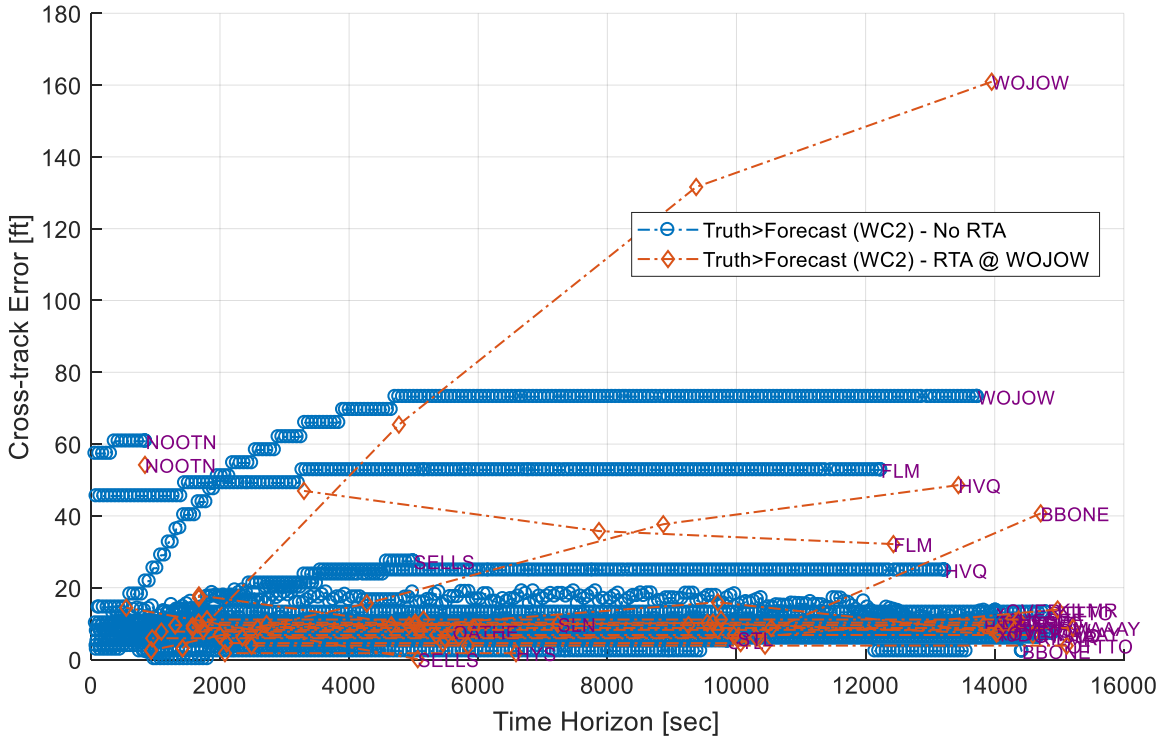

Figure 66. FMS cross-track error for the points of the long route, with true wind magnitude greater than forecast condition, without RTA (No RTA) and with an RTA (RTA1) in the cruise portion of flight [RL1, RT1, WC2].

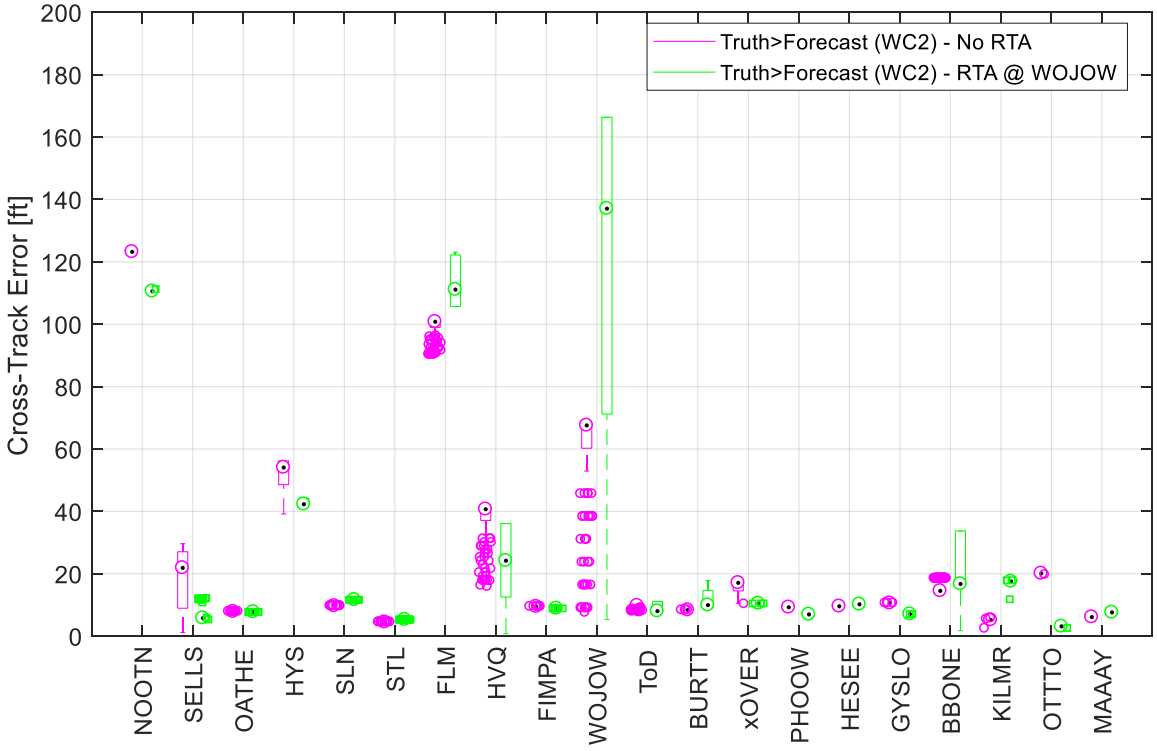

Figure 67. Boxplot of the EPP cross-track error of each point of the long route with true wind magnitude greater than forecast condition, without RTA (No RTA) and with an RTA (RTA1) in the cruise portion of flight [RL1, RT1, WC2].

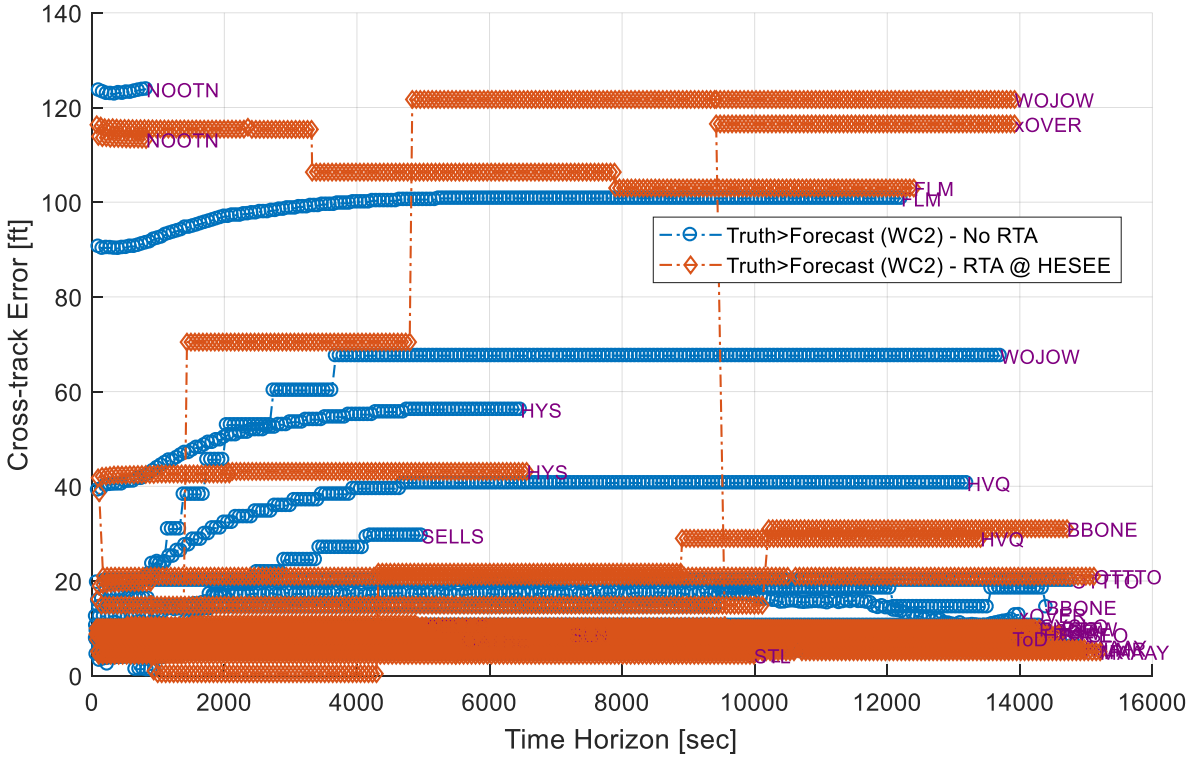

Figure 68. EPP cross-track error for the points of the long route, with true wind magnitude greater than forecast condition, without RTA (No RTA) and with an RTA (RTA2) just after top-of-descent [RL1, RT1, WC2].

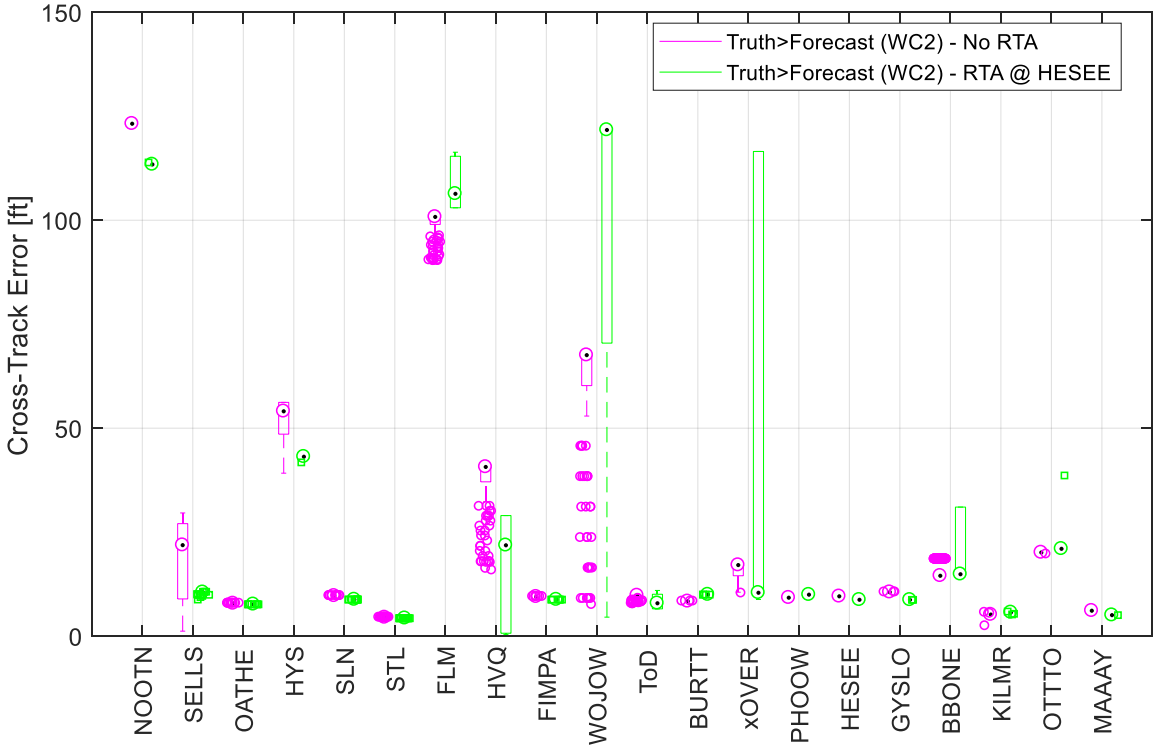

Figure 69. Boxplot of the EPP cross-track error of each point of the long route with true wind magnitude greater than forecast condition, without RTA (No RTA) and with an RTA (RTA2) just after top-of-descent [RL1, RT1, WC2].

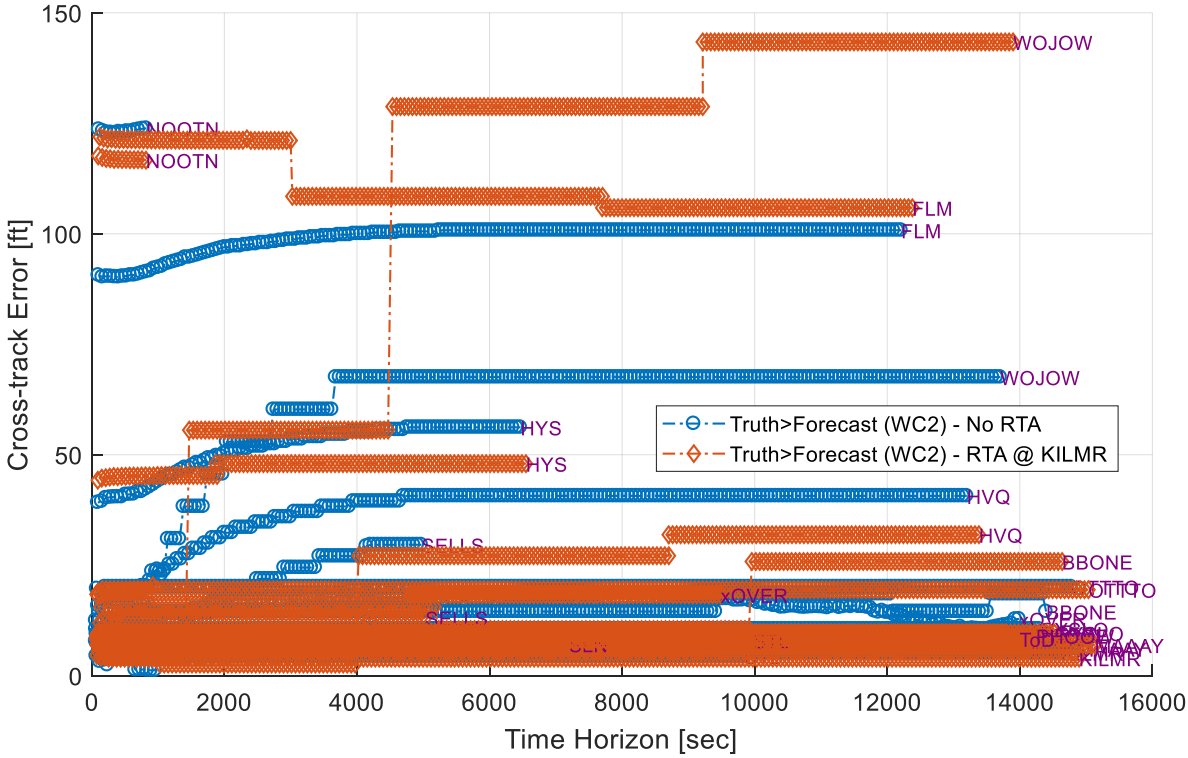

Figure 70. EPP cross-track error for the points of the long route, with true wind magnitude greater than forecast condition, without RTA (No RTA) and with an RTA (RTA3) in the terminal area [RL1, RT1, WC2].

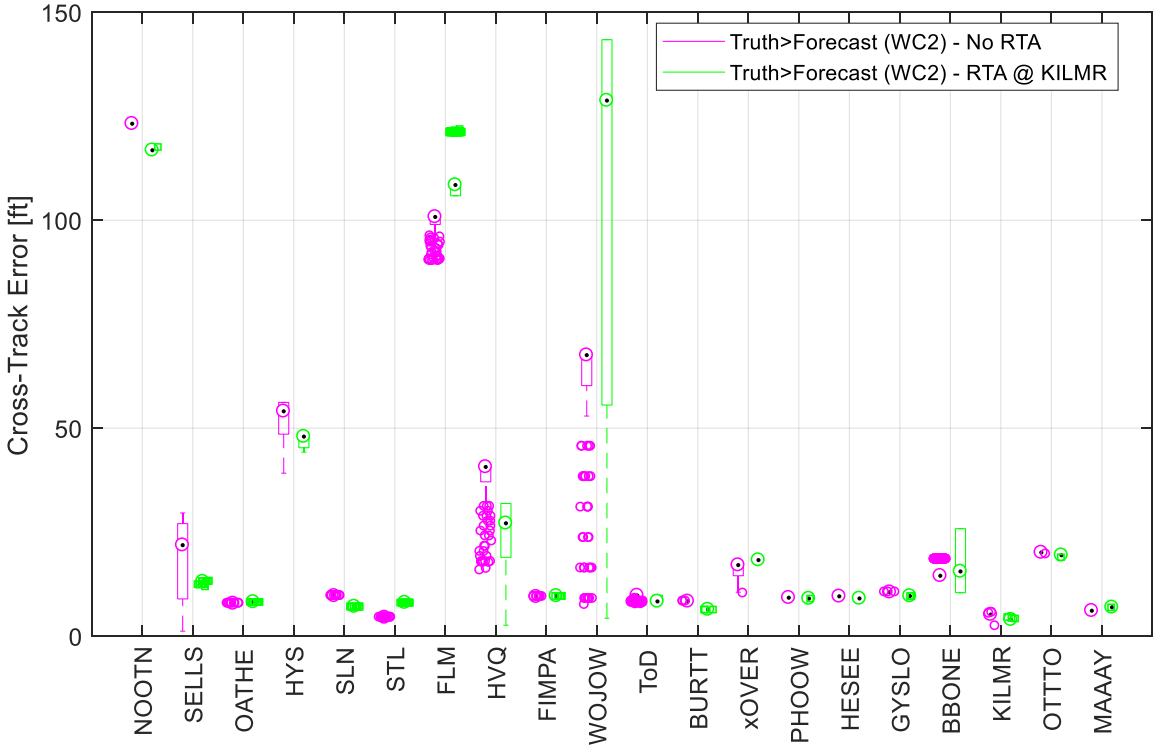

Figure 71. Boxplot of the EPP cross-track error of each point of the long route with true wind magnitude greater than forecast condition, without RTA (No RTA) and with an RTA (RTA3) in the terminal area [RL1, RT1, WC2].

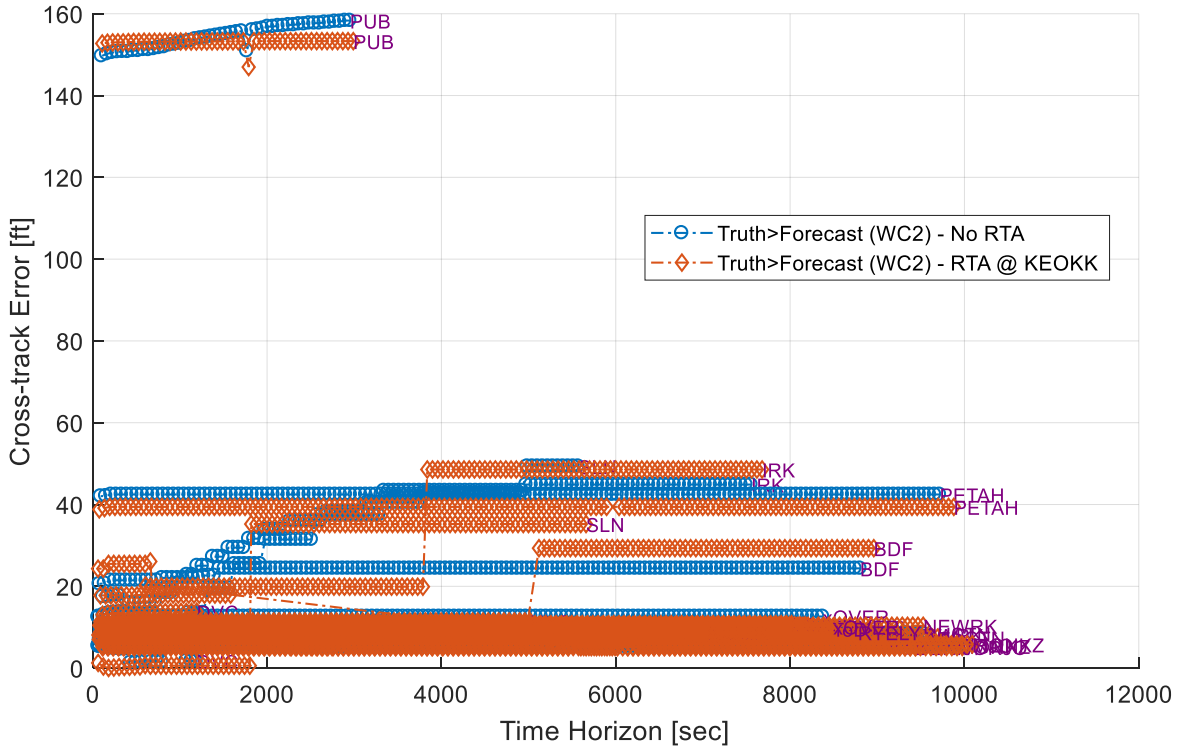

Figure 72. EPP cross-track error for the points of the medium route, with true wind magnitude greater than forecast condition, without RTA (No RTA) and with an RTA (RTA1) in the cruise portion of flight [RL2, RT1, WC2].

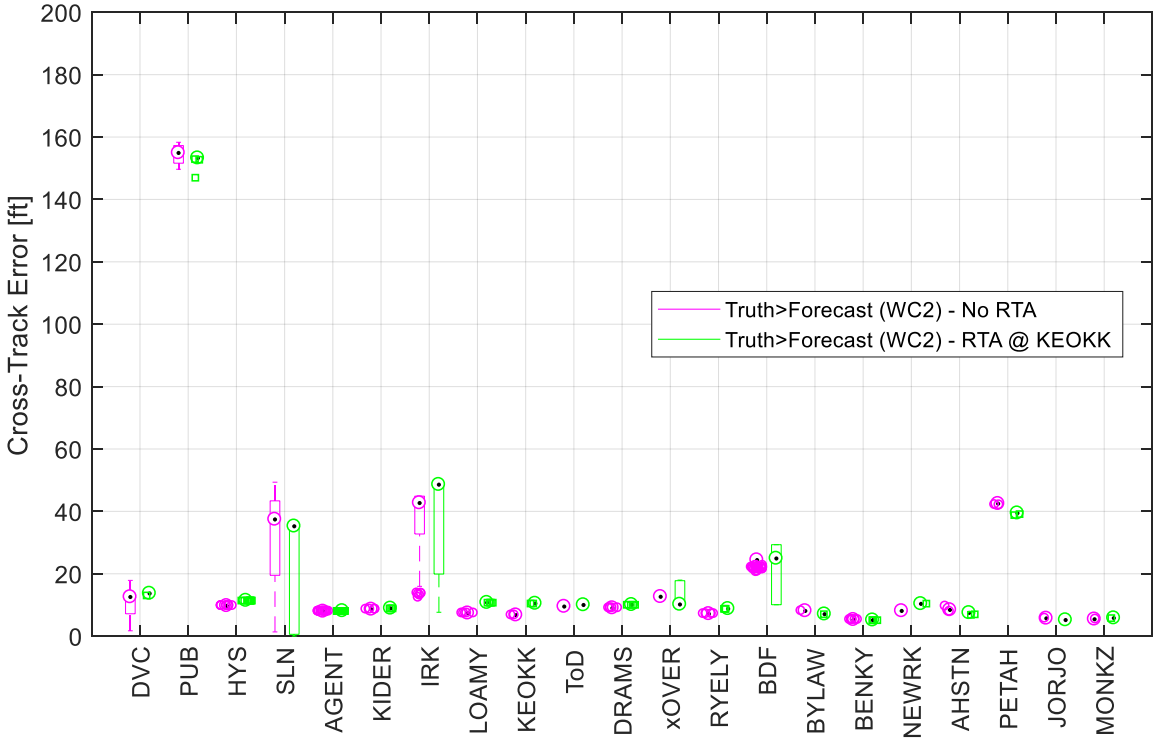

Figure 73. Boxplot of the EPP cross-track error of each point of the medium route with true wind magnitude greater than forecast condition, without RTA (No RTA) and with an RTA (RTA1) in the cruise portion of flight [RL2, RT1, WC2].

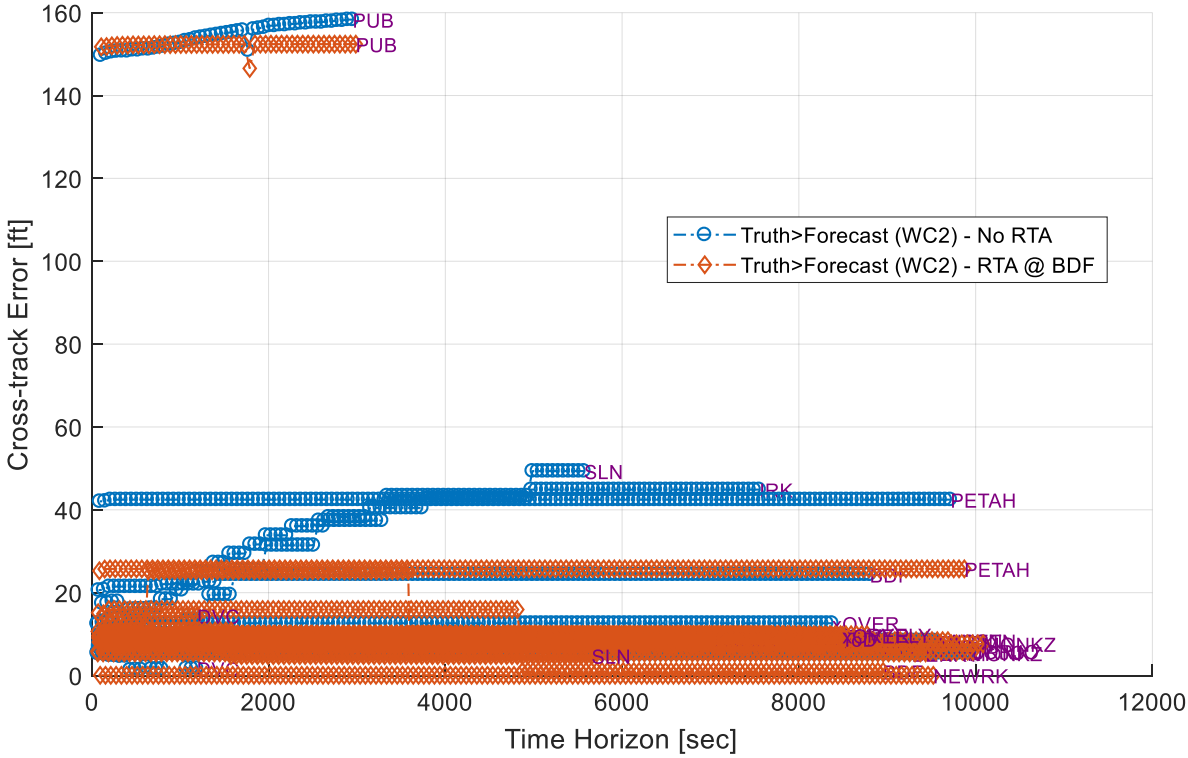

Figure 74. EPP cross-track error for the points of the medium route, with true wind magnitude greater than forecast condition, without RTA (No RTA) and with an RTA (RTA2) just after top-of-descent [RL2, RT1, WC2].

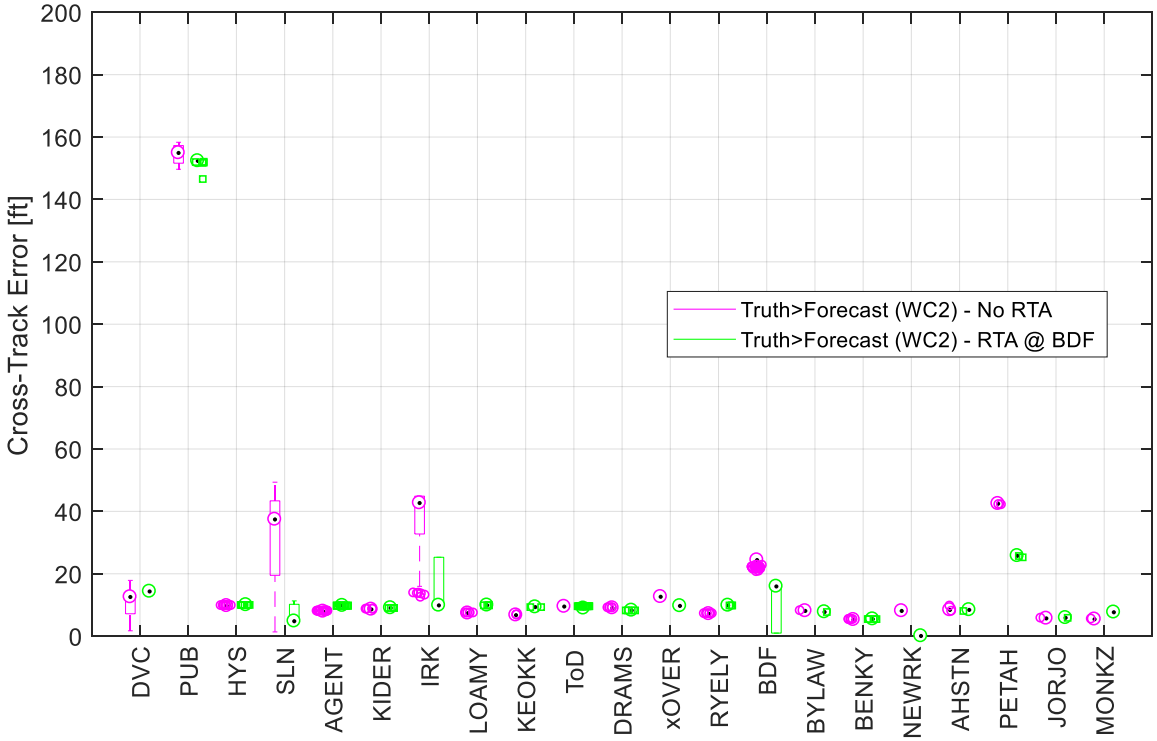

Figure 75. Boxplot of the EPP cross-track error of each point of the medium route with true wind magnitude greater than forecast condition, without RTA (No RTA) and with an RTA (RTA2) just after top-of-descent flight [RL2, RT1, WC2].

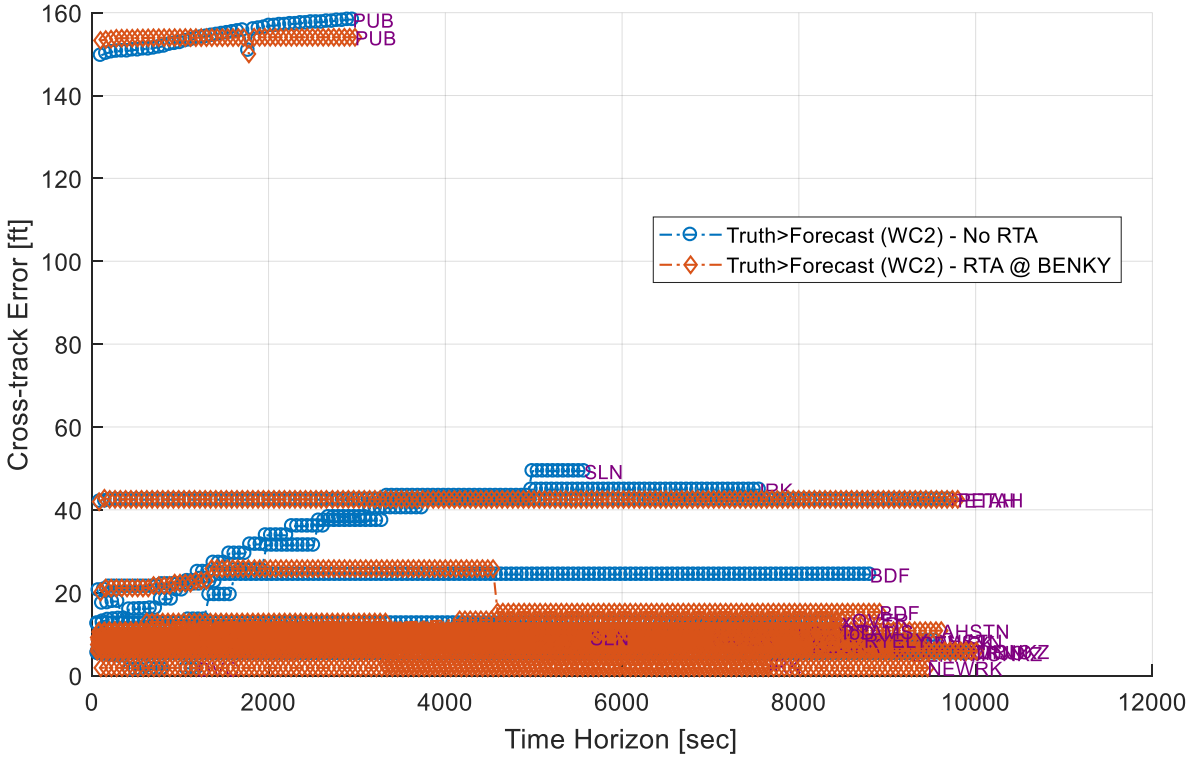

Figure 76. EPP cross-track error for the points of the medium route, with true wind magnitude greater than forecast condition, without RTA (No RTA) and with an RTA (RTA3) in the terminal area [RL2, RT1, WC2].

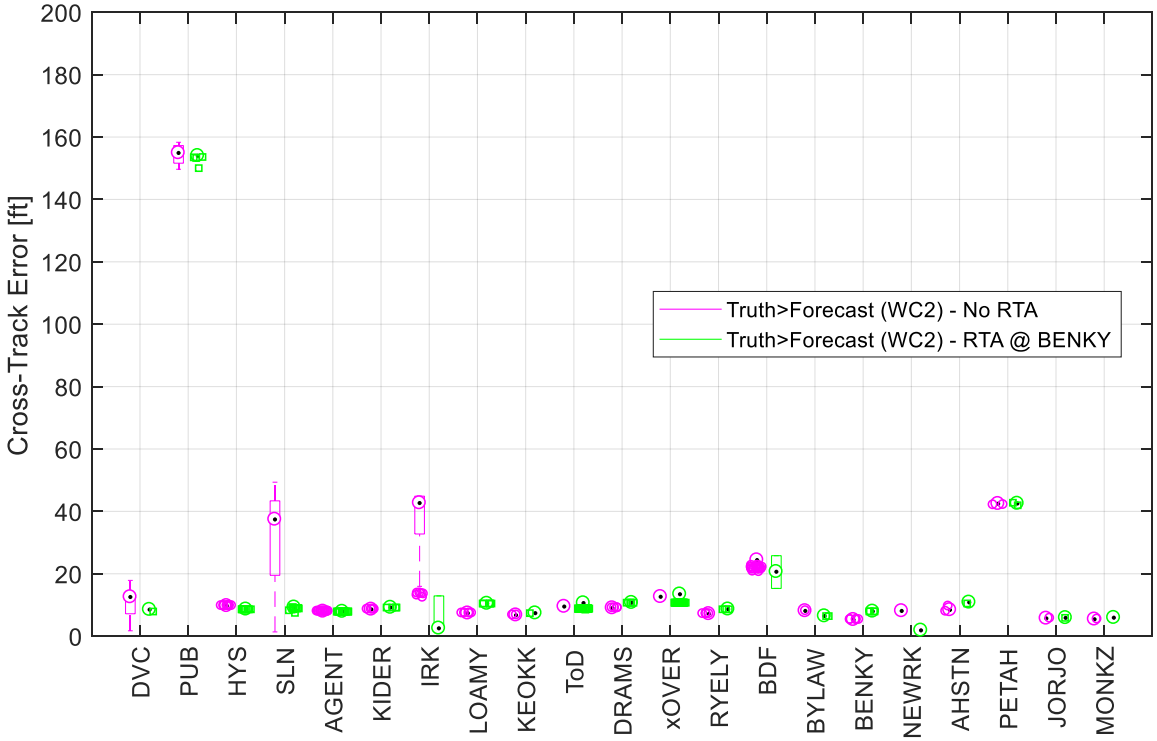

Figure 77. Boxplot of the EPP cross-track error of each point of the medium route with true wind magnitude greater than forecast condition, without RTA (No RTA) and with an RTA (RTA3) in the terminal area [RL2, RT1, WC2].

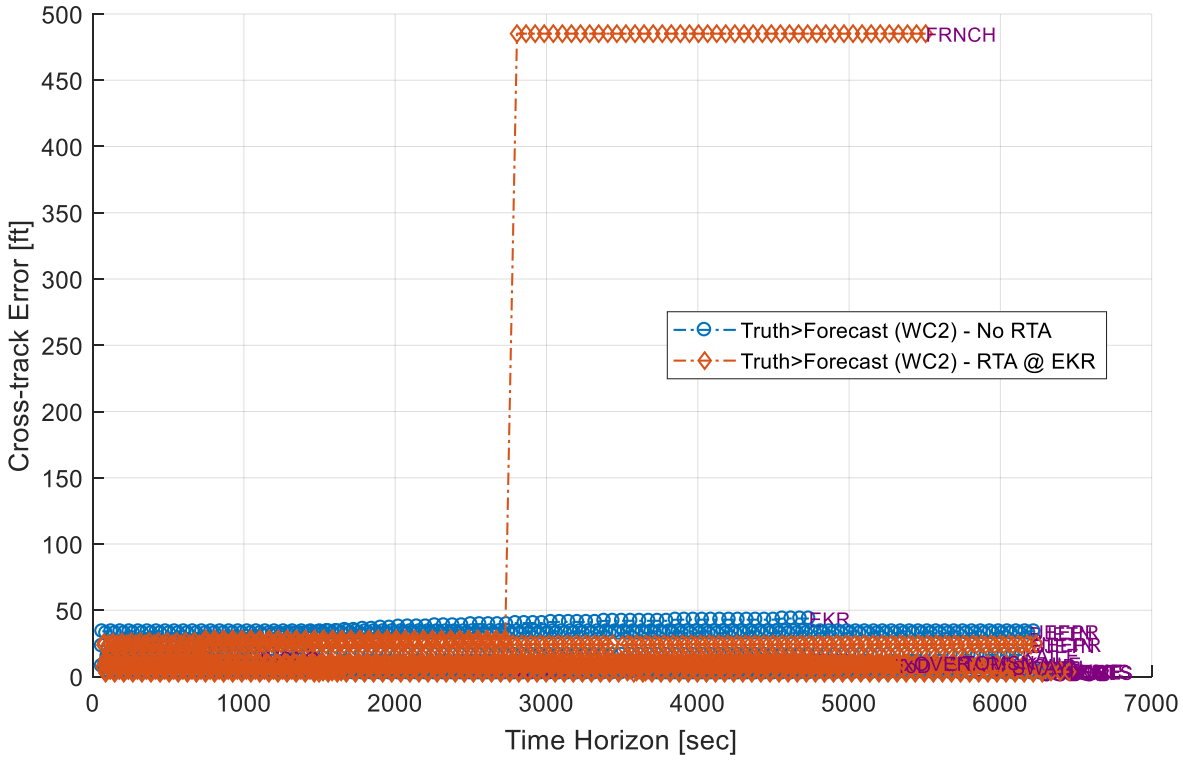

Figure 78. EPP cross-track error for the points of the short route, with true wind magnitude greater than forecast condition, without RTA (No RTA) and with an RTA (RTA1) in the cruise portion of flight [RL3, RT1, WC2].

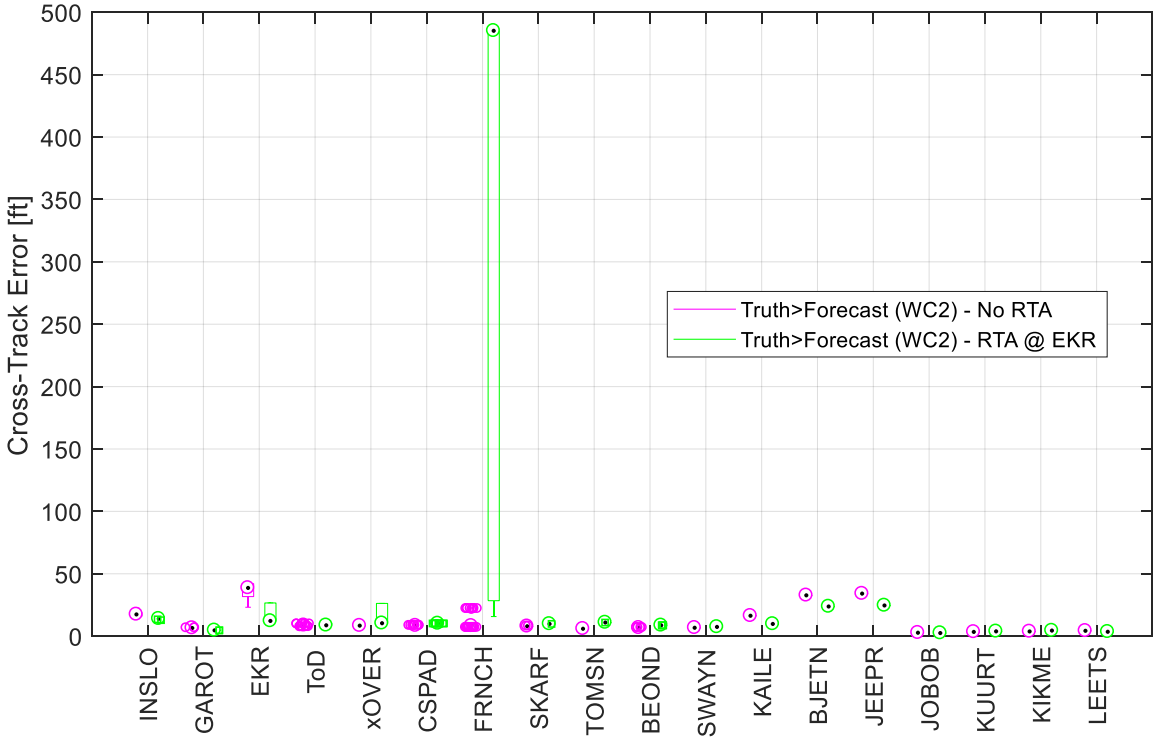

Figure 79. Boxplot of the EPP cross-track error of each point of the short route with true wind magnitude greater than forecast condition, without RTA (No RTA) and with an RTA (RTA1) in the cruise portion of flight [RL3, RT1, WC2].

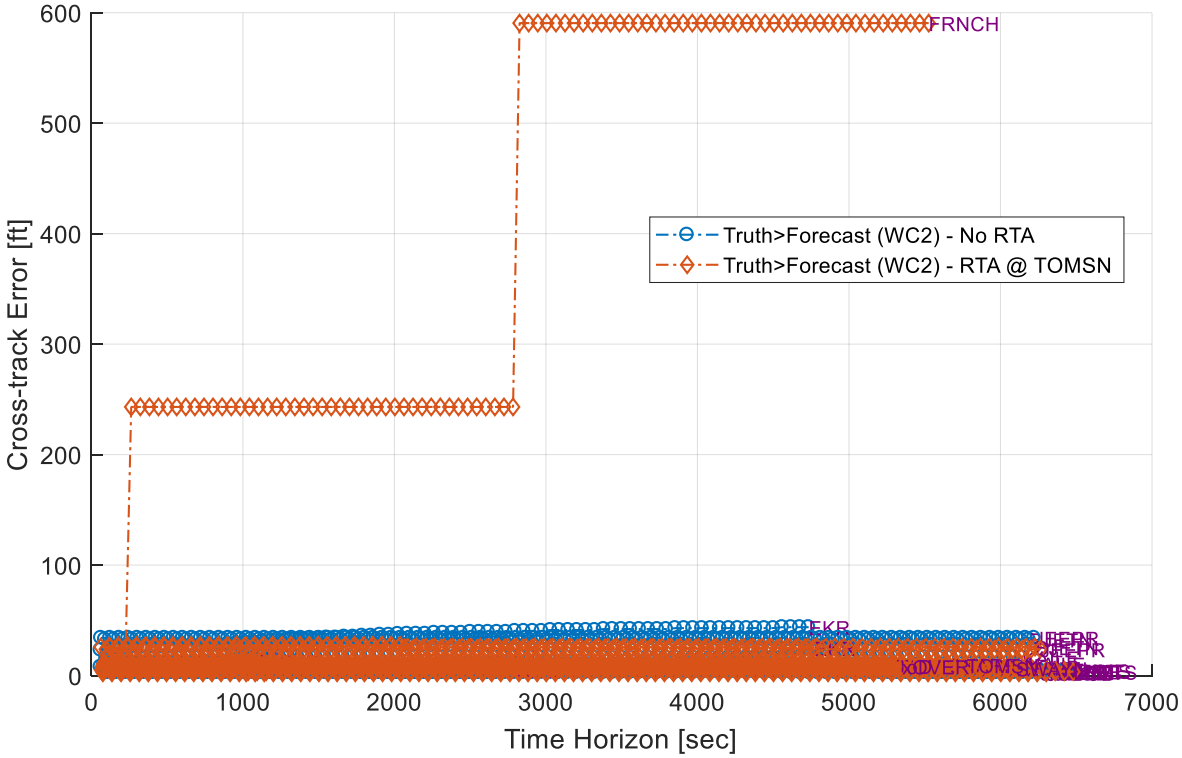

Figure 80. EPP cross-track error for the points of the short route, with true wind magnitude greater than forecast condition, without RTA (No RTA) and with an RTA (RTA2) just after top-of-descent [RL3, RT1, WC2].

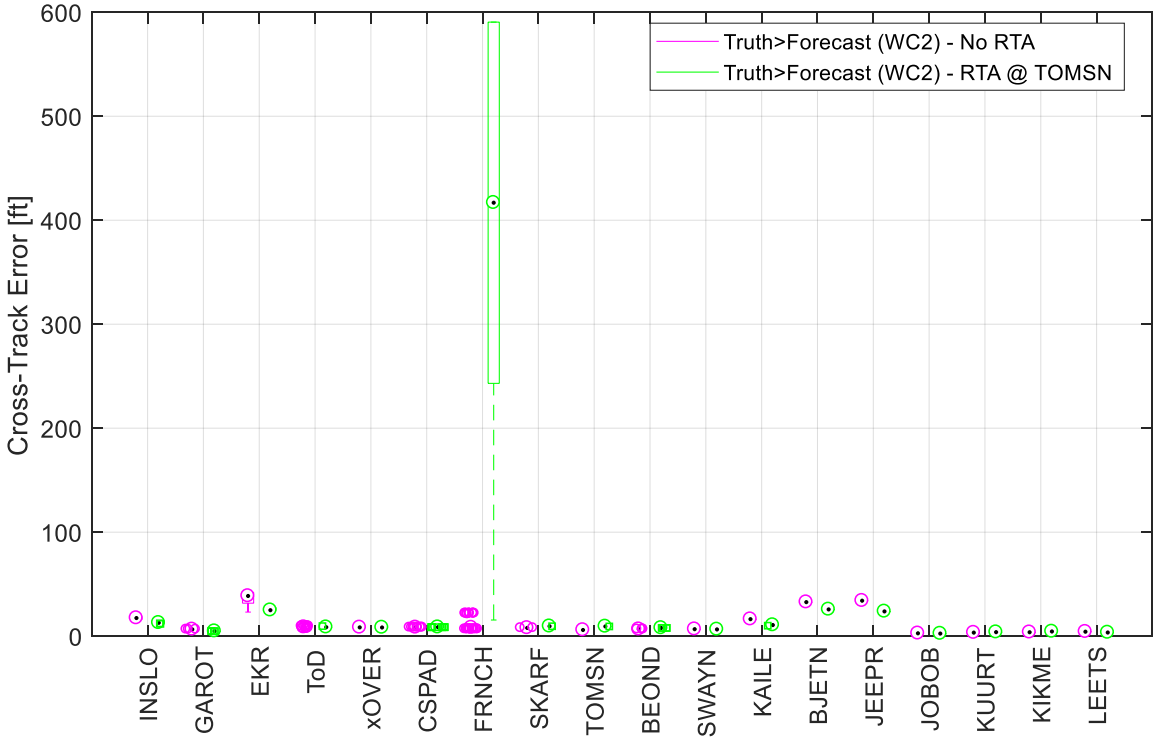

Figure 81. Boxplot of the EPP cross-track error of each point of the short route with true wind magnitude greater than forecast condition, without RTA (No RTA) and with an RTA (RTA2) just after top-of-descent flight [RL3, RT1, WC2].

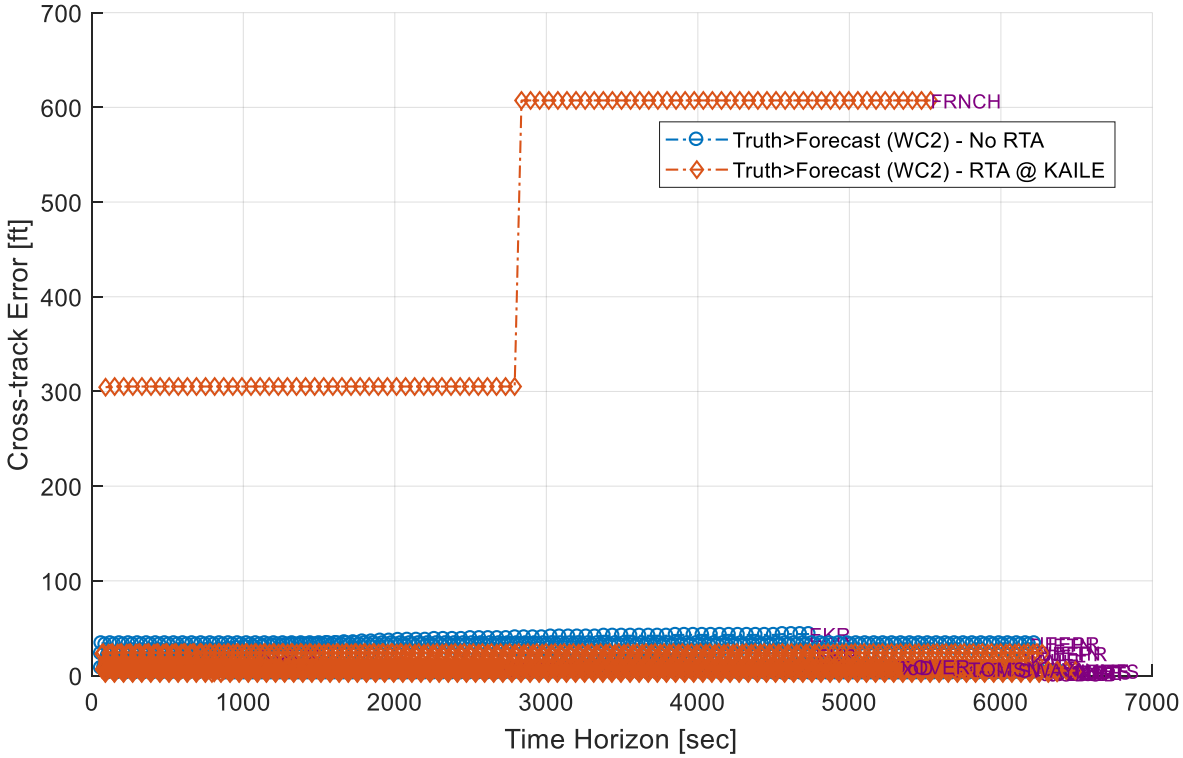

Figure 82. EPP cross-track error for the points of the short route, with true wind magnitude greater than forecast condition, without RTA (No RTA) and with an RTA (RTA3) in the terminal area [RL3, RT1, WC2].

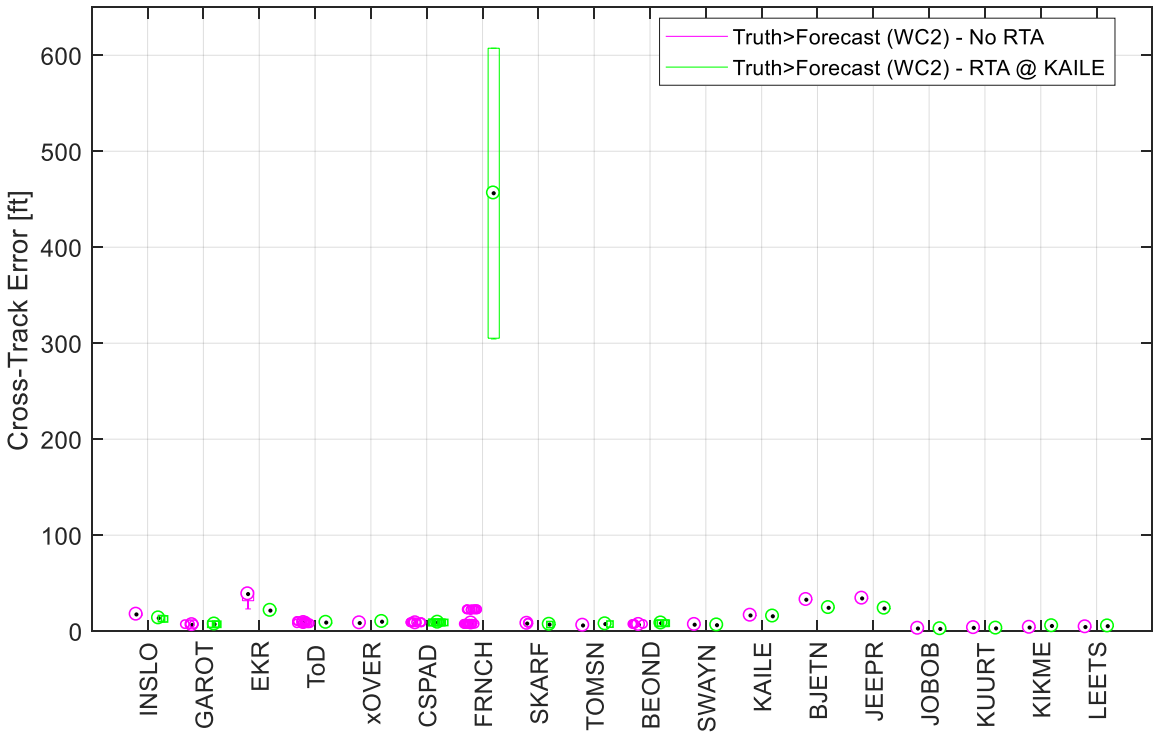

Figure 83. Boxplot of the EPP cross-track error of each point of the short route with true wind magnitude greater than forecast condition, without RTA (No RTA) and with an RTA (RTA3) in the terminal area [RL3, RT1, WC2].

2. *Vertical Error*

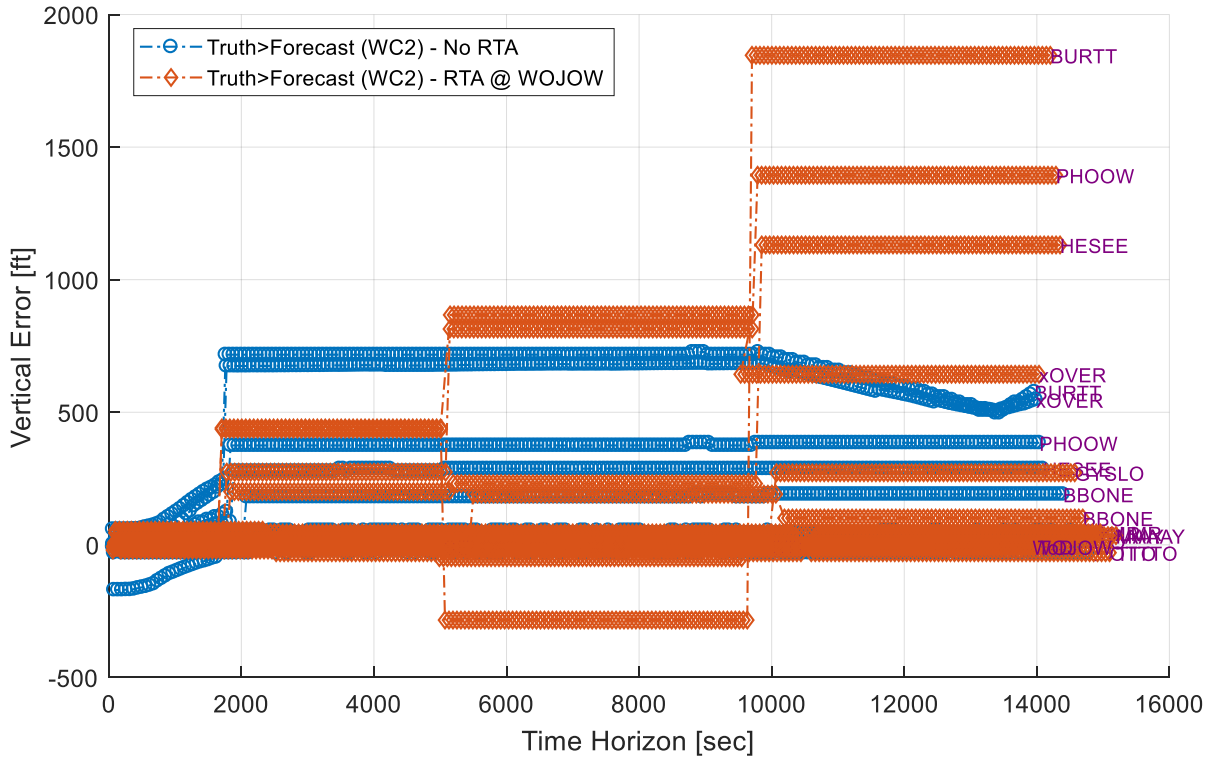

Figure 84. EPP vertical error for the points of the long route, with true wind magnitude greater than forecast condition, without RTA (No RTA) and with an RTA (RTA1) in the cruise portion of flight [RL1, RT1, WC2].

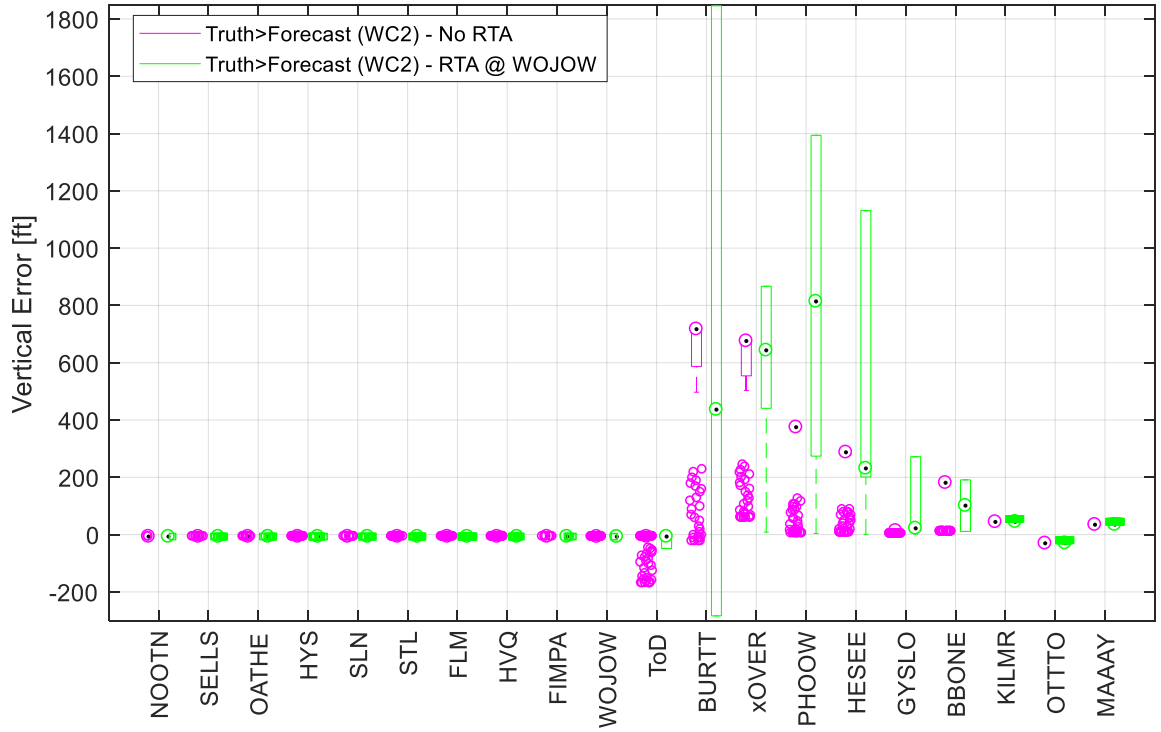

Figure 85. Boxplot of the EPP vertical error of each point of the long route with true wind magnitude greater than forecast condition, without RTA (No RTA) and with an RTA (RTA1) in the cruise phase of flight [RL1, RT1, WC2].

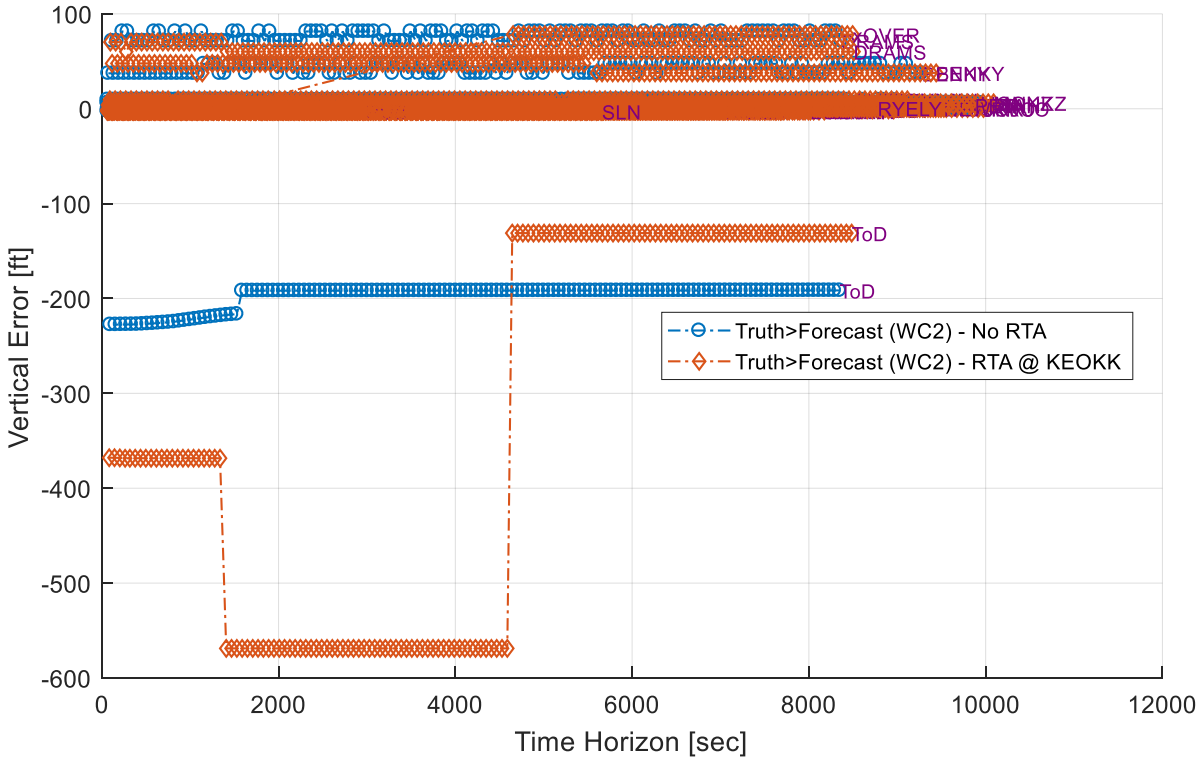

Figure 86. EPP vertical error for the points of the medium route, with true wind magnitude greater than forecast condition, without RTA (No RTA) and with an RTA (RTA1) in the cruise portion of flight [RL2, RT1, WC2].

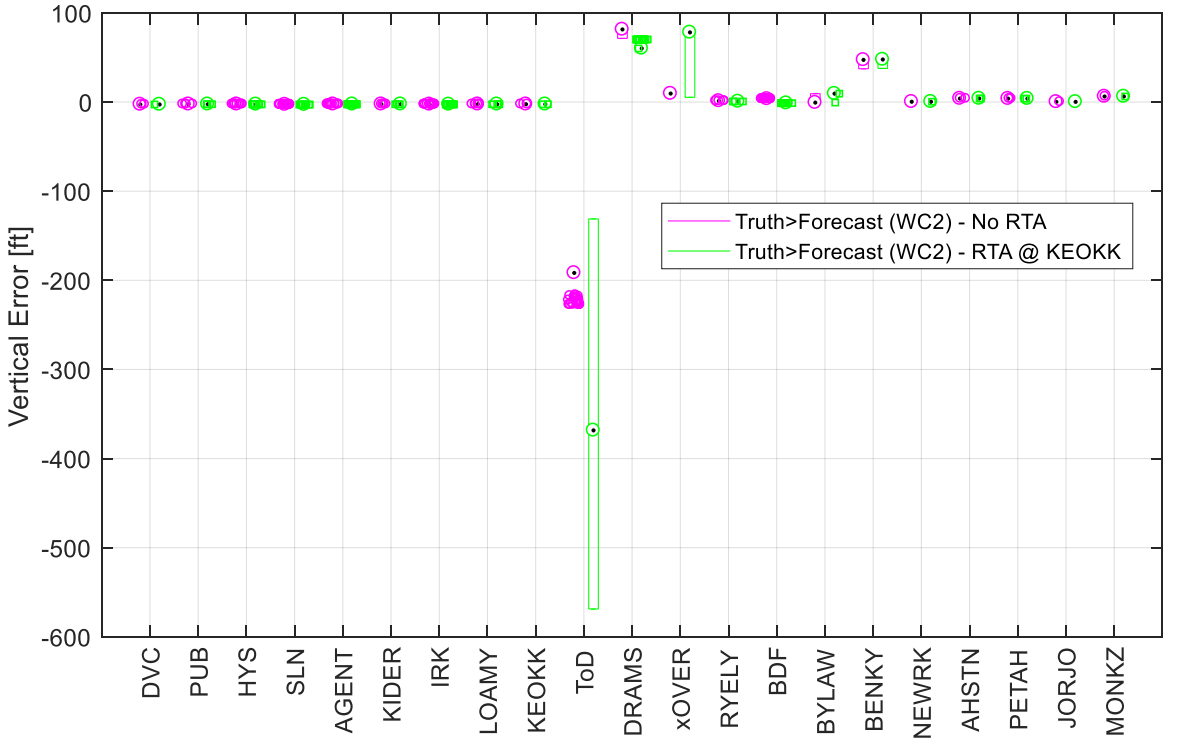

Figure 87. Boxplot of the EPP vertical error of each point of the medium route with true wind magnitude greater than forecast condition, without RTA (No RTA) and with an RTA (RTA1) in the cruise portion of flight [RL2, RT1, WC2].

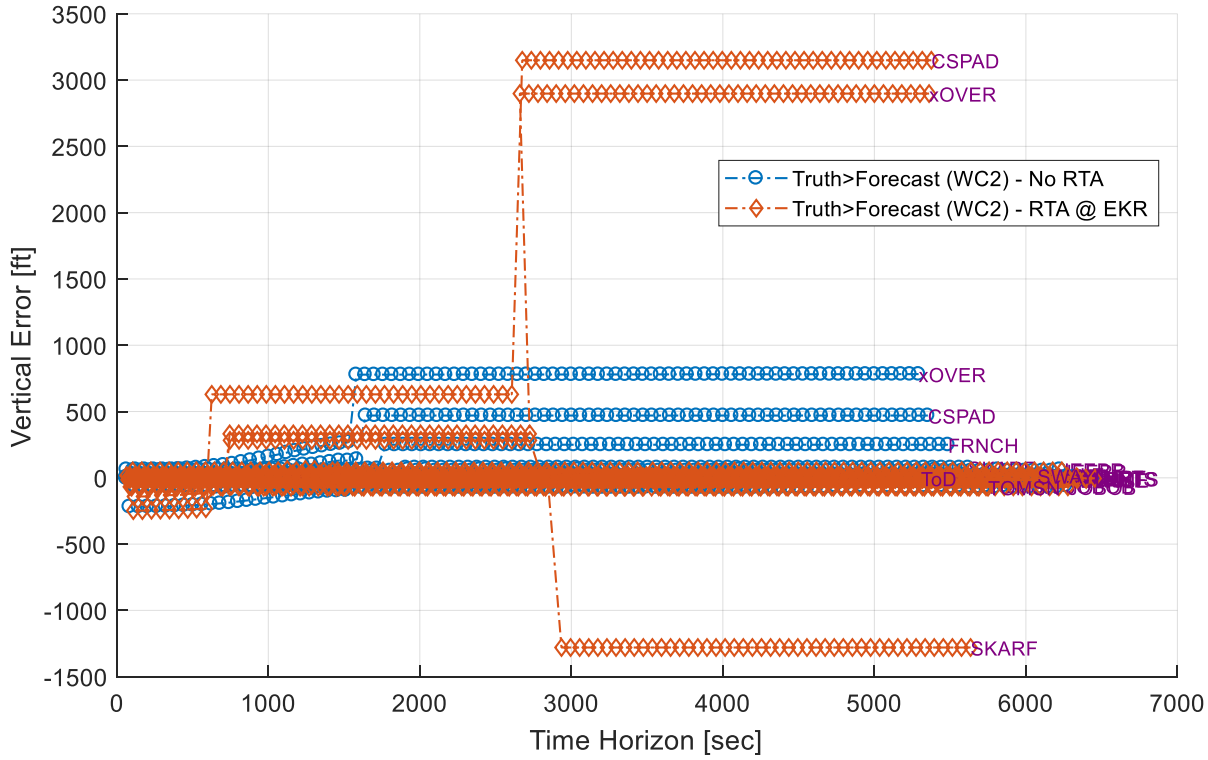

Figure 88. EPP vertical error for the points of the short route, with true wind magnitude greater than forecast condition, without RTA (No RTA) and with an RTA (RTA1) in the cruise portion of flight [RL3, RT1, WC2].

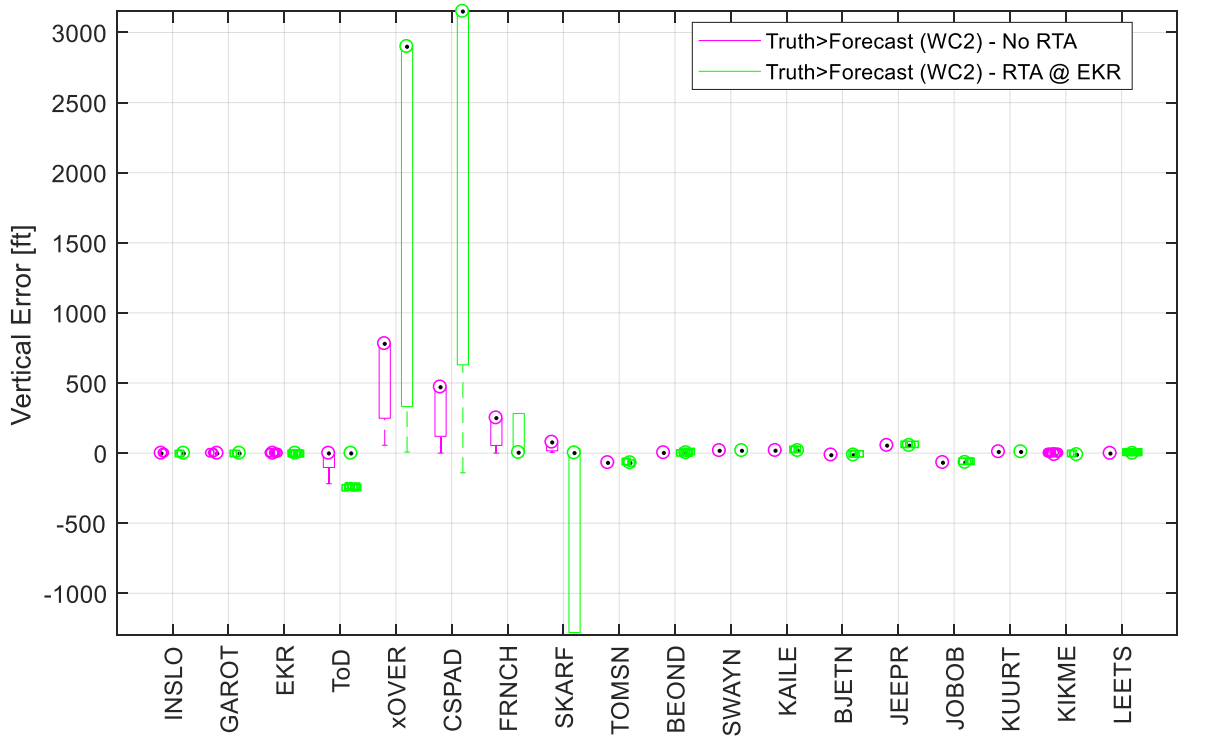

Figure 89. Boxplot of the EPP vertical error of each point of the short route with true wind magnitude greater than forecast condition, without RTA (No RTA) and with an RTA (RTA1) in the cruise portion of flight [RL3, RT1, WC2].

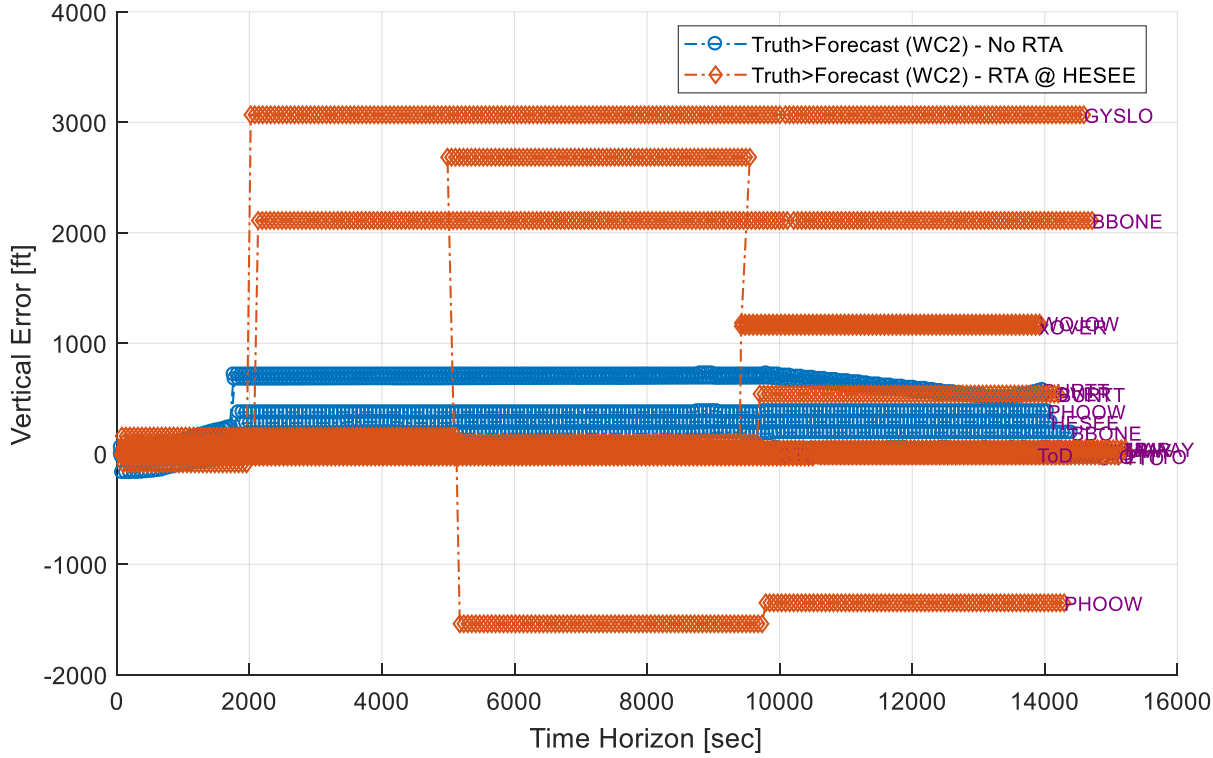

Figure 90. EPP vertical error for the points of the long route, with true wind magnitude greater than forecast condition, without RTA (No RTA) and with an RTA (RTA2) just after top-of-descent [RL1, RT1, WC2].

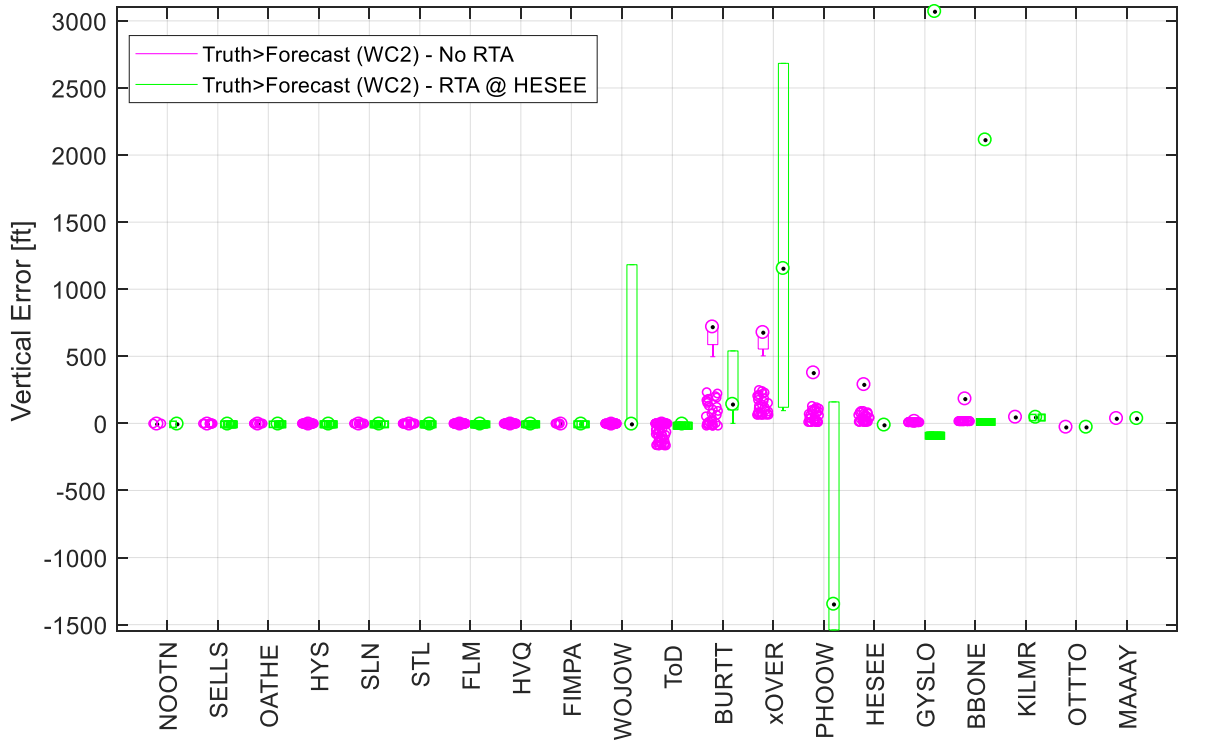

Figure 91. Boxplot of the EPP vertical error of each point of the long route with true wind magnitude greater than forecast condition, without RTA (No RTA) and with an RTA (RTA2) just after top-of-descent [RL1, RT1, WC2].

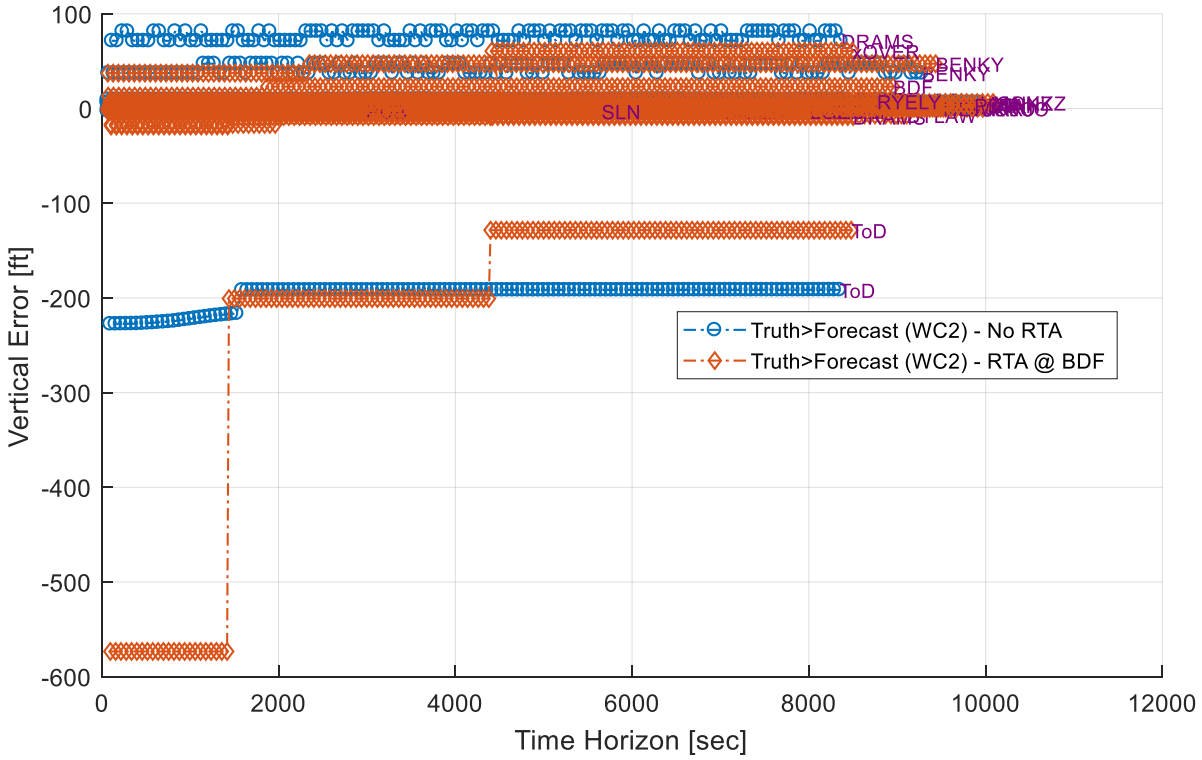

Figure 92. EPP vertical error for the points of the medium route, with true wind magnitude greater than forecast condition, without RTA (No RTA) and with an RTA (RTA2) just after top-of-descent [RL2, RT1, WC2].

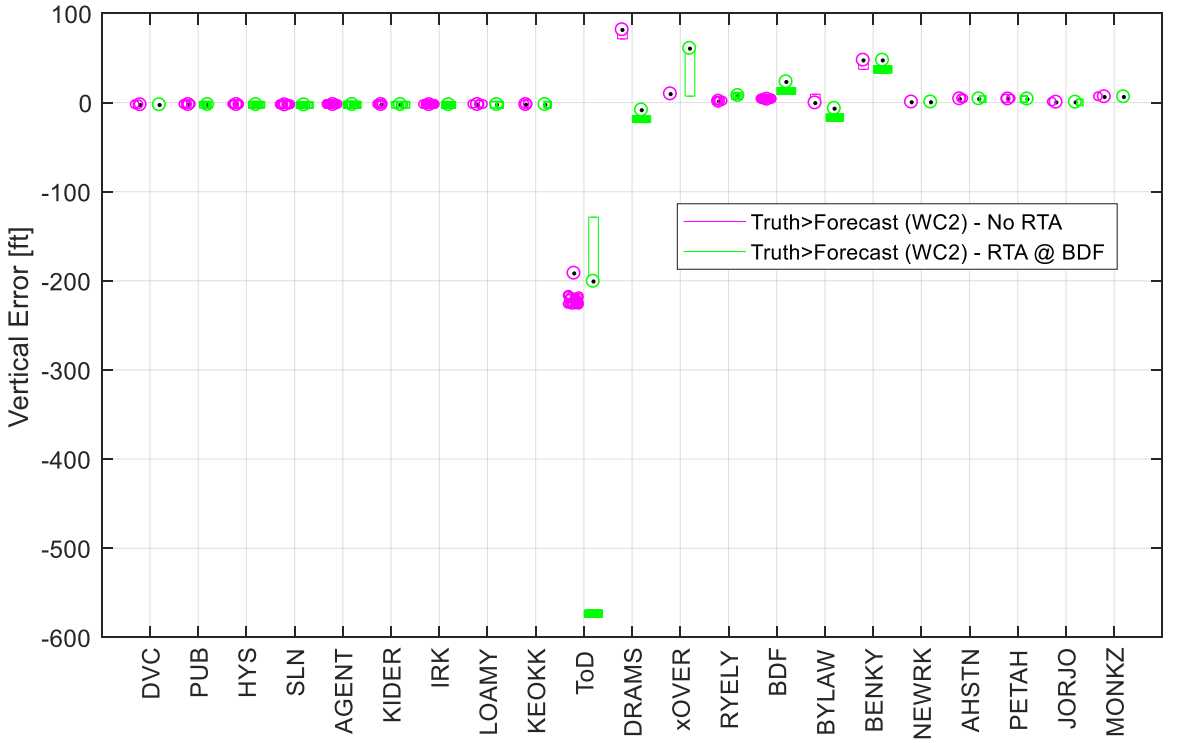

Figure 93. Boxplot of the EPP vertical error of each point of the medium route with true wind magnitude greater than forecast condition, without RTA (No RTA) and with an RTA (RTA2) just after top-of-descent [RL2, RT1, WC2].

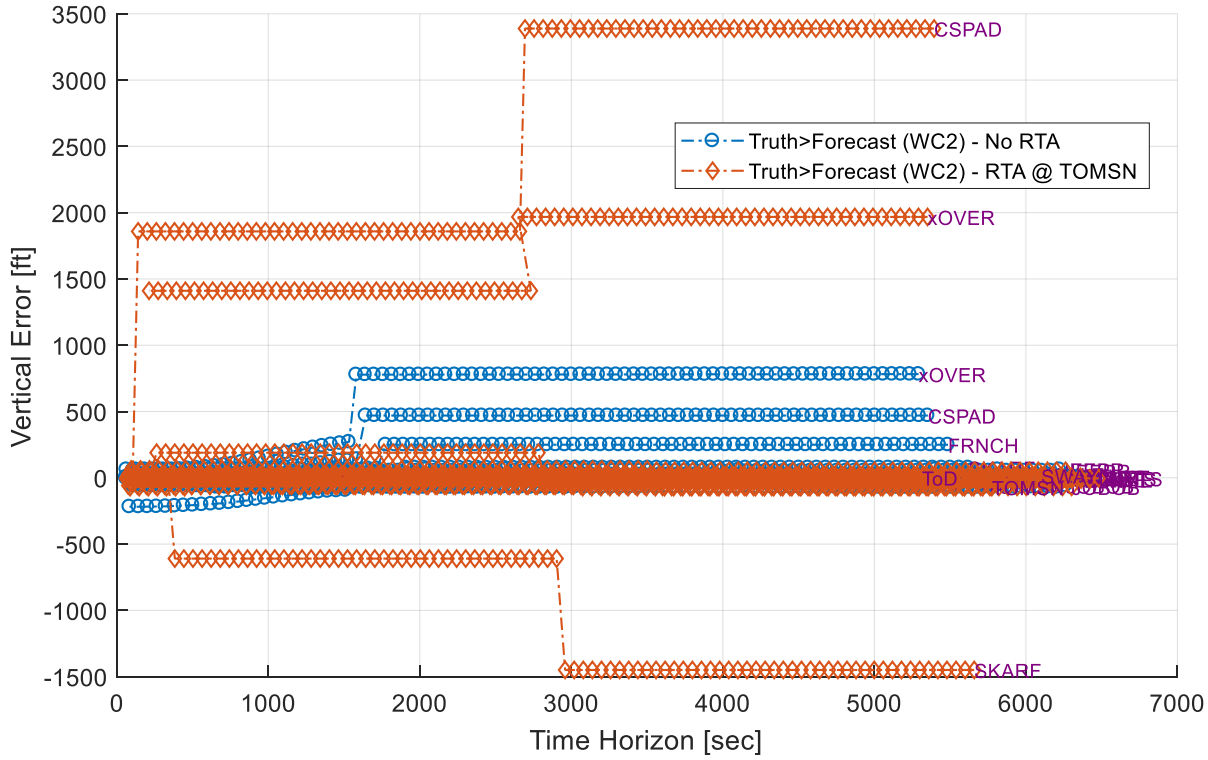

Figure 94. EPP vertical error for the points of the short route, with true wind magnitude greater than forecast condition, without RTA (No RTA) and with an RTA (RTA2) just after top-of-descent [RL3, RT1, WC2].

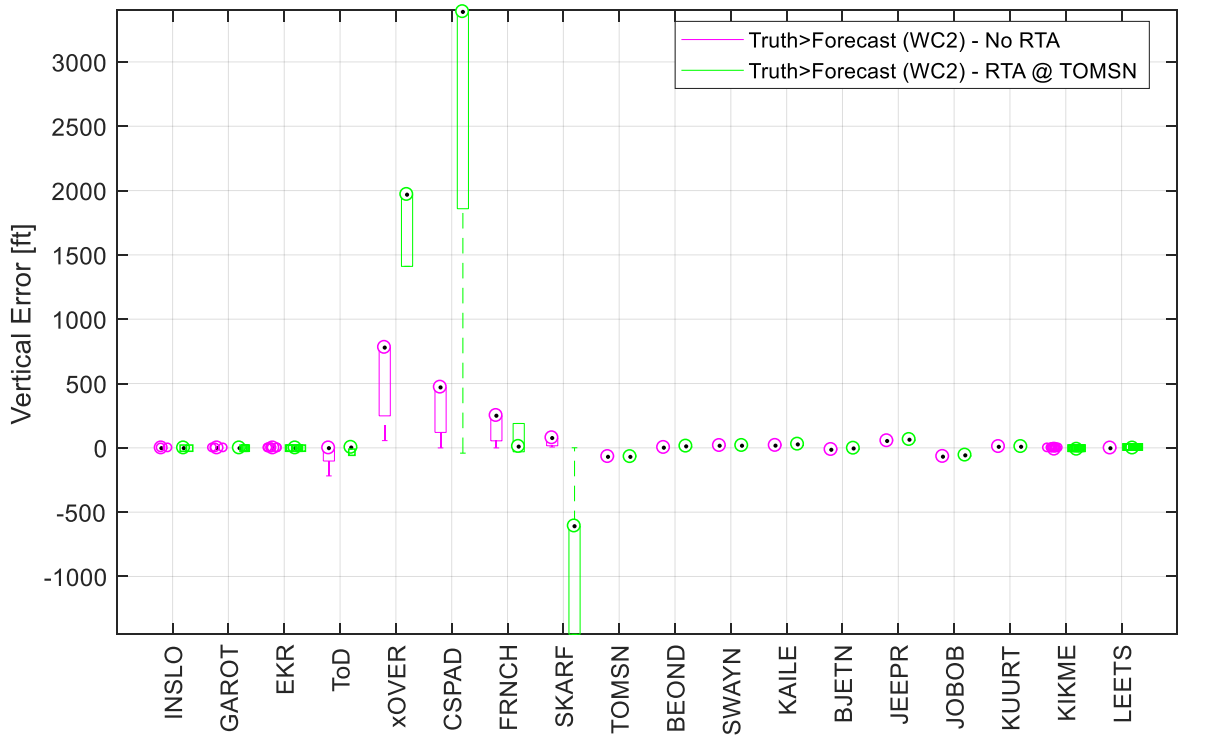

Figure 95. Boxplot of the EPP vertical error of each point of the short route with true wind magnitude greater than forecast condition, without RTA (No RTA) and with an RTA (RTA2) just after top-of-descent flight [RL3, RT1, WC2].

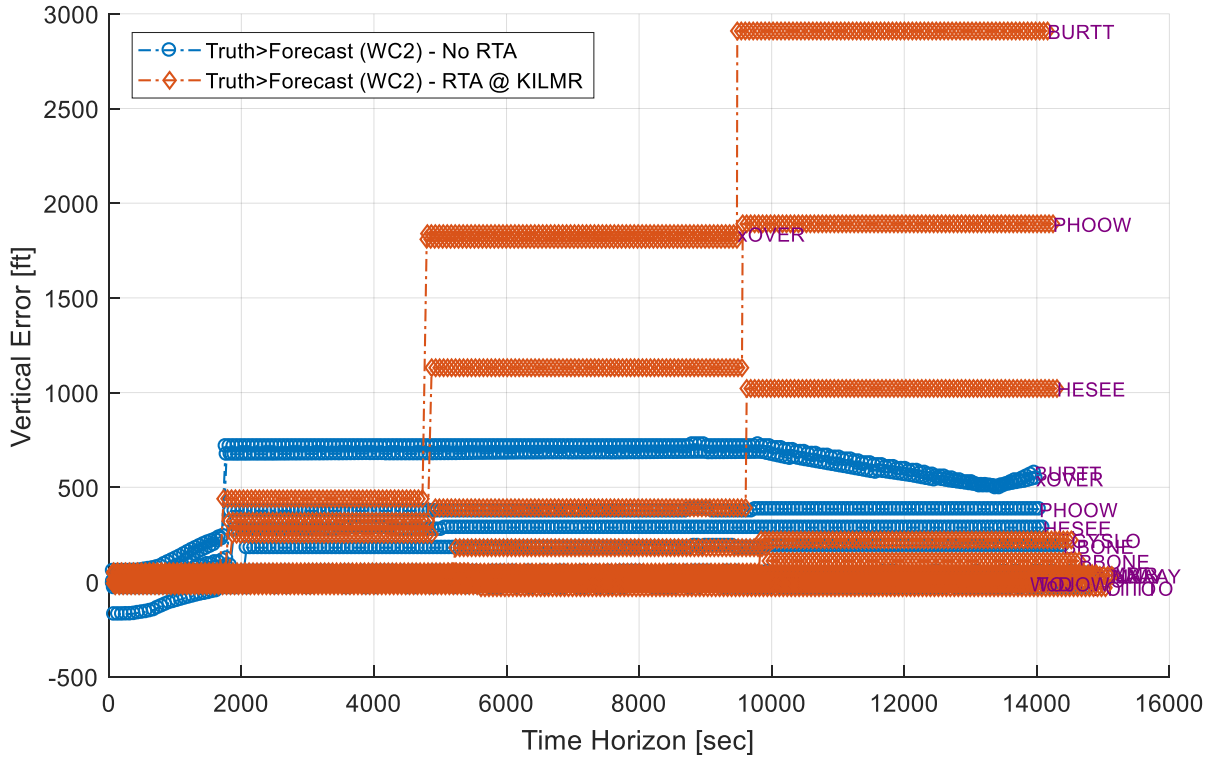

Figure 96. EPP vertical error for the points of the long route, with true wind magnitude greater than forecast condition, without RTA (No RTA) and with an RTA (RTA3) in the terminal area [RL1, RT1, WC2].

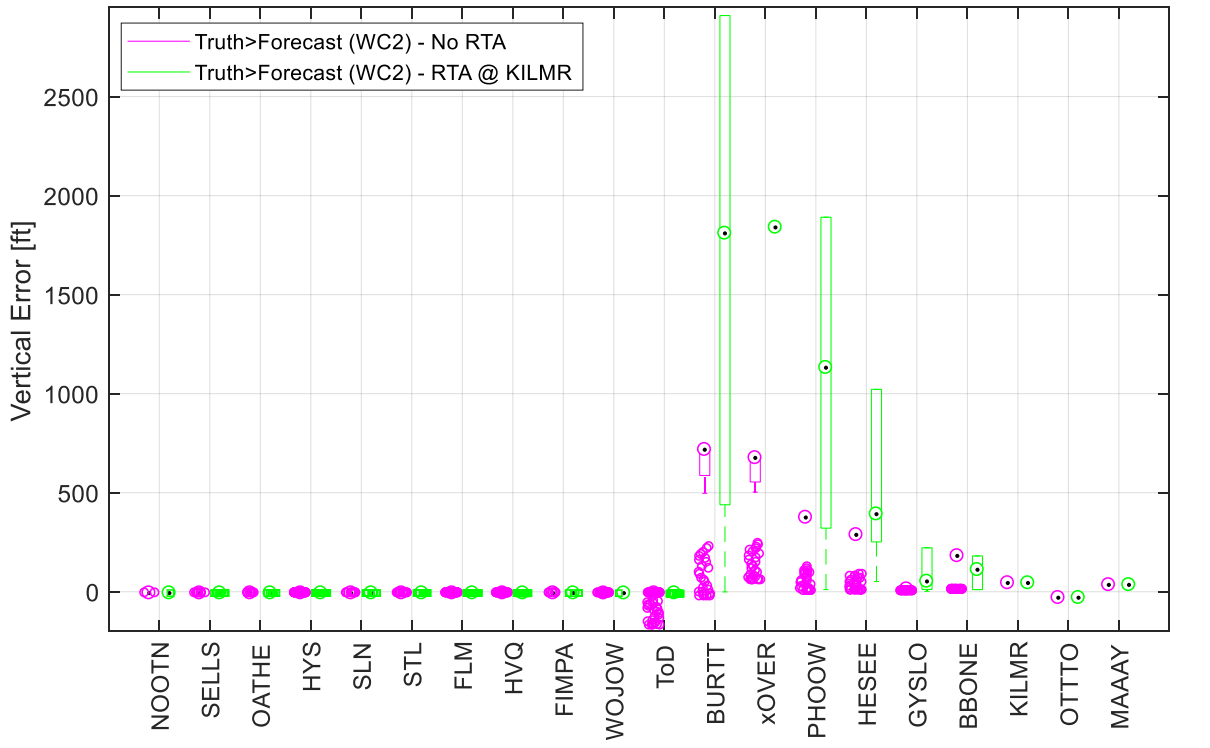

Figure 97. Boxplot of the EPP vertical error of each point of the long route with true wind magnitude greater than forecast condition, without RTA (No RTA) and with an RTA (RTA3) in the terminal area [RL1, RT1, WC2].

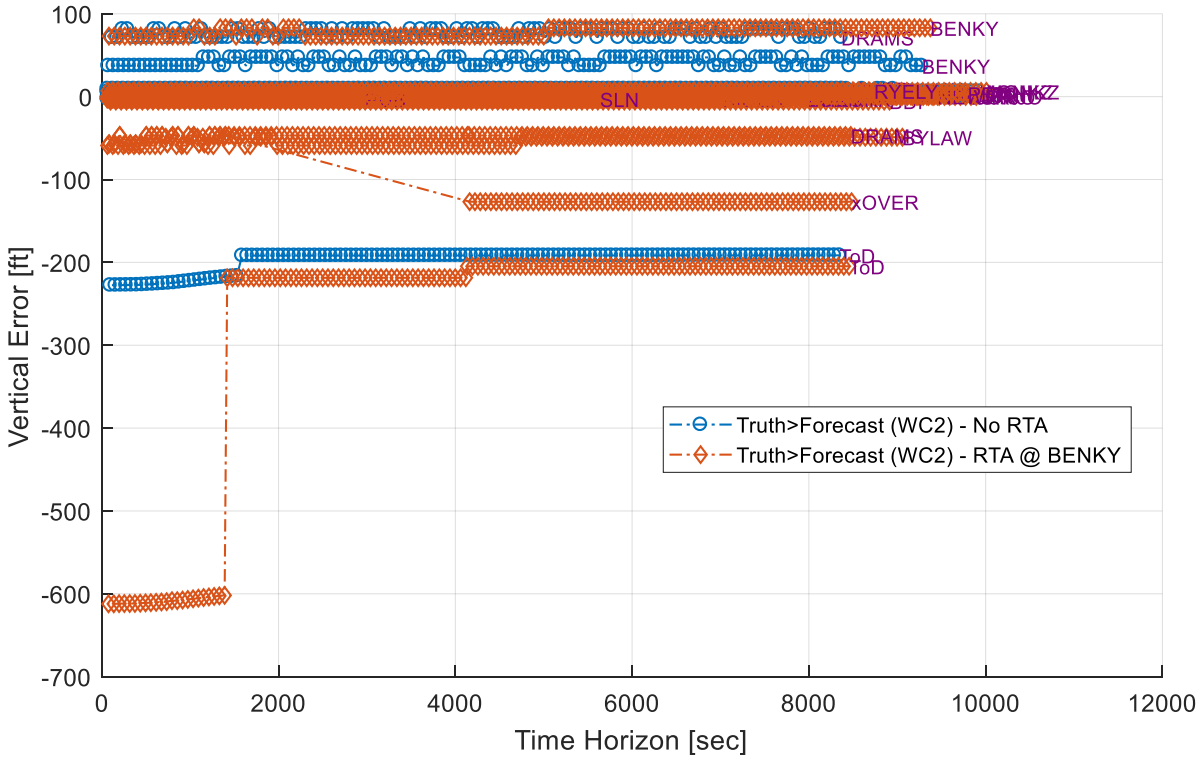

Figure 98. EPP vertical error for the points of the medium route, with true wind magnitude greater than forecast condition, without RTA (No RTA) and with an RTA (RTA3) in the terminal area [RL2, RT1, WC2].

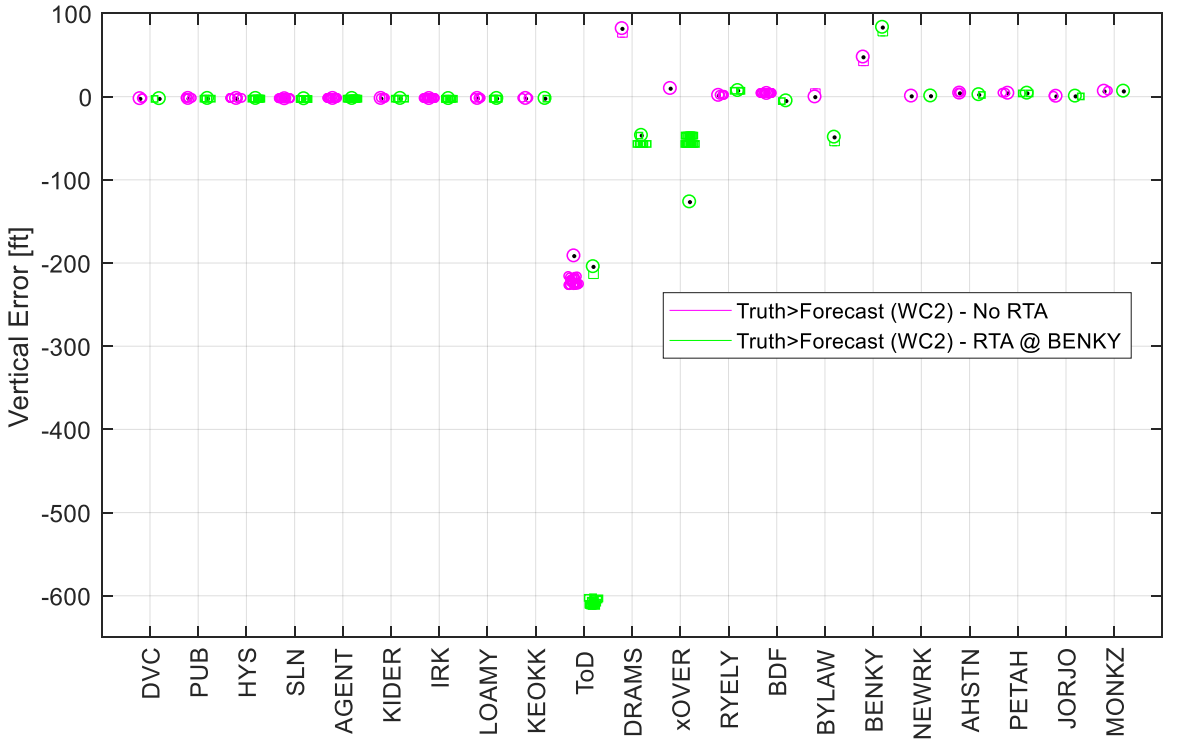

Figure 99. Boxplot of the EPP vertical error of each point of the medium route with true wind magnitude greater than forecast condition, without RTA (No RTA) and with an RTA (RTA3) in the terminal area [RL2, RT1, WC2].

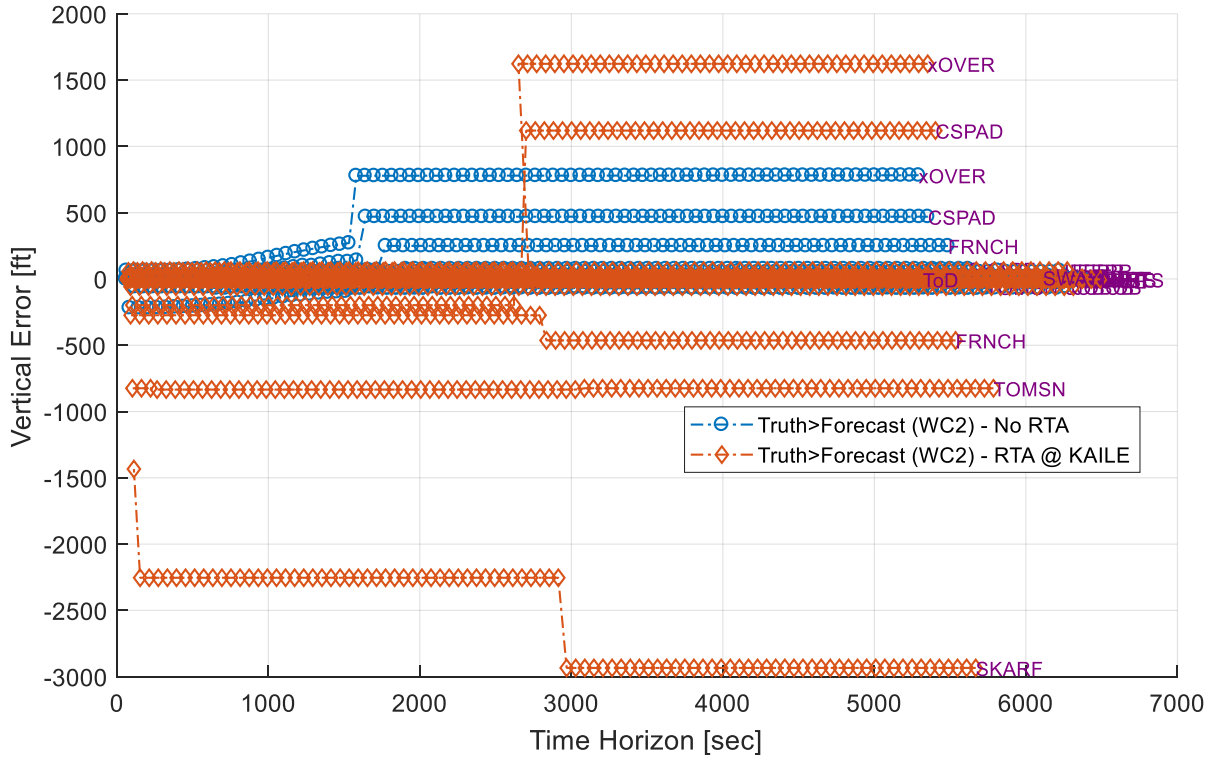

Figure 100. EPP vertical error for the points of the short route, with true wind magnitude greater than forecast condition, without RTA (No RTA) and with an RTA (RTA3) in the terminal area [RL3, RT1, WC2].

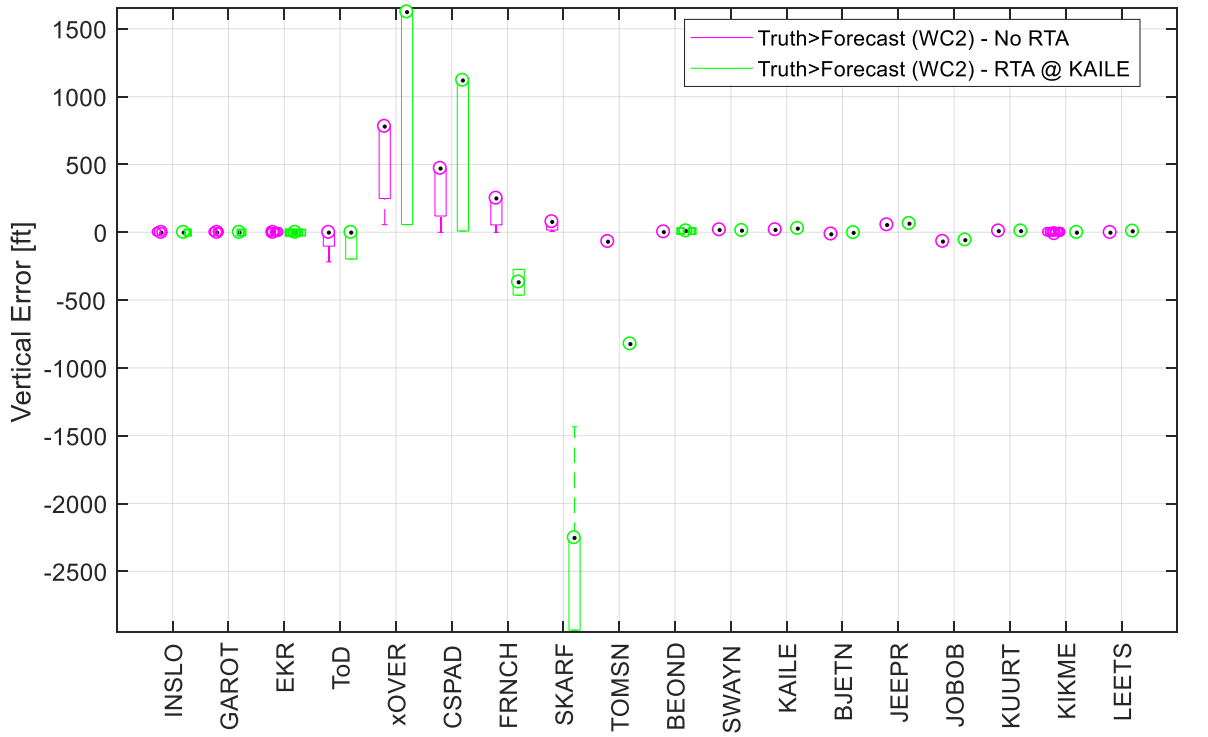

Figure 101. Boxplot of the EPP vertical error of each point of the short route with true wind magnitude greater than forecast condition, without RTA (No RTA) and with an RTA (RTA3) in the terminal area [RL3, RT1, WC2].

3. Time Error

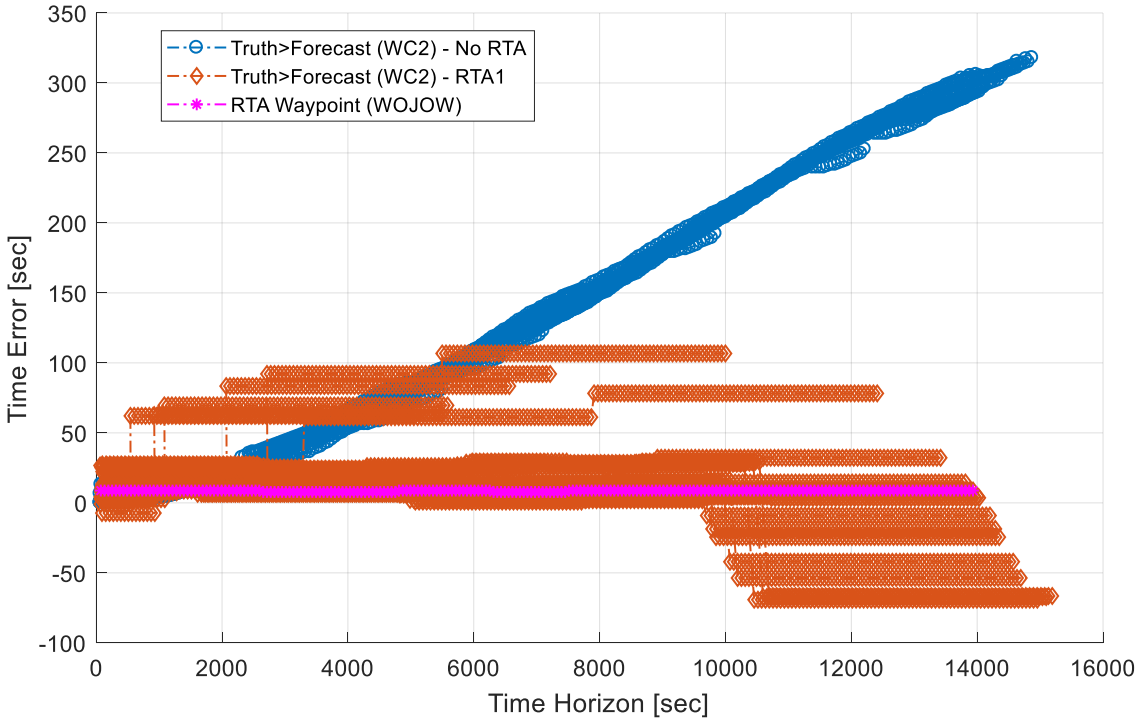

Figure 102. Time error for EPP points of the long route, true wind magnitude greater than forecast condition, without RTA (No RTA) and with an RTA (RTA1) in the cruise phase of flight [RL1, RT1, WC2].

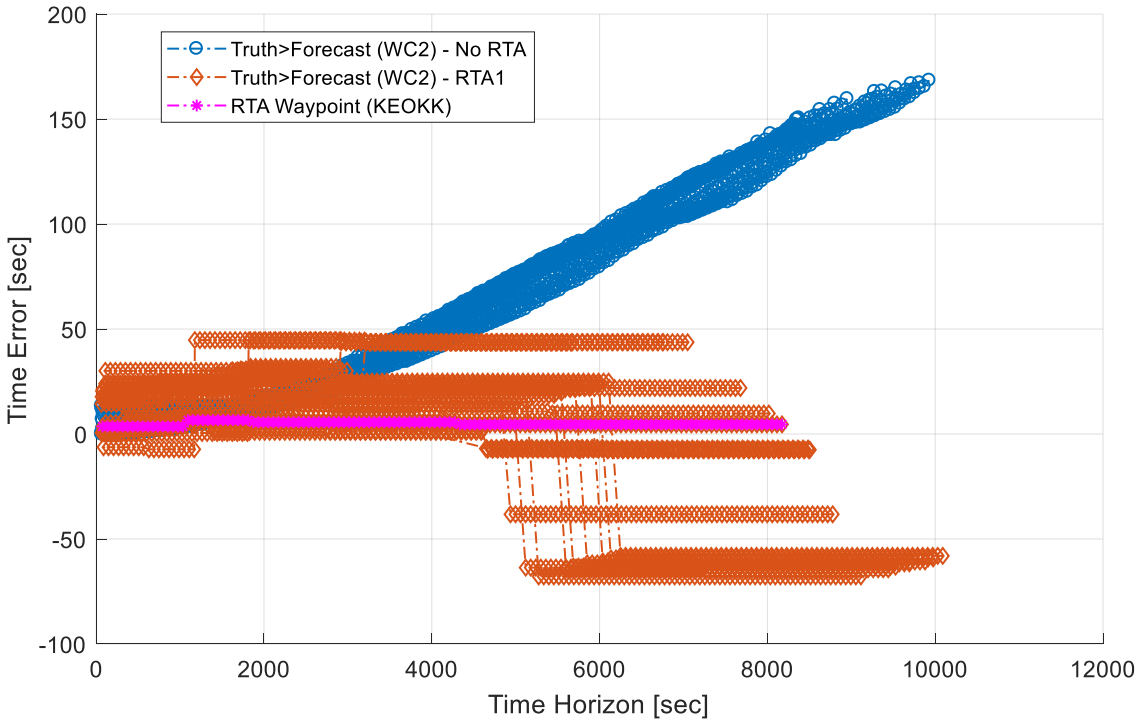

Figure 103. Time error for EPP points of the medium route, true wind magnitude greater than forecast condition, without RTA (No RTA) and with an RTA (RTA1) in the cruise phase of flight [RL2, RT1, WC2].

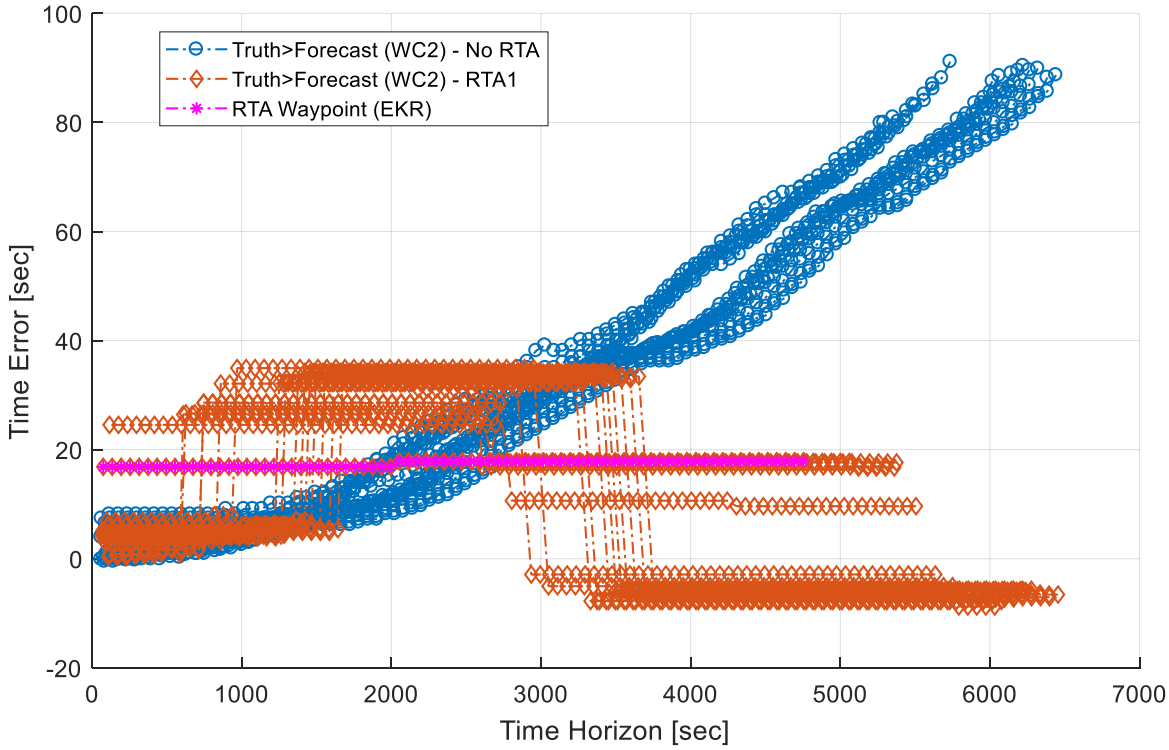

Figure 104. Time error for EPP points of the short route, true wind magnitude greater than forecast condition, without RTA (No RTA) and with an RTA (RTA1) in the cruise phase of flight [RL3, RT1, WC2].

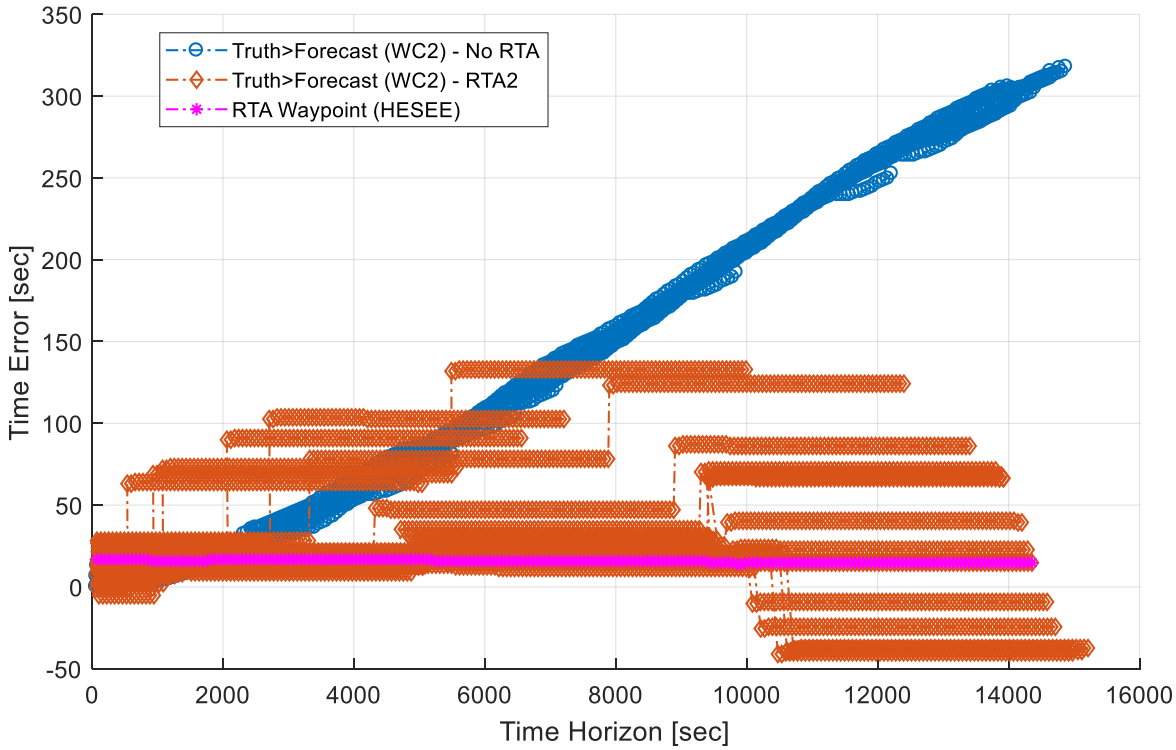

Figure 105. Time error for EPP points of the long route, true wind magnitude greater than forecast condition, without RTA (No RTA) and with an RTA (RTA2) in just after the top-of-descent [RL1, RT1, WC2].

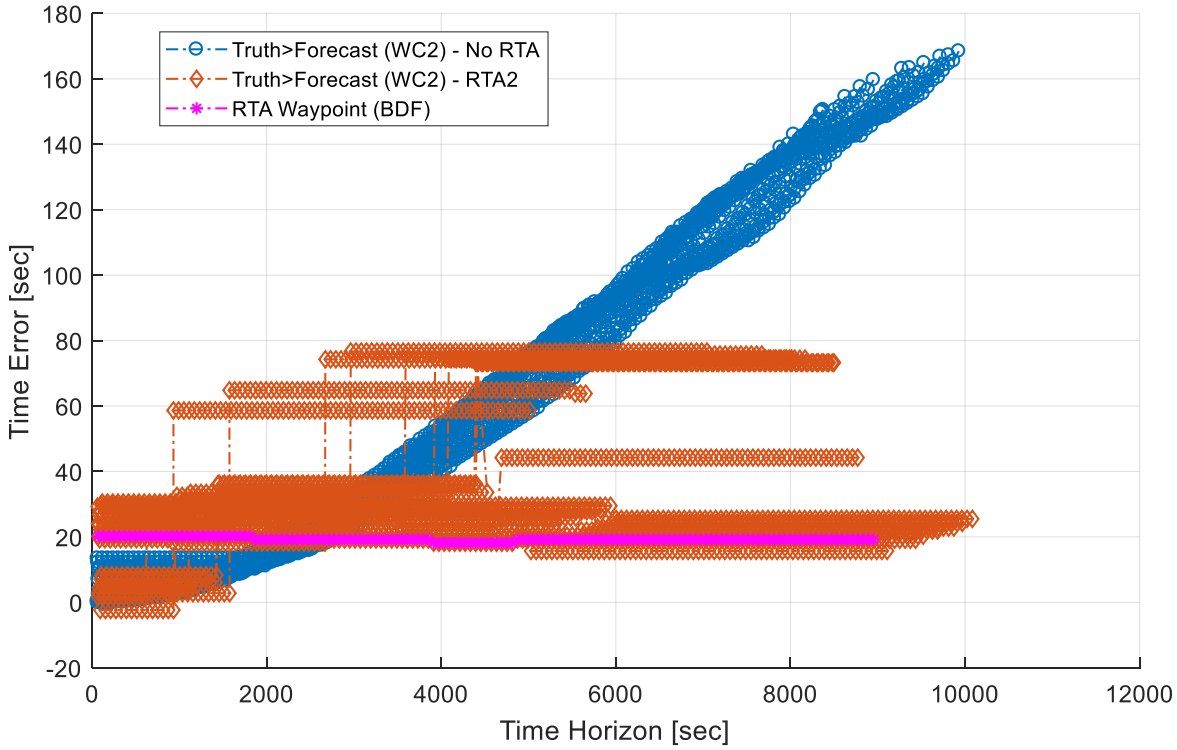

Figure 106. Time error for EPP points of the medium route, true wind magnitude greater than forecast condition, without RTA (No RTA) and with an RTA (RTA2) in just after the top-of-descent [RL2, RT1, WC2].

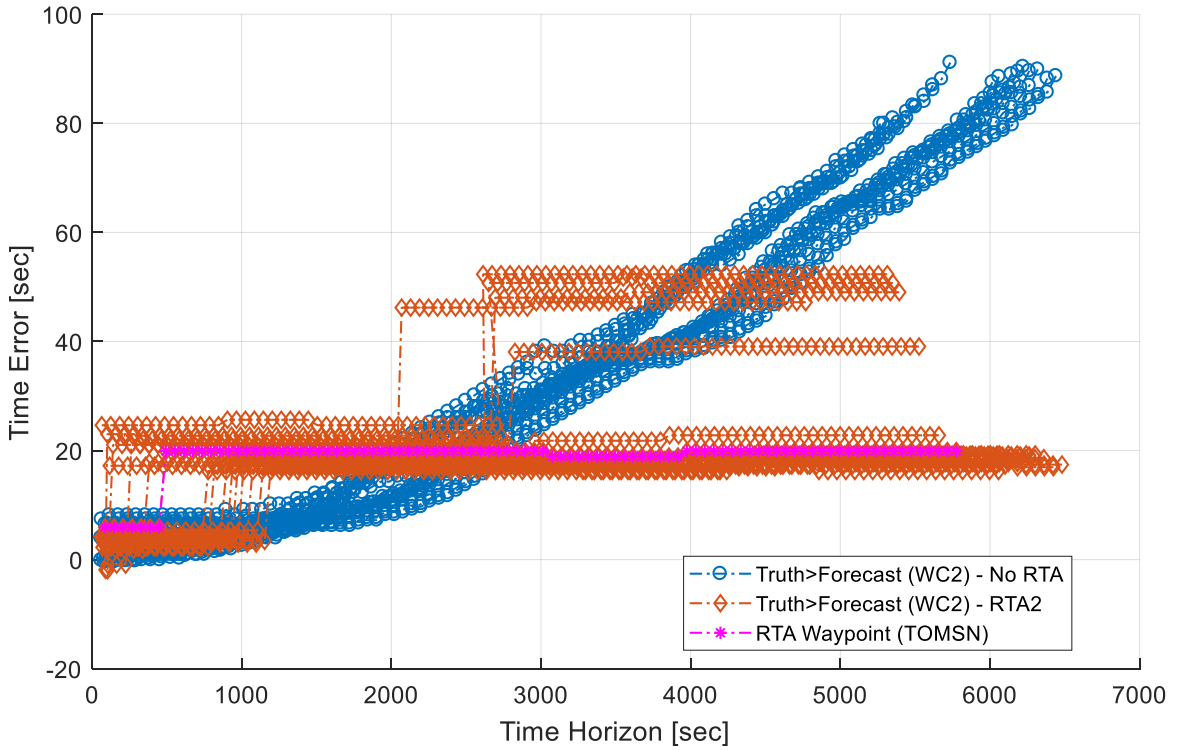

Figure 107. Time error for EPP points of the short route, true wind magnitude greater than forecast condition, without RTA (No RTA) and with an RTA (RTA2) in just after the top-of-descent [RL3, RT1, WC2].

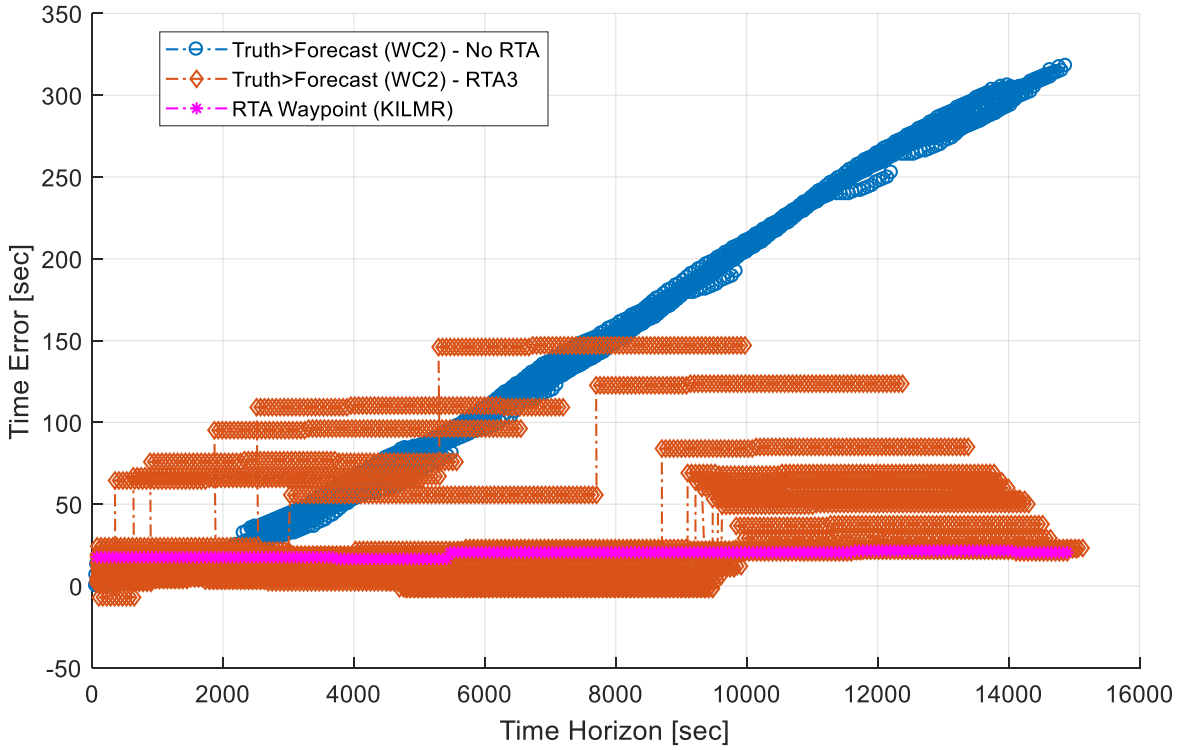

Figure 108. Time error for EPP points of the long route, true wind magnitude greater than forecast condition, without RTA (No RTA) and with an RTA (RTA3) close to the terminal area [RL1, RT1, WC2].

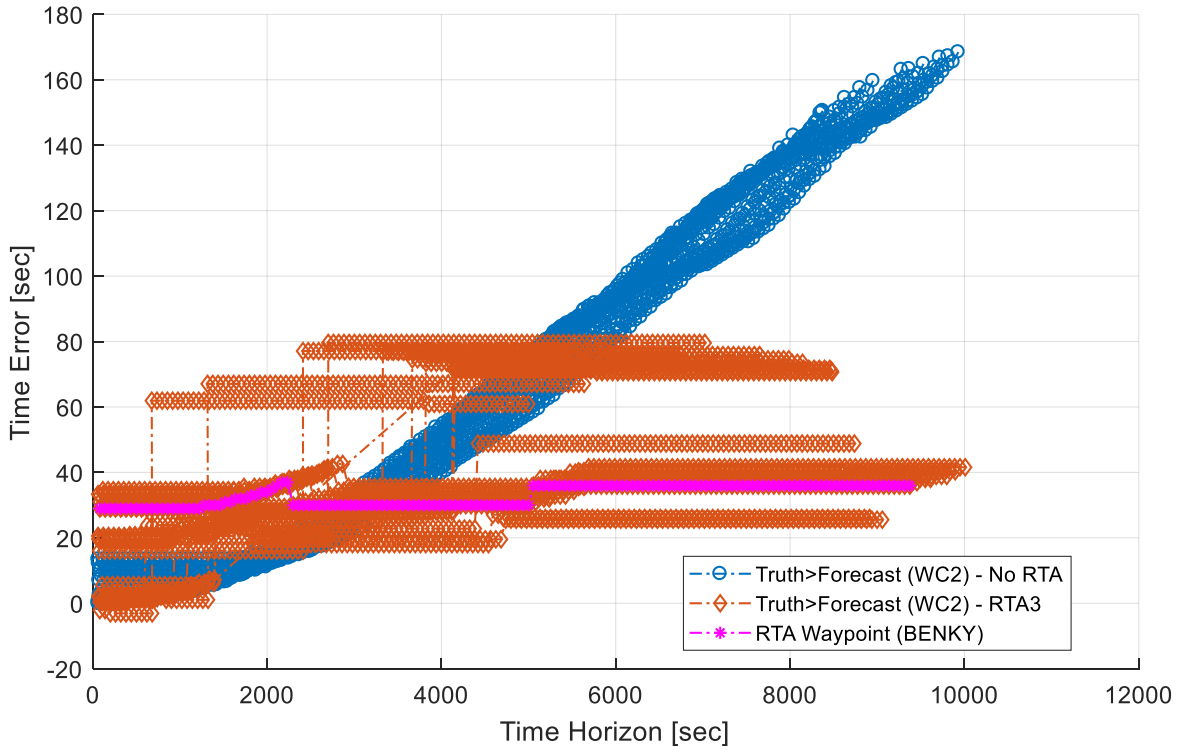

Figure 109. Time error for EPP points of the medium route, true wind magnitude greater than forecast condition, without RTA (No RTA) and with an RTA (RTA3) close to the terminal area [RL2, RT1, WC2].

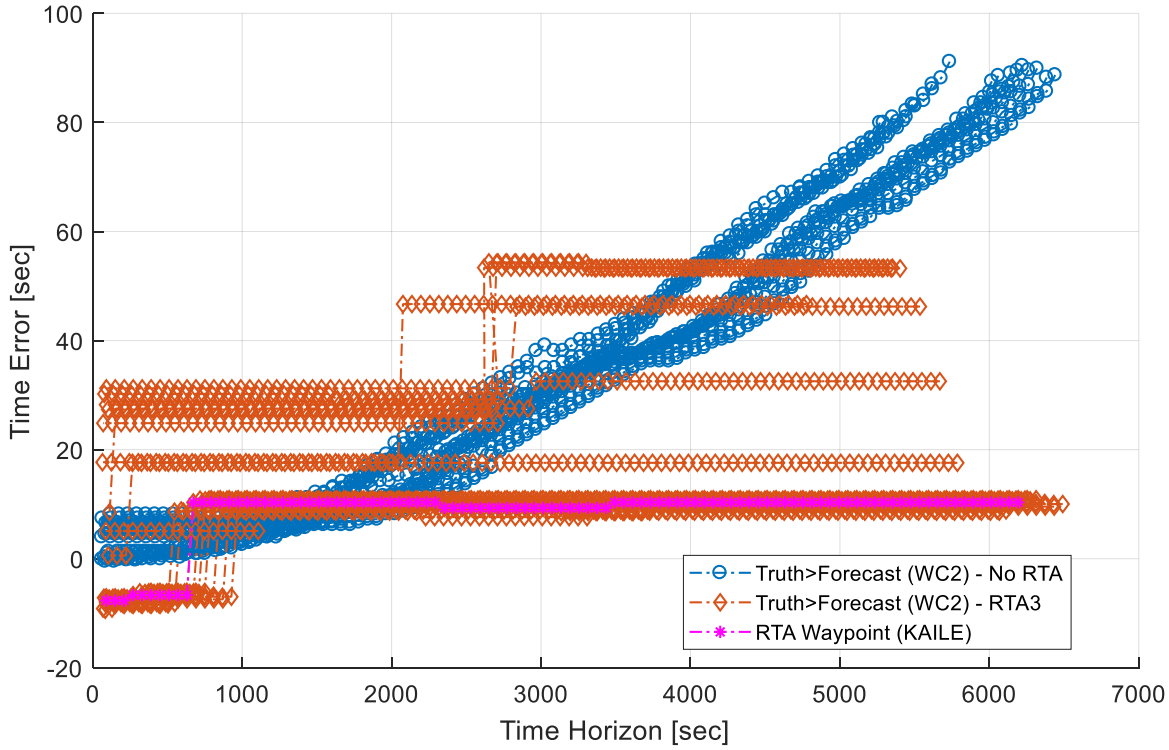

Figure 110. Time error for EPP points of the short route, true wind magnitude greater than forecast condition, without RTA (No RTA) and with an RTA (RTA3) close to the terminal area [RL3, RT1, WC2].

Appendix G: Figures – Parametric Error Models

1. *Model Identification*

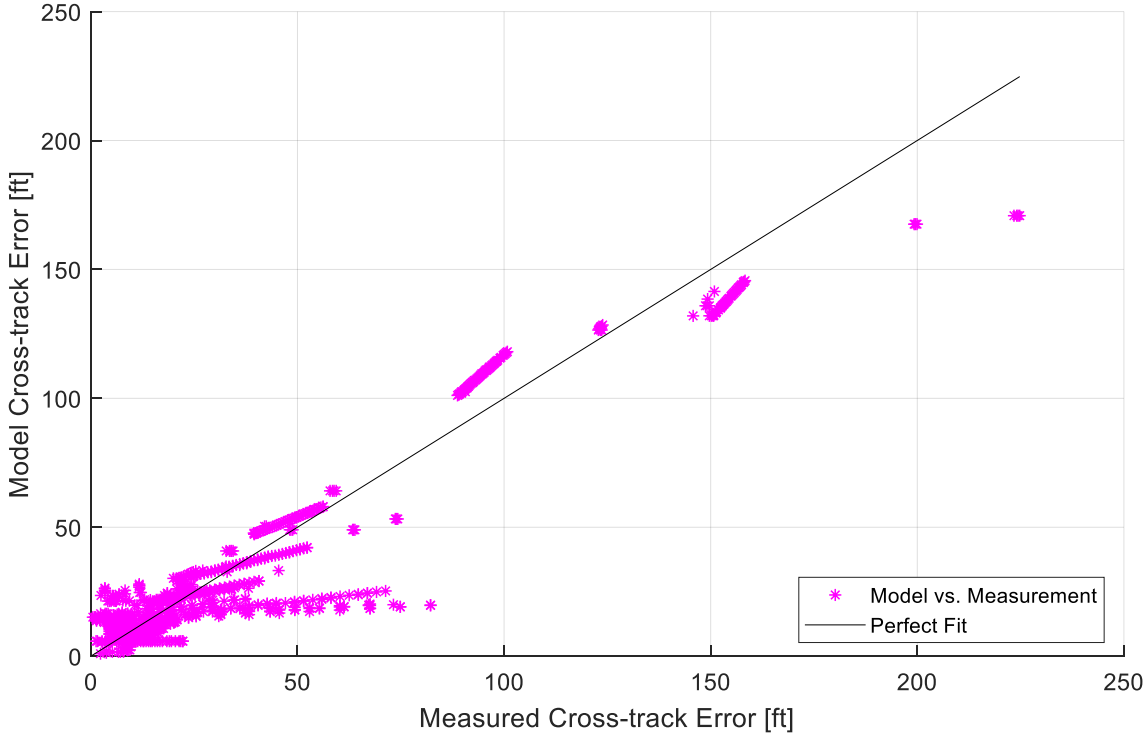

Figure 111. Cross-track error parametric model fit against the measured error data [RL1-RL3, RT1, WC0, WC1, WC2, WC5, No RTA].

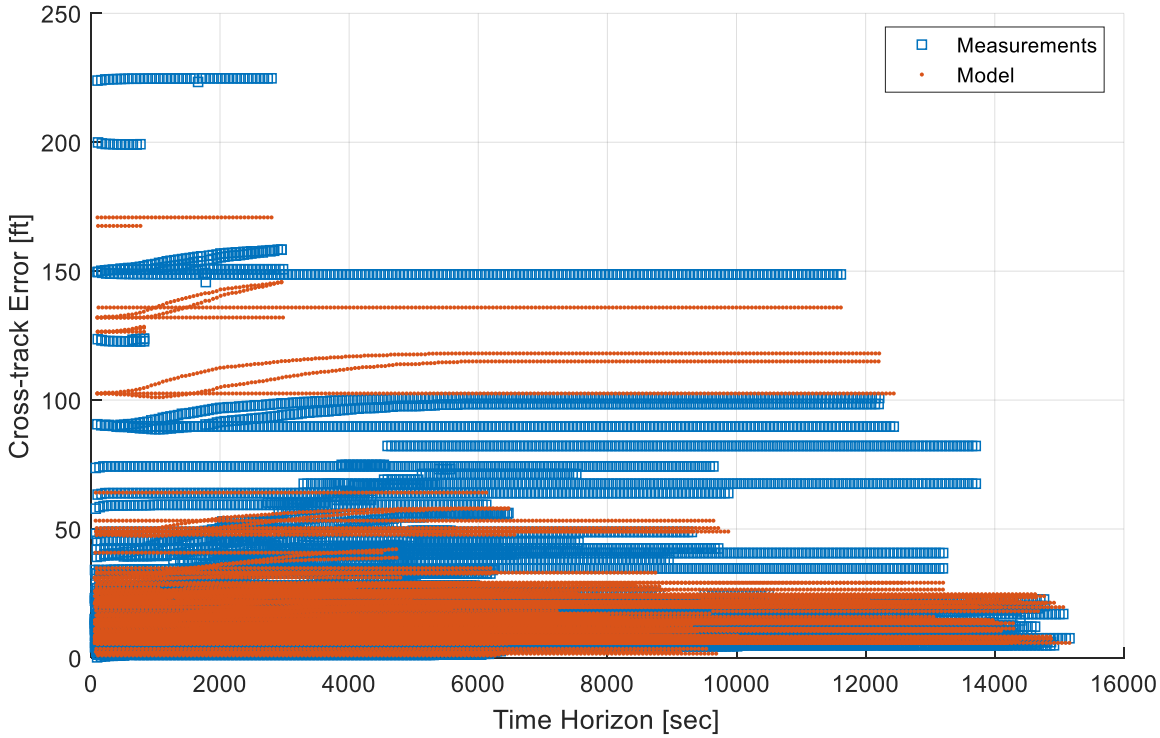

Figure 112. Modeled and measured cross-track errors versus time horizon [RL1-RL3, RT1, WC0, WC1, WC2, WC5, No RTA].

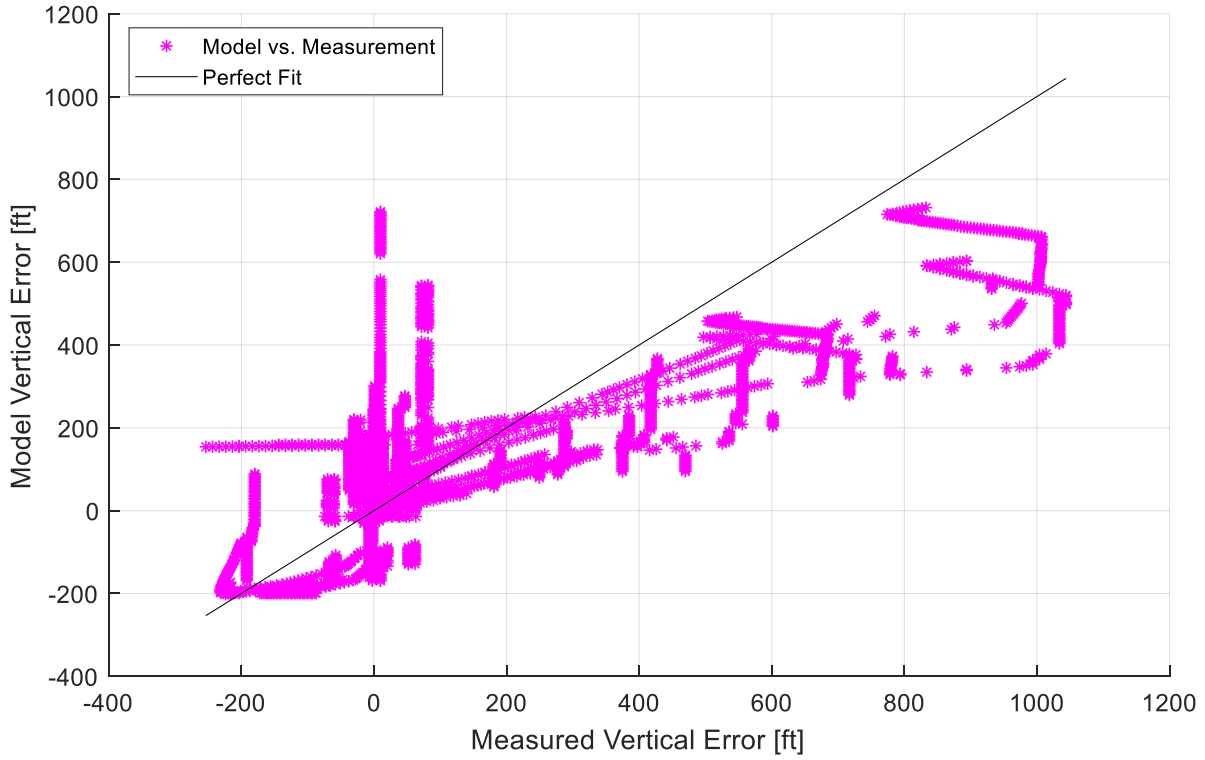

Figure 113. Vertical error parametric model fit against the measured error data [RL1-RL3, RT1, WC0, WC1, WC2, WC5, No RTA].

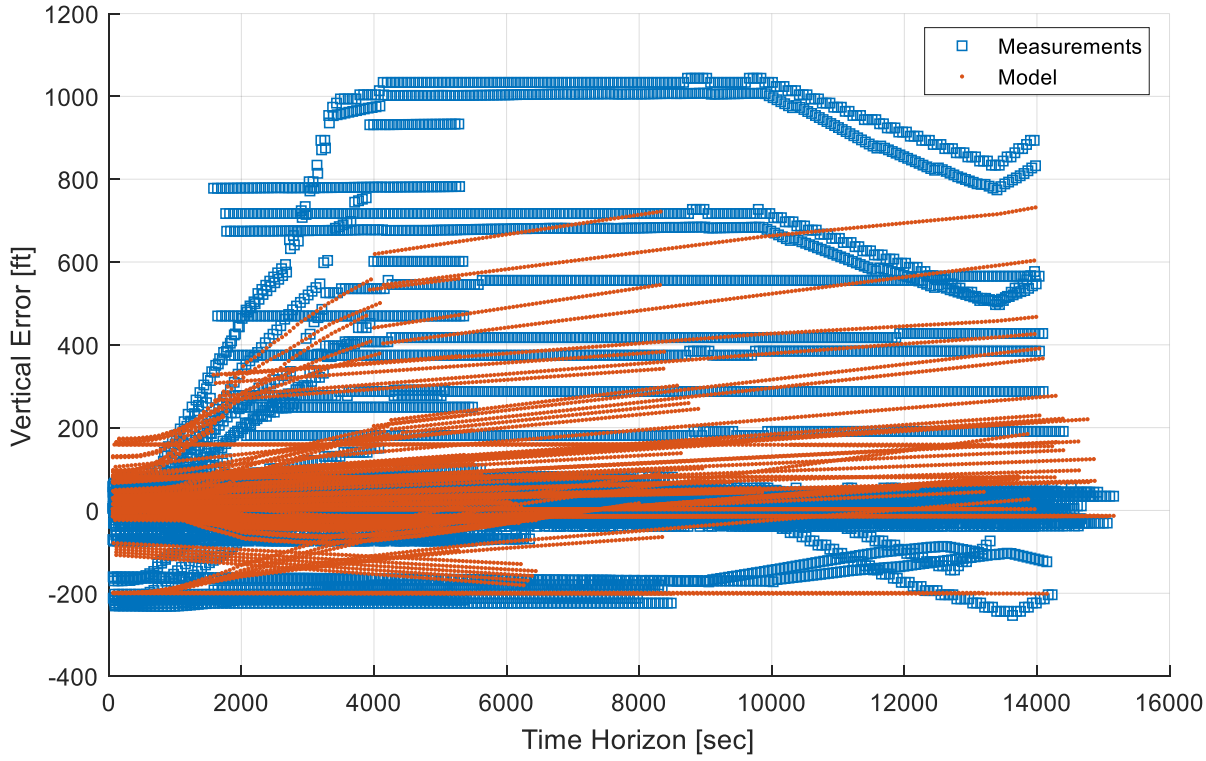

Figure 114. Modeled and measured vertical errors versus time horizon [RL1-RL3, RT1, WC0, WC1, WC2, WC5, No RTA].

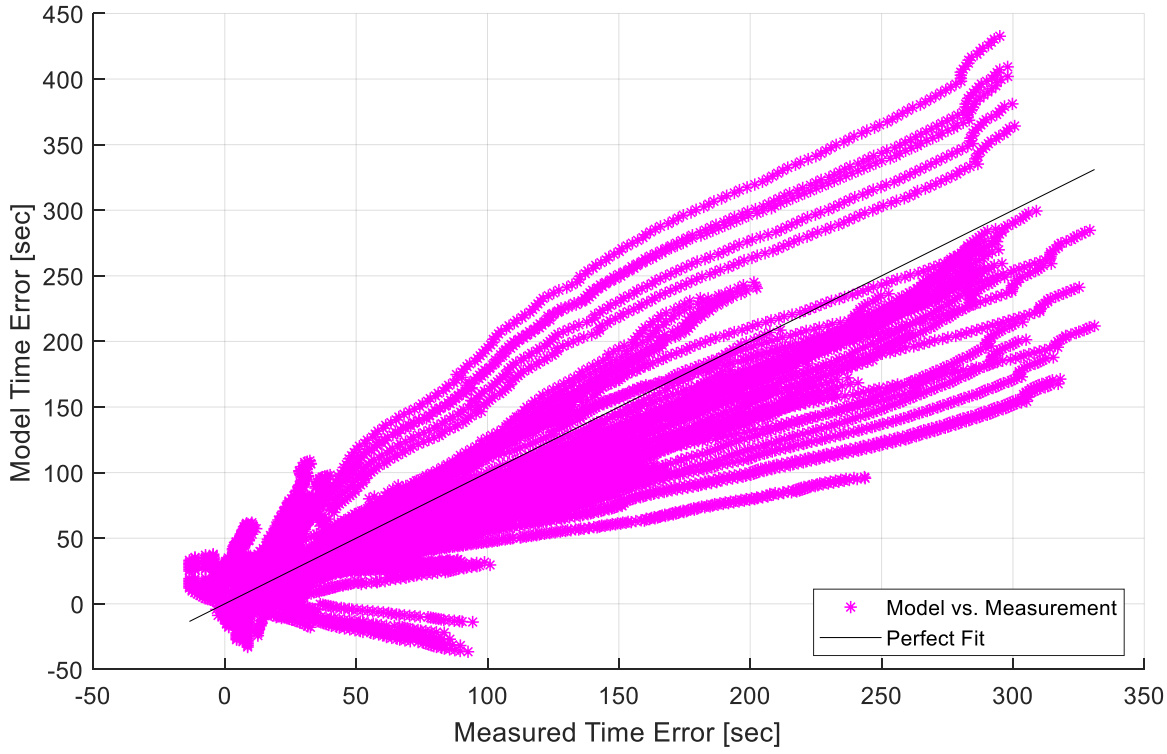

Figure 115. Time error parametric model fit against the measured error data [RL1-RL3, RT1, WC0, WC1, WC2, WC5, No RTA].

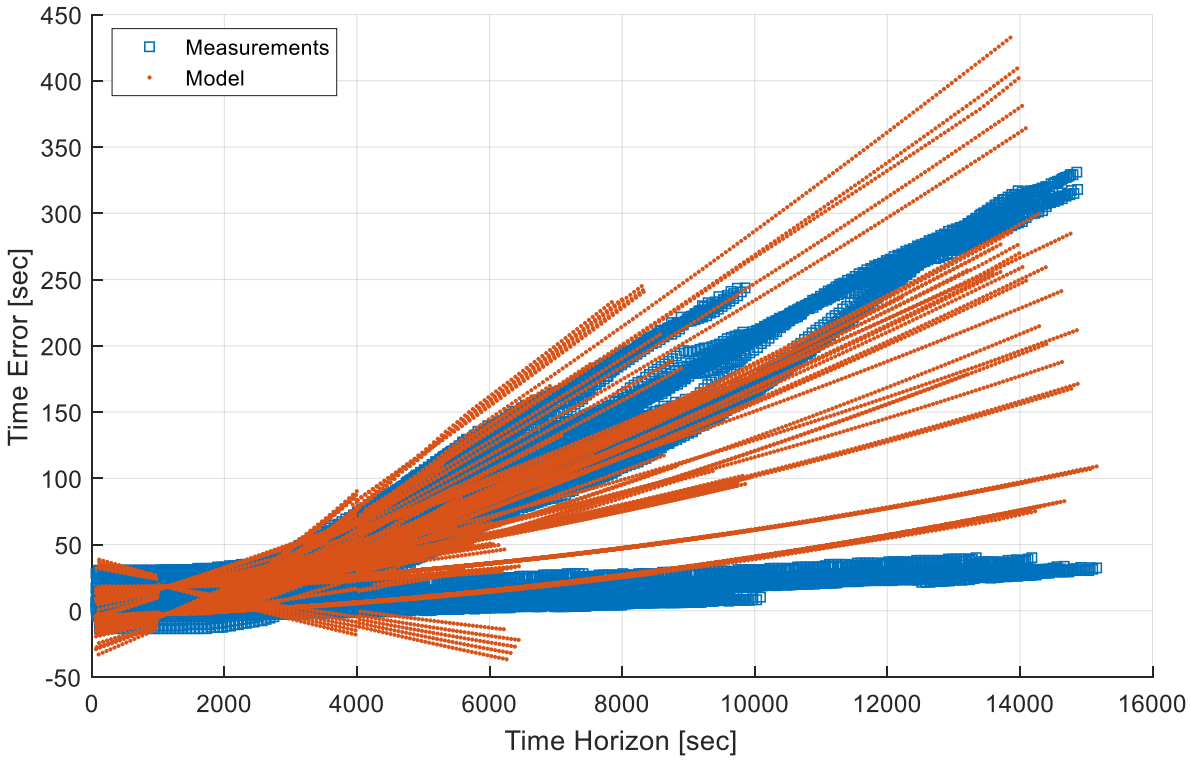

Figure 116. Modeled and measured time errors versus time horizon [RL1-RL3, RT1, WC0, WC1, WC2, WC5, No RTA].

2. Model Validation

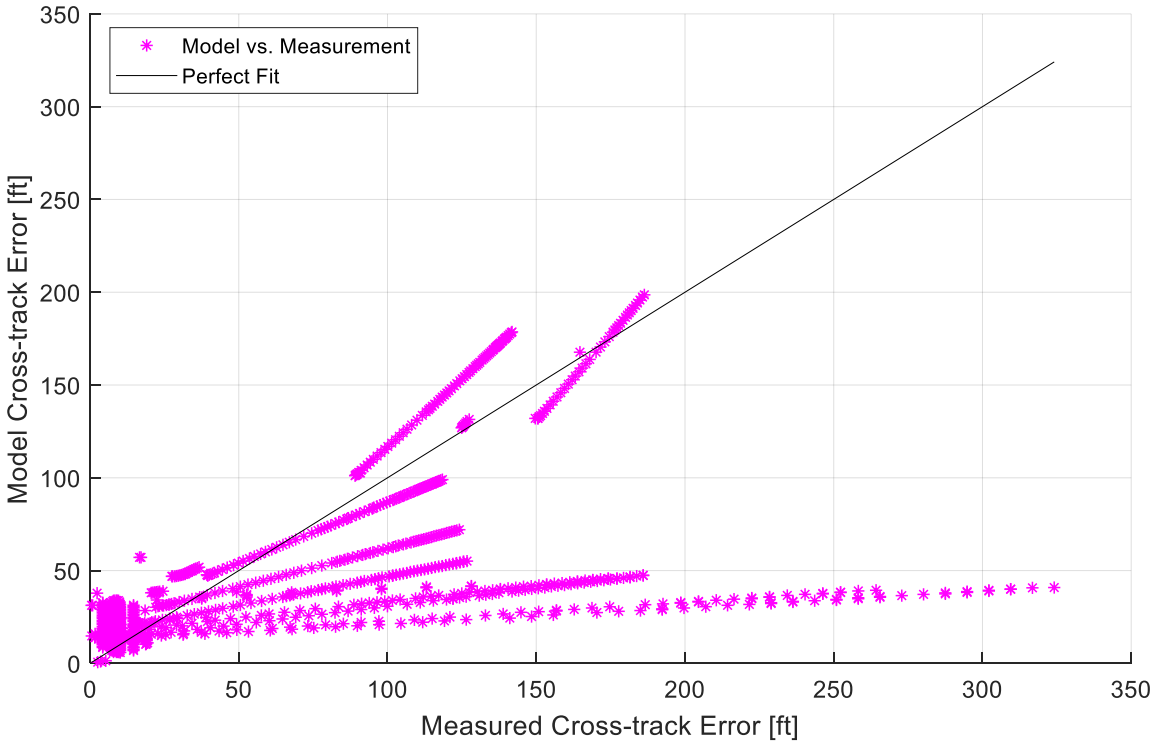

Figure 117. Cross-track error parametric model fit against the measured error data [RL1-RL3, RT1, WC7, No RTA].

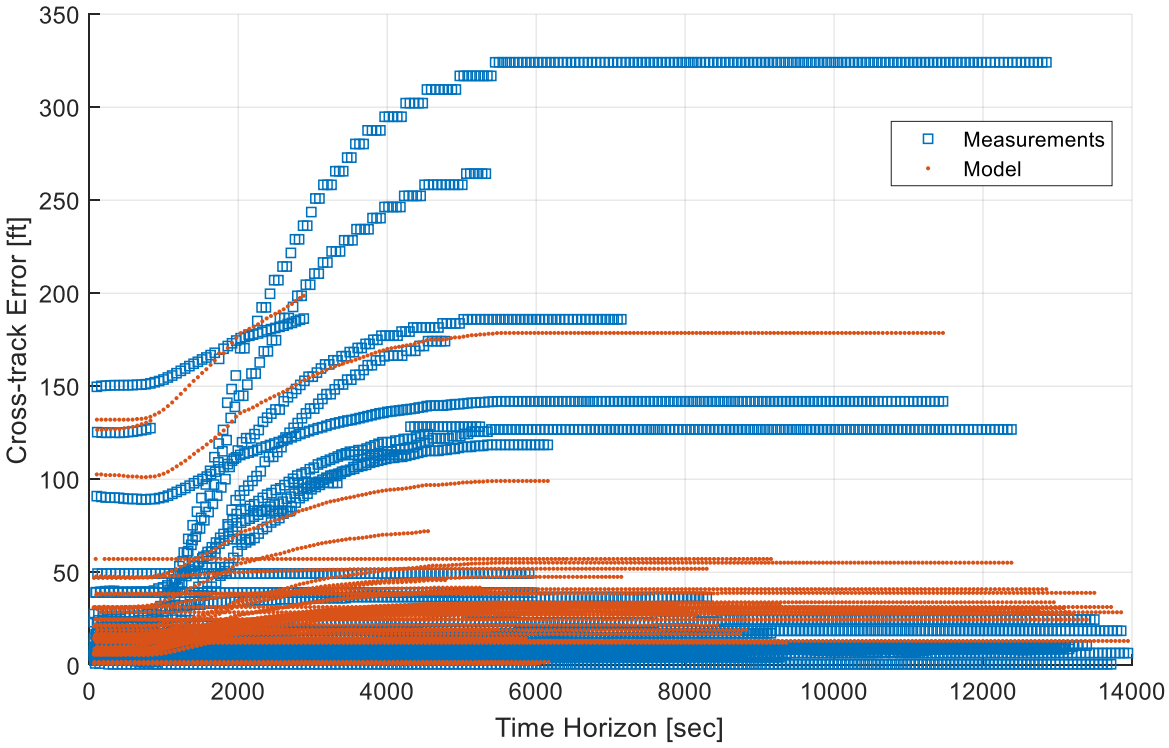

Figure 118. Estimated and measured cross-track errors versus time horizon [RL1-RL3, RT1, WC7, No RTA].

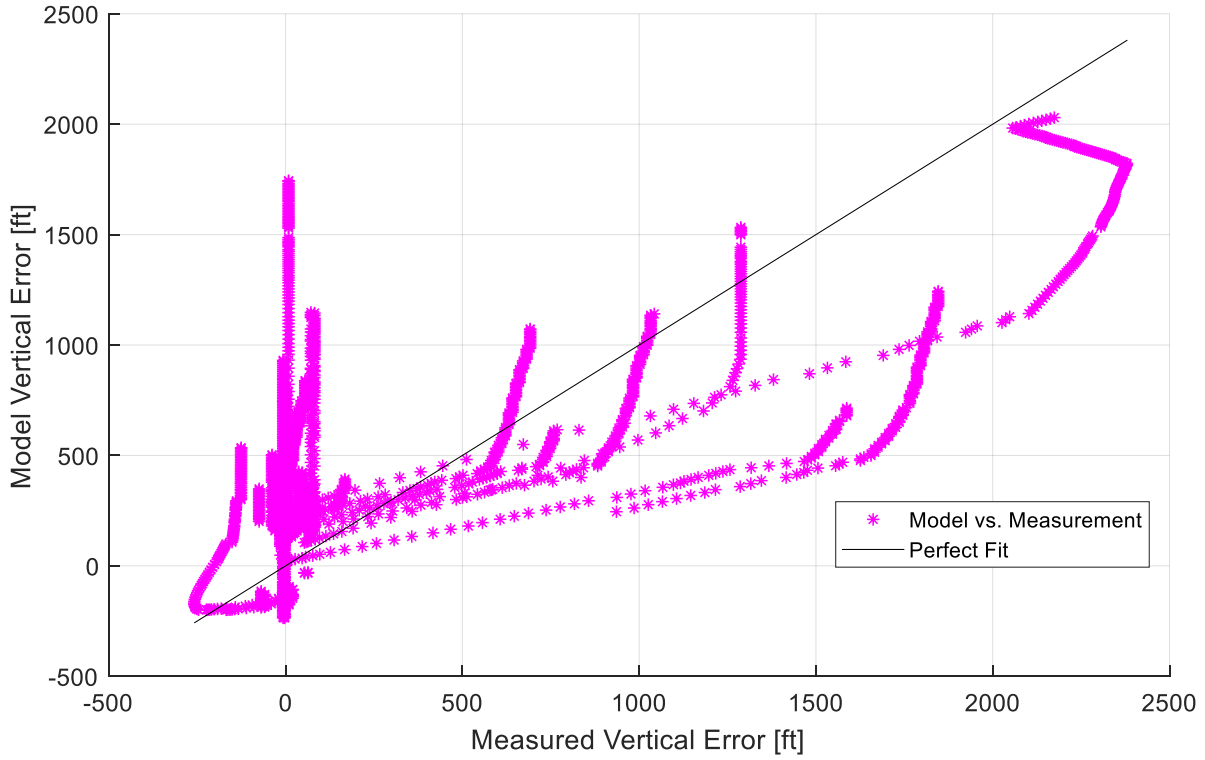

Figure 119. Vertical error parametric model fit against the measured error data [RL1-RL3, RT1, WC7, No RTA].

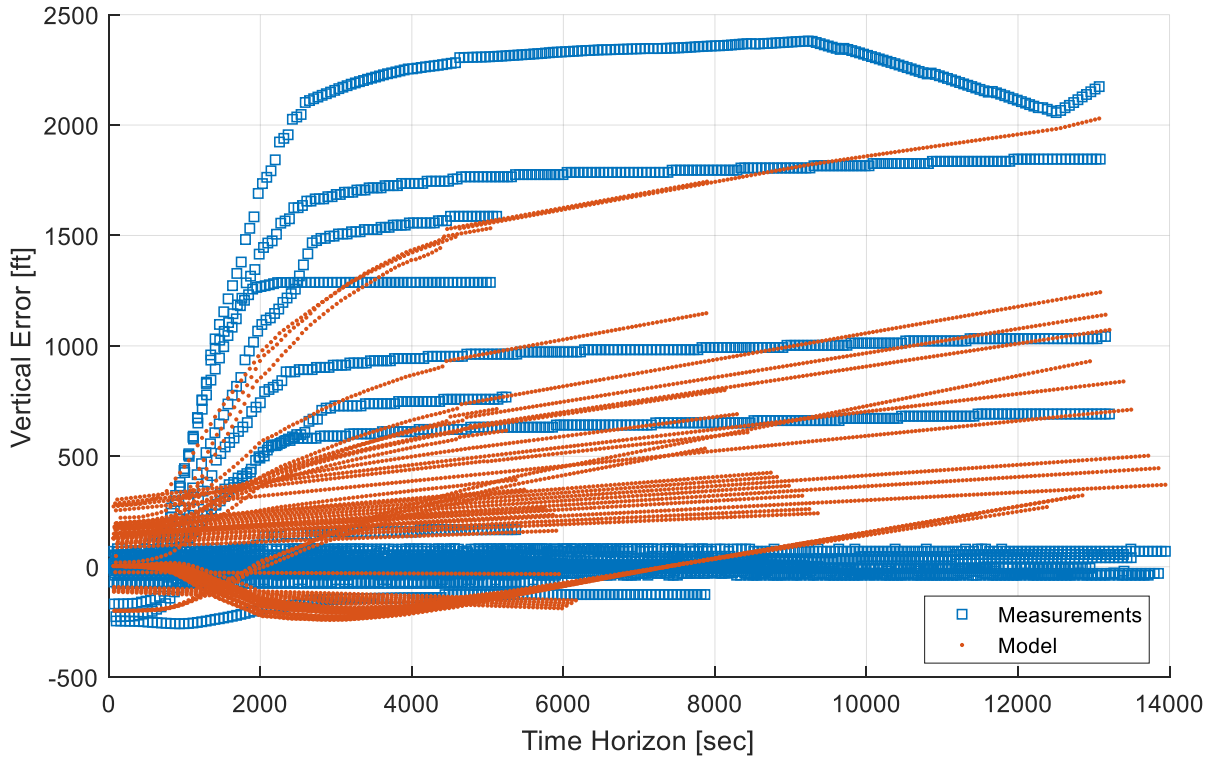

Figure 120. Estimated and measured vertical errors versus time horizon [RL1-RL3, RT1, WC7, No RTA].

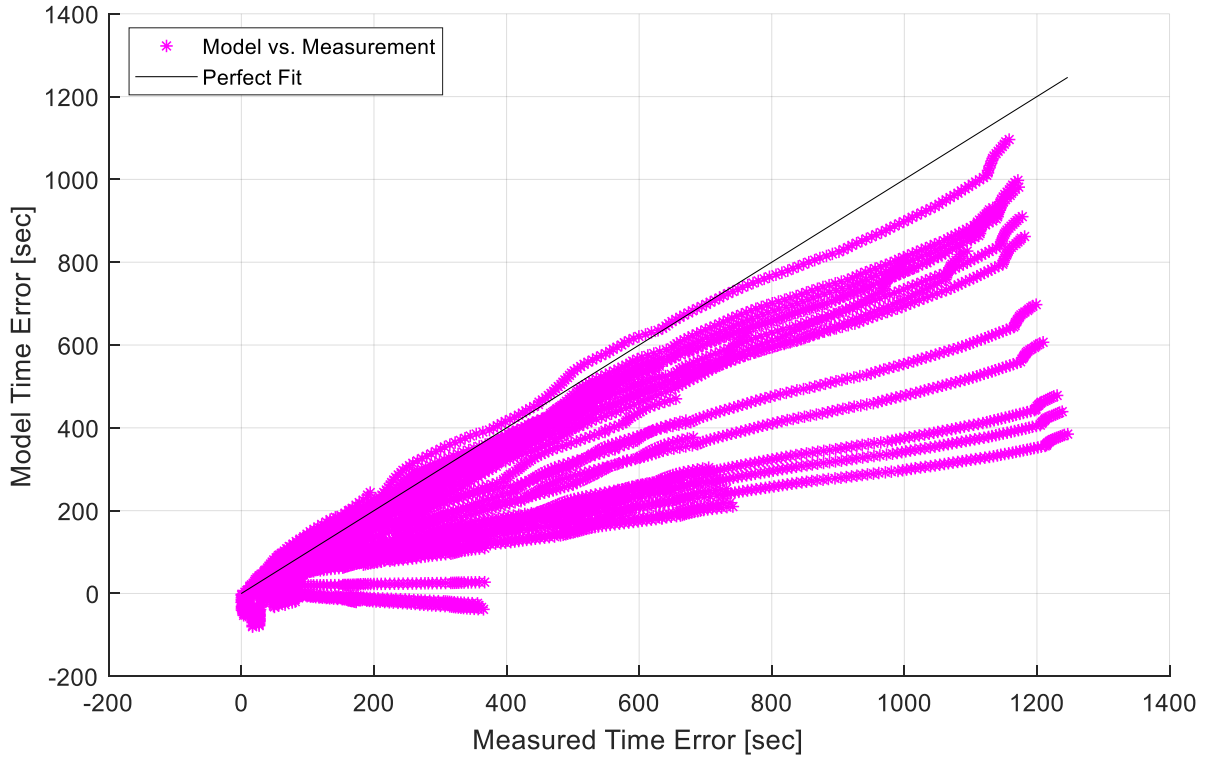

Figure 121. Time error parametric model fit against the measured error data [RL1-RL3, RT1, WC7, No RTA].

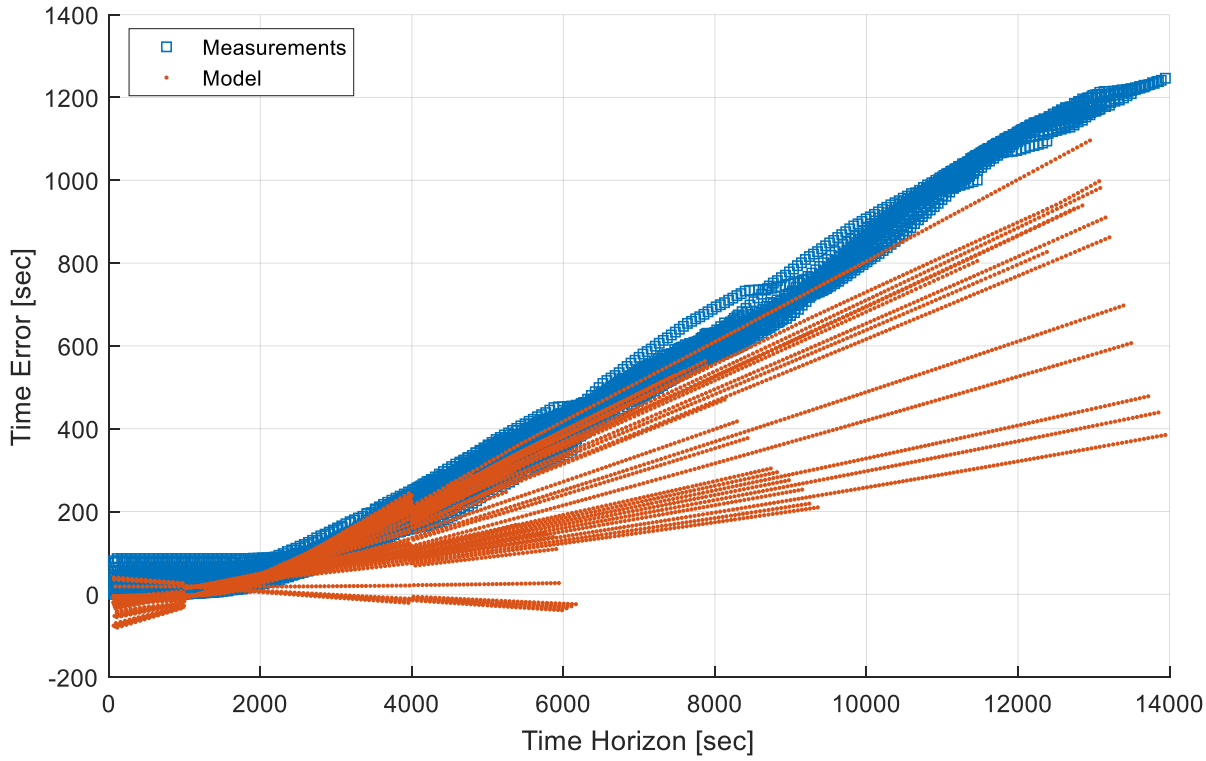

Figure 122. Estimated and measured time errors versus time horizon [RL1-RL3, RT1, WC7, No RTA].

Appendix H: Route Design

The functionality on the *flightaware.com* website was used to select realistic routes for this analysis. The research team searched for the type of aircraft used in the ATOS simulation platform (Boeing 757-200) and then selected historical routes flown on a given day that met the length requirements set in Table 2 and the direction specified in Section 3.2.1.1. Once several routes were identified, these were pared down to three routes that satisfied both the length and direction criteria. The details of each route are presented in the following sections.

The long full route [RL1, RT1] in each scenario features a flight from Los Angeles International Airport (KLAX) to Washington Dulles International Airport (KIAD). The flight is initialized at its cruise altitude of FL390 and its cruise speed of Mach 0.80 heading direct to the navigational aid NOOTN. From NOOTN, the flight proceeds direct to navigational aid SELLS, then direct to navigational aid OATHE, then direct to the VORTAC HYS, then direct to the VORTAC SLN, then direct to the VORTAC STL, then direct to the VOR-DME FLM, then direct to the VORTAC HVQ. At HVQ, the flight follows the GIBBZ2 STAR procedure to the navigational aid MATTC. In order to connect the STAR and approach procedures, the flight proceeds from MATTC direct to navigational aid IZUMI, which is the intermediate fix for the RNAV/RNP Z approach procedure to runway 19L at KIAD. Once the flight completes the turn at navigational aid IZUMI, it joins and follows the RNAV/RNP Z approach procedure to runway 19L.

The long sparse route [RL1, RT2] in each scenario features the same flight from Los Angeles International Airport (KLAX) to Washington Dulles International Airport (KIAD). The flight plan is the same as the full route except that, after the navigational aid NOOTN, the flight proceeds direct to the VORTAC HVQ, bypassing most of the en route points of the full route.

The medium full route [RL2, RT1] in each scenario features a flight from Las Vegas McCarran International Airport (KLAS) to Chicago O'Hare International Airport (KORD). The flight is initialized at its cruise altitude of FL350 and its cruise speed of Mach 0.80 heading direct to the VORTAC DVC. From DVC, the flight proceeds direct to the VORTAC PUB, then direct to the VORTAC HYS, then direct to the VORTAC SLN, then direct to the navigational aid AGENT, then direct to the navigational aid KIDER, then direct to the VORTAC IRK. At IRK, the flight follows the BENKY2 STAR procedure to the navigational aid TONIE. In order to provide a connected route to the runway, from TONIE, the flight proceeds direct to the navigational aid WAVIE, which is the intermediate fix on the RNAV Global Positioning System (GPS) approach to runway 28R at KORD. Once the flight completes the turn at WAVIE, it joins and follows the RNAV GPS approach procedure to runway 28R.

The medium sparse route [RL2, RT2] in each scenario features the same flight from Las Vegas McCarran International Airport (KLAS) to Chicago O'Hare International Airport (KORD). The flight plan is the same as the full route except that, after the VORTAC DVC, the flight proceeds direct to the VORTAC IRK, bypassing most of the en route points of the full route.

The short full route [RL3, RT1] in each scenario features a flight from San Francisco International Airport (KSFO) to Denver International Airport (KDEN). The flight is initialized at its cruise altitude of FL350 and its cruise speed of Mach 0.80 heading direct to the navigational aid INSLO. From INSLO, the flight proceeds direct to the navigational aid GAROT, then direct to the VOR-DME EKR. At EKR, the flight follows the KAILE2 STAR procedure, and then follows the Instrument Landing System (ILS) approach procedure to runway 16L at KDEN. In the short route, the STAR procedure is connected to the approach procedure, which means that no modifications to the route were required regarding removing discontinuities in the FMS.

The short sparse route [RL3, RT2] in each scenario features the same flight from San Francisco International Airport (KSFO) to Denver International Airport (KDEN). The flight plan is the same as the full route except that, after the navigational aid INSLO, the flight proceeds direct to the VOR-DME EKR, bypassing the en route navigational aid GAROT of the full route.

Table 10 provides the details of the full and sparse route conditions for all route lengths. The full route flight plans can be seen in Figure 4 while the sparse route flight plans can be seen in Figure 123.

Table 10. Route descriptions – all route lengths, full and sparse route types.

Route Length	Departure Airport	Initialization Point	Cruise Altitude	En Route Flight Plan (Full Route/RT1)	En Route Flight Plan (Sparse Route/RT2)	STAR	Approach	Arrival Airport
Long (RL1)	KLAX	35.9936° N 115.2879° W	FL390	NOOTN SELLS OATHE HYS SLN STL FLM HVQ	NOOTN HVQ	HVQ FIMPA WOJOW[1] BURTT PHOOW HESEE[1,2,3] GYSLO[2,3] BBONE[2,3] KILMR[1,2,3] OTTTO[3] MAAAY[3,4] RYPIN GIBBZ SUNYJ UDIYU MATTC (GIBBZ2)	IZUMI DOMSE R-19L (RRZ19L)	KIAD
Medium (RL2)	KLAS	36.7596° N 111.7164° W	FL350	DVC PUB HYS SLN AGENT KIDER IRK	DVC IRK	IRK LOAMY KEOKK[1] DRAMS[3] RYELY[3] BDF[1,2,3] BYLAW[2,3] BENKY[1,2,3] NEWRK ASHTN PETAH JORGO MONKZ[4] TONIE (BENKY2)	WAVIE ADAMIE WILLT FIDAK R-28R (R28R)	KORD
Short (RL3)	KSFO	38.4483° N 120.2139° W	FL350	INSLO GAROT EKR	INSLO EKR	EKR[1] CSPAD[3] FRNCH[3] SKARF[3] TOMSN[1,2,3] BEOND[2,3] SWAYN[3] KAILE[1,2,3] (KAILE2)	BJETN[3] JEEPR[3] JOBOB[3] KUURT[3] KIKME[3] LEETS[3,4] R-16L (ILS16L)	KDEN

[1] Waypoints with RTA constraints in some scenario runs.
[2] Analysis waypoint with an associated speed constraint.
[3] Analysis waypoint with an associated altitude constraint.
[4] Last waypoint considered in the analysis of each scenario (point prior to scenario termination).

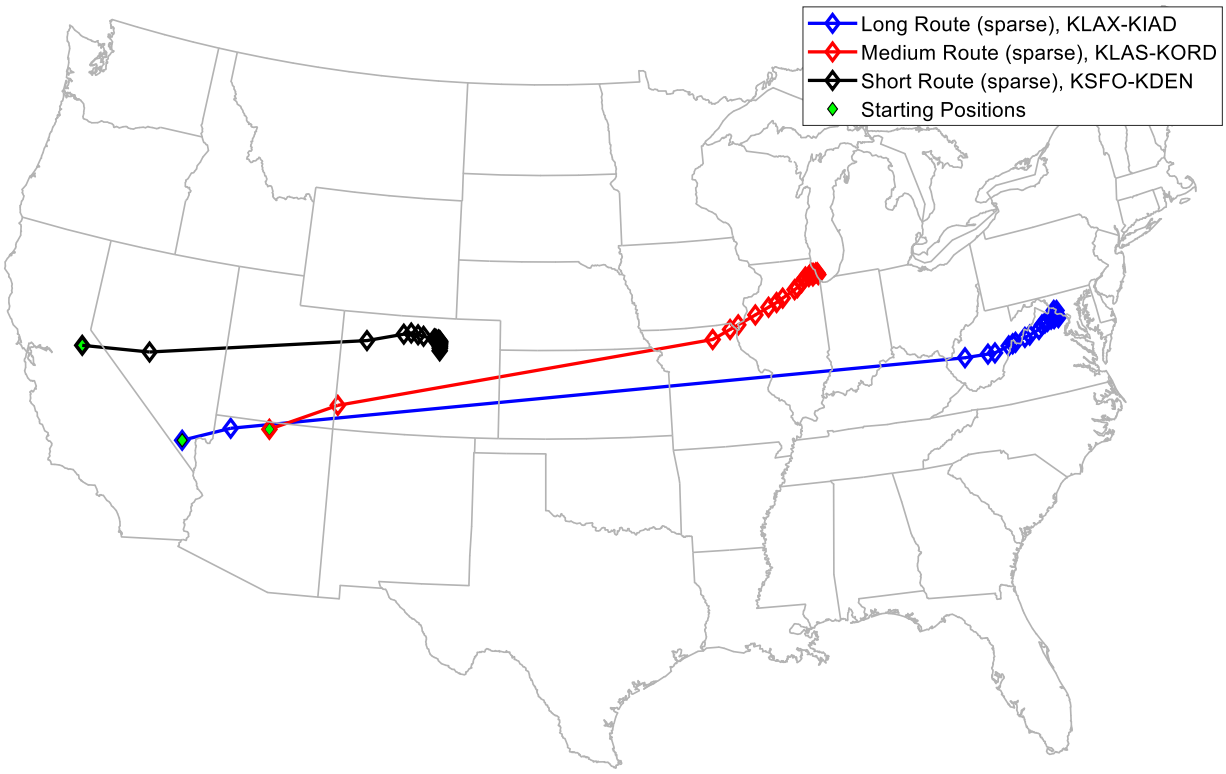

Figure 123. Sparse version of the long, medium, and short routes and their lateral waypoint locations.

Appendix I: STAR Charts and Approach Plates

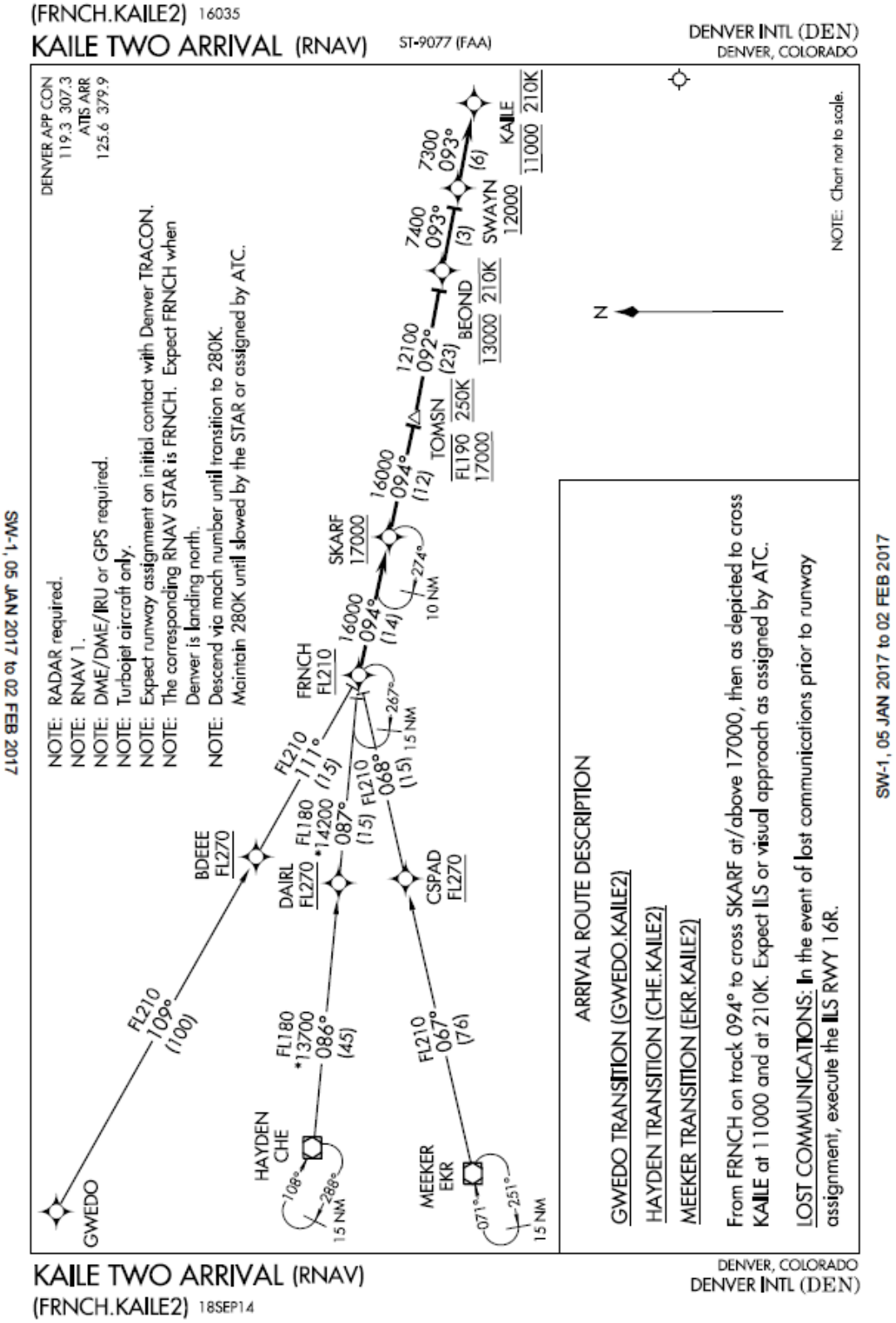

Figure 124. KAILE2 STAR chart (KDEN).

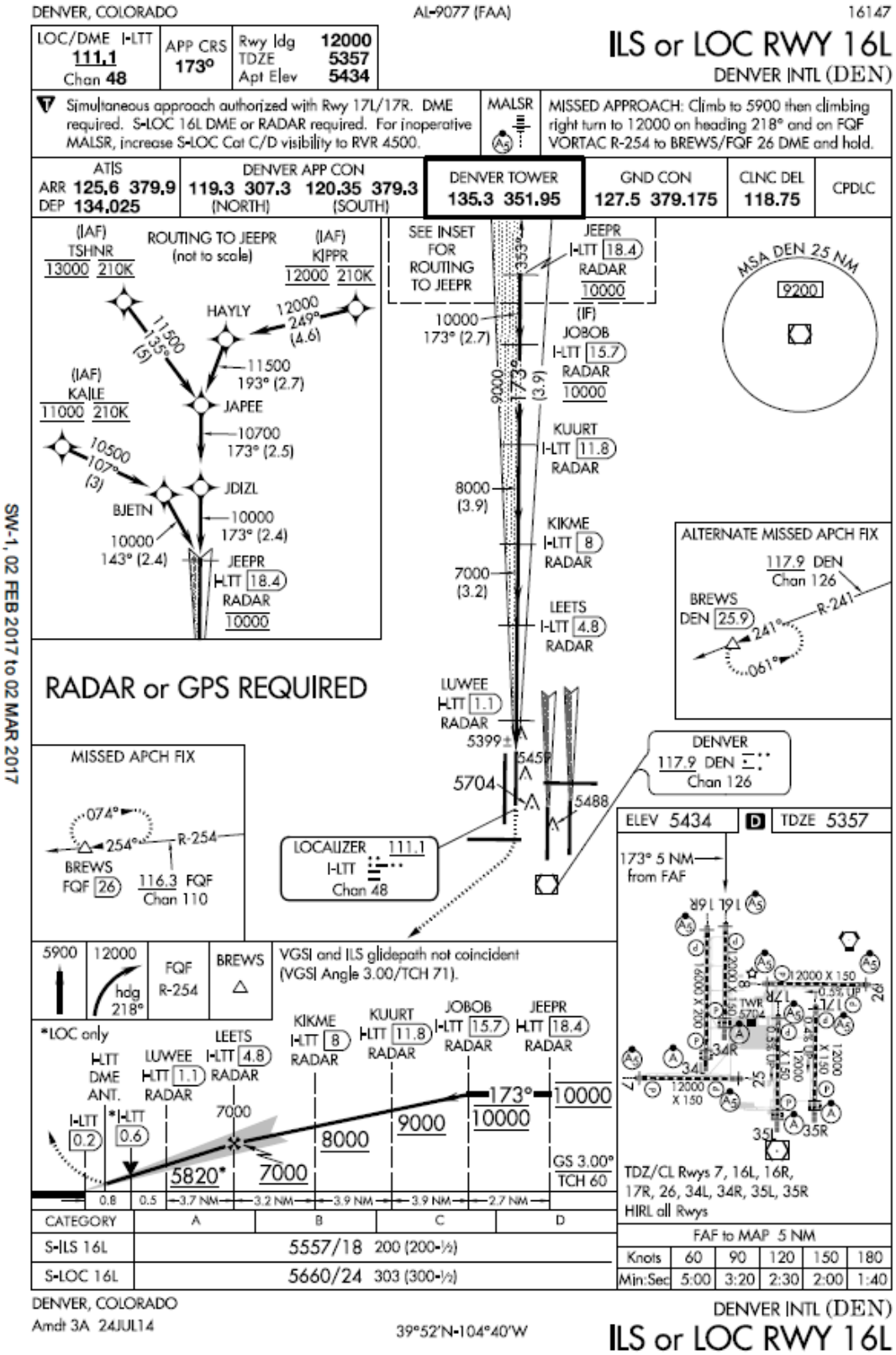

Figure 125. ILS RWY 16L approach plate (KDEN).

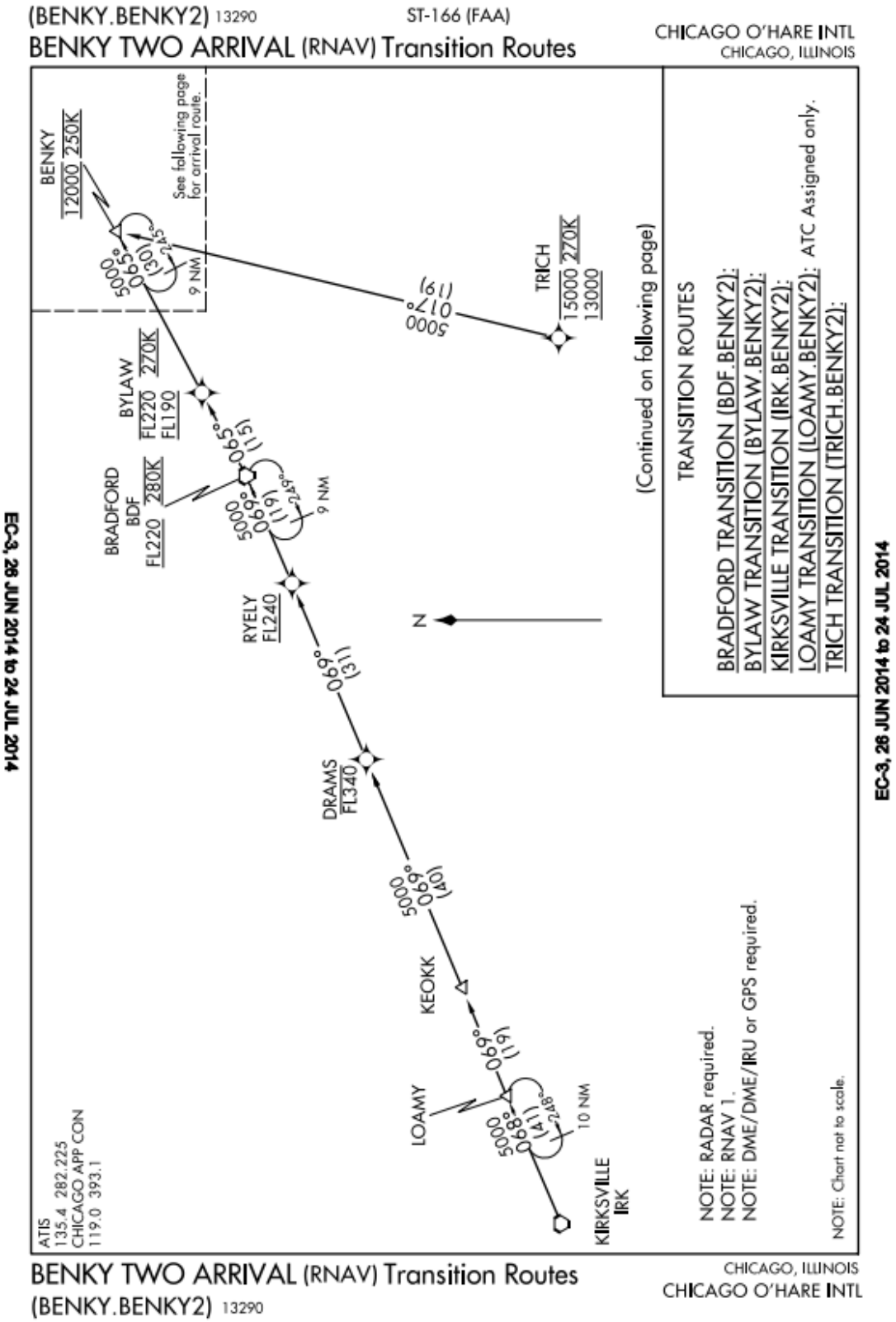

Figure 126. BENKY2 STAR transitions chart (KORD).

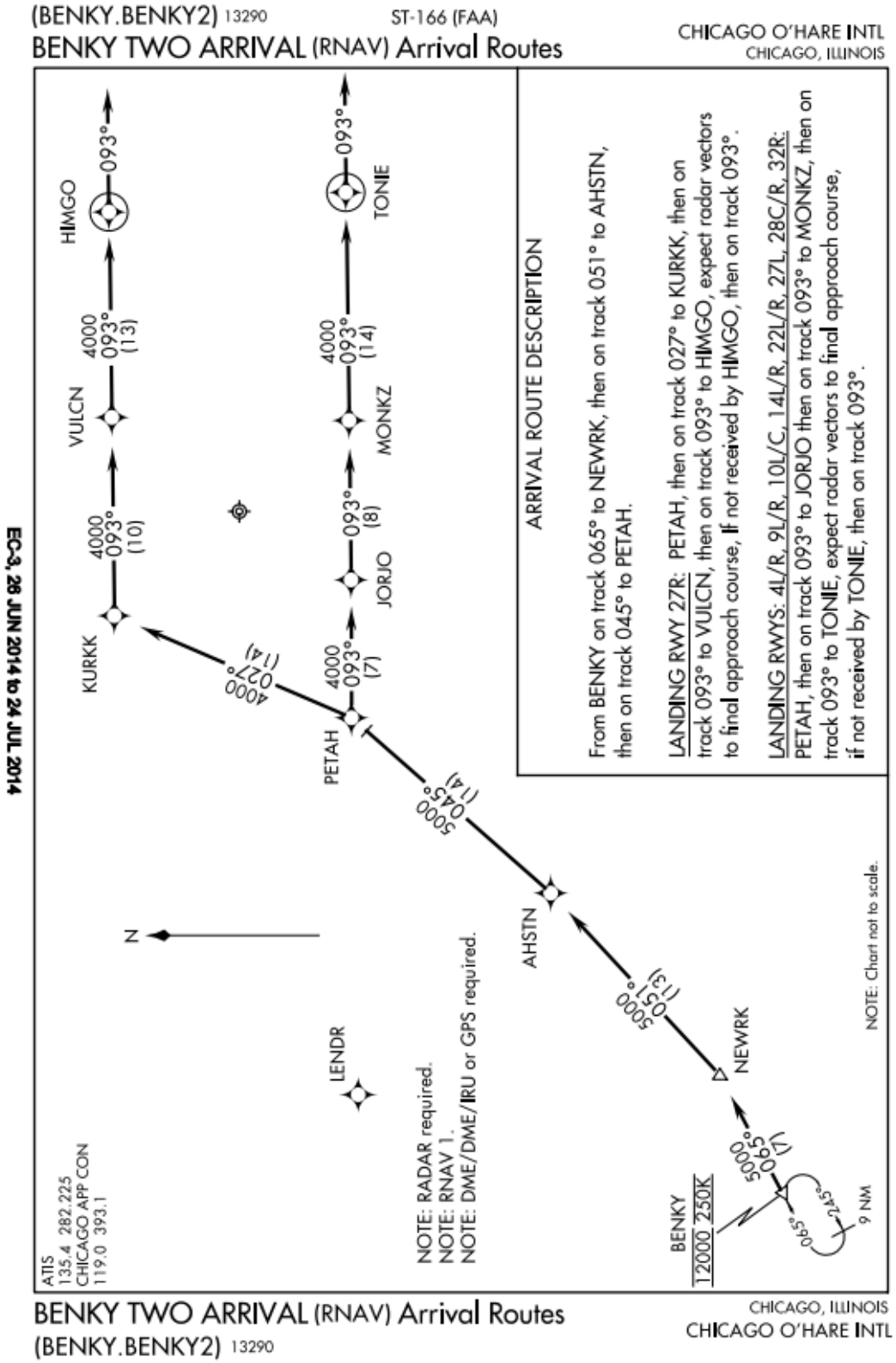

Figure 127. BENKY2 STAR arrival chart (KORD).

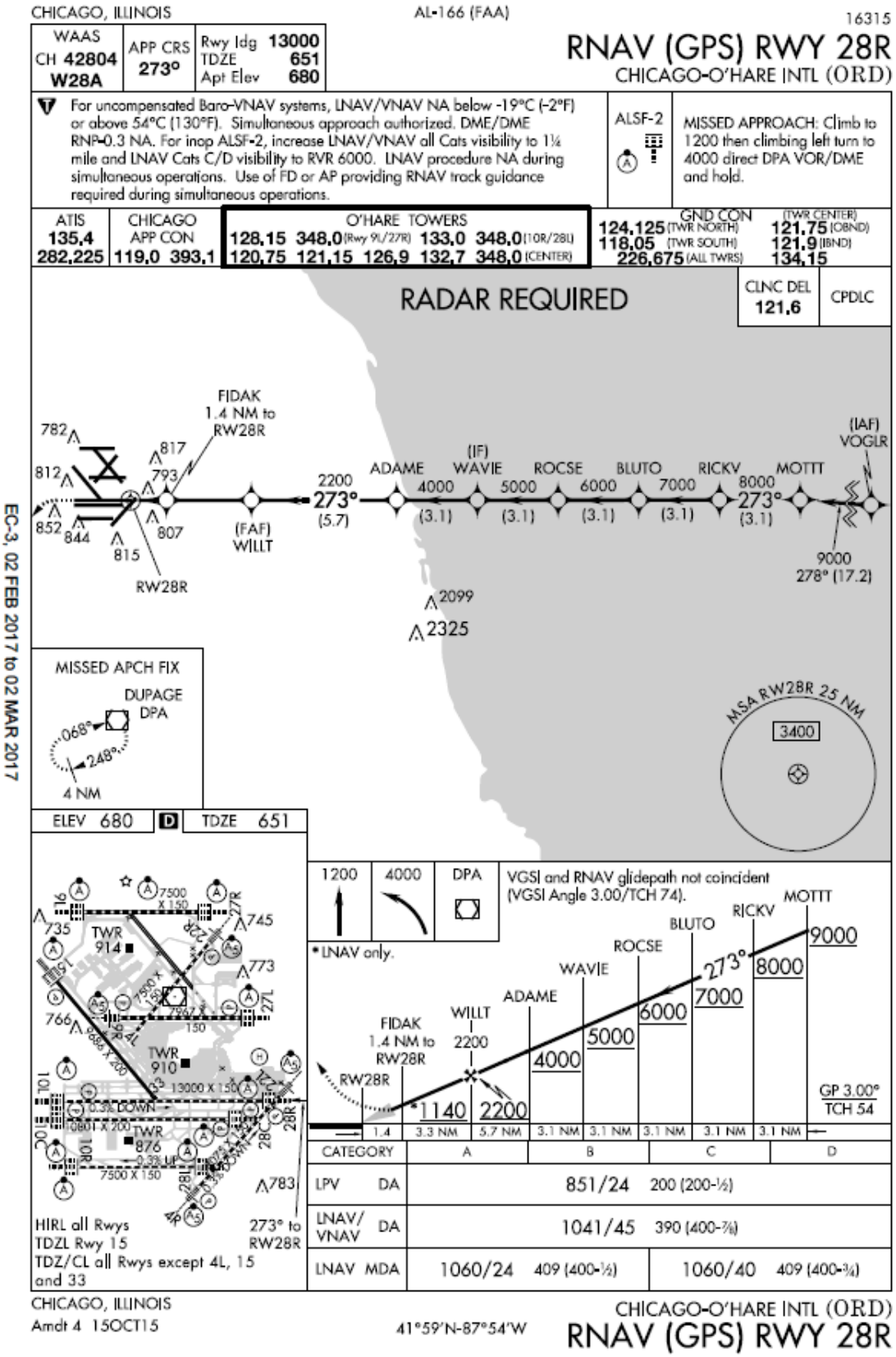

Figure 128. RNAV (GPS) RWY 28R approach plate (KORD).

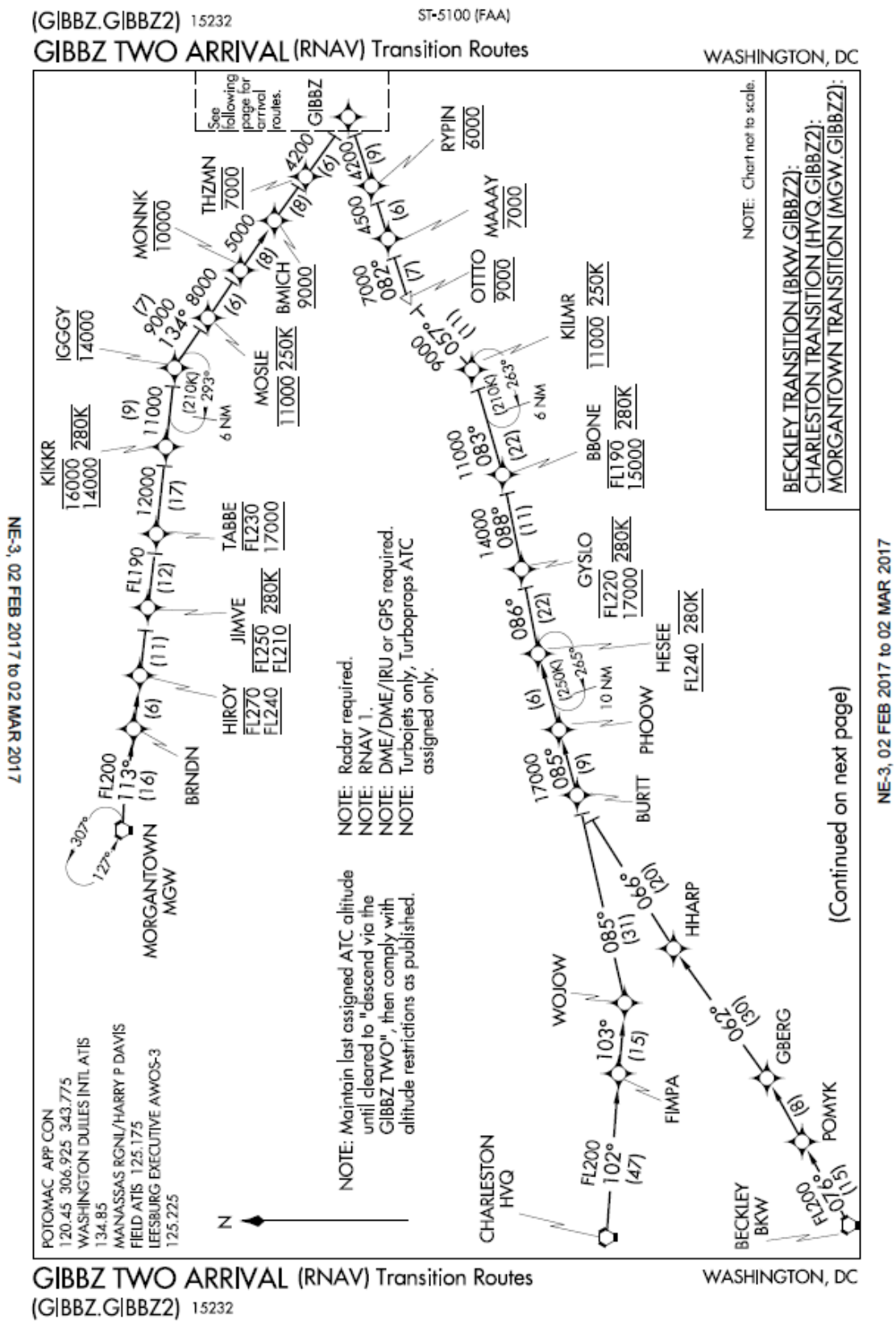

Figure 129. GIBBZ2 STAR transitions chart (KIAD).

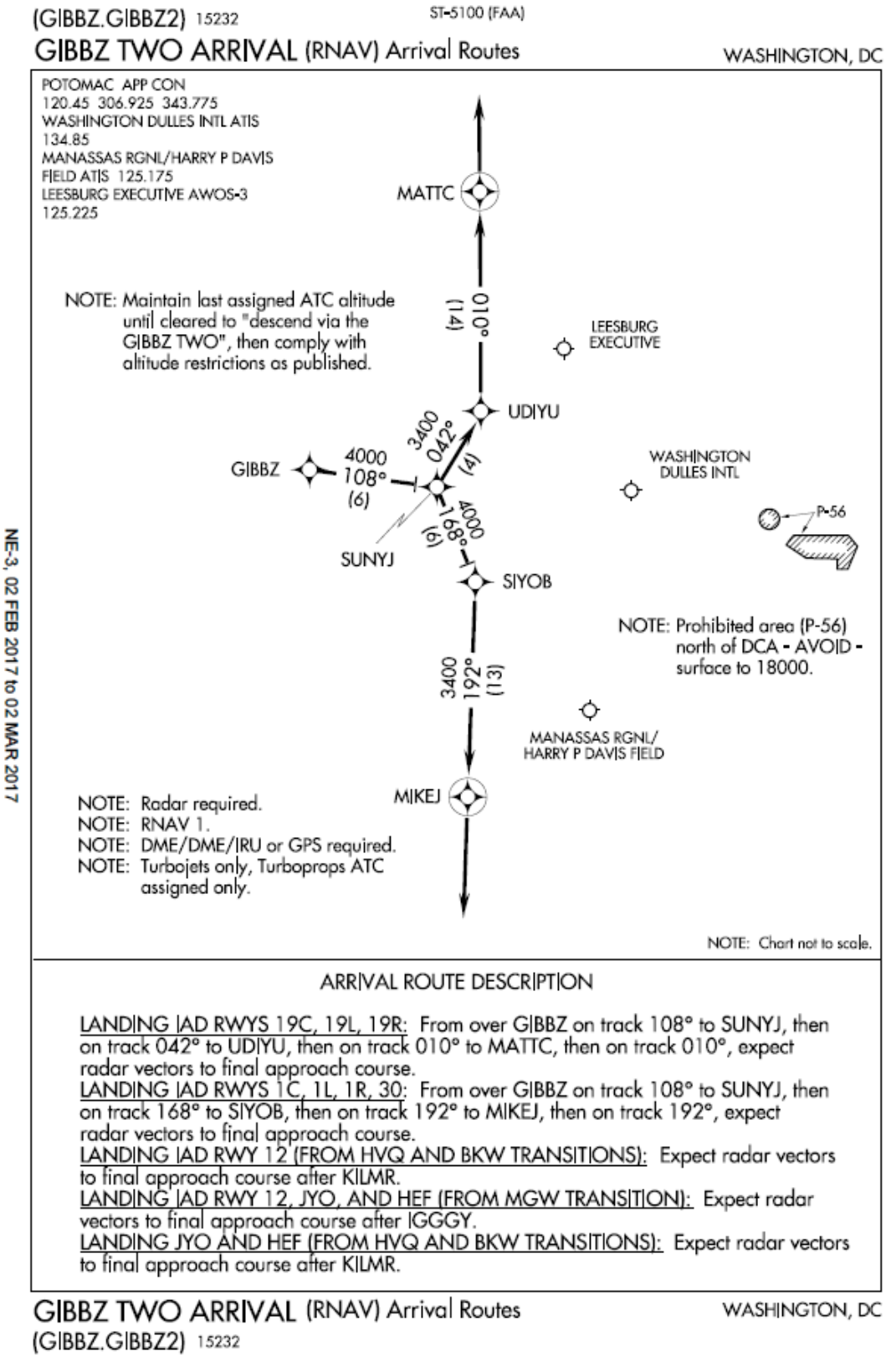

Figure 130. GIBBZ2 STAR arrival chart (KIAD).

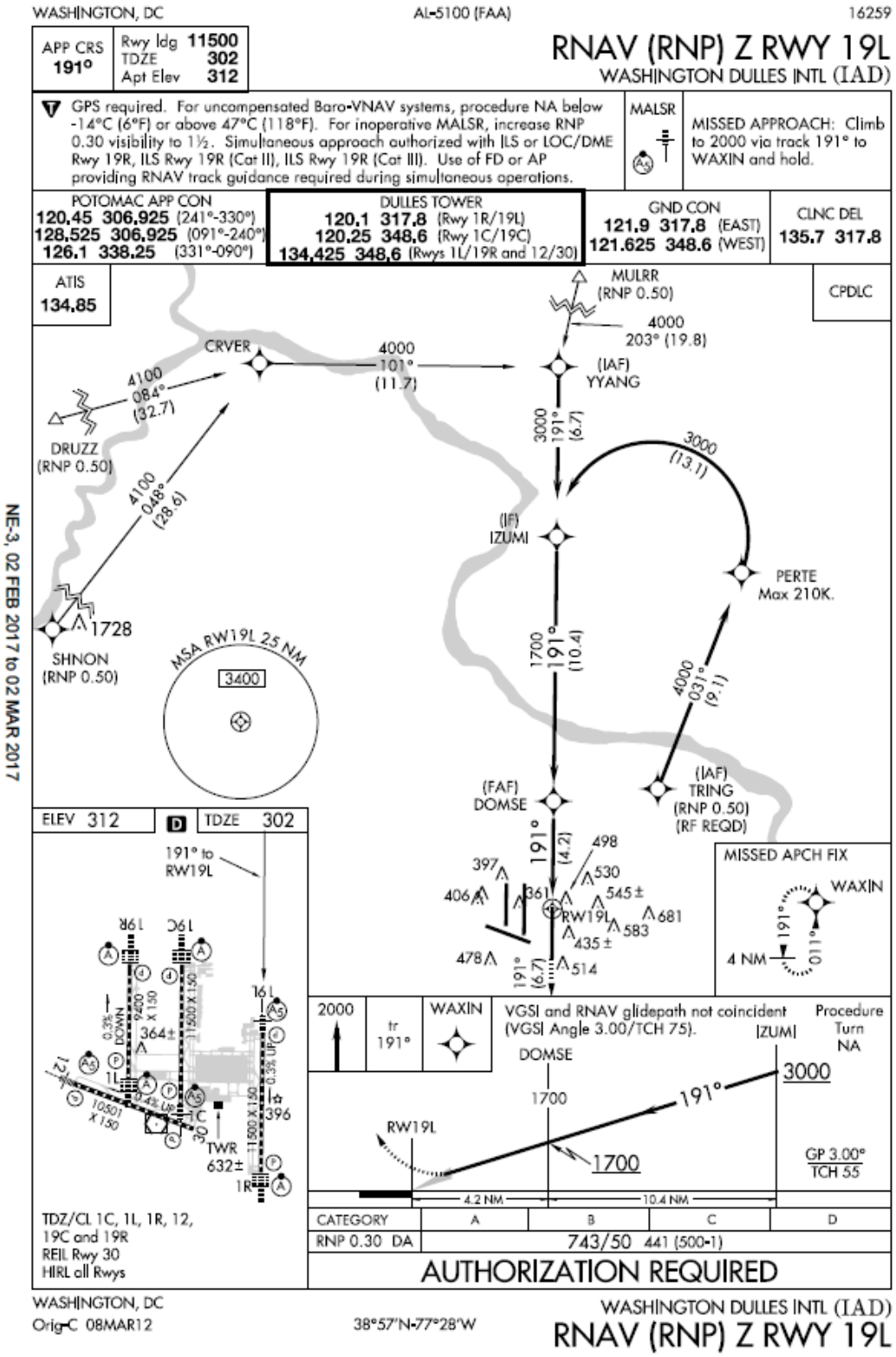

Figure 131. RNAV (RNP) Z RWY 19L approach plate (KIAD).

Appendix J: Wind Magnitude Analysis

In order to ensure that the wind magnitudes were realistic for this study, an analysis was performed to determine realistic wind magnitudes as a function of altitude. This analysis leveraged a large dataset of winds, which consisted of one month (May 2016) of Rapid Refresh (RAP), version 2 wind model data. The RAP model data used in this study provided a wind prediction every hour for 51 vertical levels in a 13-kilometer (approximately 7 nautical mile) grid over North America [20]. Wind speeds were parsed from this dataset at all prediction times (24 per day) for altitudes up to 52,000 feet mean sea level at 100 random latitude/longitude locations across the continental United States. In the analysis, the wind dataset was further curtailed to include only altitudes between 4,000 feet and 42,000 feet.

A script was written to ingest these data files (74,400 in total), parse the data files, and store the data. This post-processed data was used to determine the relationship between wind magnitude and altitude. Once the data was plotted (see Figure 132), a best-fit analysis was conducted to determine the best fit to the data for wind magnitude. Two relationships were analyzed – a linear approximation and a quadratic approximation. Based upon the results of the analyses, a linear approximation was chosen at seven percentile values – the 1st, 5th, 25th, 50th, 75th, 95th, and 99th percentiles. The results of the line fit can be seen in Figure 132.

The coefficients used in the equation $Magnitude = A * (Altitude) + B$ in order to vary the wind magnitude as a function of altitude are for each percentile. These coefficients, as well as the R^2 value for each linear approximation, are presented in Table 11. By using these coefficients in the aforementioned equation, wind files were generated with different percentile magnitudes of wind varying by altitude.

Table 11. Coefficients and R^2 values for the linear approximations of wind magnitude as a function of altitude.

Percentile	A	B	R^2 Value
1st	0.00015003	0.52633	0.94522
5th	0.00035515	0.96455	0.97482
25th	0.00082299	2.3230	0.98241
50th	0.0012070	4.6225	0.98623
75th	0.0015832	8.2710	0.98426
95th	0.0021514	15.630	0.98303
99th	0.0025367	21.844	0.97397

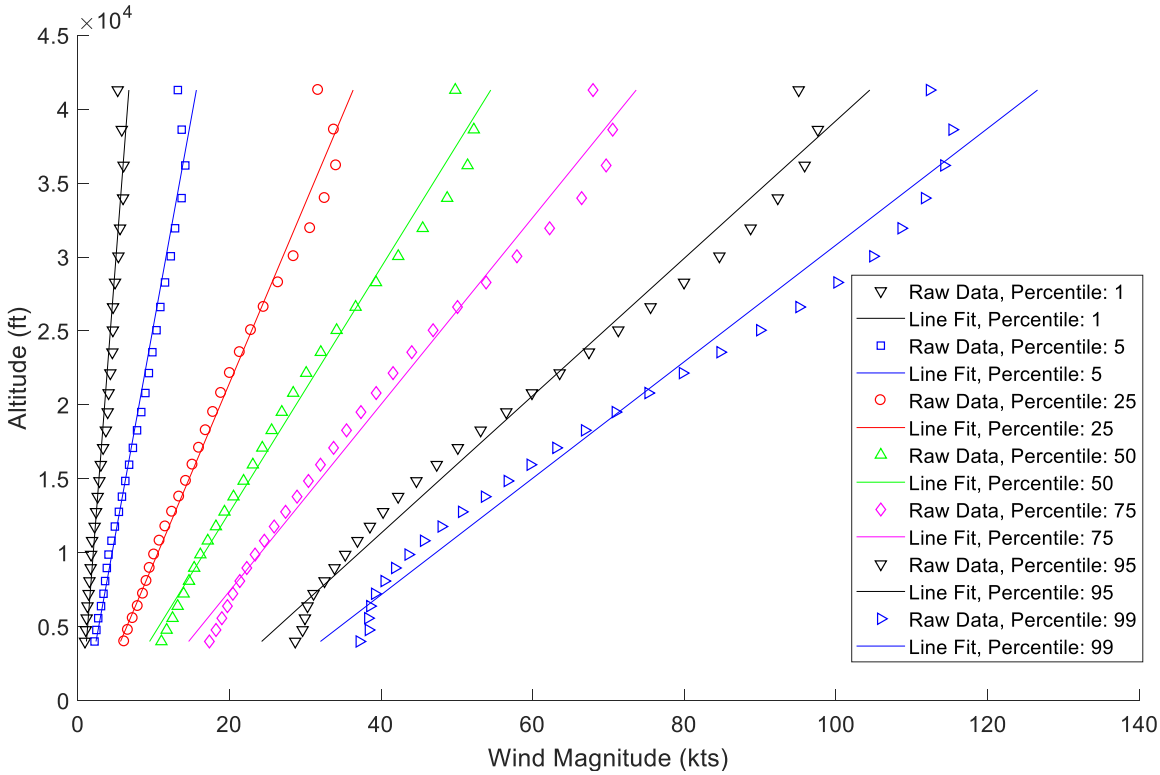

Figure 132. Linear approximation for wind magnitude as a function of altitude.

Appendix K: Turn Radius Resolution

The EPP message provides the turn radius for a waypoint at a resolution of 0.1 nautical miles. As such, the error between the actual radius and the reported radius can be as much as 0.05 nautical miles (approximately 300 feet) when using a standard rounding approach. The distance, *d*, from a fly-by waypoint to a middle-of-turn point at the geometric center of a constant radius, *R*, turn of a given track angle change, θ, can be computed by:

$$d = R\left(\frac{1}{cos\left(\frac{\theta}{2}\right)} - 1\right) \tag{10}$$

It can be shown that, given two turn radius values, the difference in the distance from the fly-by waypoint to the middle-of-turn, Δd, is given by:

$$\Delta d = -\Delta R + \frac{\Delta R}{cos\left(\frac{\theta}{2}\right)} \tag{11}$$

Equation (11) shows the maximum possible difference in the distance from a middle-of-turn point to a fly-by waypoint for a given radial difference and track angle change. The distance error here is close to zero at very small track angle changes and can be up to ~100 feet for turns of 90 degrees of track angle change. Note that the error can be double these magnitudes if the radius values are truncated or rounded using a floor or ceiling function.

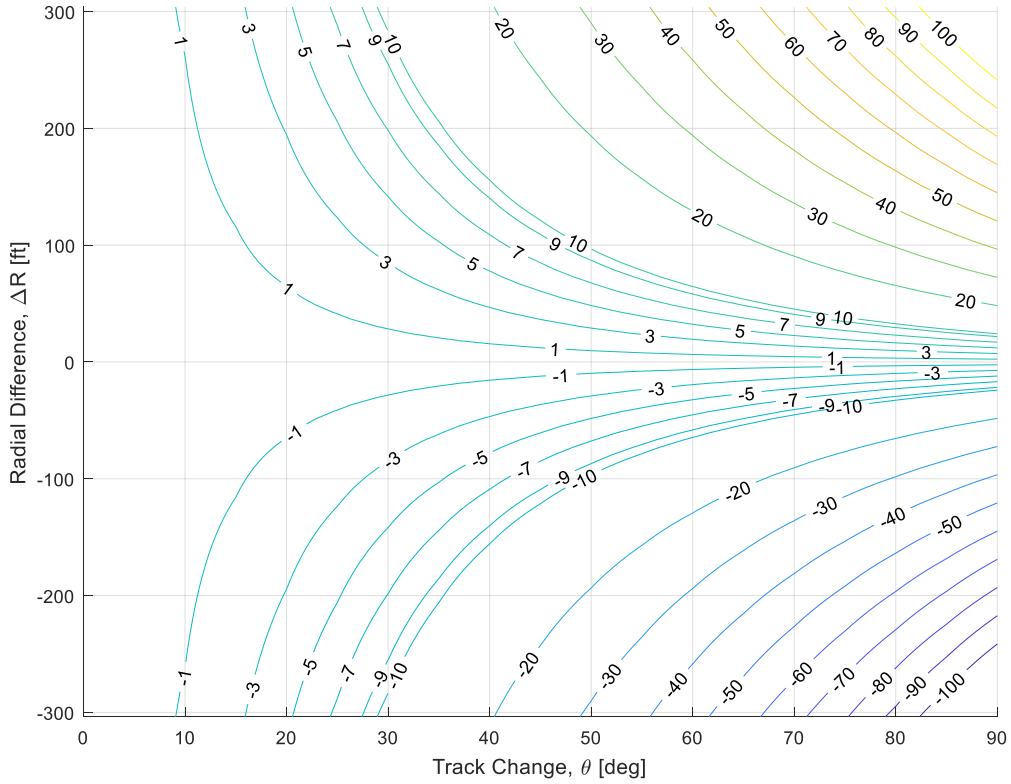

Figure 133. Maximum middle-of-turn distance error [ft] contours as a function of radial difference and track angle change.

REPORT DOCUMENTATION PAGE

Form Approved
OMB No. 0704-0188

1. REPORT DATE *(DD-MM-YYYY)*	2. REPORT TYPE	3. DATES COVERED *(From - To)*
01-03-2018	Technical Memorandum	

4. TITLE AND SUBTITLE

Preliminary Error Characterization and Parametric Error Model for the Automatic Dependent Surveillance – Contract Extended Projected Profile Message

5a. CONTRACT NUMBER

5b. GRANT NUMBER

5c. PROGRAM ELEMENT NUMBER

6. AUTHOR(S)

Guerreiro, Nelson M.; Underwood, Matthew C.

5d. PROJECT NUMBER

5e. TASK NUMBER

5f. WORK UNIT NUMBER

629660.03.10.07.01

7. PERFORMING ORGANIZATION NAME(S) AND ADDRESS(ES)

NASA Langley Research Center
Hampton, Virginia 23681-2199

8. PERFORMING ORGANIZATION REPORT NUMBER

L-20901

9. SPONSORING/MONITORING AGENCY NAME(S) AND ADDRESS(ES)

National Aeronautics and Space Administration
Washington, DC 20546-0001

10. SPONSOR/MONITOR'S ACRONYM(S)

NASA

11. SPONSOR/MONITOR'S REPORT NUMBER(S)

NASA-TM-2018-219810

12. DISTRIBUTION/AVAILABILITY STATEMENT

Unclassified-
Subject Category 03
Availability: NASA STI Program (757) 864-9658

13. SUPPLEMENTARY NOTES

14. ABSTRACT

A critical component of Trajectory-Based Operations (TBO) is the ability for a consistent and accurate 4-dimensional trajectory (4DT) to be shared and synchronized between airborne and ground systems as well as amongst various ground automation systems. The Aeronautical Telecommunication Network—Baseline 2 (ATN-B2) standard defines the Extended Projected Profile (EPP) trajectory that can be sent via Automatic Dependent Surveillance-Contract (ADS-C) from an aircraft to ground automation. The EPP trajectory message contains a representation of the reference trajectory from an aircraft's Flight Management System (FMS). In this work, a set of scenarios were run in a high-fidelity aircraft and FMS simulation to perform an initial characterization of EPP trajectory errors under a given set of conditions. The parameters investigated were the route length, route type, wind magnitude error, wind direction error, and with and without a required time-of-arrival (RTA) constraint. In addition, linear regression was used to identify a set of EPP error models for the cross-track, vertical, and time errors.

15. SUBJECT TERMS

ADS-C; Error models; Extended projected profile; FMS; TBO

16. SECURITY CLASSIFICATION OF:			17. LIMITATION OF ABSTRACT	18. NUMBER OF PAGES	19a. NAME OF RESPONSIBLE PERSON
a. REPORT	b. ABSTRACT	c. THIS PAGE			STI Help Desk(email help@sti.nasa.gov
					19b. TELEPHONE NUMBER *(Include area code)*
U	U	U	UU	127	(757) 864-9658